INFORMATION TO USERS

This manuscript has been reproduced from the microfilm master. UMI films the text directly from the original or copy submitted. Thus, some thesis and dissertation copies are in typewriter face, while others may be from any type of computer printer.

The quality of this reproduction is dependent upon the quality of the copy submitted. Broken or indistinct print, colored or poor quality illustrations and photographs, print bleedthrough, substandard margins, and improper alignment can adversely affect reproduction.

In the unlikely event that the author did not send UMI a complete manuscript and there are missing pages, these will be noted. Also, if unauthorized copyright material had to be removed, a note will indicate the deletion.

Oversize materials (e.g., maps, drawings, charts) are reproduced by sectioning the original, beginning at the upper left-hand corner and continuing from left to right in equal sections with small overlaps.

Photographs included in the original manuscript have been reproduced xerographically in this copy. Higher quality 6" x 9" black and white photographic prints are available for any photographs or illustrations appearing in this copy for an additional charge. Contact UMI directly to order.

ProQuest Information and Learning
300 North Zeeb Road, Ann Arbor, MI 48106-1346 USA
800-521-0600

Reproduced with permission of the copyright owner. Further reproduction prohibited without permission.

Reproduced with permission of the copyright owner. Further reproduction prohibited without permission.

UNIVERSITY OF ALBERTA

EXPERIMENTAL STUDIES ON "FOAMY OIL" PHENOMENA

by

Nasser Salim Albartamani

A thesis submitted to the faculty of Graduate Studies and Research in partial fulfillment of the requirements for the degree of Doctor of Philosophy

in

Petroleum Engineering

Department of Civil and Environmental Engineering

Edmonton, Alberta, Canada
Fall, 2000

Reproduced with permission of the copyright owner. Further reproduction prohibited without permission.

National Library of Canada
Acquisitions and Bibliographic Services
395 Wellington Street
Ottawa ON K1A 0N4
Canada

Bibliothèque nationale du Canada
Acquisitions et services bibliographiques
395, rue Wellington
Ottawa ON K1A 0N4
Canada

Your file Votre référence

Our file Notre référence

The author has granted a non-exclusive licence allowing the National Library of Canada to reproduce, loan, distribute or sell copies of this thesis in microform, paper or electronic formats.

The author retains ownership of the copyright in this thesis. Neither the thesis nor substantial extracts from it may be printed or otherwise reproduced without the author's permission.

L'auteur a accordé une licence non exclusive permettant à la Bibliothèque nationale du Canada de reproduire, prêter, distribuer ou vendre des copies de cette thèse sous la forme de microfiche/film, de reproduction sur papier ou sur format électronique.

L'auteur conserve la propriété du droit d'auteur qui protège cette thèse. Ni la thèse ni des extraits substantiels de celle-ci ne doivent être imprimés ou autrement reproduits sans son autorisation.

0-612-59558-7

Canada

Reproduced with permission of the copyright owner. Further reproduction prohibited without permission.

UNIVERSITY OF ALBERTA

LIBRARY RELEASE FORM

NAME OF AUTHOR:	Nasser Salim Albartamani
TITLE OF THESIS:	Experimental Studies on "Foamy Oil" Phenomena
DEGREE:	Doctor of Philosophy
YEAR THIS DEGREE GRANTED:	Fall 2000

Permission is hereby granted to the University of Alberta Library to reproduce single copies of this thesis and to lend or sell such copies for private, scholarly, or scientific research purposes only.

The author reserves all other publication and other rights in association with the copyright in the thesis, and except as hereinbefore provided, neither the thesis nor any substantial portion thereof may be printed or otherwise reproduced in any material form whatever without the author's prior written permission.

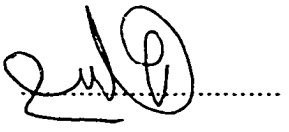

Permanent Address:

P.O. Box 768
Nizwa - 611
Sultanate of Oman

DATED: Oct. 2, 2000

Reproduced with permission of the copyright owner. Further reproduction prohibited without permission.

UNIVERSITY OF ALBERTA

FACULTY OF GRADUATE STUDIES AND RESEARCH

The undersigned certify that they have read, and recommend to the Faculty of Graduate Studies and Research for acceptance, a thesis entitled EXPERIMENTAL STUDIES ON "FOAMY OIL" PHENOMENA submitted by Nasser Salim Albartamani in partial fulfillment of the requirements for the degree of Doctor of Philosophy in Petroleum Engineering.

Dr. S.M. Farouq Ali (Supervisor)

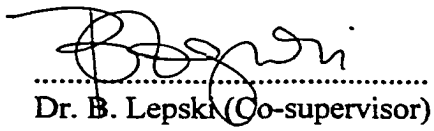

Dr. B. Lepski (Co-supervisor)

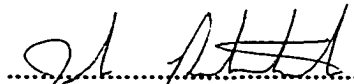

Dr. J. Ratulowski

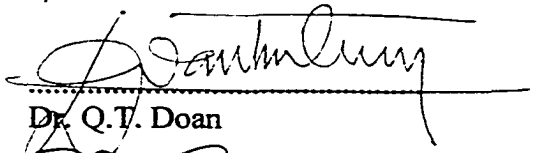

Dr. Q.T. Doan

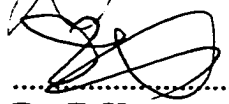

Dr. Z. Xu

Dr. B. Maini (External Examiner)

DATED: Aug. 24, 2000

Reproduced with permission of the copyright owner. Further reproduction prohibited without permission.

Abstract

This research was directed towards an experimental investigation of foamy oil phenomena, which holds considerable promise for the recovery of heavy oil from solution gas drive reservoirs exhibiting foamy oil characteristics. A recombined Lloydminster heavy oil and CO_2 was used in all the experiments. The heavy oil viscosity at ambient conditions was 14000 mPa.s. The runs were carried out at room temperature of 22 °C, ± 0.5 °C. A 0.5% (by volume) defoamer was added to several experiments to help liberate gas bubbles from the dispersed gas phase to free gas and to elucidate the effect of the pressure depletion rate on the anomalous production of foamy oil.

A series of constant composition expansion, CCE, experiments was conducted using a visual PVT cell. The CCE runs were performed with two different pressure depletion rates of 41 and 800 kPa/hr at room temperature. Furthermore, they were performed under different conditions of mixing/no mixing, with and without the addition of defomer, and in present of glass beads.

The viscosity was measured at two pressure depletion rates of 41 and 800 kPa/hr at room temperature and with and without the addition of defoamer. Three viscometers were used to measure the viscosity of foamy oil. Cambridge viscometer results showed an increase in foamy oil apparent viscosity with the decrease in pressure depletion rate. For the same pressure depletion rate, the addition of defoamer increased the foamy oil apparent viscosity. Capillary viscometer results were all within 5% from each other. Haake viscometer data were not reliable due the development of free gas phase within the chamber.

Reproduced with permission of the copyright owner. Further reproduction prohibited without permission.

A series of depletion visualization experiments were carried out using a high-pressure (6895kPa, 1000 psi) micromodel. The micromodel runs were performed with and without the presence of porous media and the addition of defoamer. Ottawa sand and Cryolite were used to pack the micromodel.

Visualization of the foamy oil depletion process revealed that several nucleation stages exist in a depletion process at the pore scale level. In all the micromodel runs, nucleation started at the furthest point from the outlet. Sand pack experiments with and without the addition of defoamer were performed at slow pressure depletion rates using two different sand packs.

Reproduced with permission of the copyright owner. Further reproduction prohibited without permission.

To My Parents,

To Samar, Hamzah, and Abdullah,

To My wife,

And

To Suleiman

For their love and support

Reproduced with permission of the copyright owner. Further reproduction prohibited without permission.

Acknowledgements

I wish to express my sincere appreciation to Dr. S.M. Farouq Ali who supervised this study at the start and continued to the end even after he left the university as a co-supervisor. My thanks go to Dr. Lepski and the supervisory committee.

I am thankful to Dr. Ratulowski for his help, suggestions, and valuable discussions. I am indebted to Dr. A. Hammami for his help in designing the micromodel, valuable suggestions during the course of this study, and obtaining the surfactant used in this study. It is no exaggeration that without the help of Dr. Hammami, this work would not be possible. The help and the experience gained during the experimental work at D.B. Robinson will be cherished for long time to come. Thanks are due to the experienced technologists at D.B. Robinson Research who helped in the setup and running of the experimental work especially Don Sieben, Craig Borman, and Dave Murray.

I must extend my special thanks to my family for their endurance of the agony of waiting for me to finish this study and for their endurance of having to travel back and forth between Oman and Canada. I am grateful to my extended family for their support and encouragement I received during this study, especially my brother Suleiman.

I am indebted to Petroleum Development Oman Company (PDO) for funding this study.

Reproduced with permission of the copyright owner. Further reproduction prohibited without permission.

Table of Contents

Chapter I

1. Introduction and Background 1

Chapter II

2. Literature Review 3

2.1 Conventional and Non-conventional Solution Gas Drive Mechanisms 3

2.2 Viscosity of Foamy Oil 5

2.3 Stages of Bubble Formation 7

2.3.1 Supersaturation 7

2.3.2 Bubble Nucleation 8

2.3.2.1 Primary Nucleation 9

2.3.2.1.1 Homogenous Primary Nucleation 10

2.3.2.1.2 Heterogeneous Primary Nucleation 10

2.3.2.2 Secondary Nucleation 11

2.3.2.3 Theory of Nucleation 11

2.3.3 Bubble Growth 13

2.3.4 Bubble Coalescence and Breakup 14

2.4 Foamy Oil Flow Modeling 15

2.4.1 Geomechanical Model 16

2.4.2 Multiphase Flow Model 17

2.4.3 Pseudo-bubble Point Model 17

2.4.4 Modified Fractional Flow Model 18

2.4.5 Low Viscosity Model 18

2.4.6 Gas Lubrication Model 19

2.4.7 Dynamic Model 19

2.5 Critical Gas Saturation 20

2.6 Solubility of Gases in Liquids 21

2.7 Brief Review of Defoamers 22

Chapter III

3. Objectives 24

Reproduced with permission of the copyright owner. Further reproduction prohibited without permission.

Chapter IV

4. Experimental Set-up and Procedure 25
4.1 Materials 25
4.1.1 Live Oil Sample Preparation 25
4.2 PVT Cell Apparatus 28
4.3 PVT Measurements 28
4.4 Foamy Oil Rheology Measurements 28
4.4.1 Cambridge Electromagnetic Viscometer 29
4.4.1.1 Calibration of CEV 29
4.4.1.2 Viscosity Measurement with CEV 31
4.4.2 Capillary Viscometer 31
4.4.2.1 Calibration 35
4.4.2.2 Viscosity Measurement with Capillary Viscometer 35
4.4.3 Haake Rotovisco RV-2 Viscometer 36
4.4.3.1 Viscosity Measurement with RV-2 Viscometer 36
4.5 Micromodel Design and Set-up 37
4.5.1 Micromodel Preparation and Packing 41
4.5.1.1 Micromodel Experimental Procedure 41
4.6 Sand Pack Core Experiments 42
4.6.1 Packing Sand Core Holders 42

Chapter V

5. Discussion of Experimental Results 45
5.1 Discussion of PVT Measurements 45
5.1.1 CCE Runs at Pressure Depletion Rate of 800 kPa/hr and Room Temperature 46
5.1.2 Comparison of the CCE Runs at Pressure Depletion Rate of 800 kPa/hr and Room Temperature 55
5.1.3 CCE Runs at Pressure Depletion Rate of 41 kPa/hr and Room Temperature 57
5.1.4 Effect of Pressure Depletion Rate 57
5.1.5 Apparent Solubility of CO_2 in Heavy Oil 61

Reproduced with permission of the copyright owner. Further reproduction prohibited without permission.

5.1.6 Reproducibility of CCE Results 64
5.2 Measurement of Viscosity of Foamy Oil 64
5.2.1 Viscosity of Foamy Oil as Measured by Cambridge Viscometer 66
5.2.1.1 Comparison of Viscosity of Foamy Oil as Measured by Cambridge Viscometer 71
5.2.2 Viscosity of Foamy Oil as Measured by Capillary Viscometer 75
5.2.3 Viscosity of Foamy Oil as Measured by Haake Rotovisco RV-2 Viscometer 77
5.2.4 Comparison of The Three Viscometers 79
5.2.5 Derivation of Foamy Oil Viscosity 83
5.3 Discussion of Micromodel Experimental Results 86
5.3.1 Micromodel Experiments with No Porous Media 87
5.3.2 Micromodel Experiments in Presence of a Porous Medium 90
5.3.3 Visualization of the Foamy Oil Phenomena 97
5.4 Discussion of Sandpack core Experimental Results 105
Chapter VI
6. Conclusions 112
Chapter VII
7. Recommendations 116
References 117
Appendix A: CCE and Viscosity Data for Different Runs 122
Appendix B: Videotape of the Micromodel Depletion Process 166

Reproduced with permission of the copyright owner. Further reproduction prohibited without permission.

List of Tables

Table 4.1 Composition of the original Lloydminster oil 26

Table 4.2 Composition of Lloydminster recombined oil 27

Table 5.1 Foamy oil CCE runs done under different conditions of pressure depletion rate and room temperature 46

Table 5.2 Viscosity as measured by Cambridge viscometer 75

Table 5.3 Runs performed in the micromodel 86

Table 5.4 Descriptions of the foamy oil depletion process captured in a videotape 167

Reproduced with permission of the copyright owner. Further reproduction prohibited without permission.

List of Figures

Figure 4.1 Schematic of the Cambridge Viscometer and PVT cell set-up. 30

Figure 4.2 Calibration of viscosity vs. temperature for Cambridge Viscometer using S2000 viscosity standard Lot# 96202 fluid. 32

Figure 4.3 Calibration of viscosity vs. temperature data for Cambridge Viscometer using S600 viscosity standard Lot# 99301 fluid. 33

Figure 4.4 Schematic of the capillary viscometer and PVT cell se-up.....34

Figure 4.5 Schematic of the RV-2 Viscometer set-up 38

Figure 4.6 Top and side view of the micromodel 39

Figure 4.7 Schematic of the micromodel experimental set-up.....40

Figure 4.8 Schematic of the sand-pack Experimental Set-up.....43

Figure 5.1 CCE of foamy oil for pressure depletion rate of 800 kPa/hr for the case of no mixing, insert showing bubble point pressure.....47

Figure 5.2 CCE of foamy oil for no mixing case at a depletion rate of 800 kPa/hr and room temperature 48

Figure 5.2T Total volume of foamy oil for no mixing case at a depletion rate of 800 kPa/hr and room temperature. 151

Figure 5.3 CCE of foamy oil for mixing case at a depletion rate of 800 kPa/hr and room temperature 50

Figure 5.3T Total volume of foamy oil for mixing case at a depletion rate of 800 kPa/hr and room temperature. 152

Figure 5.4 CCE of foamy oil for 0.5% (by vol.) defomer and no mixing case at a depletion rate of 800 kPa/hr and room temperature 51

Figure 5.4T Total volume of foamy oil for 0.5% (by vol.) defomer and no mixing case at a depletion rate of 800 kPa/hr and room temperature. 153

Figure 5.5 CCE of foamy oil for 0.5% (by vol.) defomer and mixing case at a depletion rate of 800 kPa/hr and room temperature 53

Figure 5.5T Total volume of foamy oil for 0.5% (by vol.) defomer and mixing case at a depletion rate of 800 kPa/hr and room temperature. 154

Reproduced with permission of the copyright owner. Further reproduction prohibited without permission.

Figure 5.6 Schematic of the PVT cell and glass beads arrangement 52

Figure 5.7 CCE of foamy oil for glass beads bed case at a depletion rate of 800 kPa/hr and room temperature 54

Figure 5.7T Total volume of foamy oil for glass beads bed case at a depletion rate of 800 kPa/hr and room temperature. 155

Figure 5.8 Comparison of CCE runs for different situations at a depletion rate of 800 kPa/hr and room temperature 56

Figure 5.9 CCE of foamy oil for no mixing case at depletion rate of 41 kPa/hr and room temperature 58

Figure 5.9A CCE data and Bubble point determination for the case of no mixing and pressure depletion rate of 41 kPa/hr and room temperature 123

Figure 5.9T Total volume of foamy oil for no mixing case at depletion rate of 41 kPa/hr and room temperature 156

Figure 5.10 CCE of foamy oil for mixing case at depletion rate of 41 kPa/hr and room temperature 59

Figure 5.10A CCE data and Bubble point determination for the mixing case and pressure depletion rate of 41 kPa/hr and room temperature. 124

Figure 5.10T Total volume of foamy oil for mixing case at depletion rate of 41 kPa/hr and room temperature. 157

Figure 5.11 Comparison of CCE at depletion rate of 41 kPa/hr and room temperature for mixing and no mixing cases 60

Figure 5.11A CCE of foamy oil at the depletion of 800 kPa/hr and room Temperature with glass beads filled PVT cell 125

Figure 5.11T Comparison of total volume at depletion rate of 41 kPa/hr and room temperature for mixing and no mixing cases. 158

Figure 5.12 Comparison of CCE at depletion rates of 800 kPa/hr and 41 kPa/hr of foamy oil for different conditions and room temperature 62

Figure 5.12A CCE of foamy oil at pressure depletion rate of 800 kPa/hr and room temperature, for the case of mixing (repeat) insert showing bubble point pressure. 126

Reproduced with permission of the copyright owner. Further reproduction prohibited without permission.

Figure 5.13 Comparison of apparent solubility of CO2 in foamy oil for different situations at a depletion rate of 800 kPa/hr and room temperature 63

Figure 5.13A CCE of foamy oil at pressure depletion rate of 800 kPa/hr and room temperature, for the case of mixing, insert showing bubble point pressure..... 127

Figure 5.14 Reproducibility of CCE runs at depletion rates of 800 kPa/hr and 41 kPa/hr of foamy oil and room temperature..... 65

Figure 5.14A CCE of foamy oil at the depletion of 800 kPa/hr and room Temperature with 0.5% defoamer added for mixing case..... 128

Figure 5.15 Viscosity of foamy oil with 0.5% (by vol.) defoamer as measured by Cambridge viscometer for the pressure depletion rate of 800 kPa/hr and room temperature 67

Figure 5.15A1 CCE of foamy oil at the depletion of 800 kPa/hr and room Temperature with 0.5% defoamer added for no mixing case..... 129

Figure 5.15A Viscosity of foamy oil at 2068 kPa (300 psi) for 800 kPa/hr pressure depletion rate and room temperature 130

Figure 5.16 Viscosity of foamy oil as measured by Cambridge viscometer for the pressure depletion rate of 800 kPa/hr and room temperature 68

Figure 5.16A Viscosity of foamy oil at 4689 kPa (680 psi) for 800 kPa/hr pressure depletion rate and room temperature 131

Figure 5.17 Viscosity of foamy oil as measured by Cambridge viscometer for pressure depletion rate of 41 kPa/hr and room temperature.... 70

Figure 5.17A Viscosity of foamy oil at 5516 kPa (800 psi) for 800 kPa/hr pressure depletion rate and room temperature 132

Figure 5.18 Comparison of viscosity of foamy oil sample at different scenarios at 5516 kPa (800 psi) and room temperature..... 72

Figure 5.18A Viscosity of foamy oil at 6343 kPa (920 psi) for 800 kPa/hr pressure depletion rate and room temperature 133

Figure 5.19 Comparison of viscosity at 2069 kPa (300 psi) for the same oil sample for different scenarios as a function of time 73

Reproduced with permission of the copyright owner. Further reproduction prohibited without permission.

Figure 5.19A Viscosity of foamy oil at 6895 kPa (1000 psi) for 800 kPa/hr pressure depletion rate and room temperature 134

Figure 5.20 Comparison of viscosity of foamy oil as measured by Cambridge viscometer for different depletion rates 74

Figure 5.20A Viscosity of foamy oil at 7584 kPa (1100 psi) performed at a pressure depletion rate of 800 kPa/hr and room temperature..... 135

Figure 5.21 Predicted viscosity using experimental data and Islam and Chakma Equation 76

Figure 5.21A Viscosity of foamy oil with o.5% (by vol.) defoamer at 2068 kPa (300 psi) for pressure depletion rate of 800 kPa/hr and room temperature 136

Figure 5.22 Viscosity as measured by capillary viscometer at different depletion rates and room temperature 78

Figure 5.22A Viscosity of foamy oil with o.5% (by vol.) defoamer at 5516 kPa (800 psi) for pressure depletion rate of 800 kPa/hr and room temperature 137

Figure 5.23 Comparison of Viscosity measured by Roto Viscometer at a Depletion Rate of 800 and 41 kPa/hr..... 80

Figure 5.23A Viscosity of foamy oil with o.5% (by vol.) defoamer at 6343 kPa (920 psi) for pressure depletion rate of 800 kPa/hr and room temperature 138

Figure 5.24 Comparison of viscosity as measured by the three viscometers at 41 kPa/hr 81

Figure 5.24A Viscosity of foamy oil with o.5% (by vol.) defoamer at 6895 kPa (1000 psi) for pressure depletion rate of 800 kPa/hr and room temperature..... 139

Figure 5.25 Comparison of viscosity as measured by three viscometers at 800 kPa/hr 82

Figure 5.25A Viscosity of foamy oil with 0.5% (by Vol.) defoamer at 7584 kPa (1100 psi) for pressure depletion rate of 800 kPa/hr and room temperature..... 140

Figure 5.25ab Velocity distribution in a capillary for a) single oil phase, b) foamy oil phase..... 84

Reproduced with permission of the copyright owner. Further reproduction prohibited without permission.

Figure 5.26 Comparison of PVT cell CCE and micromodel pressure depletion at a pressure depletion rate of 800 kPa/hr 88

Figure 5.26A Viscosity of foamy oil at 2068 kPa (300 psi) for 800 kPa/hr pressure depletion rate and room temperature 141

Figure 5.26T Comparison of PVT cell CCE (total volume) and micromodel pressure depletion at a pressure depletion rate of 800 kPa/hr. 159

Figure 5.27 Comparison of PVT cell CCE and micromodel runs of 0.5% defoamer at a pressure depletion rate of 800 kPa/hr 89

Figure 5.27A Viscosity of foamy oil at 4689 kPa (680 psi) for 800 kPa/hr pressure depletion rate and room temperature 142

Figure 5.27T Comparison of PVT cell CCE (total volume) and micromodel runs of 0.5% defoamer at a pressure depletion rate of 800 kPa/hr. 160

Figure 5.28 Comparison of PVT cell CCE and micromodel run at pressure depletion rate of 41 kPa/hr..... 91

Figure 5.28A Viscosity of foamy oil at 5516 kPa (800 psi) for 800 kPa/hr pressure depletion rate and room temperature 143

Figure 5.28T Comparison of PVT cell (total volume) CCE and micromodel run at pressure depletion rate of 41 kPa/hr. 161

Figure 5.29 Micromodel Run 4 and 6 depletion data 92

Figure 5.29A Viscosity of foamy oil with o.5% (by vol.) defoamer at 2068 kPa (300 psi) for pressure depletion rate of 800 kPa/hr and room temperature using 10000-piston 144

Figure 5.29T Total volume for Cryolite-packed micromodel runs for 41 and 800 kPa/hr pressure depletion rates. 162

Figure 5.30 Micromodel Run 7 depletion data 94

Figure 5.31 Micromodel Runs 4, 6 and 7 depletion data..... 95

Figure 5.31A Viscosity of foamy oil with o.5% (by vol.) defoamer at 4689 kPa (680 psi) for pressure depletion rate of 800 kPa/hr and room temperature using 10000-piston (overlap run with 2000piston) . 145

Figure 5.31T Total volume of Cryolite-packed micromodel runs at different conditions and pressure depletion rates. 163

Reproduced with permission of the copyright owner. Further reproduction prohibited without permission.

Figure 5.32 Micromodel Runs 8, and 9 depletion data....96

Figure 5.32A Viscosity of foamy oil at 2068 kPa (300psi) for pressure depletion rate of 41 kPa/hr and room temperature....146

Figure 5.32T Total volume for sand-packed micromodel runs at 41 and 800 kPa/hr pressure depletion depletion rates....164

Figure 5.33 Comparison of Cryolite and sand packed Micromodel runs....98

Figure 5.33A Viscosity of foamy oil at 4689 kPa (680 psi) for pressure depletion rate 41 kPa/hr and room temperature....147

Figure 5.33T Comparison of total volume for Cryolite and sand packed micromodel runs....165

Figure 5.34 Bubble nucleation at the beginning the depletion process....100

Figure 5.34A Viscosity of foamy oil at 5516 (800 psi) for pressure depletion rate of 41 kPa/hr and room temperature....148

Figure 5.35 Spherical bubbles being nucleated....101

Figure 5.35A Viscosity of foamy oil at 6343 kPa (920 psi) for pressure depletion rate of 41 kPa/hr and room temperature....149

Figure 5.36 Spherical bubbles being nucleated near a larger moving bubble 101

Figure 5.36A Viscosity of foamy oil at 7584 kPa (1100 psi) for pressure depletion rate of 41 kPa/hr and room temperature....150

Figure 5.37 Spherical bubbles being nucleated behind a larger moving bubble....102

Figure 5.38 Initial condition of the sand-packed micromodel at a pressure of 6895 kPa (1000 psi)....103

Figure 5.39 Growth of gas phase at a pressure of about 4137 kPa (600 psi)..103

Figure 5.40 Growth of gas phase at a pressure of 3450 kPa (500 psi)....103

Figure 5.41 Growth of gas phase at a pressure of 2415 kPa (350 psi)....103

Figure 5.42 Cumulative oil production of Run 2 performed in the long sand pack....106

Figure 5.43 Cumulative oil production of Run 6 performed in the short sand pack....108

Reproduced with permission of the copyright owner. Further reproduction prohibited without permission.

Figure 5.44 Cumulative oil production of Run 5 performed in the long sand pack. 109

Figure 5.45 Cumulative oil production of Run 2 performed in the long sand pack. 110

Reproduced with permission of the copyright owner. Further reproduction prohibited without permission.

Chapter I

1. Introduction and Background

"Foamy oil" phenomenon is associated with primary cold production, a non-thermal recovery process, from heavy-oil reservoirs producing under solution-gas drive mechanism. The "foamy oil" hypothesis to explain the unusually high production is still much debated and whether it exists within a reservoir is still an open question that needs to be answered. A number of heavy oil solution gas drive reservoirs show anomalously good primary performance, high oil production, and primary recovery factor (Maini et al., 1993; Sheng, 1997). Among the heavy oil reservoirs that show such behaviour, for example, are: Lindbergh, Frog Lake, Lloydminster, and Edam in Saskatchewan. Wellhead samples of these reservoirs show foamy oil. The oil is produced as an oil-continuous foam that contains dispersed gas bubbles at the wellhead. The nature of the gas dispersions in oil distinguishes foamy oil behaviour from conventional heavy oil. Moreover, the important issues that distinguish foamy oil from conventional heavy oil are: the amount of dispersed gas in oil and the time gas bubbles remain dispersed in the oil. These reservoirs are characterized by having unconsolidated sand with an average porosity of 34% (Tremblay et al., 1998), and an average permeability of 3.5 darcies (Tremblay et al., 1996). These reservoirs also experience sand production. However, some heavy oil reservoirs in North and South America exhibit foamy oil behaviour and essentially have no sand production (Claridge and Prats, 1995). Production rates from cold production wells can be up to 50 (Tremblay et al., 1996) to 100 times (Yeung and Adamson, 1992) and as high as 300 times (Yeung, 1996) higher than the rate predicted by Darcy equation without sand production and the foamy oil behaviour.

Several possible causes for the anomalous production have been suggested and are being investigated. These include the formation of wormholes and cavities around the wellbore that increase the effective well radius (Elkins, 1972; Tremblay, et al.,

Reproduced with permission of the copyright owner. Further reproduction prohibited without permission.

1996, 1998). Loughead (1992) suggested another possible mechanism that of sand dilation which results in high absolute permeability due to the production of substantial volumes of sand with the oil. Another possibility suggested was the enhancement of oil mobility by nucleation of a large number of microbubbles (Smith, 1988; Islam and Chakma, 1990). Other possible causes of the unusual behaviour are the in-situ formation of oil-continuous foam (Maini et al., 1993; Sheng, 1997) and influx of bottom water, but they did not give any explanation of this mechanism (Yeung and Adamson, 1992). Yet, another possibility of the unusually high cold production is due to non-Newtonian flow (Poon and Kisman, 1991). One or several of these possibilities might be involved to varying degrees in the anomalous behaviour of different foamy heavy-oil reservoirs. In view of the limited knowledge of foamy oil flow, this study will attempt to improve the understanding of the foamy oil flow through the evaluation of the existing theories/models describing foamy oil flow behaviour and through experimental work. In this study, the foamy oil behaviour is examined in particular the formation of foam in porous media in heavy oil solution gas drive reservoirs and the contribution of foam in the anomalous production.

Reproduced with permission of the copyright owner. Further reproduction prohibited without permission.

Chapter II

2. Literature Review

This chapter gives a review of pervious work done on the subject of foamy oil. To start with, a brief comparison between conventional solution-gas drive and solution-gas drive for foamy oil in heavy oil reservoirs is given in the following paragraphs.

2.1 Conventional and Non-conventional Solution Gas Drive Mechanism

Conventionally, the reservoir drive mechanism is called solution gas drive mechanism if the primary reservoir energy is supplied by the release of gas from the oil and the expansion of the in-place fluids as the reservoir pressure declines.

The process of solution gas drive in conventional oil reservoirs, above the bubble point, is that liquid oil is expanded resulting in production of oil at the reservoir level. As the pressure declines further below the bubble point pressure, the dissolved gas starts to evolve. The evolution is very rapid and is assumed to occur instantaneously. The evolved gas is further assumed to disengage simultaneously/ quickly from the oil to form a free gas phase. However, in some heavy oil reservoirs that exhibit foamy oil behaviour, the time it take the solution gas drive to evolve and the evolved gas to disengage from liquid oil is believed to be important (Sheng, 1997); that is the time it takes the solution gas to evolve and for the evolved gas to become free gas.

Unlike conventional oil reservoirs, the evolved gas in foamy oil reservoirs initially remains dispersed in the oil, and gradually disengages from the oil phase. The amount of evolved gas is always equal to the amount of dispersed and free gas. Foamy oil is thus not a firmly established reality. The definition and the existence in reservoirs remain controversial (Sheng, 1997).

Reproduced with permission of the copyright owner. Further reproduction prohibited without permission.

Foamy oil is the term used to describe a form of two-phase oil-gas flow in porous media in solution gas drive reservoirs. The important difference between normal two-phase and foamy oil flow is that in later a large volume of the evolved gas is trapped within the reservoir resulting in a drastic reduction in gas mobility (Maini, 1999). In addition, as gas comes out of solution, it remains partially or completely dispersed in the oil phase. After reaching certain size, bubbles start to flow with oil. During migration, bubbles continue to grow, but are likely to break-up into smaller bubbles. The break-up of bubbles into smaller ones maintains gas dispersion, which counteracts the effect of coalescence, and results in lower produced GOR and a high recovery factor (Maini, 1999). In conventional solution gas drive, gas bubbles remain trapped and continue to grow without ever leaving their original pore. Bubbles continue to grow and span several pores where they coalesce with other bubbles in other pores (Maini, 1999). Furthermore, Maini (1999) offered another hypothesis to explain the mechanism of foamy oil. Based on experimental work, he postulated that foamy oil flow involves much larger bubbles migrating with the oil and that the dispersion is created by break-up of bubbles during their migration with the oil. He stated that the main difference between conventional and foamy oil solution gas drive is that the pressure gradient in foamy oil solution gas drive is large enough to mobilize growing gas clusters after they have grown to a certain size. The requirements for the occurrence of dispersed flow under solution gas drive are: viscous forces acting on a bubble should exceed the capillary trapping forces, no gravitational segregation of the two phases, and interfacial chemistry effects that hinder bubble coalescence maybe needed. Meeting these three requirements is dependent on the rock and fluid properties and the operating conditions. In reservoirs, dispersed flow is more likely to occur in well-sorted unconsolidated sands with high permeability, viscous oil, and low oil-gas interfacial tension (Maini, 1999). Next, a review of the rheology and the gas formation mechanisms is given.

Reproduced with permission of the copyright owner. Further reproduction prohibited without permission.

2.2 Viscosity of Foamy Oil

Few investigations have been done exclusively to correlate the apparent viscosity of foamy oil to its foam quality. Einstein performed the first theoretical work done on the subject of viscosity of dispersion. He assumed that the disperse system consisted of a suspension of rigid spheres in a viscous liquid and that the spheres were sufficiently apart not to influence one another (Hatschek, 1928, p196). The equation of the viscosity of the dispersion at low concentration of the dispersed phase was derived mathematically from the fundamental equations of hydrodynamics and is given in the following form (Hatschek, 1928):

$$\mu_S = \mu\,(1 + 2.5\,\phi), \quad \text{.....(1)}$$

Where μ_S is the viscosity of dispersion, μ is the viscosity of the dispersion medium, and ϕ is the volume fraction of the dispersed phase. The above equation, which predicts a linear relation as the concentration of the dispersed phase increases, does not hold well for higher concentration. Various investigators differ about the range of applicability of this equation. Hatschek (1928, p197) stated that the viscosity of suspensions of low concentrations of 2 to 8% was anomalous, i.e., varied with the velocity gradient. Shen and Batycky (1996) put the applicability of Einstein's equation for the range of foam quality of zero to 5%. While; Mitchell (1971) used it for foam quality of the range of zero to 54% to compare his experimental results. Mitchell also gave two correlations for the viscosity of foam: one for foam quality of the range of zero to 54%, he used 45 data points to empirically derive the following equation:

$$\mu_f = \mu\,(1.0 + 3.6\,\phi). \quad \text{.....(2)}$$

For foam quality of the range of 54 to 96%, he used 87 data points to derive the following empirical equation:

$$\mu_f = \mu\,/\,(1.0 - \phi^{0.49}). \quad \text{.....(3)}$$

Reproduced with permission of the copyright owner. Further reproduction prohibited without permission.

Where μ_f is foam viscosity, μ is the viscosity of the base liquid, and ϕ is foam quality, fraction.

Pal et al. (1992) have reviewed various viscosity correlations mainly for Newtonian suspensions available in the literature. They expressed the functional relationship between relative viscosity (μ_{rel}) and the volume fraction of the dispersed phase in the following form:

$$\mu_{rel} = \frac{\mu_m}{\mu_l} = 1.0 + a\phi_d + b\phi_d^2 + c\phi_d^3 + \ldots \quad \ldots\ldots(4)$$

Where the μ_m is the mixture and μ_l is the viscosity of the continuous liquid phase.

Islam and Chakma (1990) measured viscosities of pre-generated foamy oils in a capillary tube of diameter of 3.2 mm. The results of their experiments showed that the bulk foamy oil viscosity, μ_b can be correlated to the gas volume fraction, ϕ:

$$\mu_b = \mu_o^{1-\phi}\,\mu_g^{\phi} \quad \ldots\ldots(5)$$

Where μ_o and μ_g are the viscosities of the oil and gas, respectively. The above correlation predicts a decrease in the gas bubble-dispersed oil apparent viscosity with an increase in the gas volume fraction. This contradicts the theoretical prediction for suspension, i.e., Einstein's equation for solid dispersed phase. Moreover, According to Shen and Batycky (1990) the above empirical correlation is a slight modification of Arrhenius equation (Hatschek, 1928) for single-phase solutions of liquids, and is not appropriate for suspensions.

Bora (1998) measured foamy oil viscosity using a plate and a cone rotational viscometer, and he concluded that the foamy oil viscosity was slightly higher than that of the live oil at the same pressure and temperature. Due to his initial erratic results as there was no variation of foamy oil viscosity being measured with pressure, foam was generated by using a sintered filter elements of different pore openings. By using the sintered filters to generate foam, the process of bubble formation as they come out of

Reproduced with permission of the copyright owner. Further reproduction prohibited without permission.

solution would have been altered. Thus, the measured viscosity would not represent apparent foamy oil solution gas drive viscosity.

In the next sections, the various steps involved in the evolution of gas bubbles and the formation of free gas phase within the reservoir formations are discussed.

2.3 Stages of Bubble Formation

In solution gas drive reservoirs, hypothetically speaking, if there is a process by which gas is impeded from forming a continuous phase after coming out of solution, the oil recovery would be higher. Foamy oil behaviour is hypothesized to some degree on the ability of the liquid oil due to its high viscosity (and most likely due to natural surfactants) to slow down or even alter the formation of a continuous gas phase. The various steps involved in formation of gas phase in solution gas drive mechanism are: Supersaturation, Bubble Nucleation, Bubble Growth, and Bubble Coalescence and Decay. A review of the steps of bubble formation in porous media is given in the following sections.

2.3.1 Supersaturation

Oil is said to be supersaturated when it contains more dissolved gas than that predicted by the PVT relationships (Stewart et al., 1954). Firoozabadi et al. (1994) define supersaturation, S, as the difference between the equilibrium pressure, p_e, and system pressure, p,

$$S = p_e - p \quad \text{.....(6)}$$

For a new gas phase formation, the liquid should be supersaturated (Firoozabadi et al., 1994). Therefore, supersaturation is the driving force for the evolution of new bubbles in a gas-oil system. The higher the degree of supersaturation, the larger the number of bubbles formed and the higher is the recovery efficiency (Stewart et al., 1954). Kennedy and Olson (1952) stated that Supersaturation depends on the rate of pressure reduction. According to Ostwald's "Law of Stages", "a supersaturated state does not spontaneously transform directly into that phase which, under the conditions ruling, is

Reproduced with permission of the copyright owner. Further reproduction prohibited without permission.

the most stable of the possible states but into the phase which is next more stable than itself" (Dunning, 1969). But Dunning (1969) stated that there are exceptions to the rule due to the relative rates of nucleation and crystal growth for the stable and unstable forms.

Bora (1998) conducted visual micromodel studies on gas formation in solution gas drive. He concluded that a high degree of supersaturation was required to initiate the formation of visible bubbles. Also, he performed experiments with oils containing asphaltenes and deasphalted oils. He observed that the critical supersaturation was similar in both types of oil.

2.3.2 Bubble Nucleation

Frequently microscopic pits, or crevices on solid surfaces trap gas pockets at which vapor bubble growth may begin (Clift et al., 1978). These microscopic cavities act as nucleation sites for a bubble to form in the body of a liquid when the molecules of that liquid vaporize into a cavity in the liquid. A cavity is considered as any space within the liquid phase unoccupied by liquid molecules, either empty or occupied by vapor. A cavity is formed as a result of a liquid molecule removal from its equilibrium position due to local thermal fluctuations (Bernath, 1952). The fate of a cavity whether to grow to a nucleus rests on the probability of the availability of sufficient energy, which must be supplied by the surroundings, to supply the required work of nucleus formation. Bernath (1952) and others (La Mer, 1952; Blander and Katz, 1975) give the work required to form a nucleus by the following relation:

$$W = \sum_{1}^{n} (\mu_i - \mu_l) = \sigma A_n - (p_n - p_L) V_n \quad \text{.....(7)}$$

Where μ_i is the chemical potential of a gas bubble containing i molecules; and μ_l is the liquid chemical potential. The term σA_n represents the work spent in forming the surface, and the second term represent the work gained in forming the interior mass.

Reproduced with permission of the copyright owner. Further reproduction prohibited without permission.

With the aid of Laplace's equation, $r_n = 2\sigma/(p_n - p_L)$, the above relation can be written in the following form, which does not include any geometrical forms:

$$W=\left(\frac{1}{3}\pi r_n^2\sigma\right)=\frac{1}{3}A_n\sigma=\left(\frac{16\pi\sigma^3}{3(p_n-p_L)^2}\right) \quad \text{.....(8)}$$

Where r_n is the radius of the nucleus, A_n and V_n are the surface area and the volume of a nucleus, respectively; σ is the surface tension evaluated at the bulk liquid temperature; p_n and p_L are the pressures of the nucleus and that of the liquid phase, respectively. As can be seen from the above equation, the work of nucleus formation is dependent on the surface tension and the size of the nucleus. The work of nucleus formation is greatest within the liquid phase and is less at an interface. Also, as the angle of wetting of the liquid on a surface becomes smaller than 180°, the work increases; at 90° it is one half and at complete wetting (0°), it is a maximum, as the gas phase must break the adhesive bond between the liquid and the wall (Bernath, 1952).

There are two types of nucleation processes: primary and secondary. Most phase transformations proceed discontinuously through the birth and the subsequent growth of small embryos or nuclei of new phase. In the absence of a foreign matter, catalytic agents, these nuclei appear at random throughout the original phase, and the nucleation process is termed homogeneous (Andres, 1969). Nucleation rate is slowed down as the liquid viscosity increases (Walton, 1969). This means that the gas would remain in solution longer than it is predicted by the equation of states, hence supersaturation would be higher for more viscous oil.

2.3.2.1 Primary Nucleation

Bubble formation in the absence or presence of pre-existing gas bubbles and/or foreign matter, such as walls, is called a primary nucleation (Wankat, 1990). The primary nucleation is further subdivided into two categories as follows:

Reproduced with permission of the copyright owner. Further reproduction prohibited without permission.

2.3.2.1.1 Homogenous Primary Nucleation

Homogeneous nucleation occurs in the bulk liquid which is free of foreign matter and preferably the liquid wets the solid surfaces (Kamath and Boyer, 1993). Blander and Katz (1975) stated that homogeneous nucleation occurs when the liquid completely wets the surface of contact. It is formed by the spontaneous formation of bubbles in a liquid when a thermodynamic fluctuation of sufficient magnitude occurs to form a cluster of certain critical size (Yortsos and Parlar, 1989). The critical size represents a metastable equilibrium such that the particles which are larger than the critical radius continue to grow to a macroscopic bubble. Gas cluster that does not reach the critical radius redissolves back into liquid oil. A certain degree of supersaturation is needed to help smaller particles to grow, since there is a tendency for the bigger particles to grow and the smaller ones to dissolve.

The nucleation energy required to form a nucleus of certain critical size is defined as the amount of work, W, required to bring the gas molecules together to form a nucleus. The nucleation energy is related to the nucleation rate, J (m^{-3} s^{-1}), by the following relation (Wankat, 1990; Blander and Katz, 1975; Kashchiev and Firoozabadi, 1993):

$$J=\frac{dN}{dt}=Z\exp\left(\frac{-W}{kT}\right)=Z\exp\left(-\frac{16\pi\sigma^3}{3kT(p_g-p_o)^2}\right) \quad \text{.....(9)}$$

Where N is the number density of nucleus per unit volume, k is Boltzmann constant, T is the absolute temperature, σ is the surface tension, Z is Zeldovich factor, given by $Z=(\sigma\, kT/B)^{0.5}/[p_g A(r_c)]$; $A(r_c)$ is the surface area of the critical radius and B is a constant equals $2/3+p_o/3p_g$. p_g and p_o are the gas and oil pressures, respectively.

2.3.2.1.2 Heterogeneous Primary Nucleation

Heterogeneous nucleation is initiated by foreign nuclei due to the catalytic effect of their surfaces, as well as by grain boundaries and pores (La Mer, 1952).

Reproduced with permission of the copyright owner. Further reproduction prohibited without permission.

Furthermore, for heterogeneous nucleation, La Mer stated that an essential condition is that the newly formed phase must wet the surface in the presence of the bulk phase. Hence, heterogeneous nucleation could not occur in a porous medium if gas is completely non-wetting phase and the bulk phase is free of foreign matter. The presence of such matter in or around the bulk liquid lowers the critical supersaturation and the nucleation rate is enhanced. Critical supersaturation is defined as the value of supersaturation required for the formation of a detectable volume of new gas phase (Firoozabadi, et al., 1994). Yortsos and Parlar (1989) investigated different nucleation processes and concluded that the heterogeneous nucleation is the most plausible mechanism in porous media.

2.3.2.2 Secondary Nucleation

Secondary nucleation requires a pre-existing nucleus to induce the formation of a new nucleus. This mechanism is utilized in crystallization techniques in which crystal seeds, catalyst, are added intentionally to a solution to help induce crystallization. This method of nucleation is limited in a reservoir, but it may happen to some extent, if the liquid contains a trapped gas.

2.3.2.3 Theory of Nucleation

In under saturated reservoirs, as the pressure declines below the bubble point, gas starts to build up within the reservoir. The process of gas evolution out of the liquid phase requires energy. Therefore, the liquid has to be supersaturated, that is the pressure of the liquid phase must be lower than the equilibrium pressure for a gas bubble to emerge. Supersaturation, S, was defined earlier by Equation (6). Thermodynamically, the driving force for gas formation is supersaturation, and it is given approximately by (Kashchiev and Firoozabadi, 1993):

$$\Delta\mu = \mu_l(p) - \mu_g(p) = k\,T \ln (p_e/p) \quad \text{.....(10)}$$

Reproduced with permission of the copyright owner. Further reproduction prohibited without permission.

in which μ_l and μ_g are the chemical potential of the liquid and gas, respectively; k is Boltzmann constant; p_e and p are the equilibrium and system pressures, respectively. When $p= p_e$, there is no driving force for the formation of gas phase formation (S =0, $\Delta\mu$=0), in other words no supersaturation; and the liquid is said to be in the saturated state (at equilibrium). Gas phase formation is motivated only when the liquid is supersaturated, that is $p< p_e$, i.e., $S > 0$, $\Delta\mu > 0$. Thus, for formation of nucleus, the liquid phase must pass through a state of metastable equilibrium before it attains its equilibrium state (saturated state). According to Kashchiev and Firoozabadi (1993), during the initial stage of gas formation, coalescence plays no role on gas build up, since the bubbles are relatively small and sufficiently far from each other. Depending on the nature of gas bubble formation, nucleation can be divided to two categories: progressive nucleation in which new bubble nuclei appear continuously between the existing bubbles, and instantaneous nucleation in which all bubble nuclei are formed at once and thereafter they only grow. Kashchiev and Firoozabadi (1993) have investigated both the progressive and instantaneous nucleation. They gave the total volume of gas phase resulting from progressive nucleation by the following form:

$$V_g(t) = V_o \int_0^t J(t') \, v_b(t,t') \, dt' \quad \text{.....(11)}$$

And from instantaneous nucleation by:

$$V_g(t) = V_o \, N_o \, v_b(t,0) \quad \text{.....(12)}$$

In the above expressions, the compressibility of the liquid and the volume of the nucleus bubbles were neglected. V_o, N_o, and v_b are the initial volume of the liquid phase at t=0, number of bubbles per unit volume, and the volume at time t of a bubble nucleated at a time $t = t'$, respectively.

Reproduced with permission of the copyright owner. Further reproduction prohibited without permission.

2.3.3 Bubble Growth

Bubble growth starts after a bubble exceeds a certain critical size. Bubble growth in porous media is driven by one of the following situations (Li and Yortsos, 1993):

1. Fixed supersaturation far field, where the pressure or temperature is suddenly lowered and kept constant thereafter for the remainder of the process.
2. Constant liquid withdrawal, at a fixed volumetric flow rate.
3. Constant rate of supersaturation increase in the far field, due to a reduction in liquid pressure at a fixed rate.

The bubble will grow irreversibly with a growth rate $G \equiv dr/dt$, where r is the bubble radius. It is generally accepted that an isolated bubble growth is controlled by mass, momentum, and/or heat transfer across the bubble/liquid interface (Kashchiev and Firoozabadi, 1993). According to these authors, the different regimes of growth result in different r(t) dependences which, in general, are rather complicated. However, the bubble growth, G, can be approximated for a number of cases by:

$$G(t) = (\omega + \nu)\, K \left[s(t)^{\omega}\right] t^{(\nu-1)} \quad \text{.....(13)}$$

where K is the kinetic constant of bubble growth, the powers, $\omega > 0$ and $\nu > 0$, depend on the particular growth regime of gas bubbles. They gave several mathematical expressions for different growth regimes, i.e., constant supersaturation, variable supersaturation. They concluded from their theoretical analysis that the volume of newly formed gas saturation:

1. is a stronger function of time and especially of supersaturation for progressive nucleation than for instantaneous nucleation;
2. increases sharply with time for progressive nucleation, while for instantaneous nucleation it increases gradually, and
3. shows higher sensitivity to the supersaturation rate in the case of progressive nucleation than in the case of instantaneous nucleation.

Reproduced with permission of the copyright owner. Further reproduction prohibited without permission.

Li and Yortsos (1993) have modeled solution gas drive by the convective-diffusion equation:

$$\phi\frac{\partial C}{\partial t}+\mathrm{u}\,.\,\nabla \mathrm{C}=\phi \mathrm{D}\,\nabla^2 C\,, \qquad (14)$$

where ϕ is the porosity, u is Darcy velocity, with no gravity effects, D is the diffusion coefficient, and C is the solute concentration. These authors postulated that the pattern of bubble growth to be controlled mainly by capillary and viscous forces, and to a lesser degree by mass transfers. They expected a percolation pattern for sufficiently small cluster sizes and a departure towards a viscous fingering pattern for larger sizes. They stated that bubble growth rate depends on mass transfer as well as on the competition of capillary and viscous forces.

2.3.4 Bubble Coalescence and Breakup

The last stage in the process of bubble formation leading to the gas phase build up is bubble coalescence. Once a bubble has formed, gas bubbles from the surrounding liquid diffuse towards that bubble. Li and Yortsos (1991) have performed experiments in visual micromodel and Hele Shaw cells of bubble growth in solution gas drive. They concluded that, in micromodel experiments, bubble grew from various nucleation sites, which were activated at different stages of the process. Furthermore, they observed that the bubbles grew as ramified clusters, which have the general features of a percolation process. In Hele Shaw cells, growth of compact clusters was observed. As the growth of gas bubbles increases, the gas bubbles form gas channels. This will lead to the critical gas saturation. When the critical gas saturation is exceeded, gas will start to flow. Critical gas saturation, S_{gc}, is defined as the saturation at which free gas starts to flow. It is generally accepted that S_{gc} increases with an increase in the pressure decline rate, most likely as a result of the nucleation fraction, (Li and Yortsos, 1993) and some of the experiments have shown such tendencies (Kamath and Boyer, 1993). Kamath and Boyer (1995) have investigated the external and internal drive processes for measuring critical gas saturation. They concluded that the critical gas saturation

Reproduced with permission of the copyright owner. Further reproduction prohibited without permission.

obtained from external drive is significantly different from that obtained from depletion experiments; the critical gas saturation found by the depletion experiment gave an upper limit while external drive gave lower bound value. Moreover, they stated that the spurious nucleation from pre-existing trapped gas bubbles can invalidate the laboratory depletion results. Also, they suggested a methodology for measuring critical gas saturation, which is as follows:

1. Depletion experiments should be conducted with a thoroughly evacuated core. Reservoir bubble point live oil should be used to equilibrate the core at high pressure. Deplete the core at a reasonable rate, i.e., 100 psi/day. Shut the experiment at various time and measure the change in pressure.
2. Conduct a capillary-controlled external gas drive experiment.
3. Repeat the depletion experiment at a lower pressure decline rate if the uncertainty in the critical gas saturation is unacceptable.

Wilkinson et al. (1993) reviewed and conducted experiments on the influence of gas density and liquid viscosity on bubble break up. The bubble break up is assumed to occur only when a destabilizing force that acts on the bubble is larger than the surface tension force that tends to oppose bubble deformations. In the case of large bubbles, the destabilizing force is due to gravity, whereas in small bubbles the stabilizing force is due to shear stresses, generated by velocity differences. They concluded that both higher liquid viscosity and higher surface tension oppose bubble break up for both small and large bubbles. Their experiments were conducted in two pipes of different materials. It seems that gas bubbles in heavy oil will tend to break up gradually, which in turn raises the critical gas saturation.

2.4 Foamy Oil Flow Modeling

Many researchers have tried to formulate or hypothesize a method by which foamy oil behaviour can be described; or more precisely to describe the anomalous production from heavy oil solution gas drive which is unexplained by Darcy's law. The characteristic behaviours of these reservoirs are as follows (Loughead and Saltuklaroglu, 1992; Maini, et al. 1993):

Reproduced with permission of the copyright owner. Further reproduction prohibited without permission.

1) Slower decline in reservoir pressure,

2) Lower than expected GORs,

3) Higher absolute permeability,

4) Higher critical gas saturation (35% to 40%),

5) Foamy produced crude oil, and

6) Higher ultimate recovery in primary production phase.

The possible causes for these unusual phenomena were given in the Introduction. Numerical simulation of foamy oil behaviour is still primarily based on empirical adjustments to the conventional solution gas drive models. For history matching, the following parameters can be adjusted (Loughead and Saltuklaroglu, 1992): the critical gas saturation, gas-oil relative permeabilities, pressure dependent oil viscosity, fluid/rock compressibilities, and absolute permeability. The next section reviews the several available models that attempt to describe the foamy oil behaviour in heavy oil reservoirs producing under solution gas drive.

2.4.1 Geomechanical Model

Smith (1988) attempted to simulate the anomalous production of Lloydminster area by theoretical techniques, postulating that the anomalous production was due to combinations of fluid flow phenomena and matrix deformation resulting from the production of unconsolidated sand. He used a modified pressure buildup analysis to infer apparent in-situ viscosities for foamy oil. The analysis showed a reduced apparent viscosities of the order of 100 to 500 mPa.s, compared to 1700 to 3500 mPa.s for live oil viscosity. The flow was thought of as being a two-phase flow. He suggested that two-phase flow in pipes was applicable for pore flow. The pressure drop in the reservoir pores was taken to be a combination of two effects: liquid holdup and Fanning type pressure loss. The hold up effect was given as a reduction in the mean fluid density as:

$$\rho = \rho_{sat}\left(\frac{p}{p_{sat}}\right)^{\beta} \quad \text{.....(15)}$$

Reproduced with permission of the copyright owner. Further reproduction prohibited without permission.

where β is the compressibility constant given by $c_o = \beta / p$. β for Lloydminster is about 0.25. The viscous pressure loss was determined in a Fanning equation with a mixture viscosity that was intermediate between the liquid and that of the gas. The mixture viscosity was inputted in heavy oil pseudo pressure function. Then he used this function in Darcy's radial flow equation to account for the effects of the dispersed gas on enhanced liquid phase compressibility. The model was in agreement in its prediction with the performance of Lloydminster field. The weakest point of the model is using a lower viscosity to explain the higher productivity without explaining why would a mixture viscosity be lower than the bulk phase (Claridge and Prats, 1995). Also the model failed to capture the dynamic effects associated with foamy oil.

2.4.2 Multiphase Flow Model

Islam and Chakma (1990) presented a mathematical model based on a series of experiments. They conducted two types of experiments. The first set of experiments was conducted in capillary tubes to investigate the mechanics of bubble flow. The second set of experiments was conducted in unconsolidated sand cores to study the mechanics of bubble flow. They proposed an empirical relation for mixture viscosity of liquid and microbubbles flow. The relation was given earlier in the viscosity section as equation number (5). The authors did not give any comparison between the experimental and the predicted data, nor they gave any range of applicability of their correlation. Furthermore, the microbubbles were pre-generated which may not represent solution-gas-drive-originated bubbles.

2.4.3 Pseudo-bubble Point Model

Kraus et al. (1993) developed what was referred to as pseudo-bubble point model. The model was not general and was developed specifically for the incorporation into a particular simulator, Scientific Software Intercomp thermal simulator. The authors described in detail the method by which foamy oil properties could be incorporated into a conventional black simulator. The goal of the development of the model was to account for the observed effects in the field as well as

Reproduced with permission of the copyright owner. Further reproduction prohibited without permission.

in laboratory studies of foamy oil. The effects were: enhance fluid compressibility, natural pressure maintenance mechanism, and the delay of gas production. The model concept was stated as follows. When gas bubbles are liberated in heavy oil solution gas reservoirs, the bubbles are entrained. A reduction in pressure is required for the entrained bubbles to disengage and form a continuous mobile free gas phase. Thus the model consisted of three components, oil, dissolved gas, and entrained gas. The entrained gas enhances the effective compressibility of the oil phase in proportion to the mole fraction of the entrained gas in the foamy oil. Thus, the foamy oil behaves as if it has an "effective" or pseudo-bubble point pressure below the conventional bubble point pressure.

2.4.4 Modified Fractional Flow Model

Lebel (1994) described a modified fractional flow model to match laboratory measurements of foamy oil and gas flow. As gas saturation builds up from zero, the fractional flow of gas increases linearly until it reaches a limiting entrained gas saturation value. Beyond this limiting volume fraction of entrained gas saturation, further increase in gas saturation results in the formation of free gas. The effective foamy oil viscosity decreases only slightly from that of the oil as the gas content increases. The density of the foamy oil was a volume weighted average density of the oil and the gas components. The model simulates an important feature of foamy oil that is part of the evolved gas is entrained in the oil phase. This requires only modified relative permeability and fluid properties to be implemented into a conventional simulator. However, time dependent properties of foamy oil cannot be simulated.

2.4.5 Low Viscosity Model

Claridge and Prats (1995) proposed a foamy oil model based on the assumption that the asphaltenes present in the crude oil adhere to gas microbubbles. Coating of the microbubbles by asphaltenes, without a compositional change in liquid oil phase, stabilizes the microbubbles. The microbubbles continue to flow with the oil phase. The net effect of the coating of asphaltene onto the microbubbles is to reduce

Reproduced with permission of the copyright owner. Further reproduction prohibited without permission.

substantially the viscosity of foamy oil. There is no experimental evidence of the phenomena that asphaltenes adhere to gas microbubbles. The chemical structure of hydrocarbon gives a different picture. The structure of petroleum consists of asphaltene molecules in the center surrounded by resin. These resins are surrounded by saturates, gas (Hammami et al., 1998). Furthermore, there is no experimental or theoretical evidence to support a decrease in viscosity by asphaltene adhesion to surfaces of gas bubbles. But on the contrary, Bora (1998) stated, based on viscosity measurements on rotational viscometer, that the presence of asphaltene did not have any effect on foamy oil viscosity.

2.4.6 Gas Lubrication Model

Shen and Batycky (1996) suggested a foamy oil viscosity model to account for the effects of gas bubbles on oil recovery. They based their model on their re-interpretation of the experimental data on foamy oil published by Maini et al. (1993). They stated that the mobility of foamy oil was enhanced due to bubble nucleation, and the reduction in oil mobility due to entrapment of gas bubbles. Foamy oil mobility decreases with increasing gas fraction and increases with increasing nucleation rate. The authors attributed the enhancement of foamy oil mobility to the lubrication or, slippage effect. Lubrication effect was used in some experimental and theoretical works to explain the enhancement of non-wetting phase mobility in two-phase flow in capillary tubes (Yuster 1952; Odeh, 1962). The model was reviewed by Sheng (1997), where he stated that the model lacks enough evidence to support that the presence of nucleated gas bubbles enhanced mobility of heavy oils.

2.4.7 Dynamic Model

Sheng et al. (1996; Sheng 1997) proposed a dynamic model for simulating foamy oil solution gas drive experiments. The models attempted to include nucleation rate growth and coalescence of bubbles. They assumed four components present in foamy oil flow, namely: dead oil, dissolved gas, dispersed gas, and free gas. The dispersed gas was treated as a liquid component and assigned its own properties. The

Reproduced with permission of the copyright owner. Further reproduction prohibited without permission.

rate of nucleation was assumed to be an instantaneous nucleation, and assumed to be a function of supersaturation and time. The rate of coalescence was assumed proportional to the volume of fraction of dispersed gas in the oil. The model provided a good history match of the laboratory experiments. However, it uses adjustable parameters that cannot be independently determined.

2.5 Critical Gas Saturation

Critical gas saturation, S_{gc} is an important parameter in solution gas drive mechanism. The literature reported data on critical gas saturation differ widely. Based on various definitions and experimental techniques, critical gas saturation values of the range from 0.5% (Firoozabadi et al., 1992) to 40% (Maini et al., 1993) were reported. Among the definitions of the S_{gc} was given by Moulu and Longeron (1989) as the maximum gas saturation before any flow of gas may occur. They observed that the S_{gc} increased as the pressure decline rate increased. Kortekaas and van Poelgeest (1991) defined the S_{gc} as the gas saturation at which the gas channels have reached the top of the reservoir (for no-dispersion conditions) or interconnected gas channels have formed (for dispersion conditions) and gas can flow freely to the top of the reservoir. They reported S_{gc} values varying from 7% to 27%. Li and Yortsos (1991) defined the S_{gc} as the gas saturation at which gas phase first reached the production outlet. But, in a later paper, Li and Yortsos (1993) pointed out that a robust definition of S_{gc} should involve the formation of a sample-spanning cluster, which indicates a the appearance of a sample-conducting and free-flowing gas.

Critical gas saturation is usually determined by different methods: estimation from field production data or from laboratory measurements. Estimation of S_{gc} from field data requires that oil production data is available. A more common approach is to use core samples to measure the S_{gc}, which is termed external gas drive (gas displacing oil). Traditionally the S_{gc}, is determined by extrapolating an external gas drive derived relative permeability curve. This can lead to a considerable error due to the steepness of the gas-oil relative permeability ratio curve in the low gas saturation region (Kamath

Reproduced with permission of the copyright owner. Further reproduction prohibited without permission.

and Boyer, 1993). Another approach for estimating S_{gc} is the measurement of gas saturation at the point when gas saturation becomes mobile in an internal gas drive (depletion/solution gas drive). The internal and external gas drives are fundamentally different and the two methods will produce different values for S_{gc}.

2.6 Solubility of Gases in Liquids

Solubility of natural gas in crude oil is controlled by the pressure, temperature, and the composition of the gas and the crude oil. Gas is infinitely soluble in crude oil; the quantity is limited only by the pressure or by the amount of gas available (Craft and Hawkins, 1991). A crude oil is said to be under-saturated if it exists as a single phase at its initial conditions of pressure and temperature; furthermore, a slight reduction in pressure will not cause any release of gas from solution. On the other hand, if oil is in contact with free gas at its initial conditions, the oil is said to be saturated; and a slight reduction in pressure will cause gas to come out of solution. Solubility is the amount of gas that evolves from the liquid as the liquid is transported to surface conditions from the reservoir pressures (McCain, 1973). McCain (1973) writes that if the gas solubility is simply a matter of separating gas from liquid as a result of flash or differential vaporization, it would be easily determined. Unfortunately, the process in the reservoir is neither flash nor differential but some process in between. Commonly, flash and/or differential liberation data, and correlations are used to determine gas solubility in crude oil.

Solubility of gases in liquids is determined by the equations of phase equilibrium; the fugacities of each component, i, in each phase must be equal. The solubility can be described by Raoult's Law:

$$p_i = x_i\, p_i^s \qquad (16)$$

Where P_i is the partial pressure of component i, x_i is its liquid phase mole fraction and p_i^s is the saturation pressure of the pure gas component.

The general form of Raoult's law is given by Henry's Law:

Reproduced with permission of the copyright owner. Further reproduction prohibited without permission.

$$p_i = (1/H)x_i \quad \text{.....(17)}$$

The Henry's Law constant (1/H) is empirical and accounts for the liquid phase nonidealities. The gas is assumed to be ideal. Several methods are used to measure the solubility of gases in liquids. Among these are: gas-bubbler, volumetric, thin film, chromatographic, and vapor pressure methods. Details of these methods are given by Fogg and Gerrard (1991).

2.7 Brief Review of Defoamers

The phenomena of foaming and antifoaming can be traced to the Marangoni effects that are the presence of surface-tension gradients and the movement of liquid surface from regions of lower to regions of higher surface tension. These effects maybe produced by temperature or by surface activity (Ross, 1996). Antifoams prevent formation of foams. Defoamers are agents that inhibit the build up of foam, or which reduce foam by causing the bubbles to burst, thus releasing the gas inside it. Most commercial defoamers are mixtures of surface-active agents, hydrocarbons, alcohols, polymers, etc., to increase their effectiveness in multiple applications. Most commercial products perform both functions to a greater or lesser extent (McGee, 1989). There are generally two categories of defoamers and anti-foams, each having two sub-groups. The first type of defoamer is a silicone emulsion, which can be either water-based or oil-based. The oil component is either mineral oil or vegetable oil. The second type is a non-silicone defoamer, which can also be either water-based or oil-based. It is formulated to perform like a silicone-based defoamer, but does not contain the silicone fluid. Therefore, The prime action of a defoamer is its ability to reduce surface elasticity (Source: Handling of Antifoam Oils for Fermentations, H. R. Bungay, C.F. Simons and P. Hosler). According to the references (Heilen et. al., 1994; Berger and Gast, 1976; and Aubert et al., 1986) defoaming substances must be dispersed into fine droplets and the active matter has to get into the foam lamella and has to penetrate the surfactant film. The particle must enter both gas and liquid interfaces that make up the foam film. Adding a defoamer will lower the surface tension. After applying the

Reproduced with permission of the copyright owner. Further reproduction prohibited without permission.

defoamer, the bubbles tend to expand and grow larger. Thus, the defoamer has thinned the wall structure of the bubble, which first enlarges before it breaks. Consequently, the resulting lamella shows a drastic reduction in its wall elasticity, which causes the lamella to burst (Wallhorn et al., 1997).

Reproduced with permission of the copyright owner. Further reproduction prohibited without permission.

Chapter III

3. Objectives

Since the first publication on cold heavy oil production in 1988, there were numerous attempts to model foamy oil phenomena. Most of these attempts are largely based on empirical models. A comprehensive research was undertaken to provide answers and clarify some of the foamy oil hypothesises/ models experimentally. The general aim of this research was to improve the understanding of the foamy oil process in heavy oil reservoirs and to investigate the causes of the anomalous production behaviour. The specific objectives of this research were as follows:To design an experimental procedure and setup to investigate the time dependent properties of foamy oil.

2. To investigate the effect of the dispersed gas phase on the production of foamy oil (at same pressure depletion rate) by addition of defoamer.
3. To conduct study of foamy oil using a visual PVT cell at different pressure depletion rates and under different conditions of mixing/quiescent, and with/without the addition of a defoamer.
4. To measure viscosity of foamy oil at different pressure depletion rates as a function of time.
5. To investigate visually the pore level processes by conducting pressure depletion experiments in high-pressure porous media packed-micromodels.
6. To run experiments at or close to actual field pressure depletion rates in sand packs.

Reproduced with permission of the copyright owner. Further reproduction prohibited without permission.

Chapter IV

4. Experimental Set-up and Procedure

This chapter covers the description of the apparatus, materials, and procedures used in this study. The experimental research can be divided into four categories: partial PVT experiments (constant composition expansion, CCE), rheological measurements of foamy oil, micromodel experiments, and sand pack core depletion experiments. The following sections present description of the four experimental set-ups and procedures.

4.1 Materials

The oil used in all the experiments was from the Lloydminster area, Alberta. Table 4.1 shows the composition of the original oil. The oil was combined with 14% (by volume) CO_2 at a pressure of 6900 kPa (1000 psi) and room temperature. The combined live oil was then used in all runs. The analysis of the oil is shown in Table 4.2.

Ottawa Silica Sand (70-140 mesh size) was used in the sand packs and micromodel experiments. In addition, Cryolite (Na_3AlF_6), a colorless to snow-white transparent to translucent rock obtained from Ward's Natural Science Establishment, Inc., Rochester, New York, was used in most of the micromodel experiments.

4.1.1 Live Oil Sample Preparation

Live oil was prepared by recombining the crude oil with 14% (by volume) CO_2. Then the sample was mixed and rocked for two weeks at a pressure of 10350 kPa (1500 psi). The pressure of the mixing cylinder was monitored. As CO_2 dissolved into crude oil, pressure was routinely adjusted by bring it up to the initial pressure of 8300 kPa. Before using the live oil, sample pressure was brought down to 6900 kPa (1200 psi) and left for one week to stabilize. At this stage, live oil sample was ready for use in an experiment.

Reproduced with permission of the copyright owner. Further reproduction prohibited without permission.

COMPONENT	MW	LIQUID WT %	MOLE %	GROUP MOLE %
CO2	44.01	0.00	0.00	0.00
H2S	34.08	0.00	0.00	0.00
N2	28.01	0.00	0.00	0.00
C1	16.04	0.00	0.00	0.00
C2	30.07	0.00	0.00	0.00
C3	44.10	0.00	0.00	0.00
I-C4	58.12	0.00	0.02	0.02
N-C4	58.12	0.01	0.04	0.04
I-C5	72.15	0.00	0.02	0.02
N-C5	72.15	0.00	0.02	0.02
C6	86.20	0.06	0.28	
MCYC-C5	84.16	0.07	0.30	
BENZENE	78.11	0.01	0.03	
CYCL-C6	82.15	0.03	0.14	0.75
C7	100.20	0.20	0.77	
MCYCL-C6	98.19	0.00	0.00	
TOLUENE	92.14	0.00	0.00	
C8	114.23	0.23	0.77	
C2-BENZEN	106.17	0.01	0.03	
M&P-XYLEN	106.17	0.00	0.00	
O-XYLENE	106.17	0.02	0.08	
C9	128.30	0.30	0.90	2.54
C10	134.00	0.70	1.99	
C11	147.00	0.97	2.52	
C12	161.00	1.42	3.35	
C13	175.00	1.98	4.30	
C14	190.00	2.14	4.28	16.45
C15	206.00	2.54	4.69	
C16	222.00	2.47	4.25	
C17	237.00	1.94	3.12	
C18	251.00	2.19	3.33	
C19	263.00	1.82	2.63	18.02
C20	275.00	2.21	3.06	
C21	291.00	1.78	2.33	
C22	305.00	1.92	2.40	
C23	318.00	2.15	2.57	
C24	331.00	1.51	1.73	
C25	345.00	2.17	2.39	
C26	359.00	1.24	1.32	
C27	374.00	1.41	1.44	
C28	388.00	1.47	1.44	
C29	402.00	2.63	2.49	21.18
C30+	580.00	62.40	40.97	40.97
			100.00	100.00

Table 4.1 - Composition of the original Lloydminster oil.

Reproduced with permission of the copyright owner. Further reproduction prohibited without permission.

COMPONENT	MW	GAS MOLE %	LIQUID WT %	OVERALL WT %	OVERALL MOLE %	GROUP MOLE %
CO2	44.01	99.48	0.00	12.79	55.78	55.78
H2S	34.08	0.00	0.00	0.00	0.00	0.00
N2	28.01	0.00	0.00	0.00	0.00	0.00
C1	16.04	0.15	0.00	0.01	0.09	0.09
C2	30.07	0.02	0.00	0.00	0.01	0.01
C3	44.10	0.02	0.00	0.00	0.01	0.01
I-C4	58.12	0.02	0.00	0.01	0.02	0.02
N-C4	58.12	0.03	0.01	0.01	0.03	0.03
I-C5	72.15	0.02	0.00	0.01	0.02	0.02
N-C5	72.15	0.03	0.00	0.01	0.02	0.02
C6	86.20	0.05	0.06	0.07	0.15	
MCYC-C5	84.16	0.01	0.07	0.06	0.14	
BENZENE	78.11	0.00	0.01	0.01	0.01	
CYCL-C6	82.15	0.01	0.03	0.03	0.06	0.37
C7	100.20	0.04	0.00	0.01	0.02	
MCYCL-C6	98.19	0.02	0.20	0.18	0.35	
TOLUENE	92.14	0.00	0.00	0.00	0.00	
C8	114.23	0.03	0.23	0.21	0.36	
C2-BENZEN	106.17	0.00	0.01	0.01	0.02	
M&P-XYLEN	106.17	0.00	0.00	0.00	0.00	
O-XYLENE	106.17	0.00	0.02	0.02	0.04	
C9	128.30	0.04	0.30	0.28	0.42	1.20
C10	134.00	0.02	0.70	0.62	0.89	
C11	147.00	0.00	0.97	0.85	1.11	
C12	161.00	0.00	1.42	1.23	1.47	
C13	175.00	0.00	1.98	1.72	1.89	
C14	190.00	0.00	2.14	1.86	1.88	7.24
C15	206.00	0.00	2.54	2.21	2.06	
C16	222.00	0.00	2.47	2.16	1.87	
C17	237.00	0.00	1.94	1.69	1.37	
C18	251.00	0.00	2.19	1.91	1.46	
C19	263.00	0.00	1.82	1.58	1.15	7.91
C20	275.00	0.00	2.21	1.93	1.34	
C21	291.00	0.00	1.78	1.55	1.02	
C22	305.00	0.00	1.92	1.67	1.05	
C23	318.00	0.00	2.15	1.87	1.13	
C24	331.00	0.00	1.51	1.31	0.76	
C25	345.00	0.00	2.17	1.89	1.05	
C26	359.00	0.00	1.24	1.08	0.58	
C27	374.00	0.00	1.41	1.23	0.63	
C28	388.00	0.00	1.47	1.28	0.63	
C29	402.00	0.00	2.63	2.29	1.09	9.30
C30+	580.00	0.00	62.40	54.36	18.00	18.00
		100.00	100.00	100.00	100.00	
MW		44.13	380.79		192.02	

Table 4.2 - Composition of Lloydminster recombined oil.

Reproduced with permission of the copyright owner. Further reproduction prohibited without permission.

CO_2 gas was used because it is more soluble in heavy oil than any other gas. It is known that CO_2 flocculates asphaltenes; but filtration showed that there is no evidence of asphaltene deposition in the mixture (oil + CO_2) at maximum CO_2 concentration. This is also validated through the composition of the oil before and after the addition of CO_2, as shown in Tables 4.1 and 4.2.

4.2 PVT Cell Apparatus

A fully visual JEFRI PVT cell was used for the CCE runs. The PVT cell contained water as the pressure maintenance fluid. A floating piston separated the live oil sample side and the waterside in the visual cell. The PVT cell was connected to a displacement pump. The pressure was reduced continuously by setting the pump at the required pressure depletion rate. The PVT cell was also used in the pressure depletion runs prior to viscosity measurements.

4.3 PVT Measurements

Pressure-Volume-Temperature (PVT) experiments consisted of Constant Composition Expansion (CCE) runs. A fully visual JEFRI PVT cell was used to carryout the CCE runs. The PVT cell was connected to the live oil sample. The system of the PVT cell and the lines connecting it to the live oil cylinder were evacuated. Then a live oil sample was transferred under constant pressure to the PVT cell using a displacement pump. A computer controlled pump was then connected to the top of the PVT cell. The pump was then set at the desired pressure depletion rate and switched on. The volume injected into the PVT cell was measured by the injection pump and by a calibrated cathetometer. After commencement of the experiment, the cathetometer was used to measure the fluid levels, the gas height, and the gas-oil interface.

4.4 Foamy Oil Rheology Measurements

For the purpose of comparison, viscosity was measured using three different viscometers. Cambridge Electromagnetic Viscometer (CEV), a JEFRI capillary viscome-

Reproduced with permission of the copyright owner. Further reproduction prohibited without permission.

ter, and a Haake Rotovisco RV2 viscometer were used in this study. The viscosity was measured at two different pressure depletion rates of 800 kPa/hr (116 psi/hr) and 41 kPa/hr (6 psi/hr).

4.4.1 Cambridge Electromagnetic Viscometer

The CEV Model SPL440 is rated to 69 MPa (10,000 psi). The SPL440 comes with a microprocessor-based electronics Model ViscoPro2000 that is menu driven. The operation of the sensor is based on a proprietary patented technique*. The viscometer consists of a cylindrical steel vessel with a magnetic stainless steel piston immersed in the vessel cavity. Two pistons were used in the present study, 2000-cp and 10000-cp. When the test oil is charged into the vessel, it surrounds the piston completely. The piston is moved inside the vessel by applying a force on the piston using two electromagnetic coils inside the sensor body. After the piston travels the length of the test vessel, the magnetic field of the electromagnet is reversed as to allow the piston to return to its starting position. The motion of the piston surrounded by the test fluid inside the vessel is impeded by the viscous flow in the annulus between the piston and the chamber wall. Viscosity is determined by measuring piston transit time for a complete cycle of piston movement and comparing it to times of a known-viscosity calibration fluid. The viscometer comes with an electronic readout box where the viscosity and temperature are displayed. Figure 4.1 shows the CEV viscometer. The CEV viscometer is mounted at a 45° orientation from vertical. The measurement chamber is connected from both top and bottom to JEFRI PVT cell lines to allow the test sample to be charged under pressure and to facilitate chamber cleaning.

4.4.1.1 Calibration of CEV

CEV viscometer is like any other viscometer requires calibration. The CEV was calibrated for low and high-end viscosity ranges and for temperature range using two standard calibration fluids of known viscosity, 2000 and 10000 cp. The calibration

* Cambridge Applied Systems Incorporated, 196 Boston Ave, Medford, MA

Reproduced with permission of the copyright owner. Further reproduction prohibited without permission.

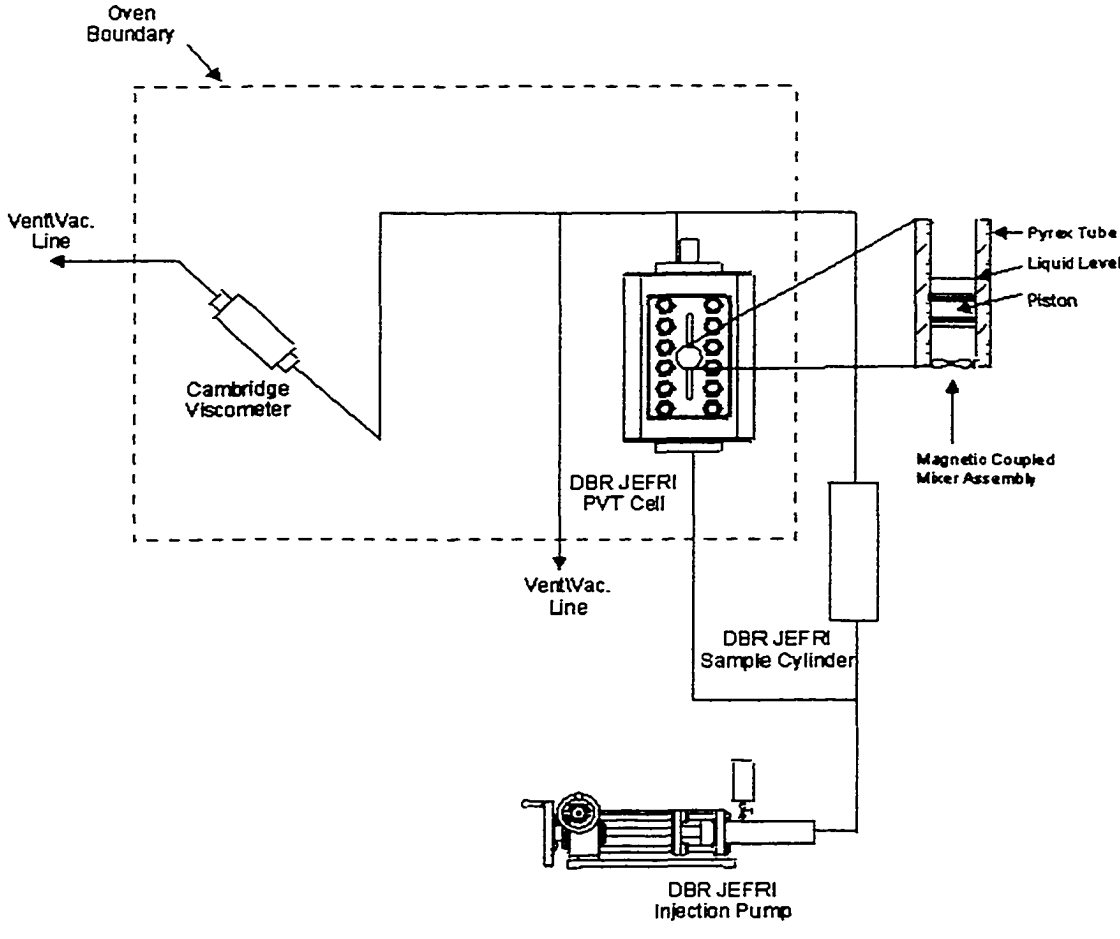

Figure 4.1- Schematic of the Cambridge Viscometer and PVT cell set-up.

Reproduced with permission of the copyright owner. Further reproduction prohibited without permission.

data is shown in Figures 4.2 and 4.3. The viscometer is less sensitive to low and moderately high pressures; therefore, pressure calibration was not needed. Despite being less sensitive to pressure, the viscometer was checked against pressure using the correction factor provided by the manufacturer and was found that the correction factor was very small. The following relation gives the correction viscosity, μ_c:

$$\mu_c = \mu\ (y+4.61E\text{-}5*p)/y)^{2.875}, \quad (20)$$

Where μ and μ_c (mPa.s) are the measured and corrected viscosity at test temperature and pressure, p (psi), respectively; and y is the annulus between the piston and the wall.

4.4.1.2 Viscosity Measurement with CEV

After The CEV viscometer was calibrated, the test chamber and the lines connecting the viscometer to the PVT cell were evacuated with a vacuum pump. Prior to foamy oil viscosity measurement, the pressure depletion rate was set in the PVT cell until the desired pressure was reached. Then a sample of the foamy oil was isobarically charged from the bottom of the PVT cell to the CEV viscometer. When the viscometer chamber was flooded with test sample, a small amount was purged to ensure a uniform sample. Then the inlet and outlet valves were closed and the viscometer was isolated from the PVT cell. At this time, the viscosity measurement was started. The measured viscosity as a function of time and temperature was sent to a computer for storage and easy retrieval. Before the next pressure was reached during the pressure depletion in the PVT cell at which a viscosity measurement was desired, the viscometer had to be cleaned and evacuated. Thus timing was crucial to insure uninterrupted pressure depletion process.

4.4.2 Capillary Viscometer

A schematic of the capillary viscometer set-up is shown in Figure 4.4. The capillary viscometer set-up consisted of high-pressure capillary tube having 1.83 m (6 ft) in length and 0.076 cm (0.03 inches) in diameter, two-32 cc cylinders, a positive displacement pump, and PVT cell. Pressure drop along the capillary tube was measured

Reproduced with permission of the copyright owner. Further reproduction prohibited without permission.

Reproduced with permission of the copyright owner. Further reproduction prohibited without permission.

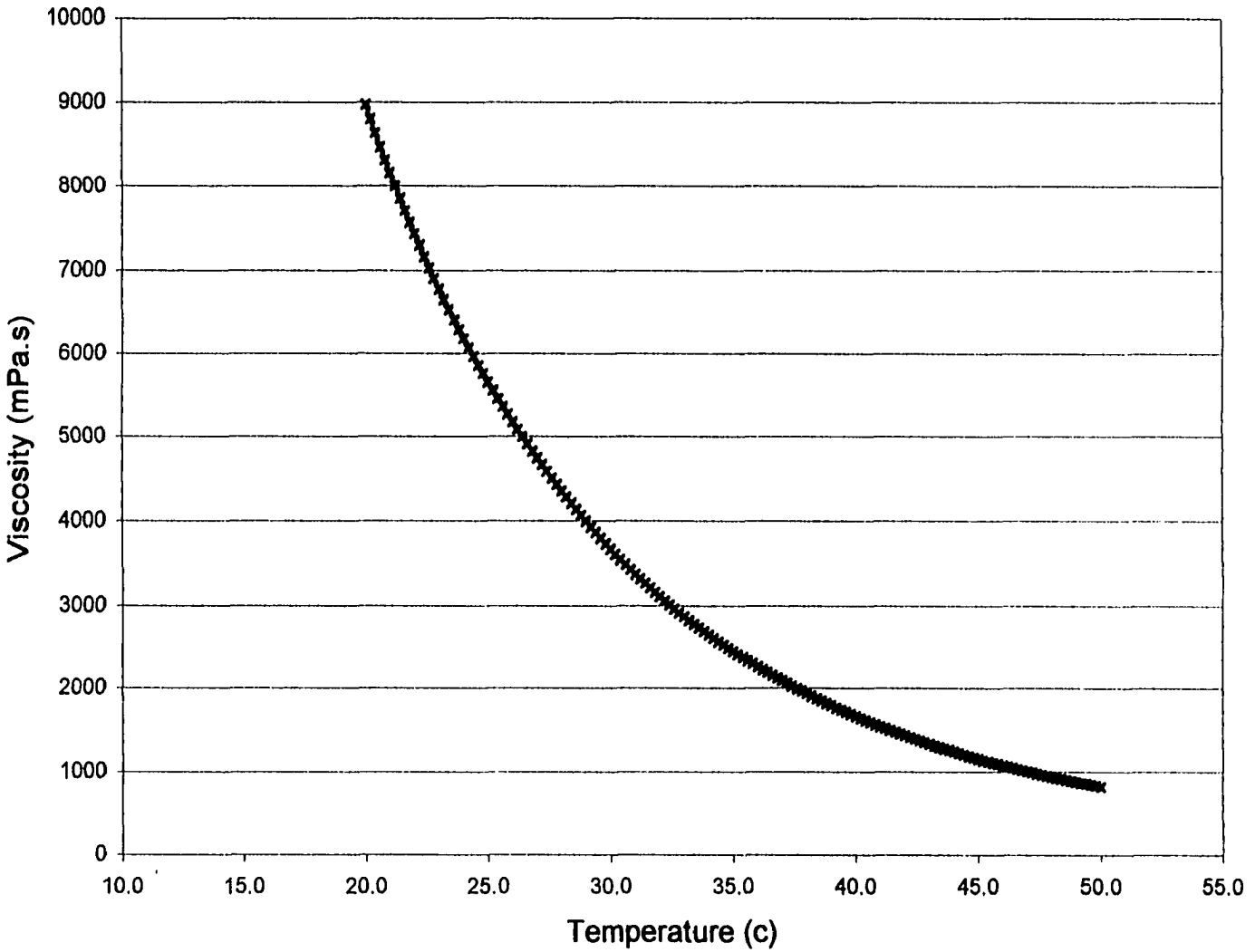

Figure 4.2 - Calibration of viscosity vs temperature for Cambridge Viscometer using S2000 viscosity standard Lot# 96202 fluid.

Reproduced with permission of the copyright owner. Further reproduction prohibited without permission.

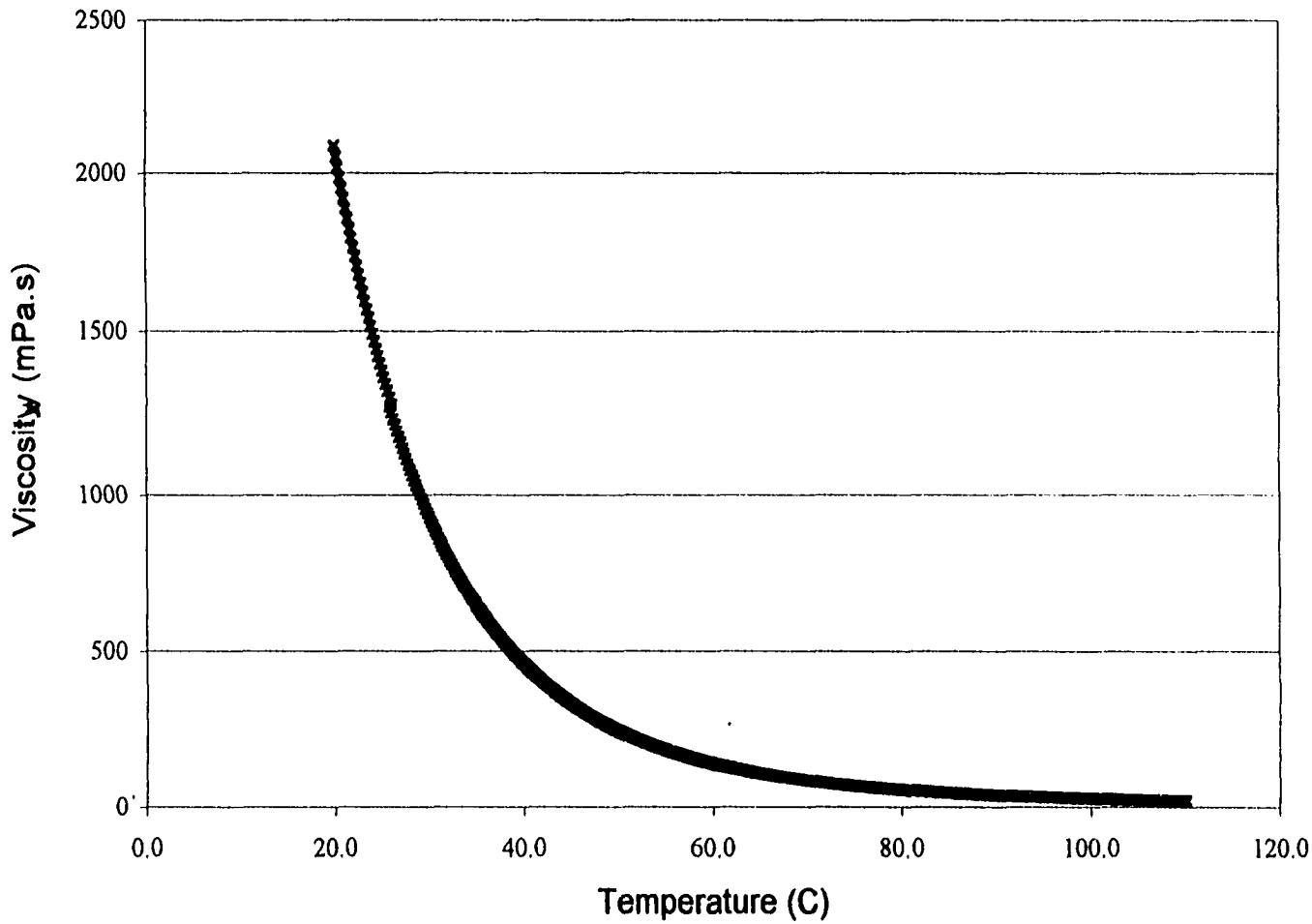

Figure 4.3 - Calibration of viscosity vs temperature data for Cambridge Viscometer using S600 viscosity standard Lot# 99301 fluid.

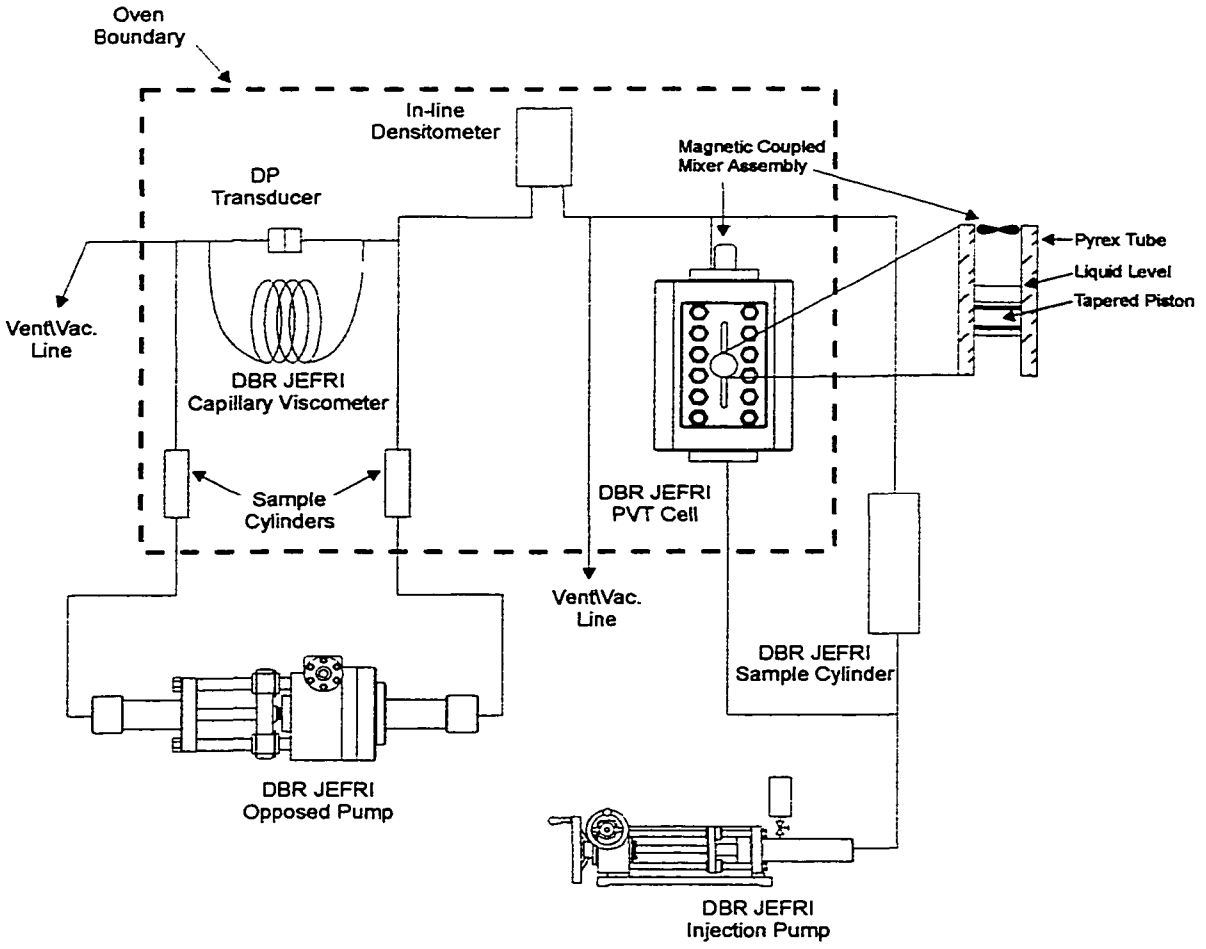

Figure 4.4- Schematic of the capillary viscometer and PVT cell se-up.

Reproduced with permission of the copyright owner. Further reproduction prohibited without permission.

using Validyne pressure transducer. Pressure was depleted at a specified rare in the PVT cell. Then a sample was transferred isobarically, to the capillary tube and the 32-cc cylinders.

4.4.2.1 Calibration

The capillary viscometer constant was determined using a standard calibration fluid of known viscosity. The tube constant, k, is derived from Poiseuille's equation describing laminar flow in tubes which is given by:

$$\mu = \frac{\Delta p}{Q}\left(\frac{\pi r^4}{8L}\right) = \frac{\Delta p}{Q}k, \quad \text{.....21}$$

Where the m is the fluid viscosity, Δp is the pressure drop across the capillary tube of length, L, and a radius r, and Q is the volumetric flow rate.

Having determined the instrument constant, k, the viscometer was ready for foamy oil viscosity measurements.

4.4.2.2 Viscosity Measurement with Capillary Viscometer

Before a viscosity measurement was taken, pressure depletion at a set rate was initiated in the PVT cell. In addition, the capillary tube and the lines connecting it to the PVT cell were vacuumed. When the pressure was reached, at which viscosity measurement was sought, a sample was charged at isobaric pressure from the bottom of the PVT cell into the capillary tube; and additional 8 cc was charged into the two-32 cc cylinders. The oil sample was charged using two opposing pumps, one withdrawing mercury from the two-32 cc cylinders (one at a time) while the other charging oil into the capillary tube and the two cylinders. Once the capillary viscometer was charged with oil sample, an opposed pump set at a certain flow rate was used to push the sample from one cylinder to the other through the capillary tube. Knowing the pressure drop as measured by the Validyne transducer at the set flow rate, viscosity was determined using the above Poiseuille's equation and the calibration constant. The viscosity

Reproduced with permission of the copyright owner. Further reproduction prohibited without permission.

was measured at different flow rates. After the viscosity was measured, the viscometer and the lines connecting it to the PVT cell were thoroughly cleaned using solvents and dried using CO_2. At this time, the viscometer was evacuated using a vacuum pump and made ready for the next viscosity measurement at a different pressure point.

4.4.3 Haake Rotovisco RV-2 Viscometer

The Haake** Rotovisco RV-2 is a direct drive, concentric cylinder, controlled strain viscometer. It consists of an interchangeable measuring head unit, viscosity sensor system, and a control panel unit. The types of interchangeable measuring heads used were DMK 50 and DMK 500. The control panel houses the electric components and a driving motor. The power is transmitted to the measuring head through a system of gears. Shear stress is measured by a high precision torsion spring. The torsion spring deflection due to viscous drag is measured by a potentiometer and the signal is shown on a dial on the control panel. The dimensions of sensor system were cup radius of 5.1 cm, and the rotor radius 4.5 cm, and their length was 7 cm.

A pressure chamber was designed and incorporated into the viscometer to allow measurements of viscosity at high pressures. The chamber volume was about 950 cc. The large volume of live oil sample required for one viscosity measurement caused operational difficulty. For this reason, the pressure depletion of the foamy oil sample was done inside the viscometer chamber. As a result, a free gas phase was present during the viscosity measurement.

4.4.3.1 Viscosity Measurement with RV-2 Viscometer

Due to the large volume of sample needed to fill the RV-2 viscometer chamber, the pressure was depleted inside the viscometer. To insure that the live oil sample did not flash out during the transfer, the chamber was filled with CO_2 and pressurized to 7600 kPa (1200 psi). Then the CO_2 was displaced by the live oil sample at constant pressure from the bottom of the viscometer chamber. After the viscometer chamber

** Made By Gebruder- Haake, Berlin, Germany

Reproduced with permission of the copyright owner. Further reproduction prohibited without permission.

was full with live oil sample, live oil was flushed out through the outlet at the top of the chamber to insure that all CO_2 was displaced. The viscometer was connected to another cylinder where water was withdrawn at a specified pressure depletion rate. Water was withdrawn by backing up the pump at the specified drawdown rate. Figure 4.5 shows the schematic of the RV-2 viscometer set-up. As a result, the fluid in the viscometer chamber was flashed out. Viscosity was measured at the desired pressure at different speeds of rotation and the dial reading was recorded. The viscosity was calculated from the dial/scale reading, gear position number recorded on top of the control unit, and instrument constant, G. The instrument constant, G, was obtained from the geometry of the rotor and the cup and the spring constant for the measuring head.

4.5 Micromodel Design and Set-up

A special micromodel was designed to visualize the pressure depletion process. The micromodel could be run with or without porous medium. It consisted of two transparent high-pressure polycarbonate plastic windows held together by steel plates. It was 13.81 cm in length and 1.27 cm wide. The transparent windows were made of polycarbonate and have the commercial name of HYZOD GP*. The transparent windows were separated by a special graphoil gasket that acted as a spacer and a pressure sealant when the two steel plates were tightened-up. The micromodel thickness could be changed by changing the thickness of the spacer/gasket. Figure 4.6 shows the top and cross-sectional views of the micromodel.

* Manufactured by DSM Sheffield, 119 Salisbury Road, sheffield, MA

Reproduced with permission of the copyright owner. Further reproduction prohibited without permission.

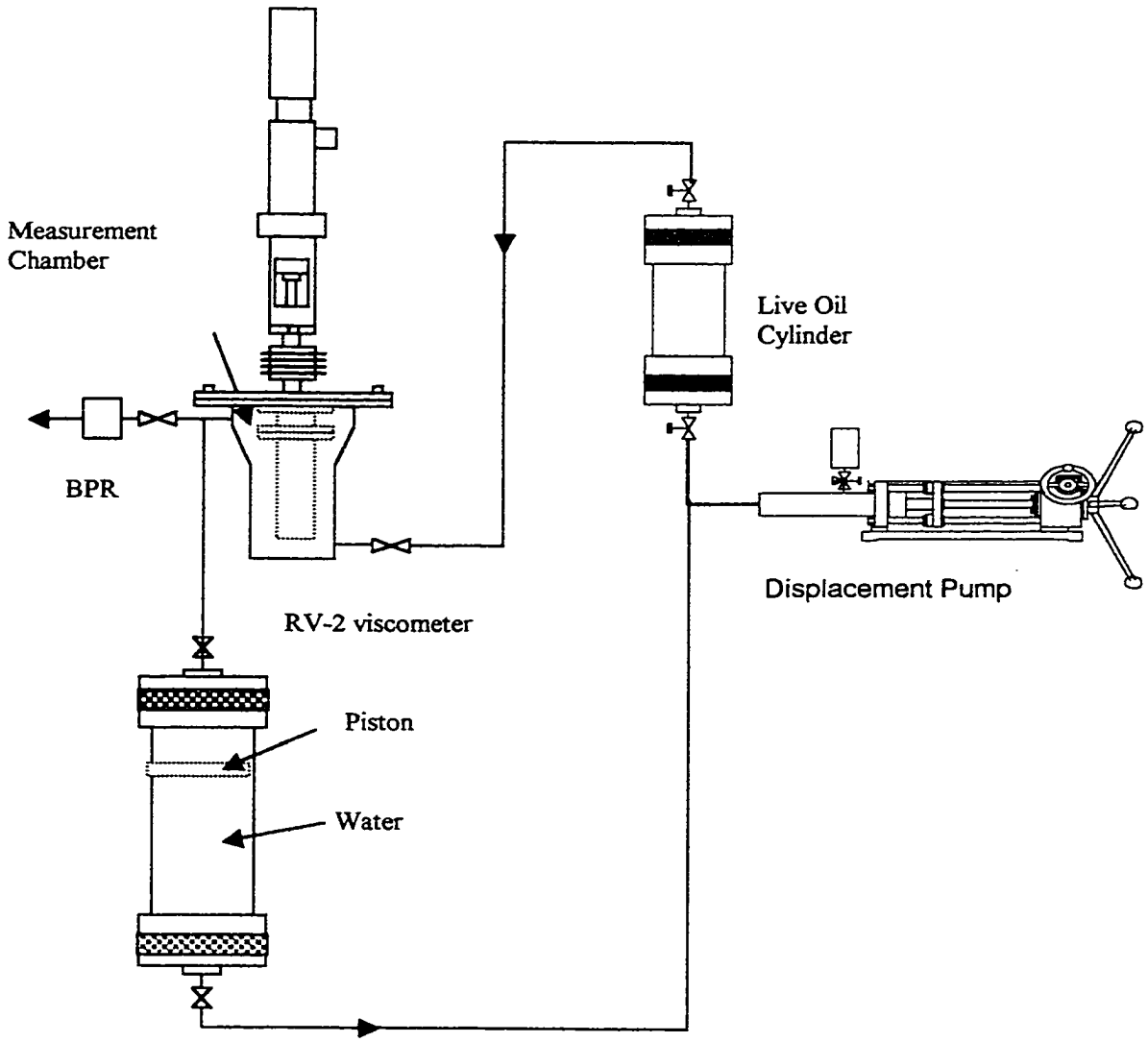

Figure 4.5 – Schematic of the RV-2 Viscometer set-up.

Reproduced with permission of the copyright owner. Further reproduction prohibited without permission.

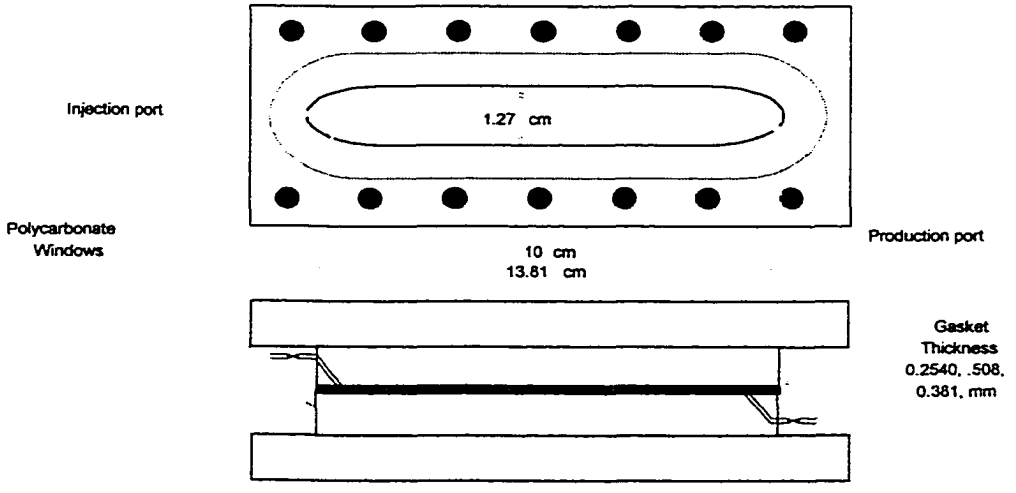

Figure 4.6 - Top and side view of the micromodel

The micromodel was connected to a 10 cc sapphire cell. The recombined oil from the micromodel was depleted in the sapphire cell and the volumes of the oil and CO_2 gas were measured in the sapphire cell using a digital cathetometer. The sapphire cell was equipped with a piston to separate the pump fluid from the production fluid out of the micromodel. The pressure depletion rate was controlled by a pump that was connected to the sapphire cell. The micromodel could withstand pressure up to 8300 kPa (1200 psi) at room temperature. Two cameras were used to film the depletion process. A regular video camera was utilized for taking wide view images of the depletion process, overall view. In addition, a CCD camera* was used to capture continuous images of the pressure depletion process. In order to increase the magnification of the images, several optical attachments were added to the CCD camera. The optical attachments were two teleconverter lenses, several extension tubes, two filter lenses, and a variable focus lens. The CCD camera was connected to a video cassette player to record the experiment. Figure 4.7 shows the schematic of micromodel experimental set-up.

* Manufactured by COHU Inc, San Diego, CA

Reproduced with permission of the copyright owner. Further reproduction prohibited without permission.

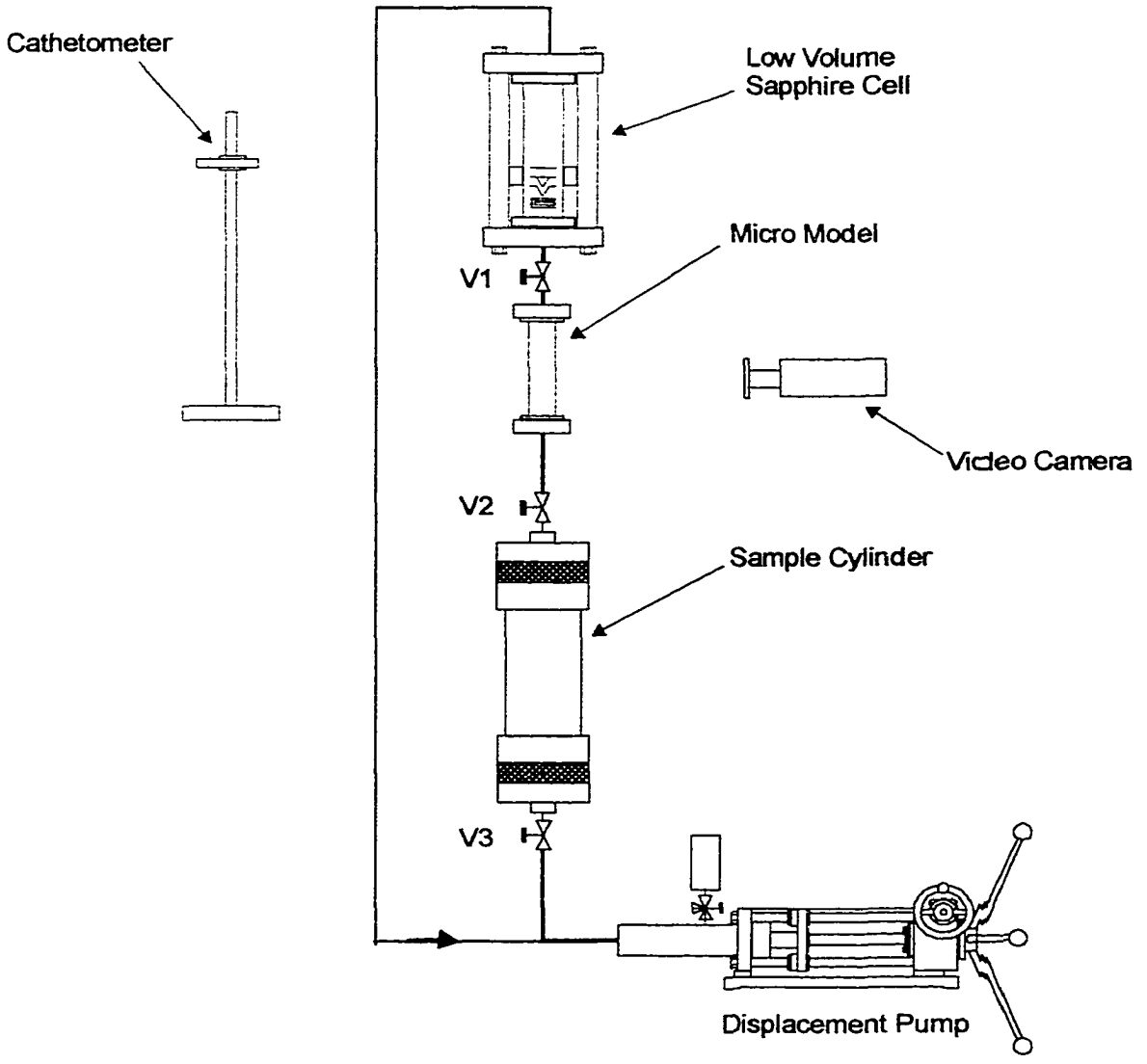

Figure 4.7 - Schematic of the micromodel experimental set-up.

Reproduced with permission of the copyright owner. Further reproduction prohibited without permission.

4.5.1 Micromodel Preparation and Packing

The first step in preparing the micromodel was to assemble the micromodel and clamp it together to a specified torque. Then, it was pressure tested for any leak using CO_2 gas to a pressure up to 8300 kPa (1200 psi). To determine the bulk volume, the micromodel was connected to a 10 cc pump and vacuumed. Then, decane was pumped from the 10cc pump into the micromodel. The bulk volume of the micromodel equals the amount of decane pumped. Having determined the bulk volume, the micromodel was dried-up by air injection. In experiments that involved a porous medium, the micromodel was packed with either Cryolite or Ottawa sand. The micromodel was placed vertically and an air vibrator was strapped onto the side of it. Next, the porous medium was poured slowly into the model while it was being vibrated. The packing procedure took about two hours. Again, the model was connected to a 10 cc pump and a vacuum was drawn to evacuate the air inside the model. Pore volume was determined in the same way as the bulk volume of the micromodel using decane.

Next, the micromodel was mounted vertically and connected to the sapphire cell and the rest of the experimental set-up as shown in Figure 4.7.

4.5.1.1 Micromodel Experimental Procedure

A pressure vessel containing live oil was connected to the bottom end of the micromodel. The vessel was equipped with a pressure tight piston to separate the live oil from the pump driving fluid that maintained constant pressure in the vessel. Live oil was pumped at constant pressure into the micromodel and decane was displaced. Produced fluid was collected into the sapphire cell, which was kept at a constant pressure by another pump. When the sapphire cell was full, it was isolated from the micromodel and the contents were expelled. After thirty pore volumes of live oil was injected into the micromodel, the live oil vessel was disconnected. At this point, the micromodel was ready for a depletion run. The pump, which was connected to the sapphire cell, was set in motion at the desired pressure depletion rate. At the same time,

Reproduced with permission of the copyright owner. Further reproduction prohibited without permission.

the CCD camera was turned on to monitor the progress of the depletion run. The height of the piston and the oil-gas interface in the sapphire cell were measured by the digital cathetometer.

4.6 Sand Pack Core Experiments

The experimental set-up is shown schematically in Figure 4.8. Two sand packs were used. The first was a 125 cm long and 4.75 cm in diameter and the second was 60 cm long and 7.6 cm in diameter. Pressure tabs where drilled at equal distance across the length of the steel core holders. In the longer core holder, twelve transducers were installed at an interval of 10 cm apart. The shorter core holder had six transducers located 10 cm along its length. Back pressure regulator was attached to the outlet end of the core holder.

4.6.1 Packing Sand Core Holders

Dry packing was used in both core holders. The packing process started by placing the core holder in a vertical position. An air vibrator was strapped on the side of the core holder. Ottawa sand was slowly poured into the core holder while it was being vibrated. After the core holder was full with sand, vibration continued for 8 hours. Next, the top end cap was mounted and a vacuum was drawn from the top end to evacuate air from the sand pack core. Following the air evacuation, pore volume was determined by first imbibing distilled water from a graduated cylinder through the bottom end of the sand pack core holder. In order to get a more accurate pore volume determination, additional distilled water was pumped through the sand pack, and an accurate mass balance was performed to obtain the pore volume of the sand pack. Following this, absolute permeability was determined using distilled water. From a known volume of produced water that was collected at a given time and pressure differential, absolute permeability was determined using Darcy's equation for linear flow.

To establish irreducible water saturation, an oil (dead oil) flood was carried out. Then the dead oil was displaced by live oil at a backpressure higher than the saturation

Reproduced with permission of the copyright owner. Further reproduction prohibited without permission.

Reproduced with permission of the copyright owner. Further reproduction prohibited without permission.

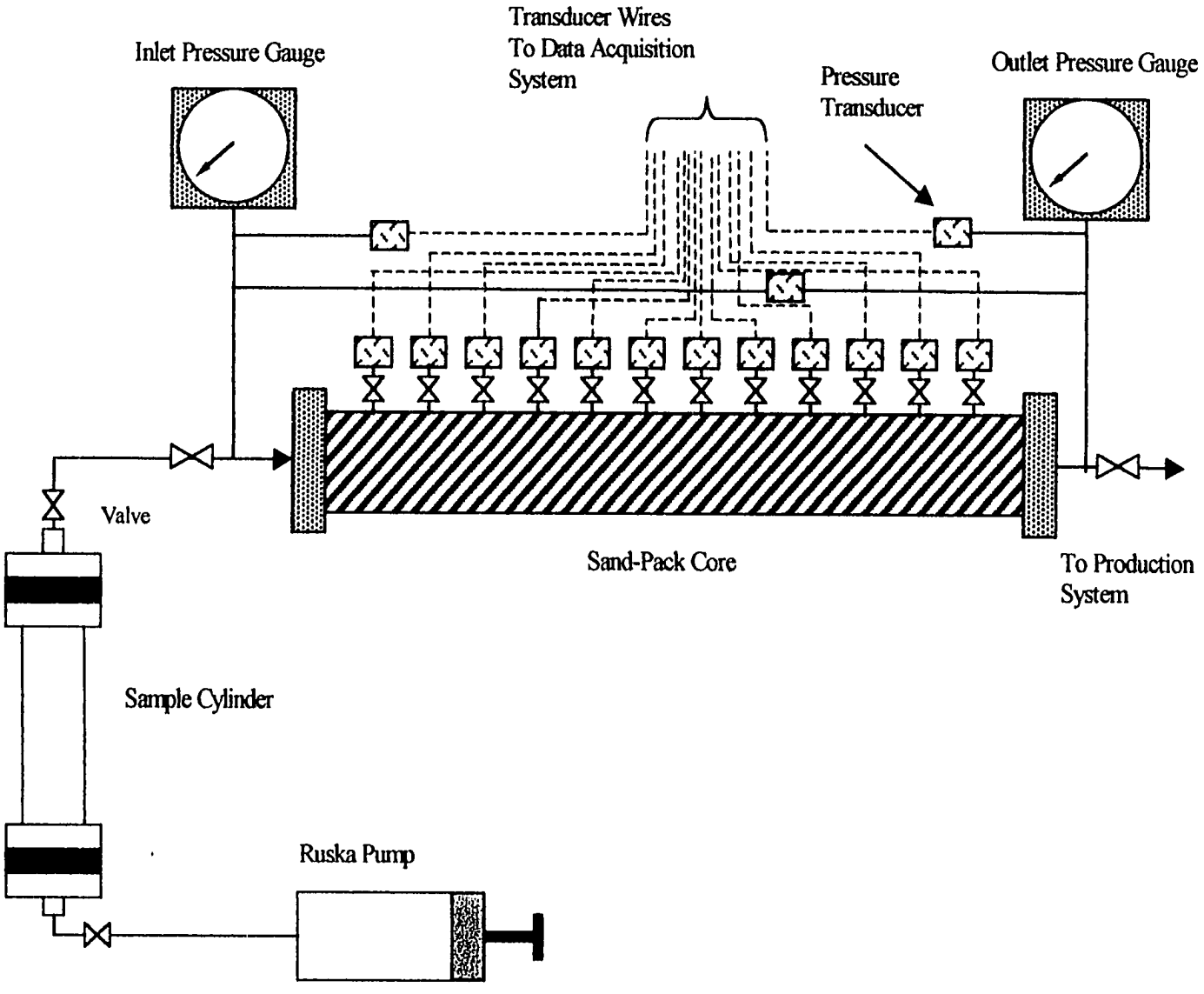

Figure 4.8 - Schematic of the sand-pack Experimental Set-up.

pressure of the live oil. After injecting one and a half pore volumes of the live oil at a very slow rate, 20 cc/hr, the oil flood was stopped. The initial oil saturation was determined from mass balance of the injected and produced liquids. At this point, the model was saturated with recombined oil. At this time, the sand pack was ready for a depletion run.

Reproduced with permission of the copyright owner. Further reproduction prohibited without permission.

Chapter V

5. Discussion of Experimental Results

This chapter consists of four parts. The first part presents the results of PVT measurements. The second gives the results of foamy oil viscosity measurements. The third part discusses the micromodel runs performed to investigate the pore-level process of foamy oil, in particular bubble nucleation process. The last part deals with the sand pack experiments.

5.1 Discussion of PVT Measurements

This set of experiments was performed to investigate the effect of pressure depletion rate on the foamy oil process. Investigating foamy oil process in heavy oil was a challenging problem due in part to the high oil viscosity, and the dark color of the oil made it even harder to visualize what was happening during the, constant composition expansion (CCE) runs. So, the process of foamy oil was investigated by comparing the unaltered process, where the gas, CO_2, was allowed to come out of solution as closely as possible resembling the process in the reservoir, and by introducing external variables. Runs were performed with and without mixing/agitation, addition of defoamer, and in the presence of glass beads. During the depletion process, a magnetic mixer was used to mix the oil sample. A 0.5% (by volume) of a commercial defoamer was added to several runs to alter the foamy oil process by speeding up the disengagement of the dispersed gas phase to free gas phase. To increase the surface area available for nucleation, the PVT cell was packed with glass beads. The foamy oil volume (as percentage of the total volume) was compared for the different cases. Two pressure depletion rates were investigated, 800 and 41 kPa/hr (116 and 6 psi/hr). All the CCE runs were carried out at room temperature. Table 5.1 below summarizes the CCE runs done.

Reproduced with permission of the copyright owner. Further reproduction prohibited without permission.

Run No.	Pressure Depletion Rate (kPa/hr)	Description of CCE Run		
		Mixing/ Stirring	Addition of 0.5% (By Vol.) Defoamer	Glass Beads
1	800	No	No	No
2	800	Yes	No	No
3	800	No	Yes	No
4	800	Yes	Yes	No
5	800	No	No	Yes
6 (repeat of 1)	800	No	No	No
7	41	No	No	No
8	41	Yes	No	No
9 (repeat of 8)	41	Yes	No	No
10	800	Yes	Yes	No

Table 5.1 - Foamy oil CCE runs done under different conditions of pressure depletion rate and room temperature.

5.1.1 CCE Runs at Pressure Depletion Rate of 800 kPa/hr and Room Temperature

The first CCE run was performed with no mixing and no addition of the defoamer. This run represents the base run, and it resembles closely the foamy oil process as it happens in the reservoir. The run commenced with the switching on the pump controlling the pressure depletion rate. The pressure depletion rate was set at 800 kPa/hr. After the start of the pressure depletion the fluid levels were measured using the cathetometer. Figure 5.1 shows the bubble point pressure determination, which was found to be 5723 kPa ± 103 kPa (830 ± 15 psi). The bubble point pressure was also confirmed by PVT Pro Simulator* that gave 5716 kPa (829 psi). The Peng-Robinson equation of state was used in the simulator. This indicates little effect of supersaturation. The foamy volume (as percentage of the total volume) is shown in Figure 5.2. As seen in Figure 5.2, the foamy volume (as percentage of the total volume) shows 100% liquid below the bubble point pressure. This is due to the

* DB Robinson Research PVT simulator

Reproduced with permission of the copyright owner. Further reproduction prohibited without permission.

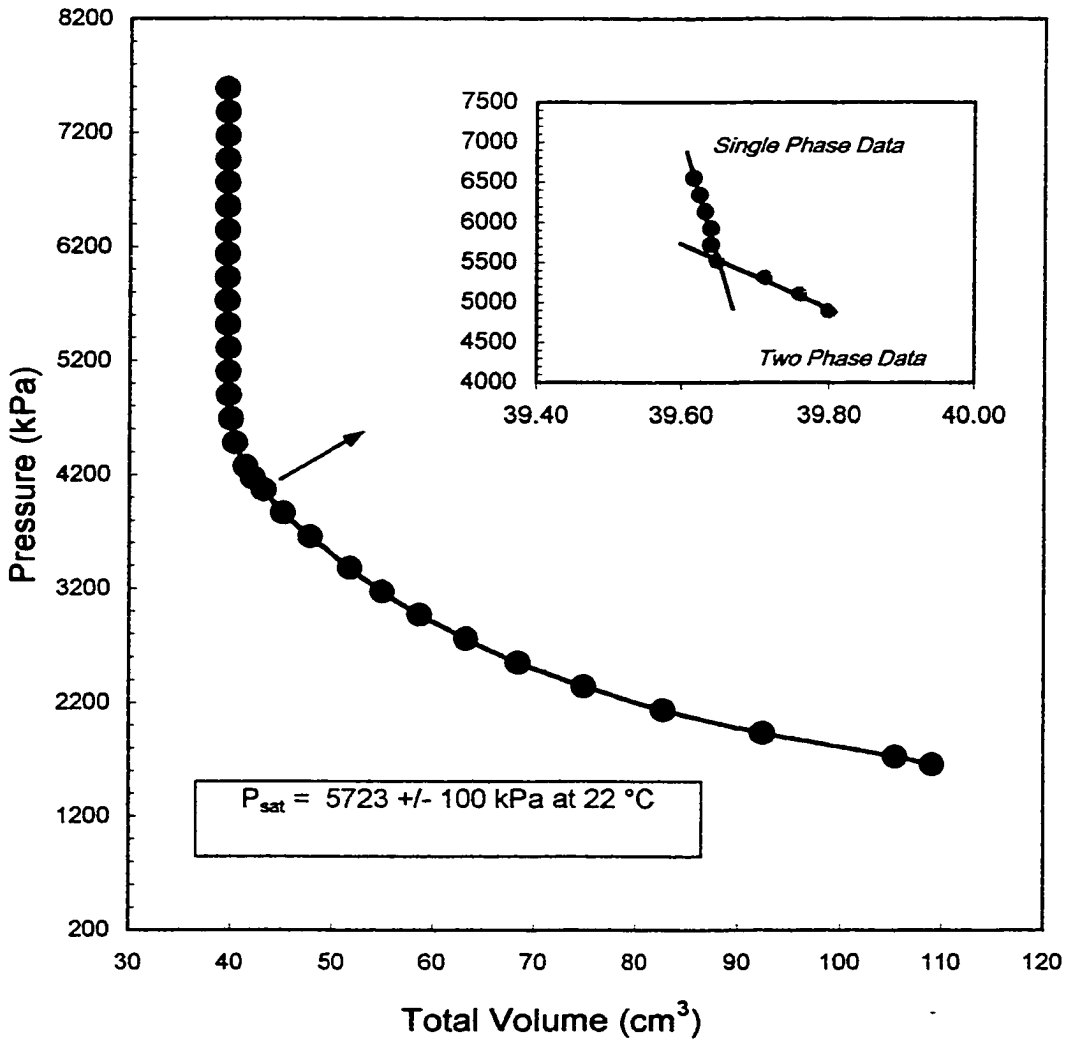

Figure 5. 1 - CCE of foamy oil for pressure depletion rate of 800 kPa/hr for the case of no mixing, insert showing bubble point pressure.

Reproduced with permission of the copyright owner. Further reproduction prohibited without permission.

Reproduced with permission of the copyright owner. Further reproduction prohibited without permission.

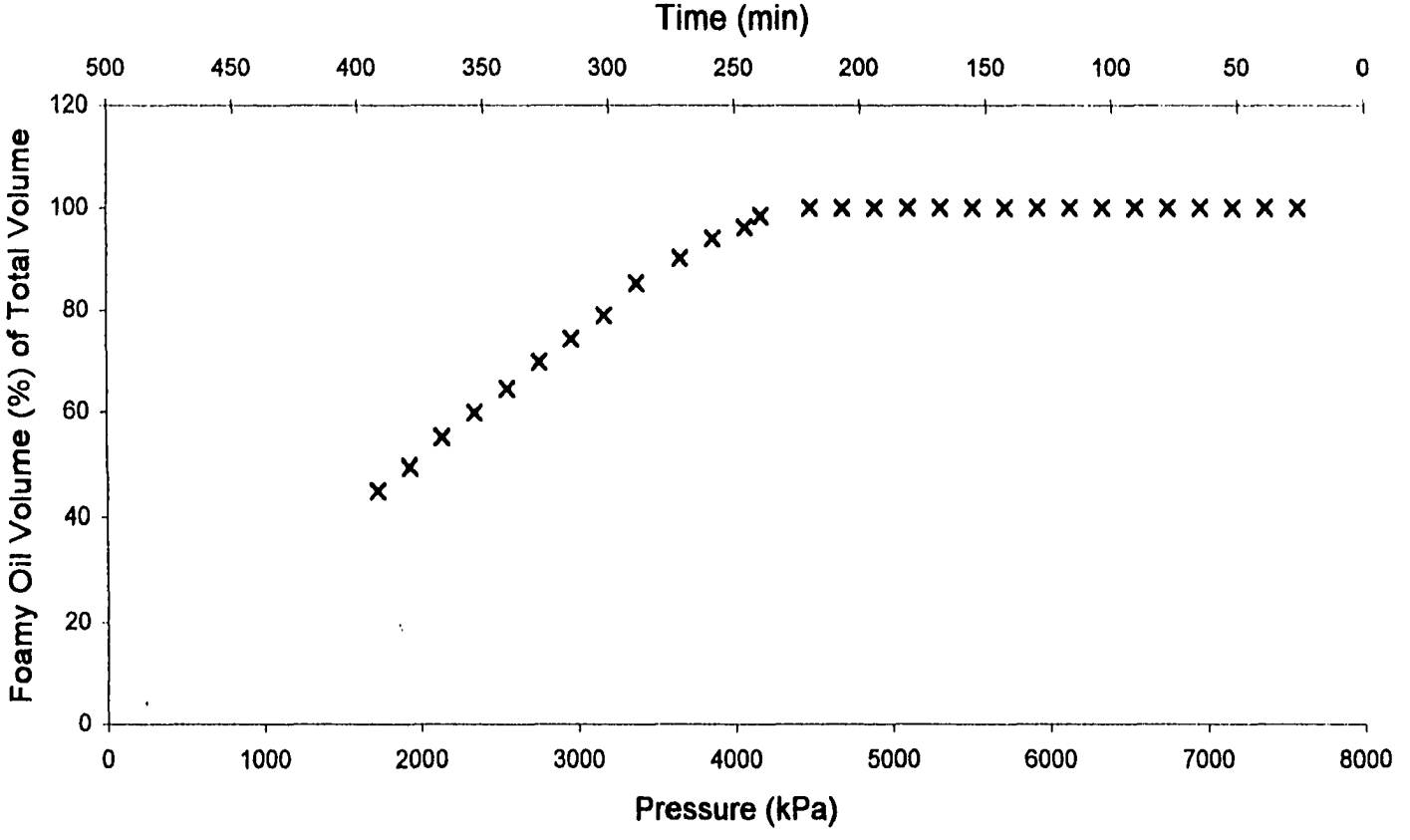

Figure 5.2 - CCE of foamy oil for no mixing case at a depletion rate of 800 kPa/hr and room temperature.

immeasurable free gas volume liberated. This graph will be used for comparison of other CCE runs.

Figure 5.3 shows the CCE data for the case when stirring was introduced by means of a magnetic mixer. This run started by setting the pressure depletion rate of the pump at 800 kPa/hr (116 psi/hr). In addition, a magnetic mixer located at the bottom of the PVT cell was turned on. The purpose of this run was to alter the foamy oil process by changing or speeding up the coalescence of the gas bubbles as they come out of solution. As a result, the disengagement of the gas bubbles from entrapped to free gas phase is hastened. Although the bubble point pressure was the same as the previous run, no-mixing case, the amount of gas liberated as free gas phase was higher. The possible explanation of this is that supersaturation was not a large contributing factor in a well-mixed system and that some of the gas bubbles remain entrapped in the oil phase. In other words, the foamy oil process is a time dependent problem, where during the evolution of gas bubbles the properties of the gas-oil system are changing.

Run 3 was performed at 800 kPa/hr (116 psi/hr) and with no-mixing. In this run, a 0.5% (by volume) of a defoamer was added. The purpose of this run was to change the interfacial tension between the gas bubbles and the oil phase. A consequence, the effect of the defoamer would manifest in an increase of free gas phase and a decrease of the foamy oil or "foaminess". Again, the bubble point pressure was found to be the same as in the previous two runs. This was confirmed visually, where minute amount of gas was seen in the PVT cell. The CCE data for this run is shown in Figure 5.4. The foamy volume (as percentage of the total volume) was intermediate between the no-mixing and mixing case runs. This indicates that the defoamer helped to speed up the disengagement of the gas bubbles into free gas phase.

Next, the combined effects of mixing and addition of 0.5% (by vol.) defoamer were introduced in Run 4. This run was conducted at a pressure depletion rate of 800 kPa/hr (116 psi/hr). Addition of the defoamer increased the rate at which gas was

Reproduced with permission of the copyright owner. Further reproduction prohibited without permission.

Reproduced with permission of the copyright owner. Further reproduction prohibited without permission.

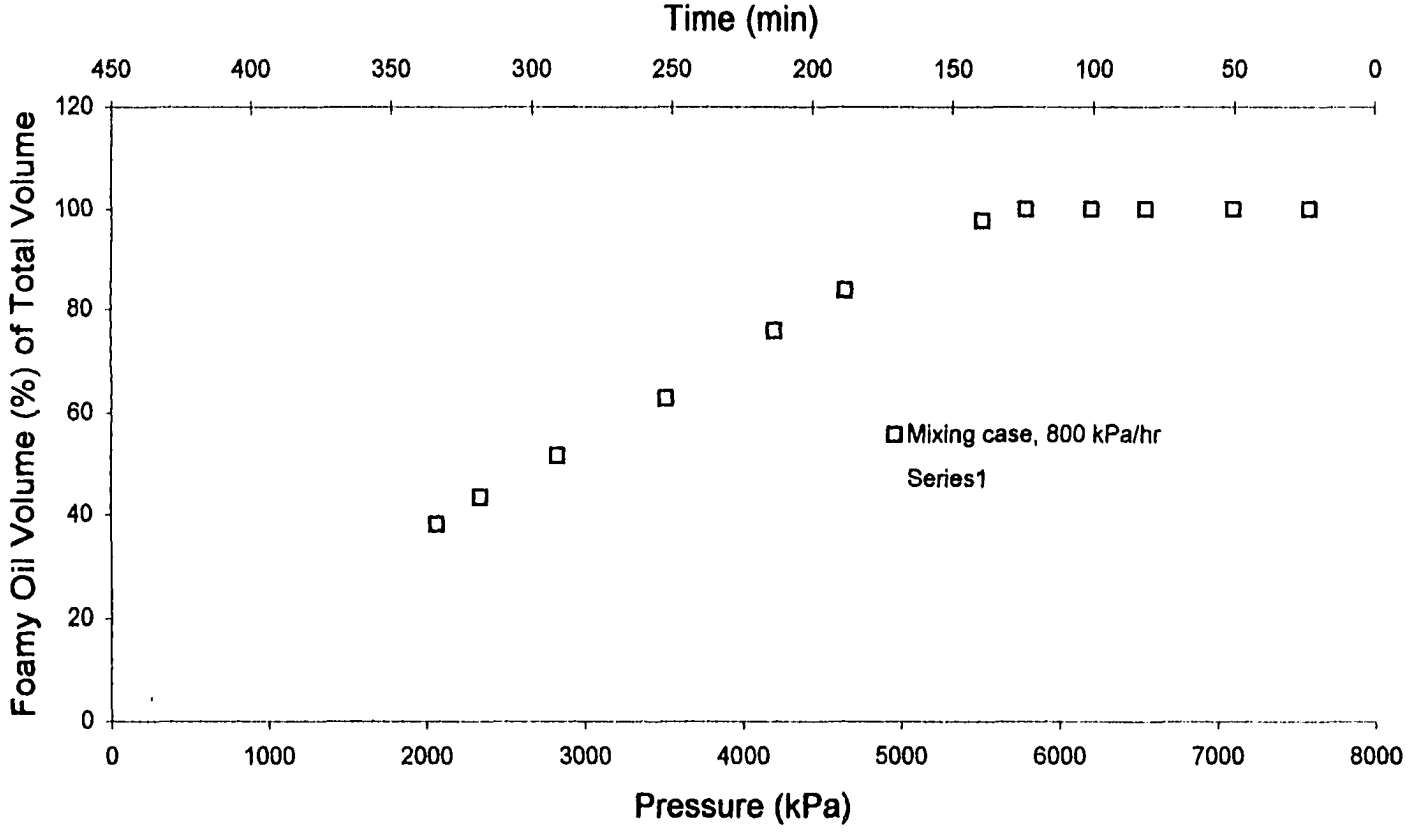

Figure 5.3 - CCE of foamy oil for mixing case at a depletion rate of 800 kPa/hr and room temperature.

Reproduced with permission of the copyright owner. Further reproduction prohibited without permission.

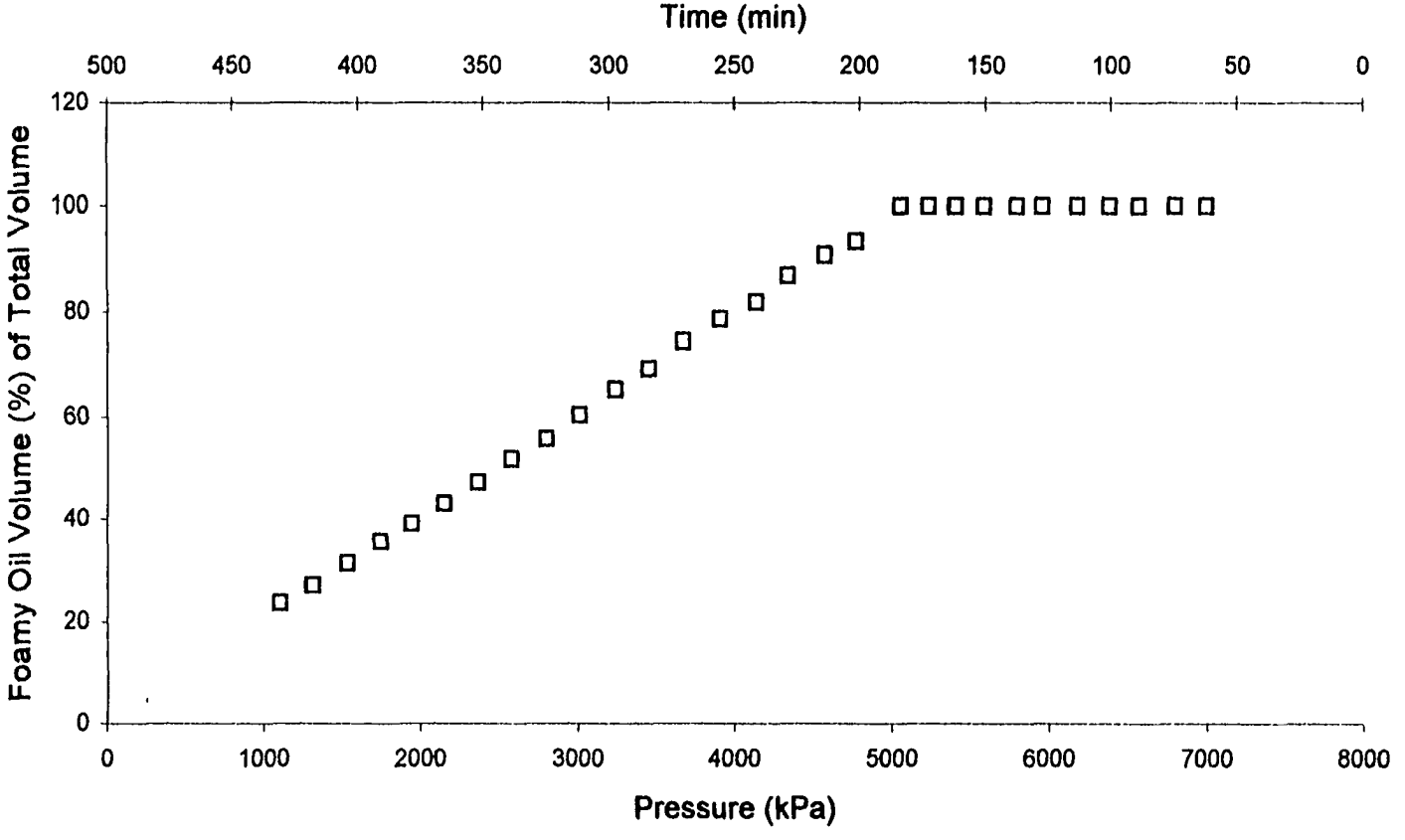

Figure 5.4 - CCE of foamy oil for 0.5% (by vol.) defoamer and no mixing case at a depletion rate of 800 kPa/hr and room temperature.

librated from the dispersed to the free gas phase. The CCE data for this run is shown in Figure 5.5.

To investigate the effect of porous medium on the CCE process, Run 5 was performed in the presence of glass beads. The PVT cell was about one-third filled with 5-mm glass beads. Two screens held the glass beads together. Figure 5.6, below, shows the schematic of the PVT cell with the glass beads and the screens. There was a little oil above the top screen just enough to maintain the initial pressure without having to crush the glass beads. This was important, as the live oil above the top screen would not affect the CCE run and mask the effect of the glass beads. The glass beads increased the surface area available for gas nucleation. The run was done at pressure depletion of 800 kPa/hr (116 psi/hr) with no addition of defoamer and no-mixing. See Figure 5.7 for the CCE data for this run. The curve of foamy volume percentage of the total volume as a function of pressure for this run was similar to the case of 0.5% (by vol.) defoamer and no-mixing, Run 3.

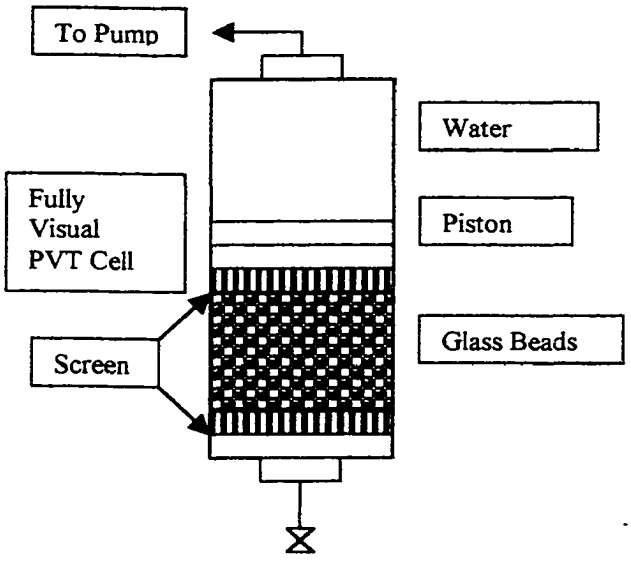

Figure 5.6 – Schematic of the PVT cell and glass beads arrangement.

Reproduced with permission of the copyright owner. Further reproduction prohibited without permission.

Reproduced with permission of the copyright owner. Further reproduction prohibited without permission.

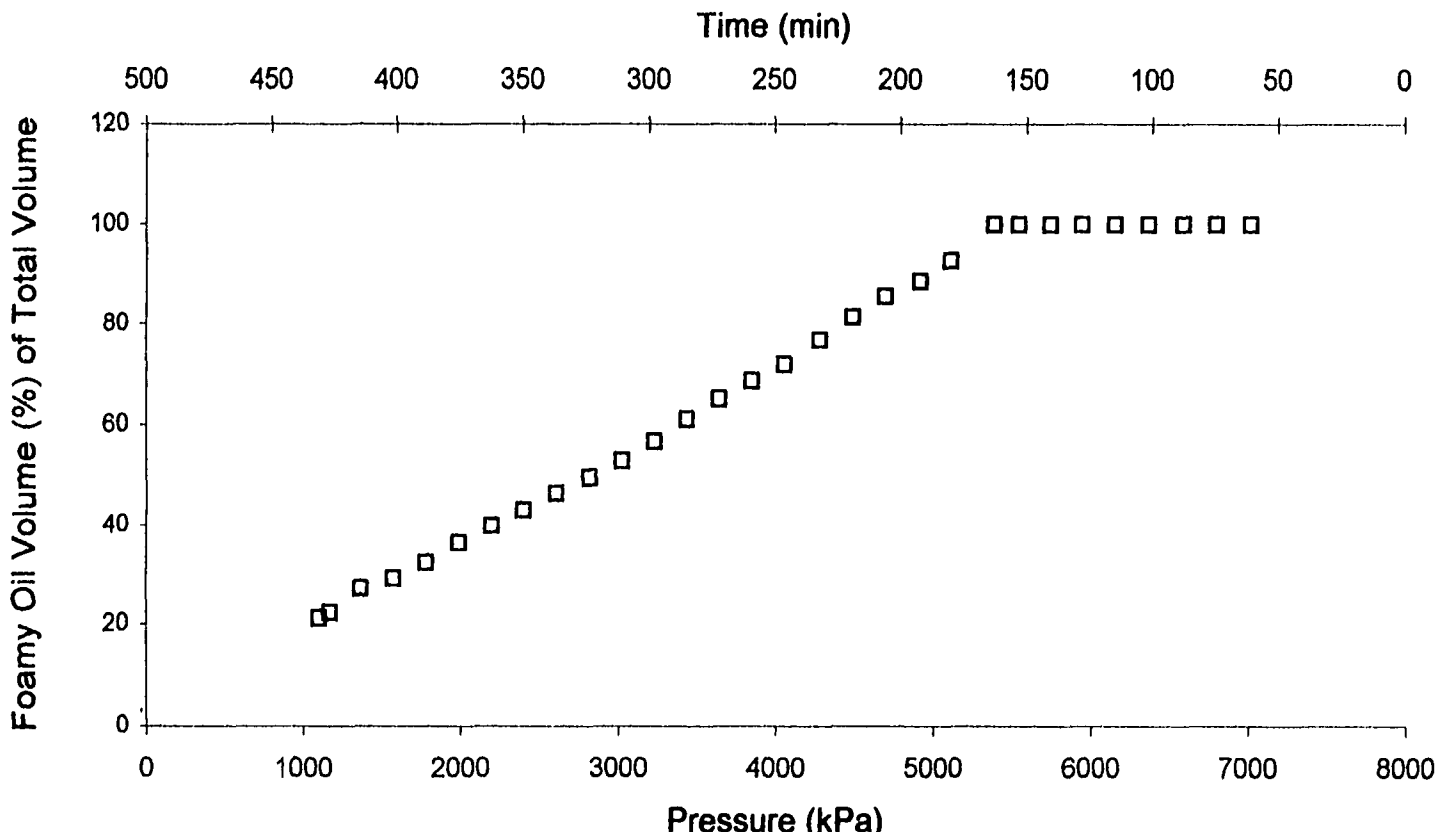

Figure 5.5 - CCE of foamy oil for 0.5% (by vol.) defoamer and mixing case at a depletion rate of 800 kPa/hr and room temperature.

Reproduced with permission of the copyright owner. Further reproduction prohibited without permission.

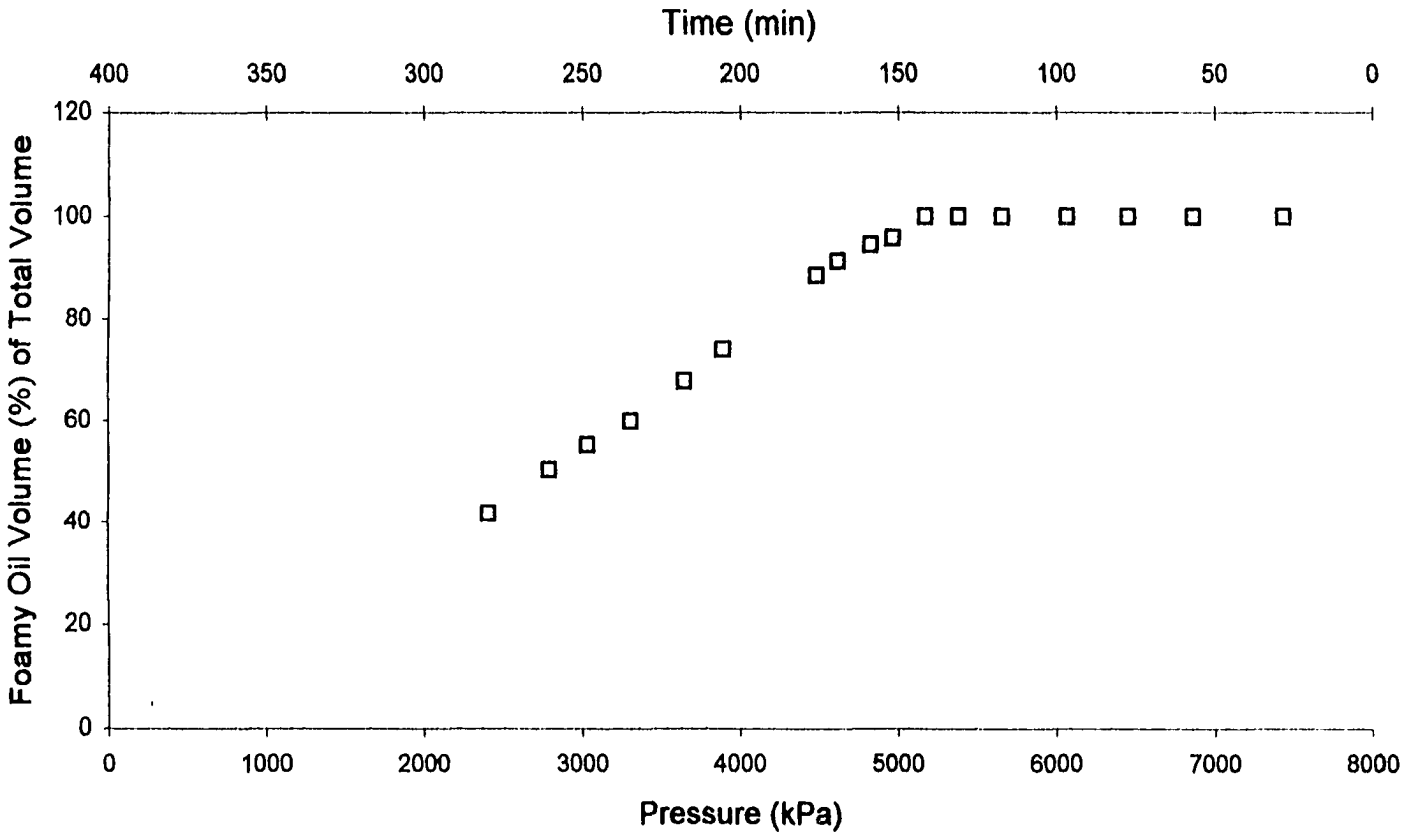

Figure 5.7 - CCE of foamy oil for glass beads bed case at a depletion rate of 800 kPa/hr and room temperature.

5.1.2 Comparison of the CCE Runs at Pressure Depletion Rate of 800 kPa/hr and Room Temperature

The different CCE runs performed at pressure depletion rate of 800 kPa/hr are plotted in Figure 5.8. As can be seen from the graph, the no-mixing case, Run 1, gave an upper limit and Runs 2 and 4, the mixing case with and without the addition of defoamer, gave a lower limit of the foamy volume percentage of the total volume. Figure 5.8 also shows one data point taken after leaving the sample for 60 hours at the end of Run 2, mixing case. This point is lower by about 2 percentage points than the last point of Run 2. Also, the pressure after leaving the sample for 60 hours rose from 2069 kPa (300 psi) to 2172 kPa (315 psi). Although the rise in pressure was within the experimental error, it is still indicative of gas bubbles disengaging from the oil phase into free gas phase due to a slight supersaturation.

It is known that the driving force in gas-oil solution is supersaturation. A fluid is said to have a degree of supersaturation if the gas remains in solution and does not evolve to gas phase below its saturation pressure (or there is an amount of gas in solution in excess of the saturation gas). The way in which gas bubbles form and grow controls the displacement of oil during the depletion process. However, in our case, supersaturation was not observed to occur or at least not to a high degree. This is evident from the bubble point pressures of all runs where the same bubble point was obtained within the experimental error. The bubble point was found from the experimental data and was confirmed visually. A few bubbles were observed at the gas-oil interface. Also, bubble point pressures for some runs were found by means of PVT simulator and were found to be the same as the experimentally determined ones. It is clear from the graph that the entrapped gas is higher for the no-mixing case at the same conditions of pressure and temperature. Therefore, the study of PVT of heavy foamy oil system is dependent on the way the experiment is carried out, and whether the mixed or not mixed case is closer represents what happens in the reservoir remains to be investigated.

Reproduced with permission of the copyright owner. Further reproduction prohibited without permission.

Reproduced with permission of the copyright owner. Further reproduction prohibited without permission.

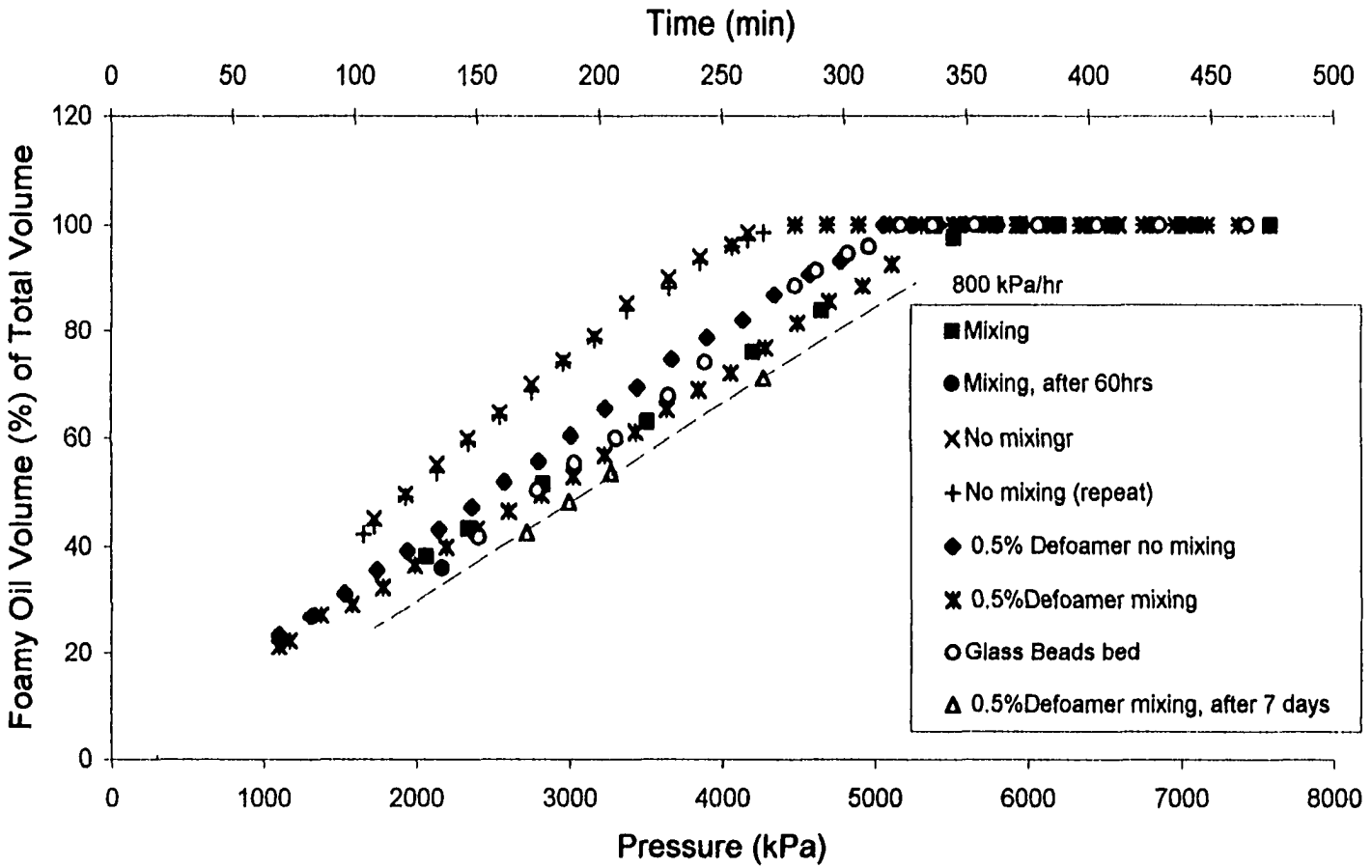

Figure 5.8 - Comparison of CCE runs for different situations at a depletion rate of 800 kPa/hr and room temperature.

5.1.3 CCE Runs at Pressure Depletion Rate of 41 kPa/hr and Room Temperature

Three runs were performed at pressure depletion rate of 41 kPa/hr (6 psi/hr). The same live oil sample used for the CCE runs at pressure depletion rate of 800 kPa/hr was used in the three runs. Run 7 was carried out at a pressure depletion rate of 41 kPa/hr at quiescent conditions. Run 8 was performed at the same pressure depletion rate as Run 7 but with the sample stirred by the magnetic mixer as depletion was in progress. The purpose of this run was to investigate the effect of pressure depletion rate on the solution gas mechanism of foamy oil. Figures 5.9 and 5.10 show the CCE data for Runs 7 and 8, respectively. The bubble point determined experimentally was the same for both runs within experimental error. See Appendix A, Figures 5.9A to 5.14A and 5.15A1 for bubble point determination for different runs. Also, included in Appendix A is the total volume data for the different runs performed. These are Figure 5.2T to 5.5T and Figure 5.7T to 11T.

Comparison of Run 7, quiescent case, and Run 8, mixing case, shows that the no-mixing case gave higher foamy volume (as percentage of the total volume) as can be seen in Figure 5.11. This indicates that gas bubbles, which were nucleated, entrapped in the oil phase in the unstirred case for longer time than that for the mixed case. If we believe, for a moment, in the hypothesis of the existence of microbubbles entrapped in the oil phase, then during the time of the gas bubbles being entrapped until their disengagement/evolution to free gas, the oil entrapped-gas system properties are different than when no entrapped gas bubble present. Therefore, in the other parts of this study we seek to quantify the effect of the entrapped gas bubbles in the displacement of oil and their role in the anomalous foamy oil production.

5.1.4 Effect of Pressure Depletion Rate

Comparison of runs done at faster, 800 kPa/hr, and slower, 41 kPa/hr, pressure depletion rates reveals that the fast depletion rate runs gave a higher foamy volume (as

Reproduced with permission of the copyright owner. Further reproduction prohibited without permission.

Reproduced with permission of the copyright owner. Further reproduction prohibited without permission.

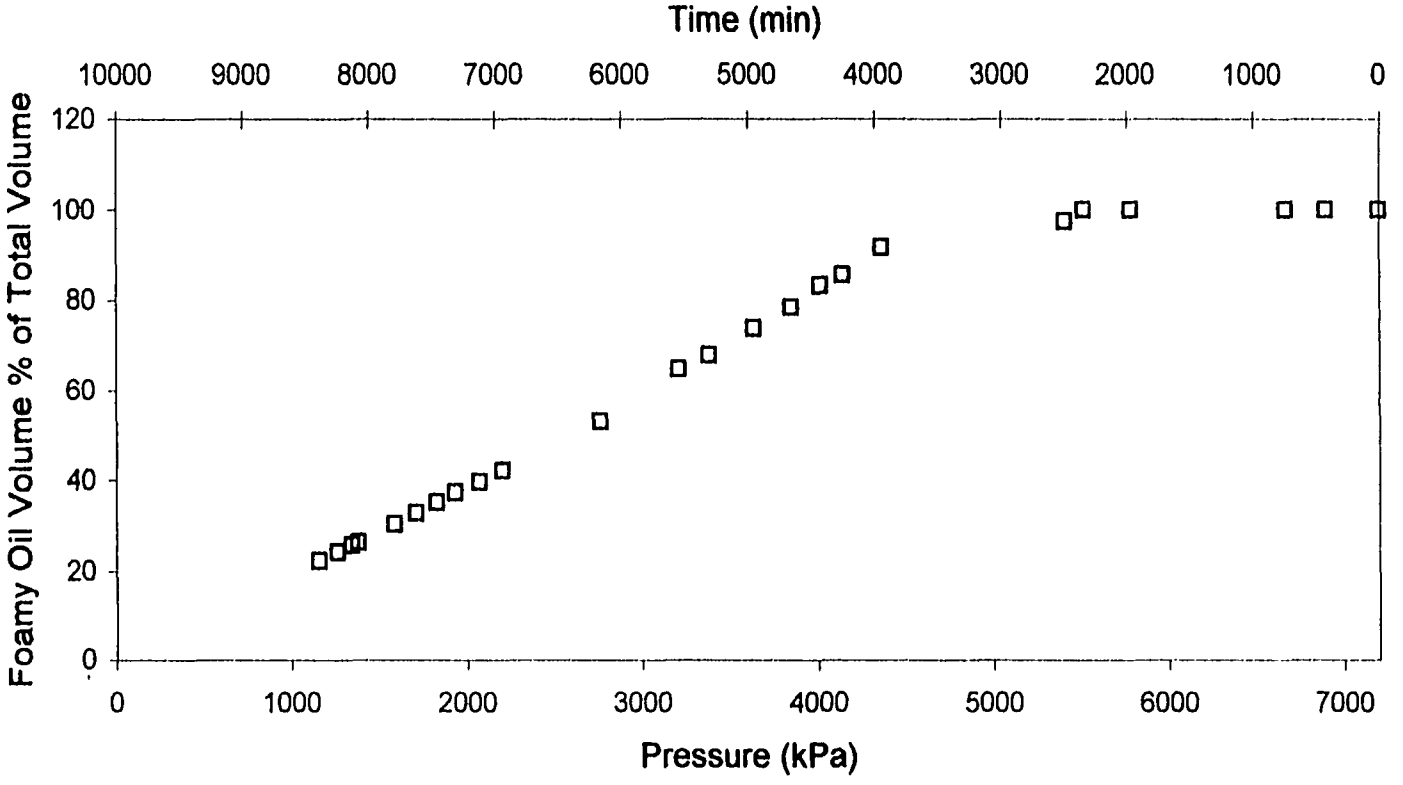

Figure 5.9 - CCE of foamy oil for no mixing case at depletion rate of 41 kPa/hr and room temperature.

Reproduced with permission of the copyright owner. Further reproduction prohibited without permission.

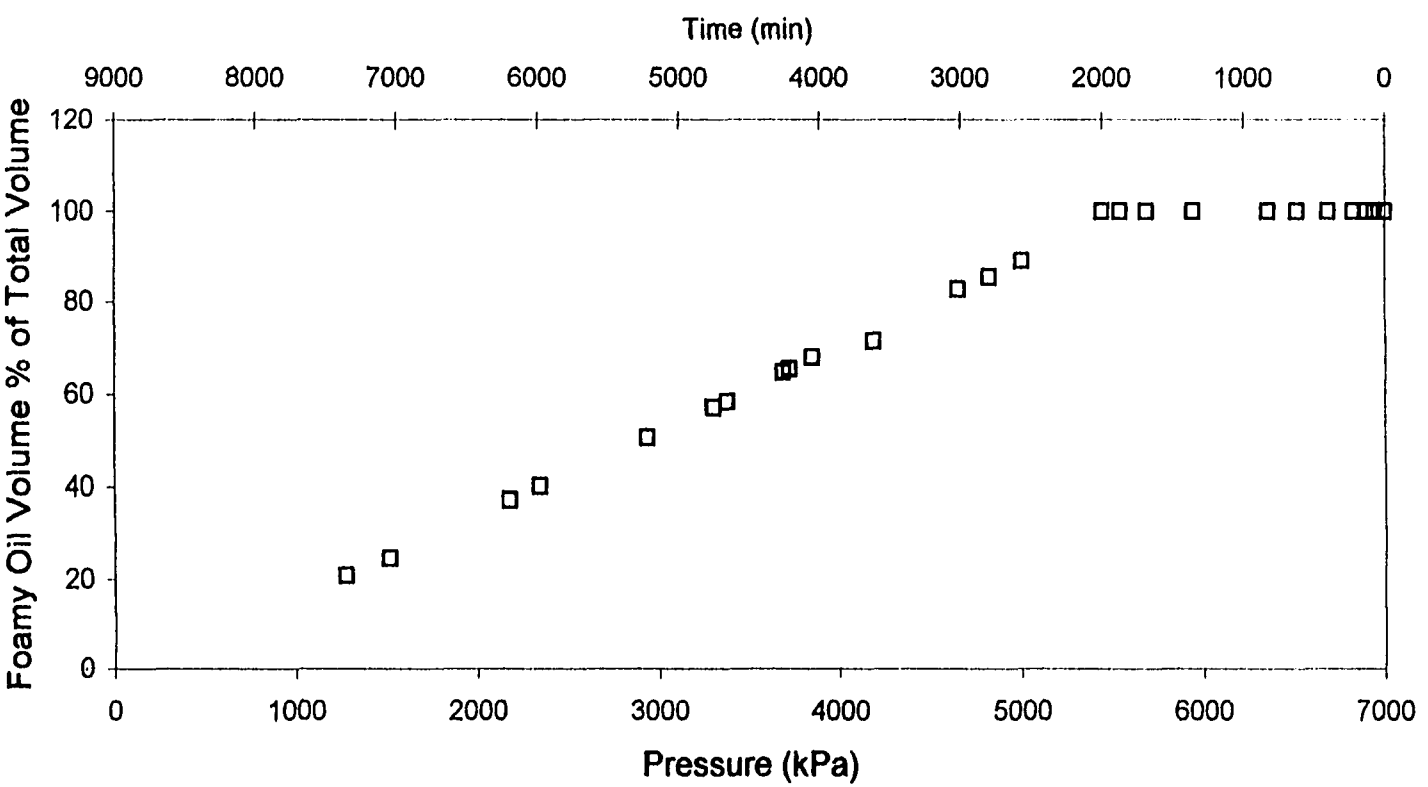

Figure 5.10 - CCE of foamy oil for mixing case at depletion rate of 41 kPa/hr and room temperature.

Reproduced with permission of the copyright owner. Further reproduction prohibited without permission.

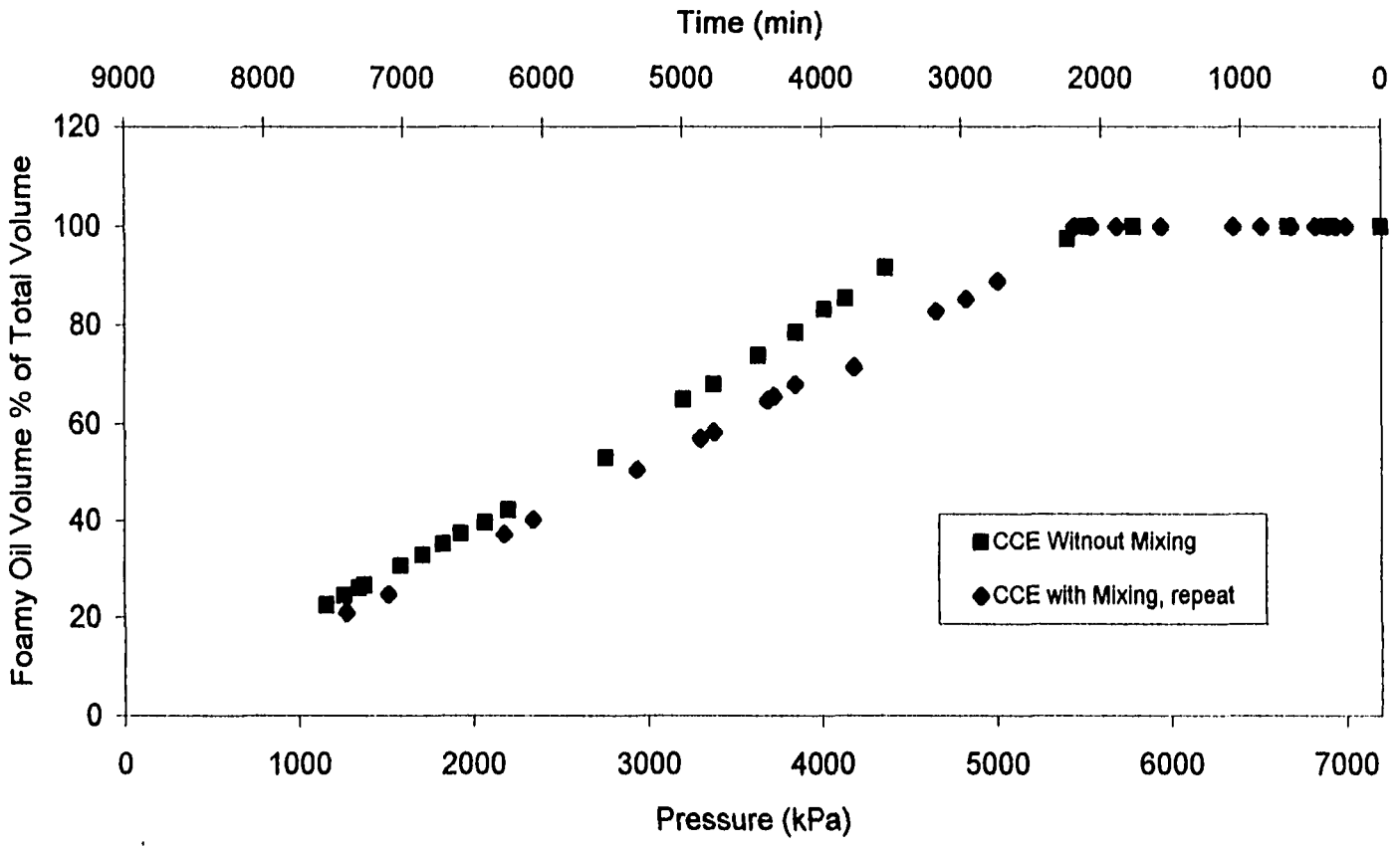

Figure 5.11 - Comparison of CCE at depletion rate of 41 kPa/hr and room temperature for mixing and no mixing cases.

percentage of the total volume) in the no-mixing case. Figure 5.12 shows the data for the fast and slow pressure depletion rates for mixing and quiescent cases. In the case when the oil sample was stirred during the depletion process both the fast and the slow pressure depletion rate experiments gave similar curves of the foamy volume (as percentage of the total volume). This indicates that stirring the sample during depletion speeded up the release of gas bubbles from being trapped to free gas phase.

5.1.5 Apparent Solubility of CO_2 in Heavy Oil

The calculation of apparent solution gas-oil ratio from the CCE experiments for the different runs performed is shown in Figure 5.13. Apparent solution gas oil ratio is the amount of gas (dissolved + dispersed) in the oil at pressure (expressed at standard conditions, 101.325 kPa, 14.7 psi, 15°C) divided by the dead oil volume. The compressibility factor, Z, for CO_2 used in the calculations of the apparent solution gas-oil ratio was found from tables (Angus et. al., 1976) at a temperature of 22 °C. A regression formula was generated which was:

$$Z^2 = 0.977 - 1.222E-4\ P \ln(P), \quad (5)$$

where P is pressure in psi < 700.

The apparent dissolved gas oil ratio was the highest for the 800 kPa/hr pressure depletion rate of the mixing case; and was the lowest for the case when the sample left for 7 days for stabilization.

A relationship of the dispersed phase with respect to pressure was found from the difference of the apparent solution gas oil ratio between the 0.5% defoamer with mixing left for 7 days and the 0.5% defoamer with mixing cases. Figure 5.13 shows the different apparent solution gas-oil ratios. This dispersed gas phase will be used in the prediction of the apparent foamy oil viscosity using Islam and Chakma, (1990) correlation.

Reproduced with permission of the copyright owner. Further reproduction prohibited without permission.

Reproduced with permission of the copyright owner. Further reproduction prohibited without permission.

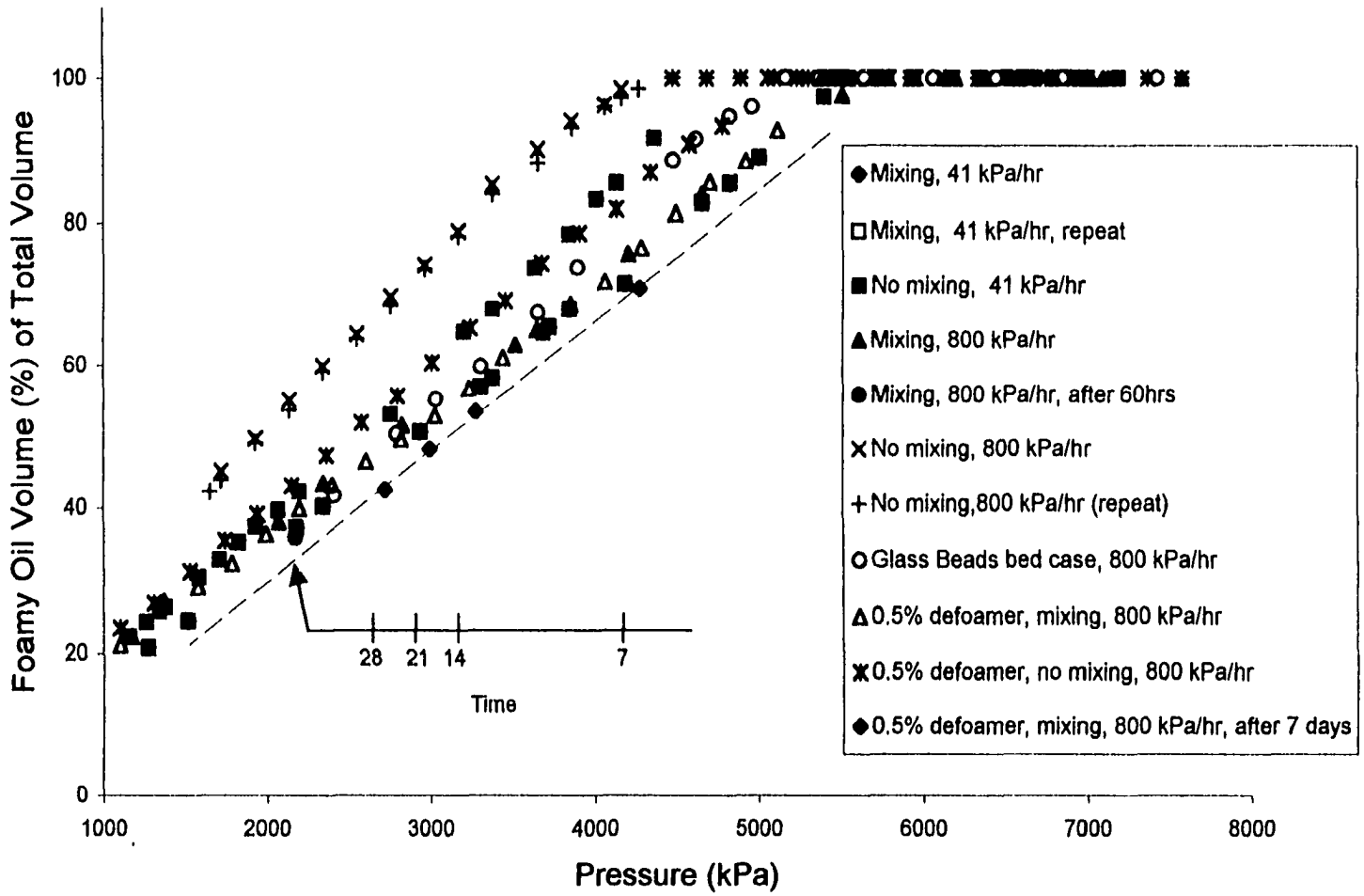

Figure 5.12. - Comparison of CCE at depletion rates of 800 kPa/hr and 41 kPa/hr of foamy oil for different conditions and room temperature.

Reproduced with permission of the copyright owner. Further reproduction prohibited without permission.

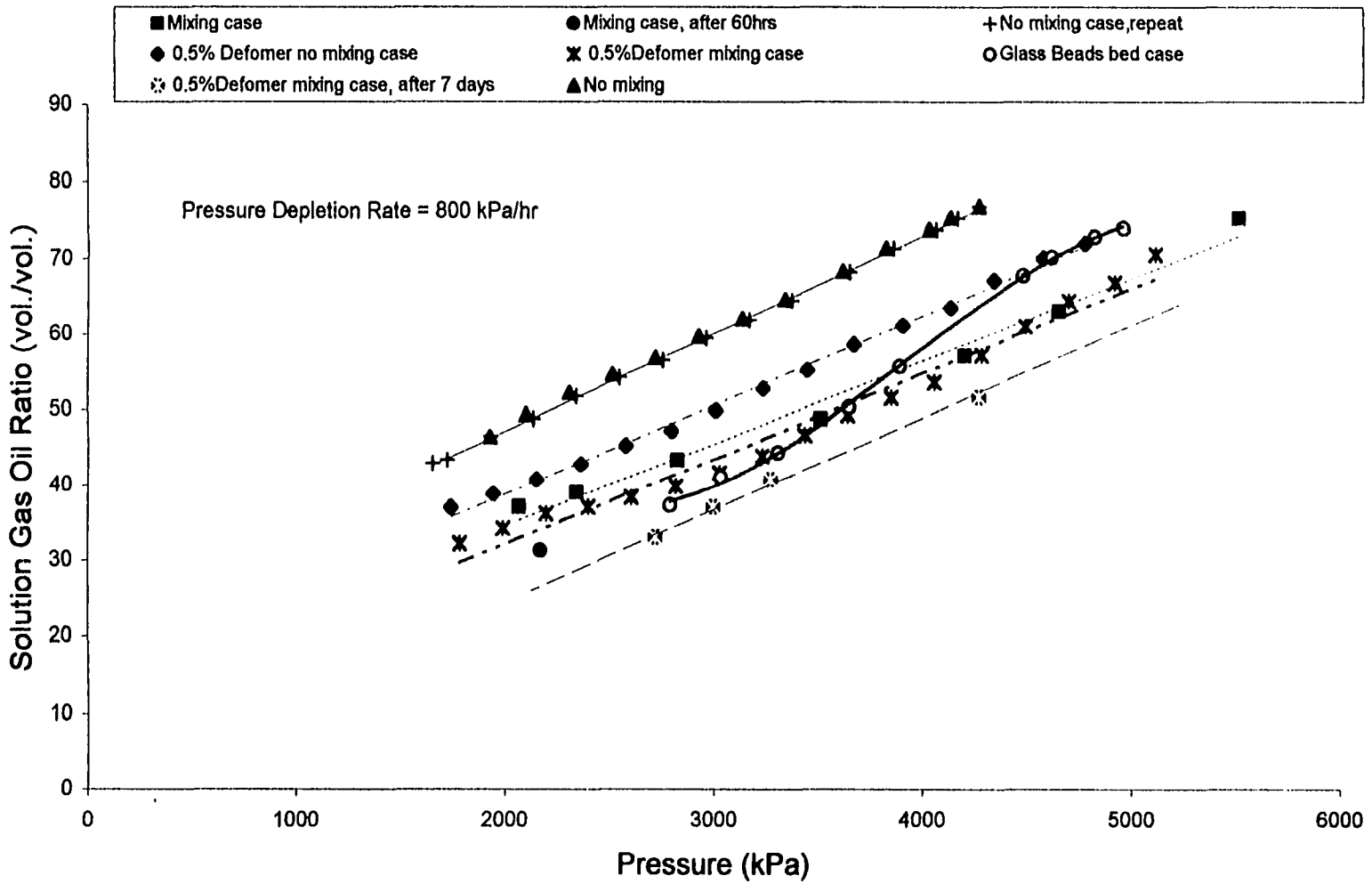

Figure 5.13 - Comparison of apparent solubility of CO_2 in foamy oil for different situations at a depletion rate of 800 kPa/hr and room temperature.

5.1.6 Reproducibility of CCE Results

To check the experimental results obtained in the CCE runs, two experiments were repeated. One was performed at pressure depletion rate of 800 kPa/hr, while the other was done at 41 kPa/hr. Run 6 was a repeat of the quiescent run at 800 kPa/hr; And Run 9 was conducted at a pressure depletion rate of 41 kPa/hr (6 psi/hr) with mixing. Figure 5.14 shows the reproducibility of the two runs to be very good.

5.2 Measurement of Viscosity of Foamy Oil

The objective of this set of experiments was to investigate the viscosity of foamy oil at different pressure depletion rates and to identify the role of viscosity, if any, on the anomalous foamy oil production. Also, to establish whether Claridge and Prats model has any experimental evidence. The viscosity was measured by three different viscometers. Those were Cambridge, capillary, and Haake RV-2 viscometers. The Cambridge and capillary viscometers were connected to a fully visual PVT cell as described previously in the Experimental Set-up and Procedures. The pressure depletion was done in the PVT cell. The third viscometer used was Haake RV-2, which was not connected to the PVT cell due to the large sample volume required to run viscosity measurement. For this reason the pressure depletion was done inside the chamber of Haake viscometer. The viscosity measurements were carried out at two different pressure depletion rates with pressure ranging from 7584 to 2068 kPa (1100 to 300 psi). When time between two pressure points was long, viscosity measurements were taken for sufficiently long period of time (longer than 2 hours) to insure a constant viscosity reading. Prior to viscosity measurement, live oil sample was depleted in the PVT cell at the desired pressure depletion rate. When the desired pressure, at which the viscosity measurement was sought, was reached, the depletion rate was stopped and a sample was pushed from the bottom of the PVT cell at constant pressure to the Cambridge and capillary viscometers. The length of time for viscosity measurement was controlled by the next pressure point. Before the next pressure point at which the viscosity was sought, the viscometers had to be cleaned and prepared for

Reproduced with permission of the copyright owner. Further reproduction prohibited without permission.

Reproduced with permission of the copyright owner. Further reproduction prohibited without permission.

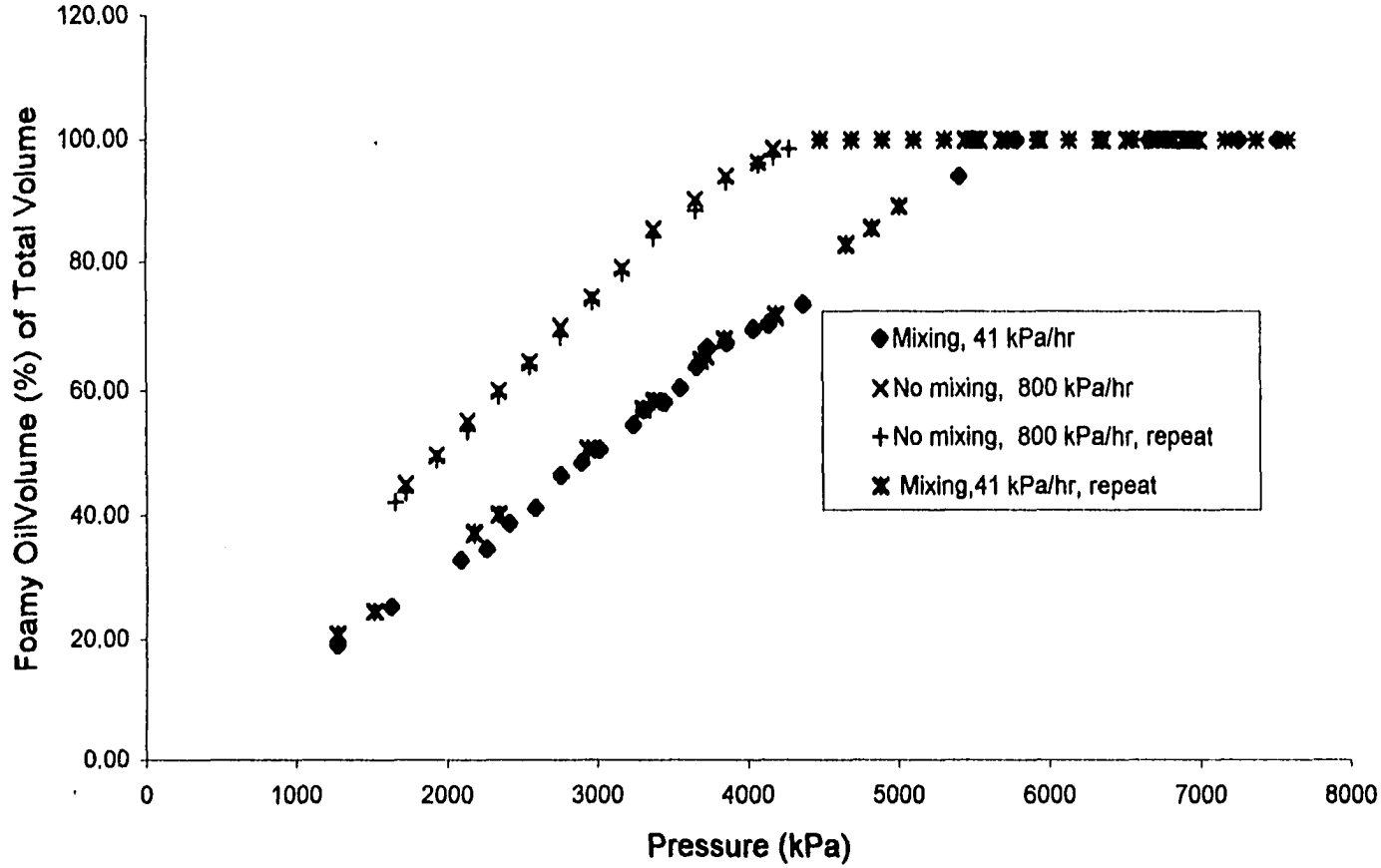

Figure 5.14 -Reproducebility of CCE runs at depletion rates of 800 kPa/hr and 41 kPa/hr of foamy oil and room temperature.

the next viscosity point measurement. Therefore, the pressures at which the viscosity was measured were spread out to allow enough time for the viscosity measurement and cleaning of the viscometers. This was done to insure a least disturbance to the pressure depletion process in the PVT cell. The viscometers and the lines were thoroughly cleaned by toluene and methylene chloride and dried by flowing air through the viscometers.

Viscosity was measured at two pressure depletion rates, 800 and 41 kPa/hr. For the 800 kPa/hr pressure depletion rate, two depletion runs were carried out with one having 0.5% (by volume) defoamer added to the live oil sample and the other was with live oil sample, nothing added. This was done as a way to alter the solution gas mechanism of foamy oil and be able to measure the effect of the gas bubbles on the viscosity of foamy oil. In addition, the addition of defoamer would help gas bubbles to coalesce and evolve to free gas phase faster. Next the experimental results of viscosity measurement are presented.

5.2.1 Viscosity of Foamy Oil as Measured by Cambridge Viscometer

The same live oil as that used in the CCE experiments was used for the viscosity measurements. The pressure depletion was done in the visual PVT cell. A sample of about 3 cc was pushed into the Cambridge viscometer. Then additional oil sample was purged through the viscometer to insure that there was no free gas flashed during the transfer process. Viscosity was measured at the desired pressure and was recorded with respect to time. Viscosity was measured at 800 kPa/hr with and without the addition of a defoamer to the live oil. Figures 5.15 and 5.16 show the results of the viscosity measurement of foamy oil with and without the addition of the defoamer, respectively. The individual viscosity points recorded as a function of time are given in Appendix A as Figures 5.15A through Figure 5.25A and 32A to 36A. The measured viscosity as a function of time was stable and reproducible as can be seen in Figures 5.26A through 5.31A . Due to the large range of viscosity being measured, two pistons were used, a 2000-cp and a 10000-cp. The pistons could be used for the viscosity

Reproduced with permission of the copyright owner. Further reproduction prohibited without permission.

Reproduced with permission of the copyright owner. Further reproduction prohibited without permission.

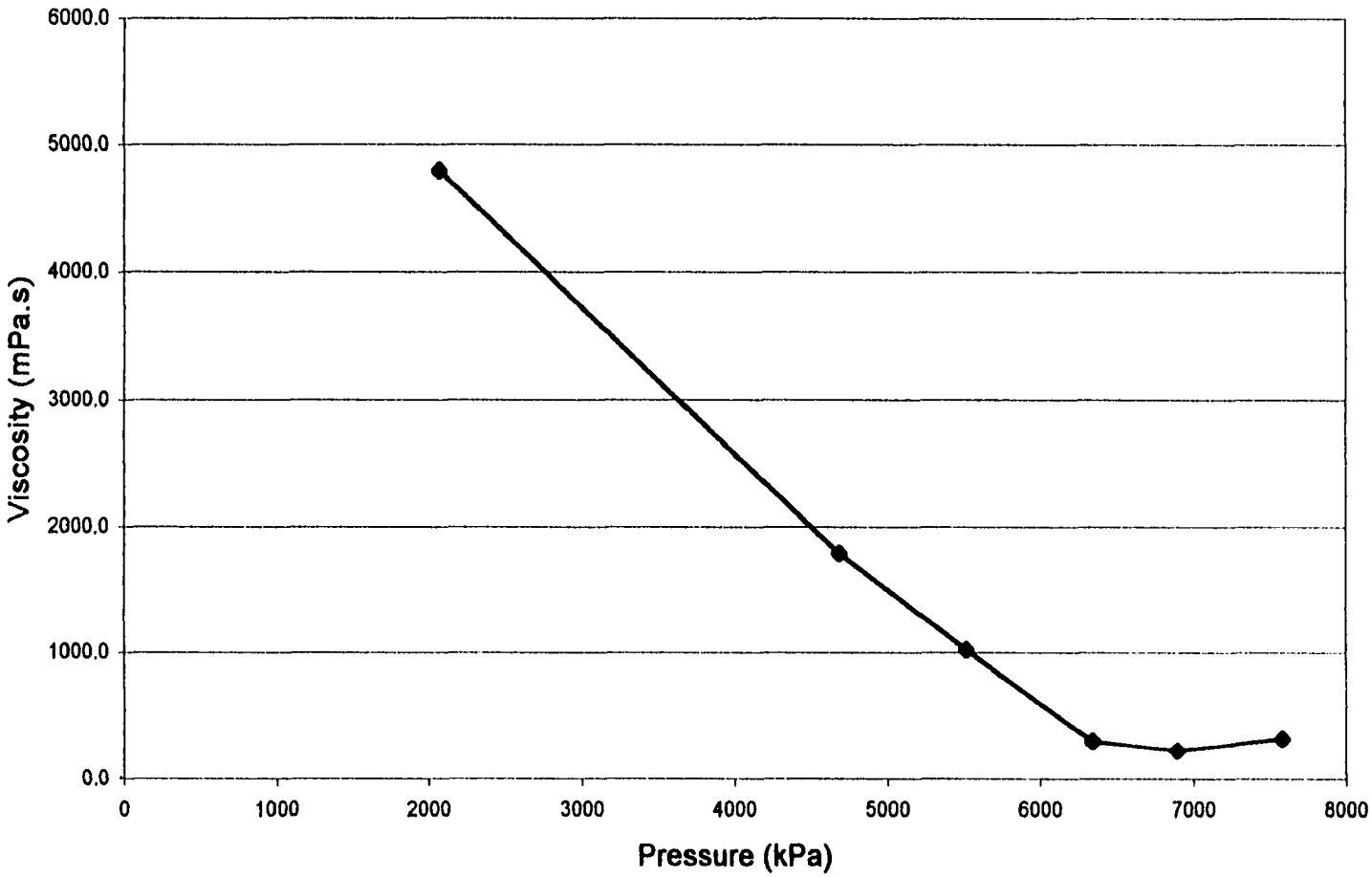

Figure 5.15 - Viscosity of foamy oil with 0.5% (by vol.) defoamer as measured by Cambridge viscometer for the pressure depletion rate of 800 kPa/hr and room temperature.

Reproduced with permission of the copyright owner. Further reproduction prohibited without permission.

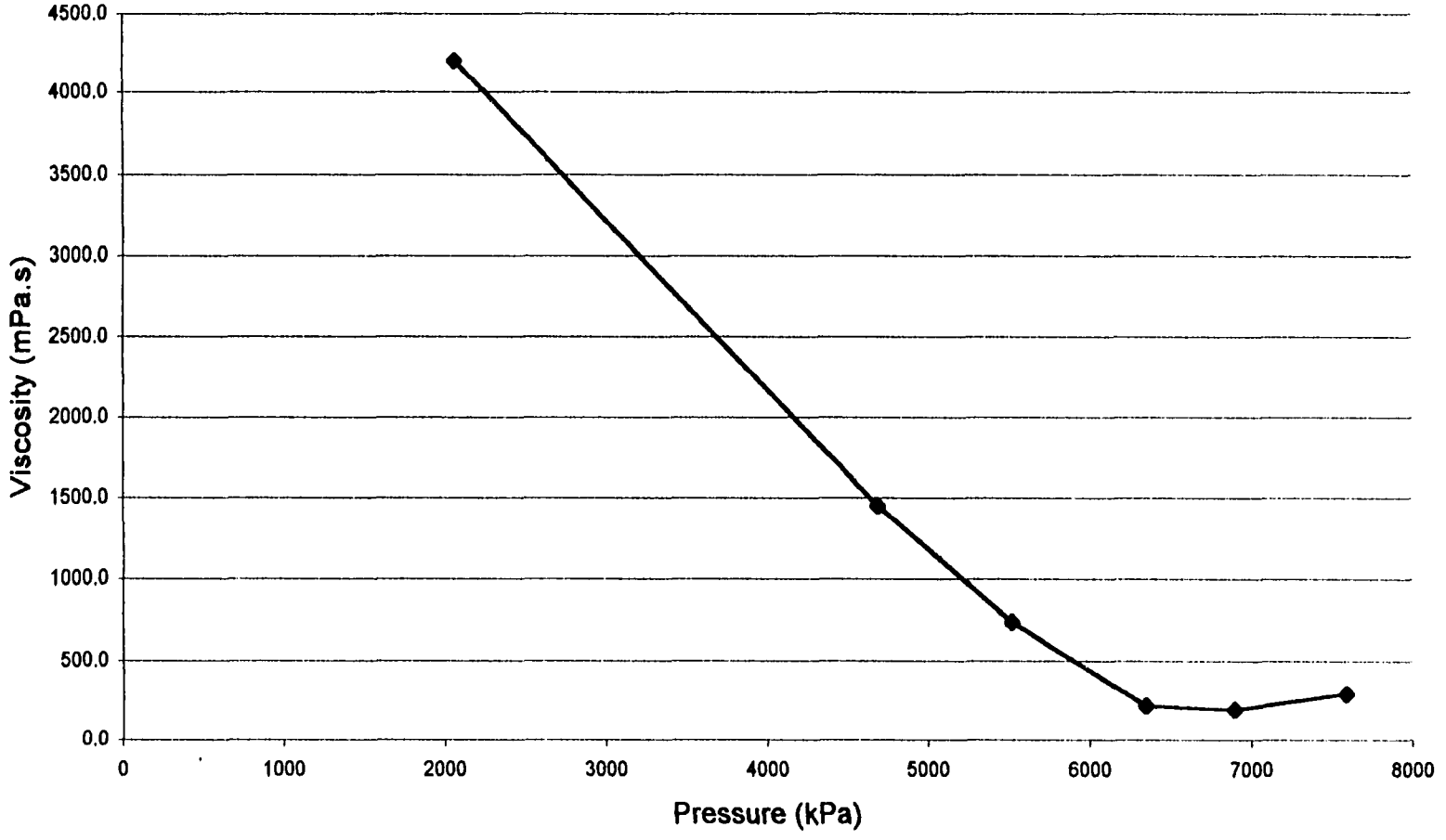

Figure 5.16 - Viscosity of foamy oil as measured by Cambridge viscometer for the pressure depletion rate of 800 kPa/hr and room temperature.

measurement in as high as 1.5 the numerical value of the piston; i.e.; a 10000-cp piston operates in a viscosity range of 1 to 15000 mPa.s (cp). The accuracy is ± 1% full-scale reading. The viscosity fluctuation was within the instrument accuracy which was 20 and 100 mPa.s for the 2000 and 10000-cp pistons, respectively. Now, if the effect of gas bubbles is to reduce the viscosity of foamy oil, then the defoamer case would be expected to have a higher viscosity than the "normal" foamy oil viscosity, with no addition of defoamer. Indeed the viscosity of the defoamed oil as measured by Cambridge viscometer was higher than the viscosity of the "normal" foamy oil at the same pressure below the bubble point pressure. This is the most likely due to fewer bubbles being entrapped in the liquid phase. The CCE experiments with 0.5% (by vol.) defoamer case gave less swelling of the liquid phase. In other words, there were fewer bubbles entrapped in the oil phase. The question of why there was no free phase developing in the chamber of the viscometer is a valid and an intriguing question that needs to be answered. But, with the set-up used, where the oil sample being measured in the Cambridge viscometer was not visual, one can only give quantitative answers. A possibility exist that the movement of the piston acts as a stirring device, so as to disperse the gas free phase into smaller bubbles that pass through the gap between the piston and the chamber wall. Another possibility is that the bubbles take longer than the duration of viscosity measurement to disengage from the liquid phase.

Figure 5.17 shows the measured viscosity at a pressure depletion rate of 41 kPa/hr. The viscosity curve was intermediate between the 800 kPa/hr with and without the addition of 0.5% defoamer cases. This will be discussed further in the comparison of the different runs below.

To investigate the time effect on foamy oil solution gas process, viscosity was measured after leaving the foamy oil sample to stabilize for one day in the first case and seven days (and 8 days for 5516 kPa, 800 psi) in the second case. Viscosity was measured at two pressure points, 5516 kPa (800 psi) and 2068 kPa (300 psi). The viscosities as measured by the Cambridge viscometer after one and seven days were found to be substantially higher than the previously measured viscosity at pressure

Reproduced with permission of the copyright owner. Further reproduction prohibited without permission.

Reproduced with permission of the copyright owner. Further reproduction prohibited without permission.

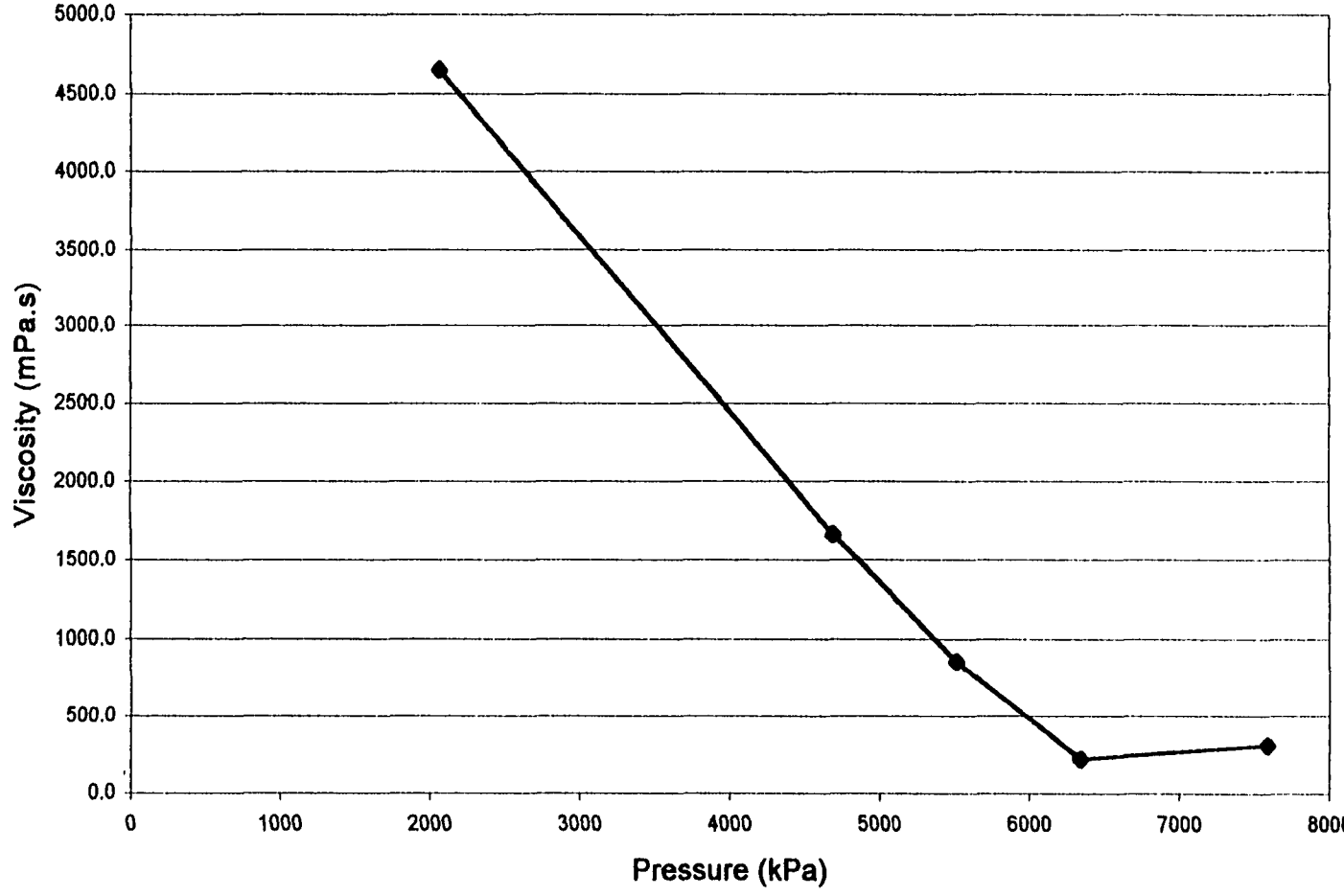

Figure 5.17- Viscosity of foamy oil as measured by Cambridge viscometer for pressure depletion rate of 41 kPa/hr and room temperature.

depletion rates of 41 and 800 kPa/hr during the depletion process. At 2068 kPa (300 psi), the same trend as that measured in the 5516 kPa (800 psi) case of increasing viscosity with time of stabilization was observed.

5.2.1.1 Comparison of Viscosity of Foamy Oil as Measured by Cambridge Viscometer

Viscosity was measured as a function of time for the pressure range of 7584 to 2068 kPa (1100 to 300 psi). The viscosity data for the different runs performed at 5516 kPa (800 psi) and 2068 (300 psi) are given graphically as a function of time in Figures 5.18 and 5.19, respectively. It is evident from the two figures that the viscosity increased as the foamy oil sample stabilization time increased. This is possibly due to the entrapped gas bubbles, so that as time passes more bubbles disengage into free gas phase.

Figure 5.20 shows viscosity vs. pressure for the runs performed at pressure depletion rates of 800 and 41 kPa/hr. As can be seen from the graph, the 0.5% defoamer case, at 800 kPa/hr, resulted in the highest viscosity and the 41 kPa/hr depletion rate gave the lowest. This is consistent with the CCE runs where the 41 kPa/hr gave the lowest foamy oil volume (as percentage of the total volume). Based on these viscosity measurements, the concluding remark is that the longer the foamy oil sample is left for stabilization the higher the viscosity. As for the pressure depletion rate, viscosity was lower for the higher-pressure depletion rate than for the lower one. Also, the viscosity at the fast depletion rate with defoamer is about the same as that for the slow depletion rate.

It is evident from Table 5.2 that the viscosity increased as the foamy oil sample stabilization time increased. Again, this is possibly due to the presence entrapped gas bubbles. As time passes, more bubbles disengage into free gas phase leaving the liquid oil with less entrapped gas bubbles. Furthermore, Equation 5, given in Literature Review Chapter, given by Islam and Chakma, (1990), was used to correlate the viscosity with respect to time using the measured CCE data and published viscosity

Reproduced with permission of the copyright owner. Further reproduction prohibited without permission.

Reproduced with permission of the copyright owner. Further reproduction prohibited without permission.

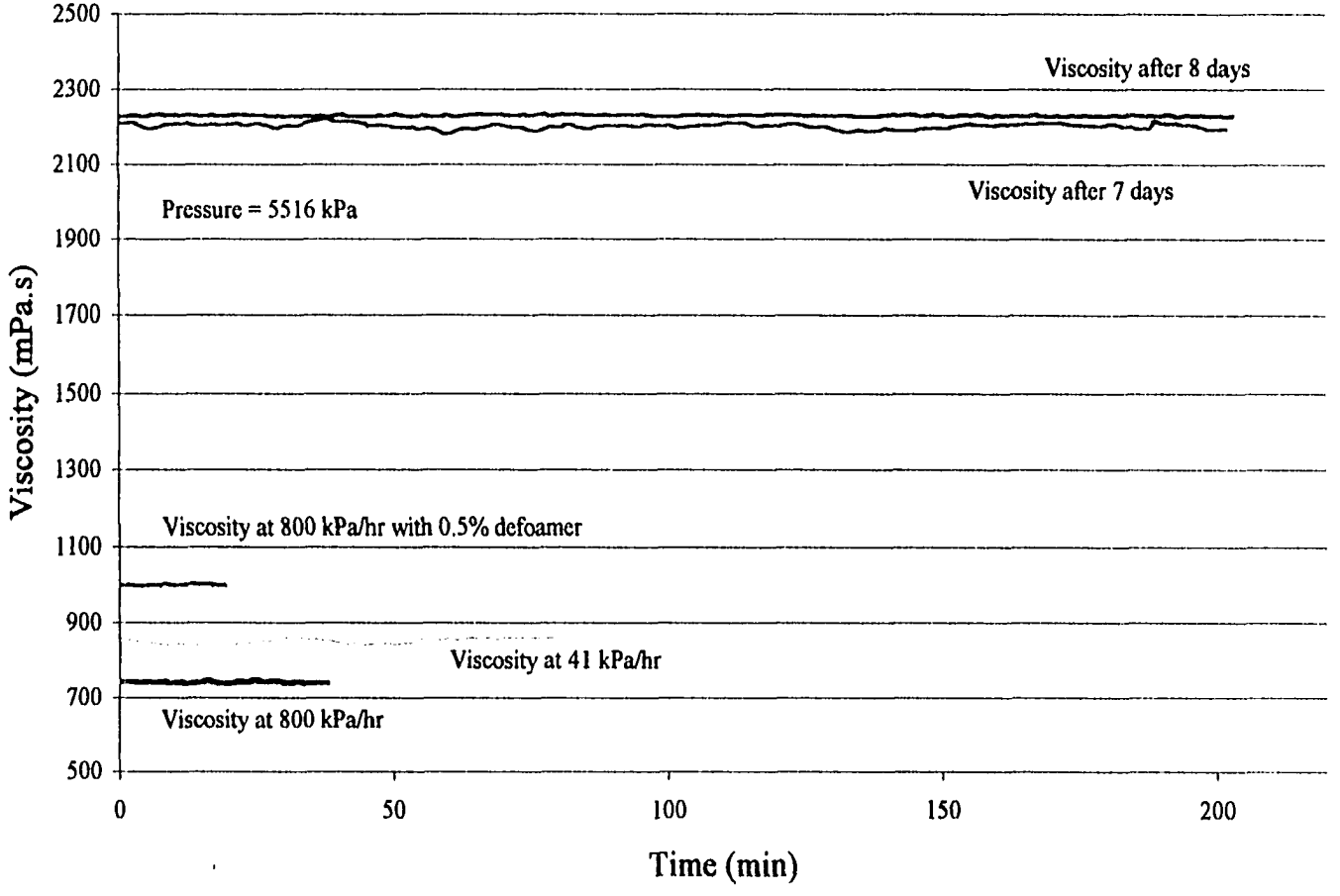

Figure 5.18 - Comparison of viscosity of foamy oil sample at different scenarios at 5516 kPa (800 psi) and room temperature.

Reproduced with permission of the copyright owner. Further reproduction prohibited without permission.

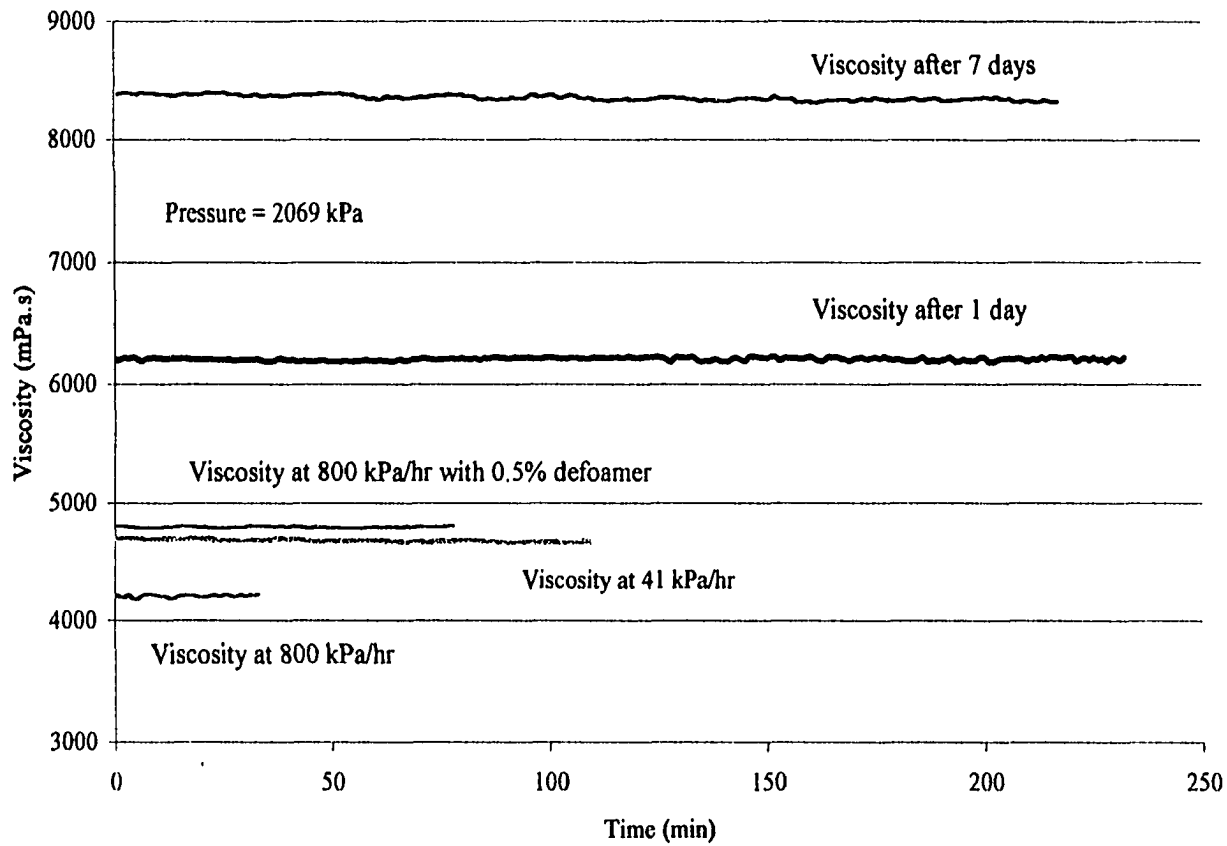

Figure 5.19 - Comparison of viscosity at 2069 kPa (300 psi) for the same oil sample for different scenarios as a function of time.

Reproduced with permission of the copyright owner. Further reproduction prohibited without permission.

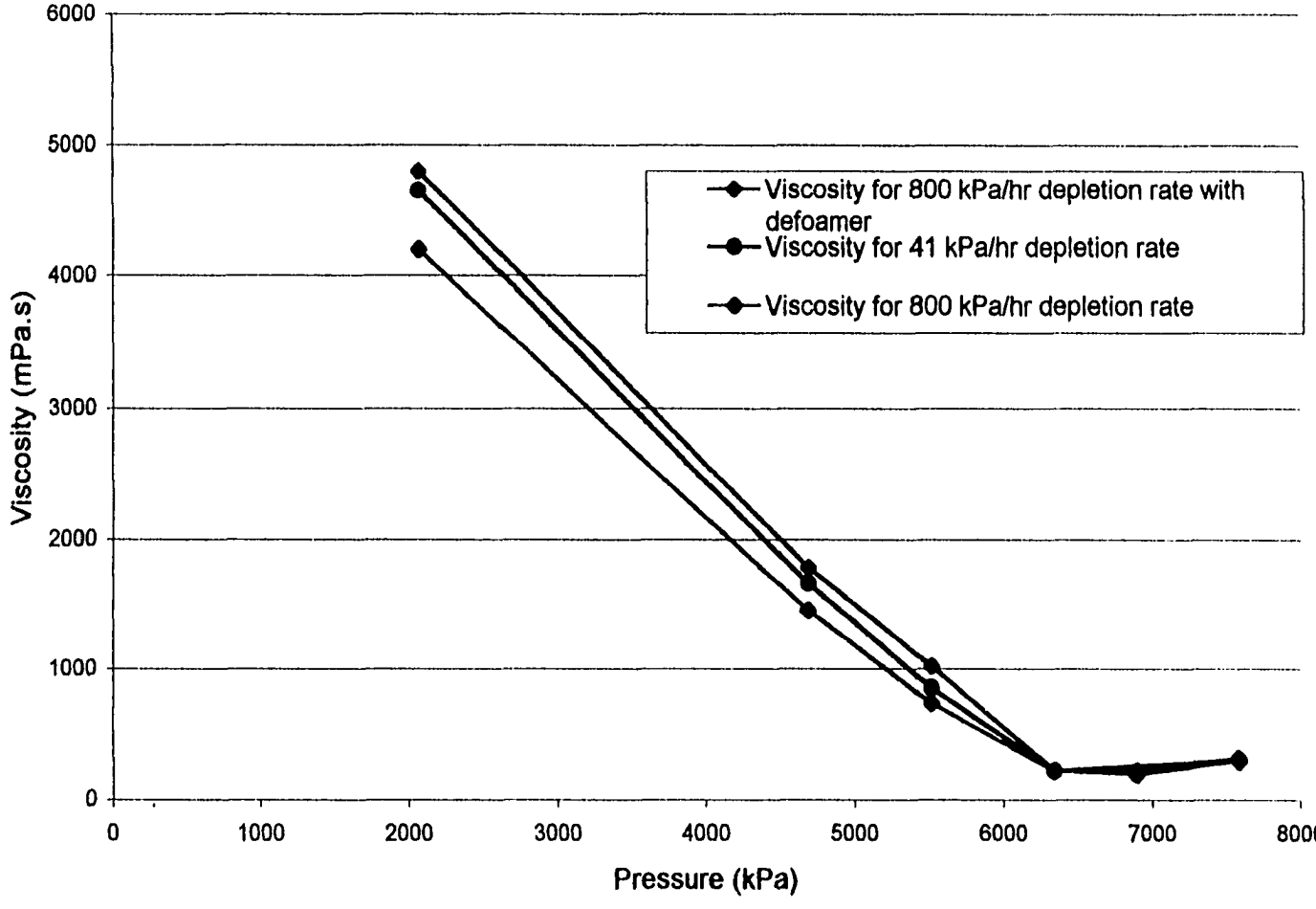

Figure 5.20 - Comparison of viscosity of foamy oil as measured by Cambridge viscometer for different depletion rates.

data for CO_2. First, a relationship of the dispersed phase with respect to pressure was found from the difference of the apparent solution gas oil ratio between the 0.5% defoamer with mixing left for 7 days and the 0.5% defoamer with mixing cases. After obtaining a relationship for the dispersed gas phase with respect to pressure, and knowing the time for the longer experiment (7 days), a linear relationship for disengagement of the dispersed gas phase was assumed with respect to time. Moreover, the assumption was made that the viscosity of foamy oil at the end of seven days represented the live oil viscosity. The viscosity at 2068 and 5516 kPa (300 and 800 psi) as a function of time is shown in Figure 5.2 1. The equation gave good agreement with the experimentally determined viscosities. The predicted value was within 16% of the measured viscosity value at 5516 kPa.

Conditions of Viscosity Measurements	Viscosity at 2068 kPa (mPa.s)	Viscosity at 5516 kPa (mPa.s)
After 1 day	6200	
After 7 days	8350	22300
After 8 days		22000
800 kPa/hr	4200	7400
800 kPa/hr, 0.5% (vol.) defoamer	4800	10000
41 kPa/hr	4680	8500

Table 5.2 – viscosity as measured by Cambridge viscometer.

5.2.2 Viscosity of Foamy Oil as Measured by Capillary Viscometer

Viscosity of foamy oil was simultaneously measured by Cambridge and capillary viscometer during the same pressure depletion process. This was done to minimize the disturbances in foamy oil properties, if any, especially to keep constant the quantity of

Reproduced with permission of the copyright owner. Further reproduction prohibited without permission.

Reproduced with permission of the copyright owner. Further reproduction prohibited without permission.

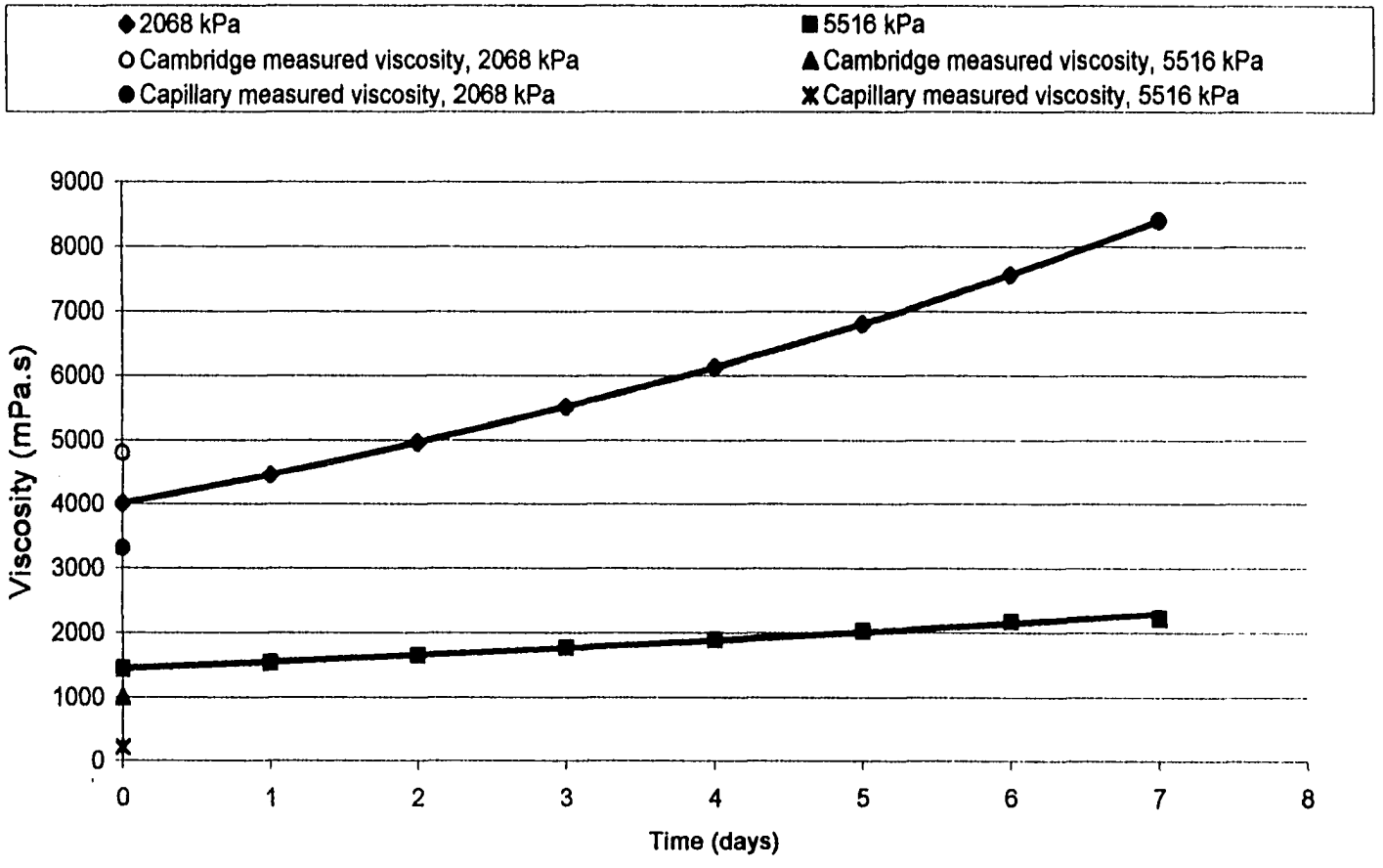

Figure 5.21- Predicted viscosity using experimental data and Islam

dispersed gas phase during any given pressure depletion run. When the pressure where the viscosity sought was reached in the PVT cell during the depletion process, a sample of about 9 cm^3 was transferred at constant pressure from the bottom of the PVT cell into the capillary tube and the two cylinders. In order to measure the viscosity in the capillary tube, the foamy oil sample was circulated through the capillary tube from one cylinder to the other using an opposed pump set at the desired flow rate. Pressure drop across the capillary tube was measured by Validyne transducer. When possible, viscosity was measured at more than one flow rate. The viscosity was measured at room temperature, and two different pressure depletion rates, 41 and 800 kPa/hr. The viscosity measurements for both depletion rates are shown in Figure 5.22. The viscosity did not show the same separation between the different runs as it was with the Cambridge measured viscosity. Moreover, the measured viscosities at different depletion rates were within 5% from each other. This renders the capillary viscometer measured viscosity for all cases to be the same or within an experimental error of 5%. This could be caused by the insensitivity of the capillary viscometer to detect the different dispersed gas phase scenarios. It is worth noting that occasionally during viscosity measurements, slugs of gas were observed (pressure transducer did not register any pressure difference) to flow through the capillary tube. This happened when the oil samples were circulated several times through the capillary tube. Pressure vs. flow rate was found to be linear which indicated a Newtonian fluid behaviour, therefore, the viscosity appeared to be independent of shear rate. Furthermore, the viscosity data were modeled using power law and the exponent was found to be one, which meant to obey Newtonian fluid model.

5.2.3 Viscosity of Foamy Oil as Measured by Haake RV-2 Viscometer

Haake viscometer was used to measure the viscosity of foamy oil. The measurement was done differently than the viscosity measurements carried out in the capillary and Cambridge viscometers. The depletion process was performed inside the viscometer chamber. This was done due to the large volume of oil required (950 cm^3)

Reproduced with permission of the copyright owner. Further reproduction prohibited without permission.

Reproduced with permission of the copyright owner. Further reproduction prohibited without permission.

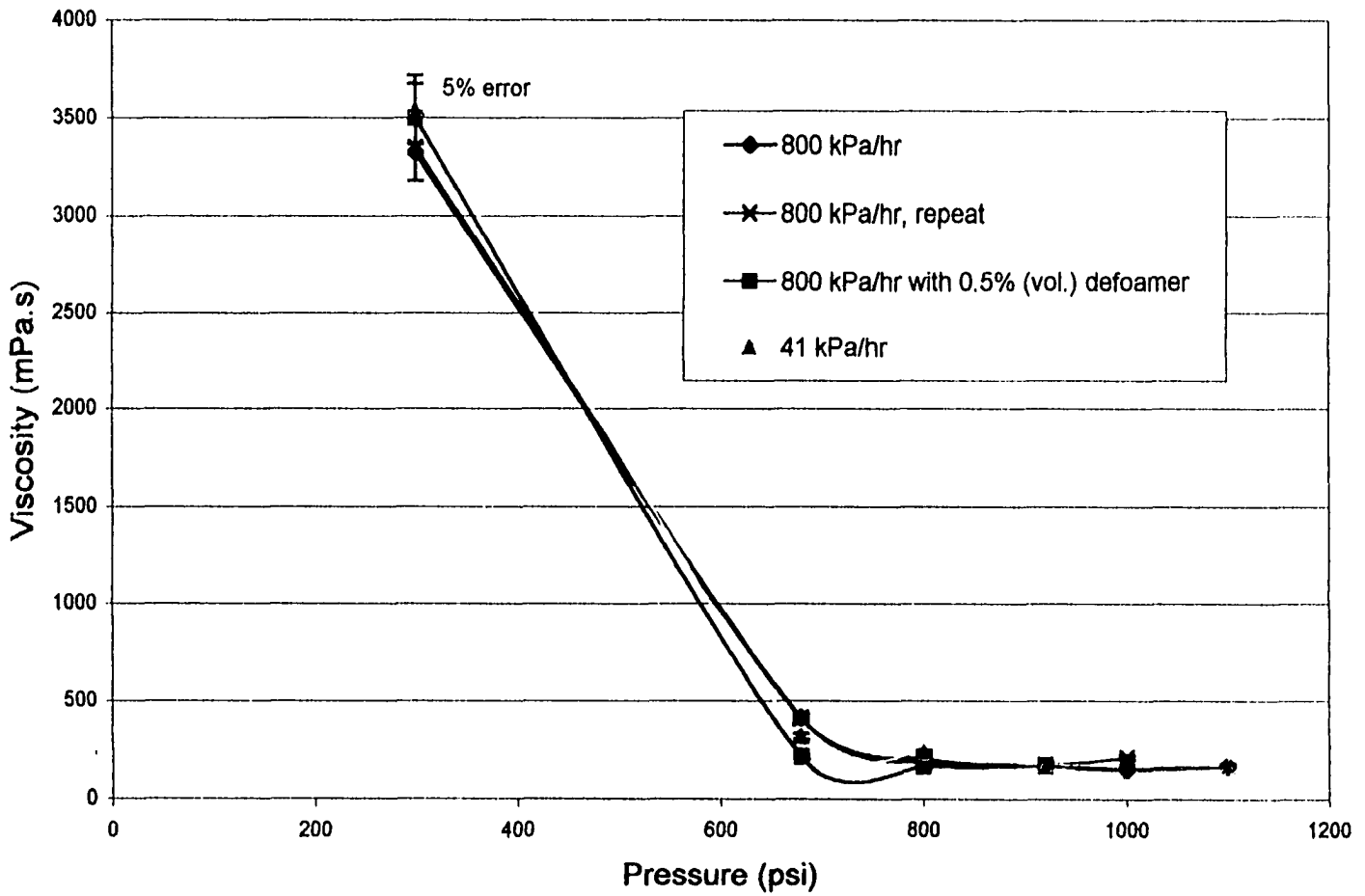

Figure 5.22 - Viscosity as measured by capillary viscometer at different depletion rates and room temperature.

to fill the viscometer chamber for one viscosity point measurement; and the PVT cell was not large enough to handle the required sample volume. The measured viscosity was not successful due to the free gas phase developing inside the chamber. Although the viscosity trend was apparent, the numerical values were very low as compared with the viscosity as measured by the other two viscometers. The measured viscosity for two pressure depletion rates, 800 and 41 kPa/hr are presented in Figure 5.23.

5.2.4 Comparison of the Three Viscometers

Figures 5.24 and 5.25 show the viscosity at 41 and 800 kPa/hr (6 and 116 psi/hr) as measured by the Cambridge and capillary viscometers as well as Haake measured viscosity. As can be seen in Figures 5.24 and 4.25, all viscometers measured the same single-phase viscosity. Below the bubble point pressure, the Cambridge viscometer measurements were higher than the capillary and Haake viscometer. This is possibly due to insensitivity of the capillary viscometer to the disperse phase. As was explained earlier, the Haake viscosity results were unreliable due to the method employed in measuring the viscosity.

Foamy oil is a two-phase system. Therefore, measured values of viscosity are only apparent single-phase viscosities of the two-phase system. These apparent viscosities may be a function of the nature of the dispersion, the geometry of the measuring device and P, T, and shear conditions of the measurements. In the case of these experiments, the nature of the dispersion is also changing with time.

We were not able to observe the system in either the Cambridge or the capillary viscometers. We cannot be certain that the nature of the dispersion was the same as observed in the PVT cell (i.e. bubble size and number, presence of free gas phase). If the presence of a dispersed gas phase in foamy heavy oil results in lower viscosity, the Cambridge viscosity results correlate better to the observed behaviour in the PVT cell. The observation that the capillary viscometer was insensitive to entrained gas volume fraction could be explained two ways. First the geometry of the capillary may result in apparent viscosity of these systems showing less sensitivity to amount of dispersed

Reproduced with permission of the copyright owner. Further reproduction prohibited without permission.

Reproduced with permission of the copyright owner. Further reproduction prohibited without permission.

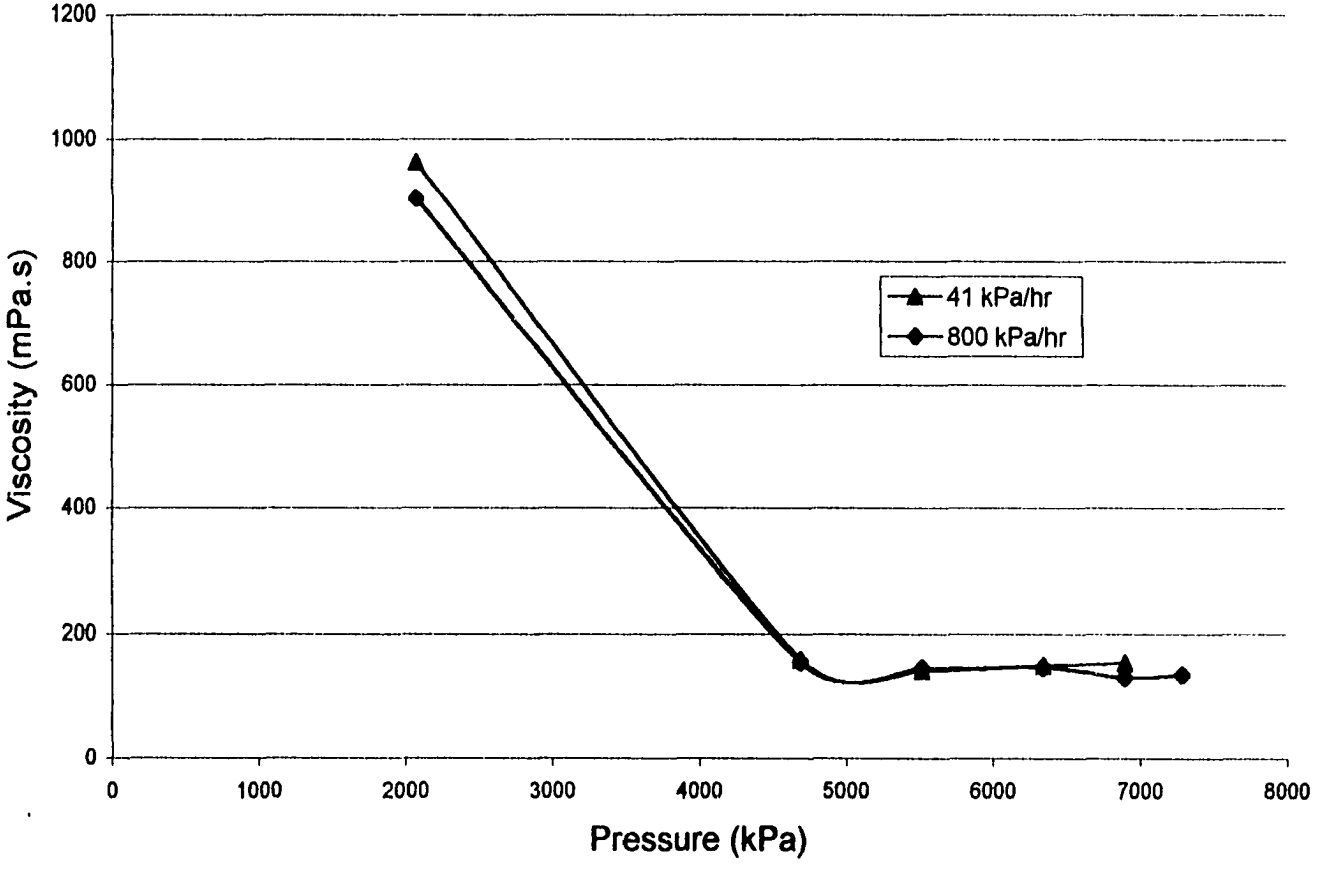

Figure 5.23 - Comparison of Viscosity measured by Roto Viscometer at a Depletion Rate of 800 and 41 kPahr

Reproduced with permission of the copyright owner. Further reproduction prohibited without permission.

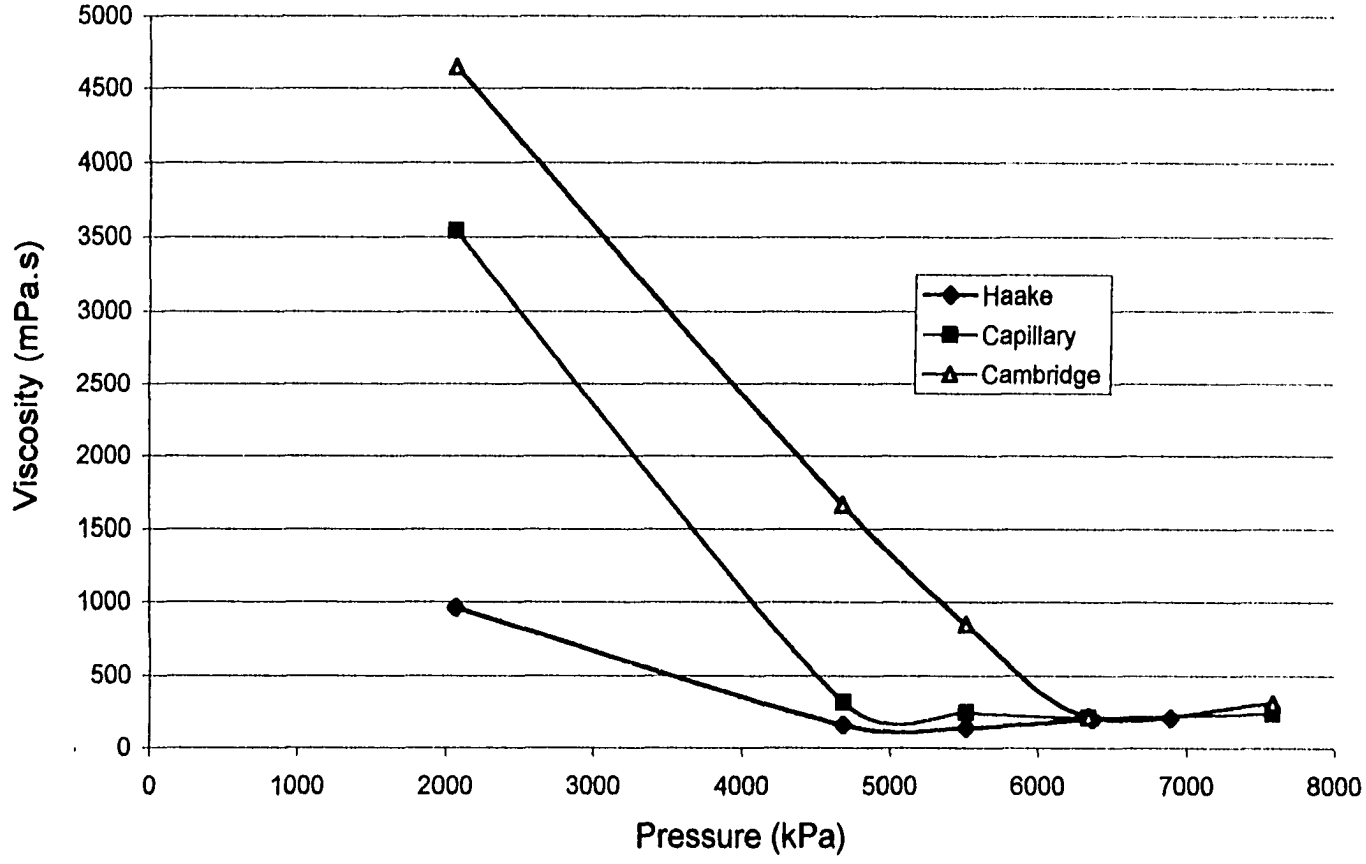

Figure 5.24 - Comparison of viscosity as measured by three viscometers at 41 kPa/hr

Reproduced with permission of the copyright owner. Further reproduction prohibited without permission.

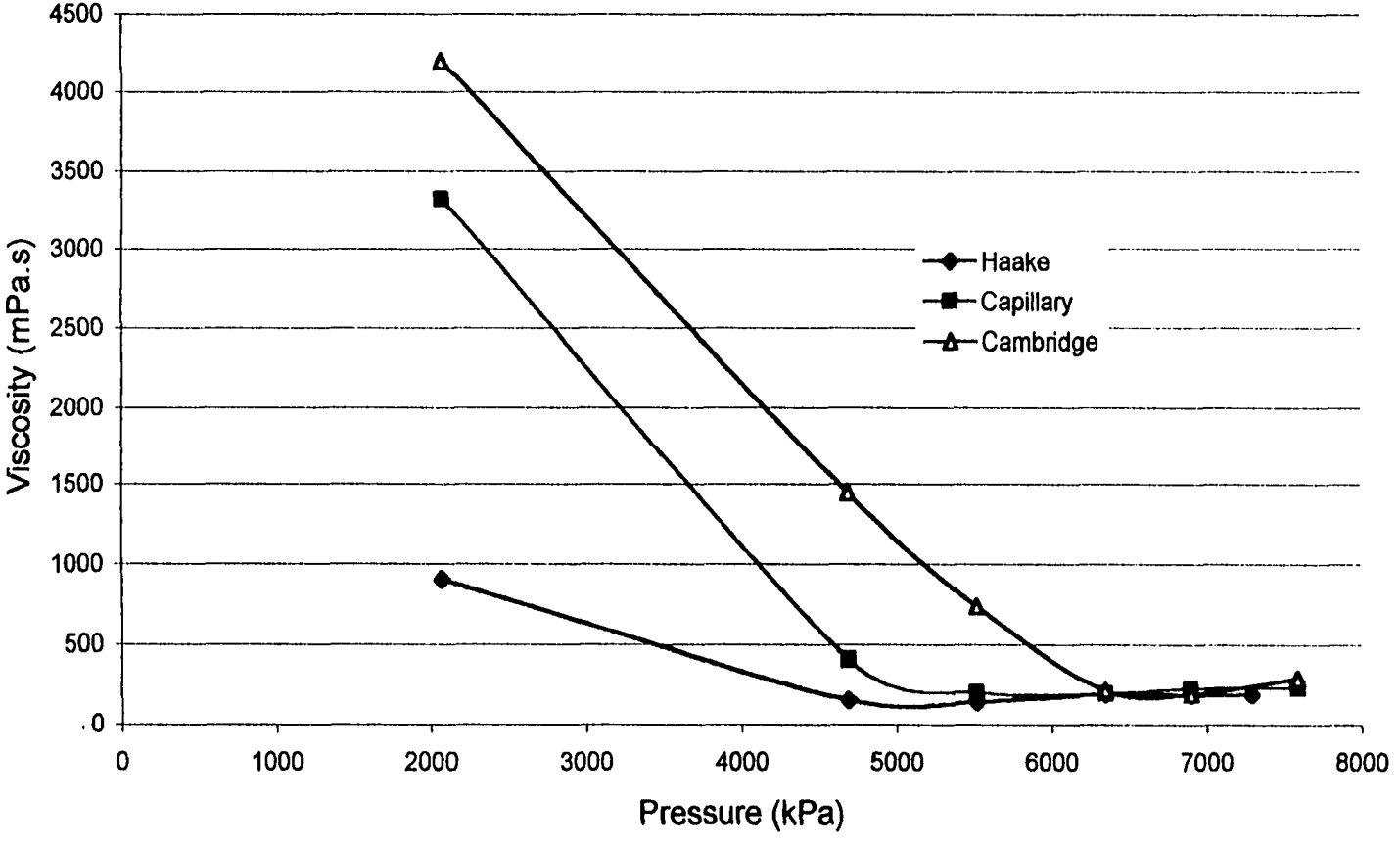

Figure 5.25 Comparison of viscosity as measured by three viscometers at 800 kPa/hr.

gas phase. This may be true if the capillary diameter is much larger than the bubble diameter. Another possibility is that the dispersion changes in the capillary. There was some evidence of phase separation in these runs.

5.2.5 Derivation of Foamy Oil Viscosity

Due to the complicated nature of foamy oil and the interaction of gas bubbles and pore geometry, it would be difficult to obtain a theoretical derivation of foamy oil viscosity. The following is an attempt to derive foamy oil viscosity and it is intended for illustration purposes to show (under restrictive assumptions) whether the foamy oil viscosity is lower or higher than the continuous oil phase viscosity.

The following assumption was made. Poiseuille's law is valid in capillary for oil and gas phases. The velocity distribution as given by Poiseuille's law for single oil phase in capillary tube is:

$$v_o = \frac{(r_c^2 - r^2)\,\Delta p}{4\mu_o L}, \quad \text{.....(22)}$$

and the velocity of the gas phase is given as:

$$v_o = v_{or_b} + \frac{(r_b^2 - r^2)\,\Delta p}{4\mu_g L}, \quad \text{.....(23)}$$

Where r_c is the radius of the capillary, r_b is the radius of the gas bubble, r is the position from the centre of the capillary, v_{or_b} is the velocity of the oil phase as $r = r_b$; Δp is the pressure drop along the capillary length, L, and μ_o and μ_g are the viscosities of oil and gas, respectively. Figure 5.25ab shows the distribution of the above velocities. The bubbles are assumed dispersed in the centre of the capillary and moving faster than the oil velocity as shown in Figure 5.25ab. The volumetric flow rate of the foamy oil, q_{fo}, is:

$$q_{fo} = \int_{r_b}^{r_c} \frac{(r_c^2 - r^2)\,\Delta p}{4\mu_o L})\,(2\pi r\,dr) \quad + \quad \int_0^{r_b} (v_{or_b} + \frac{(r_b^2 - r^2)\,\Delta p}{4\mu_g L})(2\pi r\,dr) \quad \text{.....(24)}$$

Reproduced with permission of the copyright owner. Further reproduction prohibited without permission.

Reproduced with permission of the copyright owner. Further reproduction prohibited without permission.

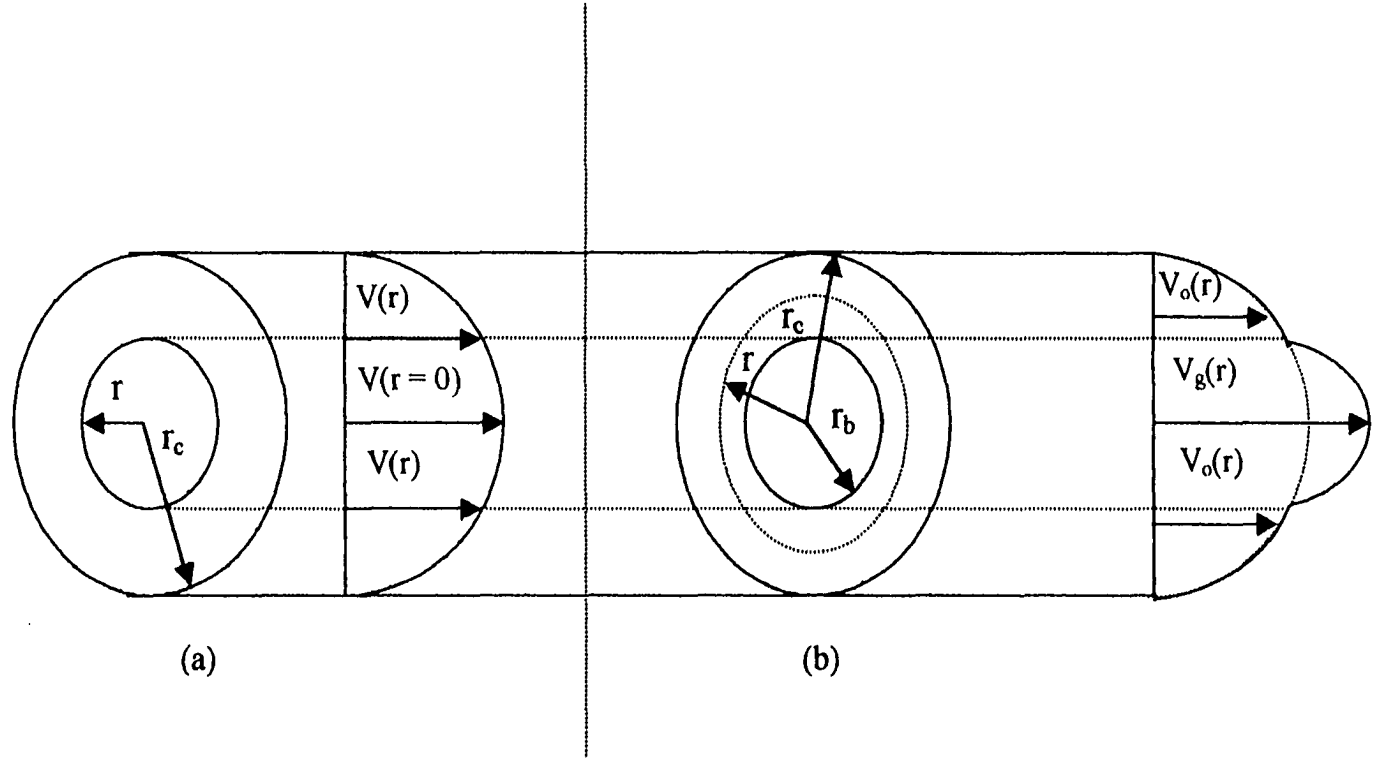

Figure 5.25ab Velocity distribution in a capillary for a) single oil phase, b) foamy oil phase.

$$q_{fo} = \frac{\pi(r_c^4 - r_b^4)\Delta p}{8\mu_o L} + \frac{\pi r_b^4 \Delta p}{8\mu_g L}). \quad \text{.....(25)}$$

Now, if the foamy oil is considered a pseudo-single phase, then the volumetric flow rate is:

$$q_{fo} = \frac{\pi r_c^4 \Delta p}{8\mu_{fo} L}, \quad \text{.....(26)}$$

Equating Equations 25 and 26,one gets

$$\mu_{fo} = \frac{\mu_o}{\left[1 + (\frac{r_b^4}{r_c^4})(\frac{\mu_o}{\mu_g} - 1)\right]}. \quad \text{.....(27)}$$

The above equation shows that the viscosity of foamy oil is reduced due to gas bubble dispersion in the oil phase.

Reproduced with permission of the copyright owner. Further reproduction prohibited without permission.

5.3 Discussion of Micromodel Experimental Results

This section presents the micromodel experimental results. The micromodel was used to investigate bubble nucleation, growth, and coalescence as well as the effect of different porous media on the foamy oil flow mechanism. When a porous medium was used, the micromodel was packed with Ottawa sand or Cryolite. Table 5.3 below summarizes the micromodel runs. In all the micromodel runs, gas/oil phases were present. No water phase was present in any micromodel run. The same recombined oil was used in all micromodel runs. All experiments were performed at room temperature of 22 °C ± 0.5 °C.

Run No.	Pressure Depletion Rate (kPa/hr)	Sand	Cryolite	0.5% Defoamer Added
1	800	No	No	No
2	800	No	No	No
3	41	No	No	No
4	41	No	Yes	No
5	800	No	No	Yes
6	800	No	Yes	No
7	800	No	Yes	Yes
8	800	Yes	No	No
9	41	Yes	No	No

Table 5.3 – Runs performed in the micromodel.

Reproduced with permission of the copyright owner. Further reproduction prohibited without permission.

5.3.1 Micromodel Experiments with No Porous Media

A set of micromodel runs was performed with no porous media present. The purpose of this set of experiments was to test the micromodel and to verify that the micromodel would give the same results as those performed in the PVT cell. Moreover, duplicating some of the PVT-cell-CCE runs would permit visualization of the process of foamy oil solution gas drive. Four runs were carried out with no porous media present. Three of the runs (Runs 1, 2 and 5) were performed at a pressure depletion rate of 800 kPa/hr while the fourth (Run 3) was done at 41 kPa/hr. In runs where no porous media present, the micromodel acted as a mini-PVT cell that permitted quantification and visualization of the process of foamy oil as the micromodel was thin enough for the light to penetrate the dark heavy oil.

Run 1 was performed at a pressure depletion rate of 800 kPa/hr with no porous medium and no defoamer added. The purpose of this run was to duplicate the CCE run performed in the PVT cell and to visualize the process of foamy oil mechanism since it was not possible to observe the phenomena in the PVT cell due to the large/thick oil sample. After transferring the oil sample into the micromodel, the experiment was started by depleting the micromodel into the sapphire cell. The fluid levels were measured in the sapphire cell. Preparation and experimental procedure of the micromodel was discussed in the Experimental Set-up and Procedure, Section 4.5. The foamy oil volume (as percentage of the total volume) versus pressure curve was in good agreement with the run conducted with PVT cell with no mixing. The micromodel and PVT cell runs are shown in Figure 5.26. The visualization of the process will be discussed later. Run 2 was a repeat of Run 1 and showed that the reproducibility was good.

The next run was carried out at the same pressure deletion rate as Run 1 with the addition of 0.5% (by vol.) defoamer. Figure 5.27 shows the PVT cell run with 0.5% defoamer added and with no mixing and the same run performed with the micromodel,

Reproduced with permission of the copyright owner. Further reproduction prohibited without permission.

Reproduced with permission of the copyright owner. Further reproduction prohibited without permission.

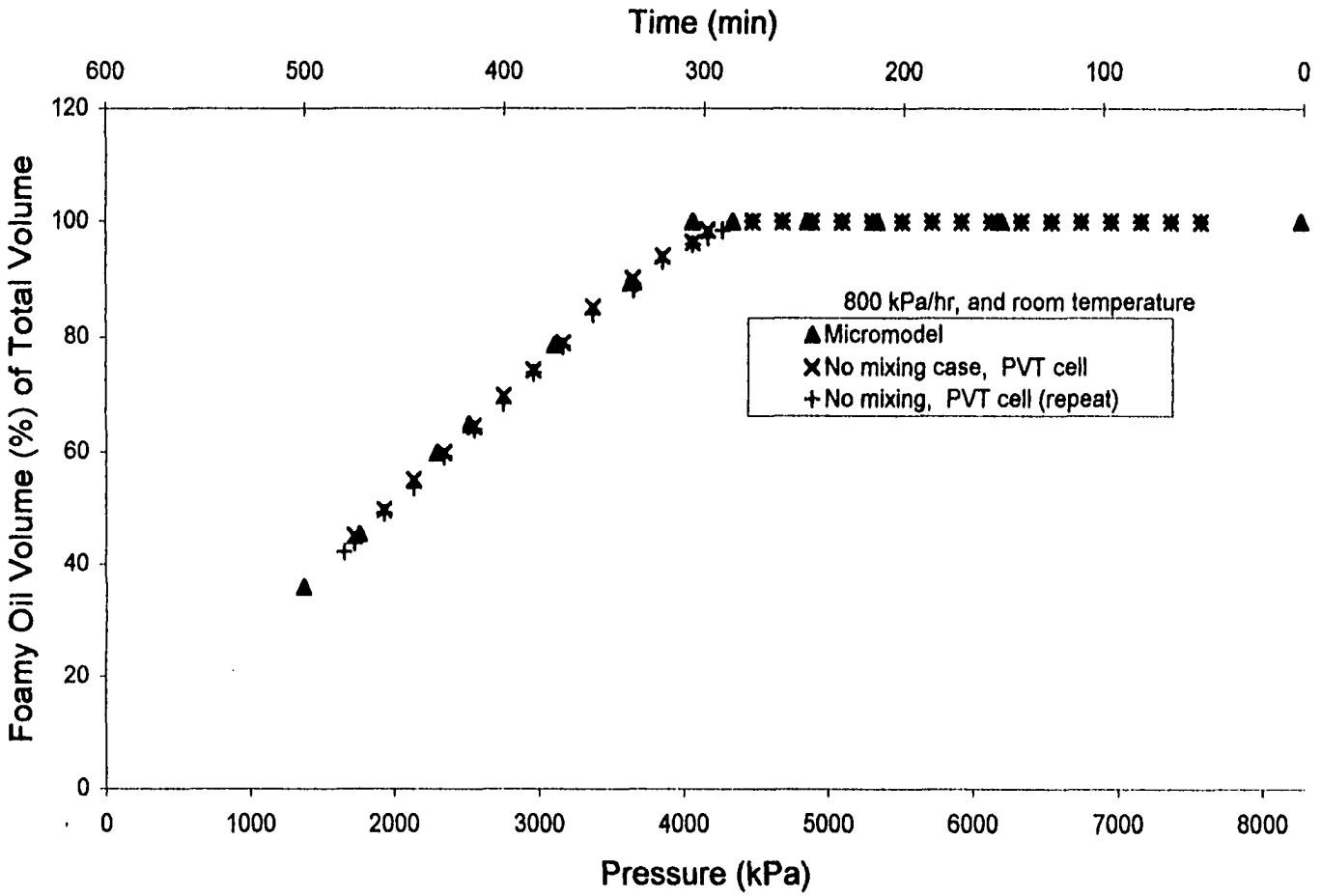

Figure 5.26 - Comparison of PVT cell CCE and micromodel pressure depletion at a pressure depletion rate of 800 kPa/hr.

Reproduced with permission of the copyright owner. Further reproduction prohibited without permission.

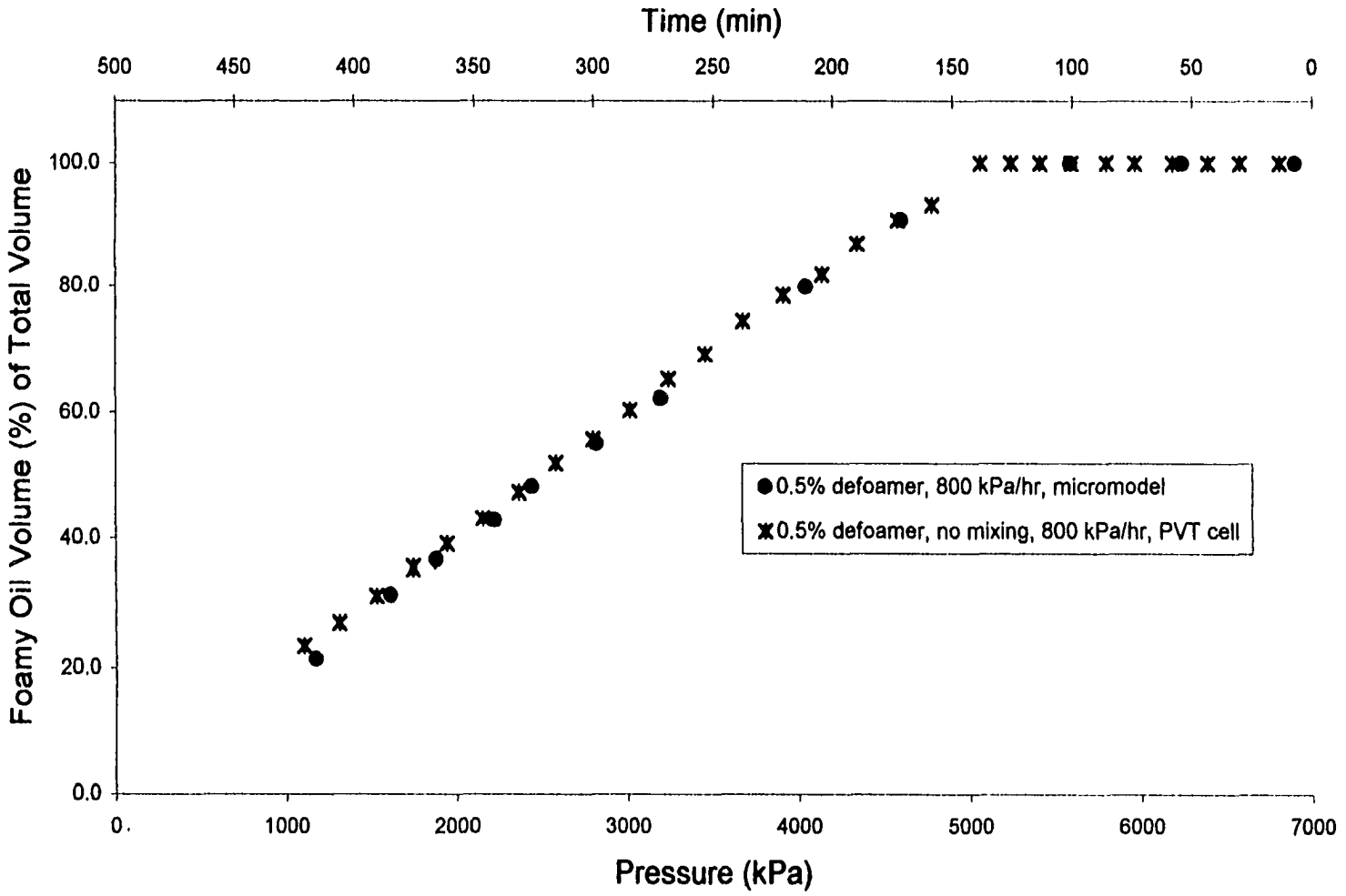

Figure 5.27. - Comparison of PVT cell CCE and micromodel runs of 0.5% defoamer at a pressure depletion rate of 800 kPa/hr.

Run 5. The graph shows the foamy oil percentage of the total volume of the two runs almost the same indicating good reproducibility.

Run 3 was the last experiment performed with no porous medium present in the micromodel. It was carried out at a slow pressure depletion rate of 41 kPa/hr. Figure 5.28 shows the data for micromodel Run 3 and the same run carried out in the PVT cell.

5.3.2 Micromodel Experiments in Presence of a Porous Medium

The rest of the micromodel experiments were performed in the presence of porous media. The micromodel was packed with either sand or Cryolite. Then the pore volume was determined using decane. Subsequently, the decane was displaced by the live oil. When 30 pore volumes were charged into the micromodel, injection was stopped. The experiment was initiated by setting the pump controlling the pressure depletion rate in motion at the desired pressure depletion rate, as explained in previous Section 4.5.1.

The first run performed in the presence of porous media was Run 4, which was done at a pressure depletion rate of 41 kPa/hr. The micromodel was packed with Cryolite. Cryolite was chosen for its highly water-wet properties (Lepski et al., 1996). To investigate the effect of pressure depletion rate on the foamy oil volume as a percentage of total volume, Run 6 was performed at a pressure depletion rate of 800 kPa/hr while the micromodel was packed with Cryolite. Figure 5.29 shows the depletion data for Runs 5 and 6. The slower depletion rate gave lower foamy oil volume as a percentage of total volume than in the case of faster depletion rate. The two curves changed slope at almost the same pressure point of 3200 kPa (464 psi). The possible explanations for this were that the critical gas saturation was not reached in both experiments until pressure declined to about 3200 kPa, or high degree of supersaturation affected the nucleation of gas bubbles. Although critical gas saturation was not measured, it could be inferred qualitatively from the visual images of the experiments. If one defines the critical gas saturation as the onset point of gas

Reproduced with permission of the copyright owner. Further reproduction prohibited without permission.

Reproduced with permission of the copyright owner. Further reproduction prohibited without permission.

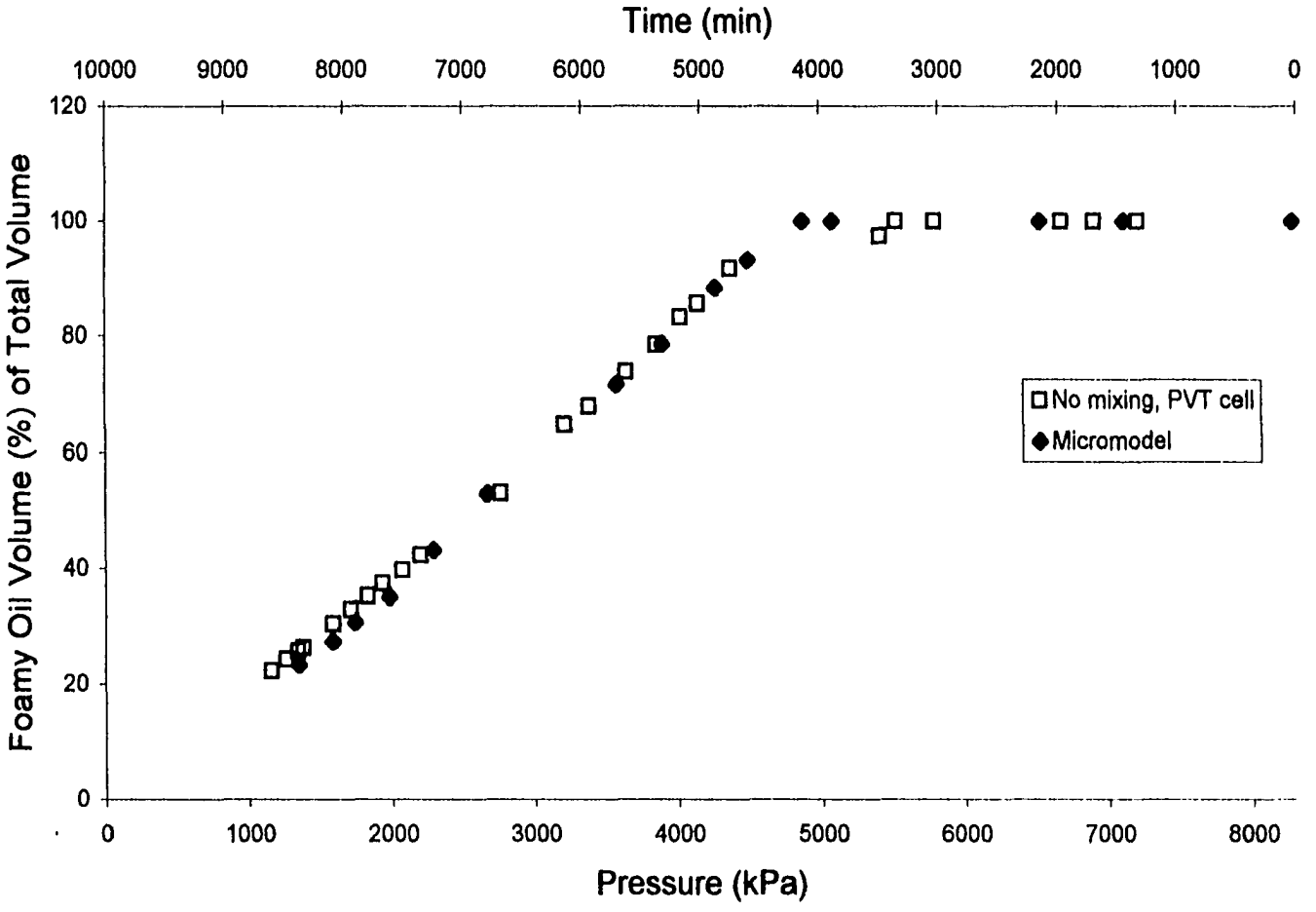

Figure 5.28 - Comparison of PVT cell CCE and micromodel run at pressure depletion rate of 41 kPa/hr.

Reproduced with permission of the copyright owner. Further reproduction prohibited without permission.

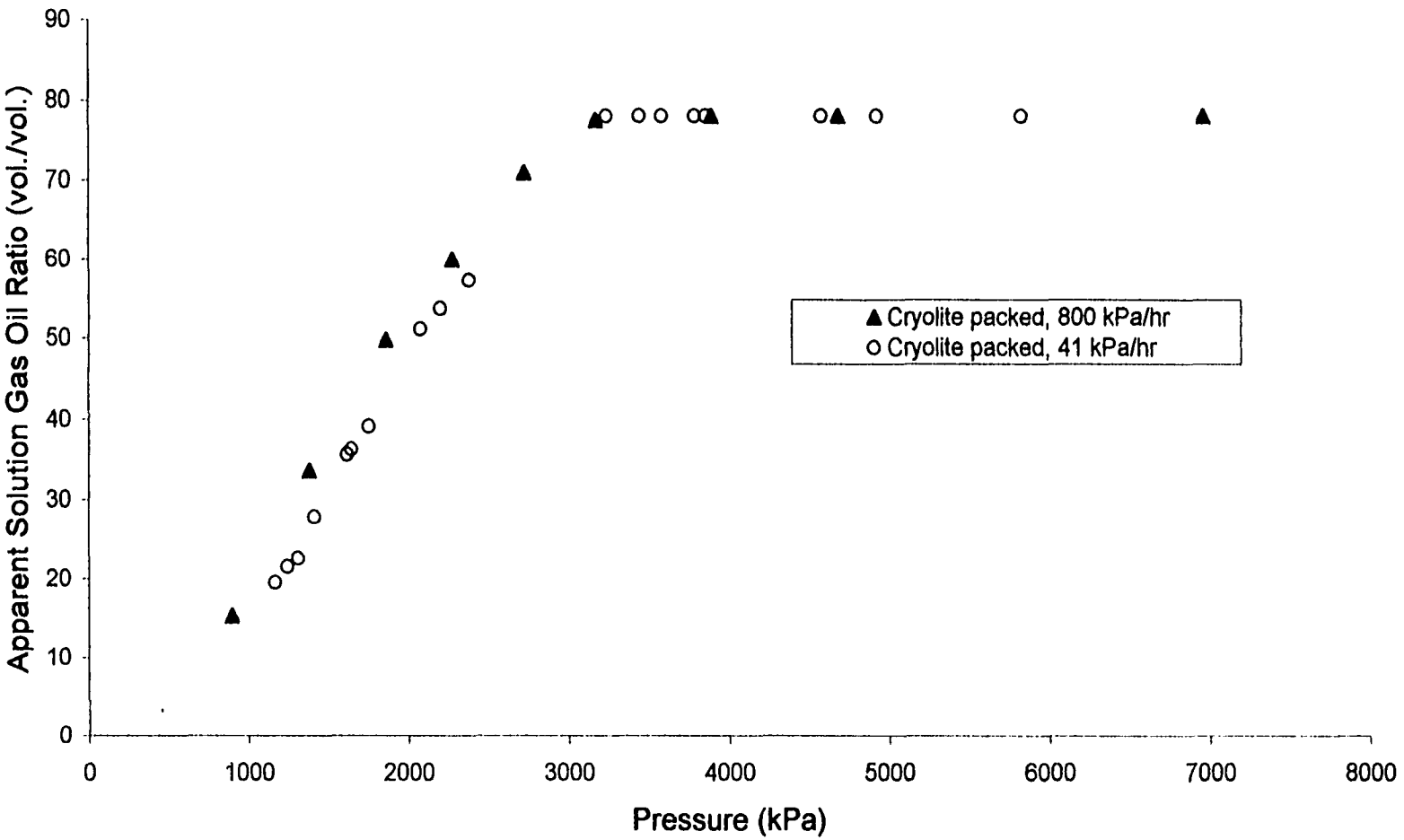

Figure 5.29 - Cryolite-packed micromodel Runs 4, and 6 at slow and fast pressure depletion rates.

production (Li and Yortsos, 1993), then critical gas saturation would be a controlling factor for the response seen in Runs 4 and 6. This will be discussed further in the next section.

To investigate the effect of gas bubble nucleation and growth a 0.5% (by volume) defoamer was added to the Cryolite run and the sample was depleted at a rate of 800 kPa/hr. Figure 5.30 depicts the depletion data of Run 7. It is redrawn for comparison purposes in Figure 5.31 along with other micromodel runs involving Cryolite. The 0.5% defoamer run resulted in lower foamy oil volume (as percentage of the total volume) than the other two runs, no defoamer added.

Sand was used in Runs 8 and 9. In both runs, sand grain size was the same. Run 8 was carried out at a pressure depletion rate of 800 kPa/hr while Run 9 was performed at a slower pressure depletion of 41 kPa/hr. Figure 5.32 plots the foamy oil volume as percentage of total volume against pressure for both runs. The slower depletion rate gave lower foamy oil volume as compared to the fast depletion rate. This is not surprising since the faster depletion rate would result in higher number of bubbles being formed, not necessarily from multiple nucleation sites as will be seen in the visual images of the runs:

Several questions need to be answered concerning the porous media packed micromodel runs.

1. Why was foamy oil volume higher in the presence of Cryolite than in sand packed micromodel?

2. did grain shape have any effect on the foamy oil process?

3. Did supersaturation contribute to the higher foamy oil volume in the Cryolite case?

These questions are answered in the following paragraphs.

Comparing the sand and Cryolite runs, Cryolite runs gave higher foamy oil volume as a percentage of total volume than runs involving sand. This could be due to the porous medium grain shape. Although the sand and Cryolite were of the same

Reproduced with permission of the copyright owner. Further reproduction prohibited without permission.

Reproduced with permission of the copyright owner. Further reproduction prohibited without permission.

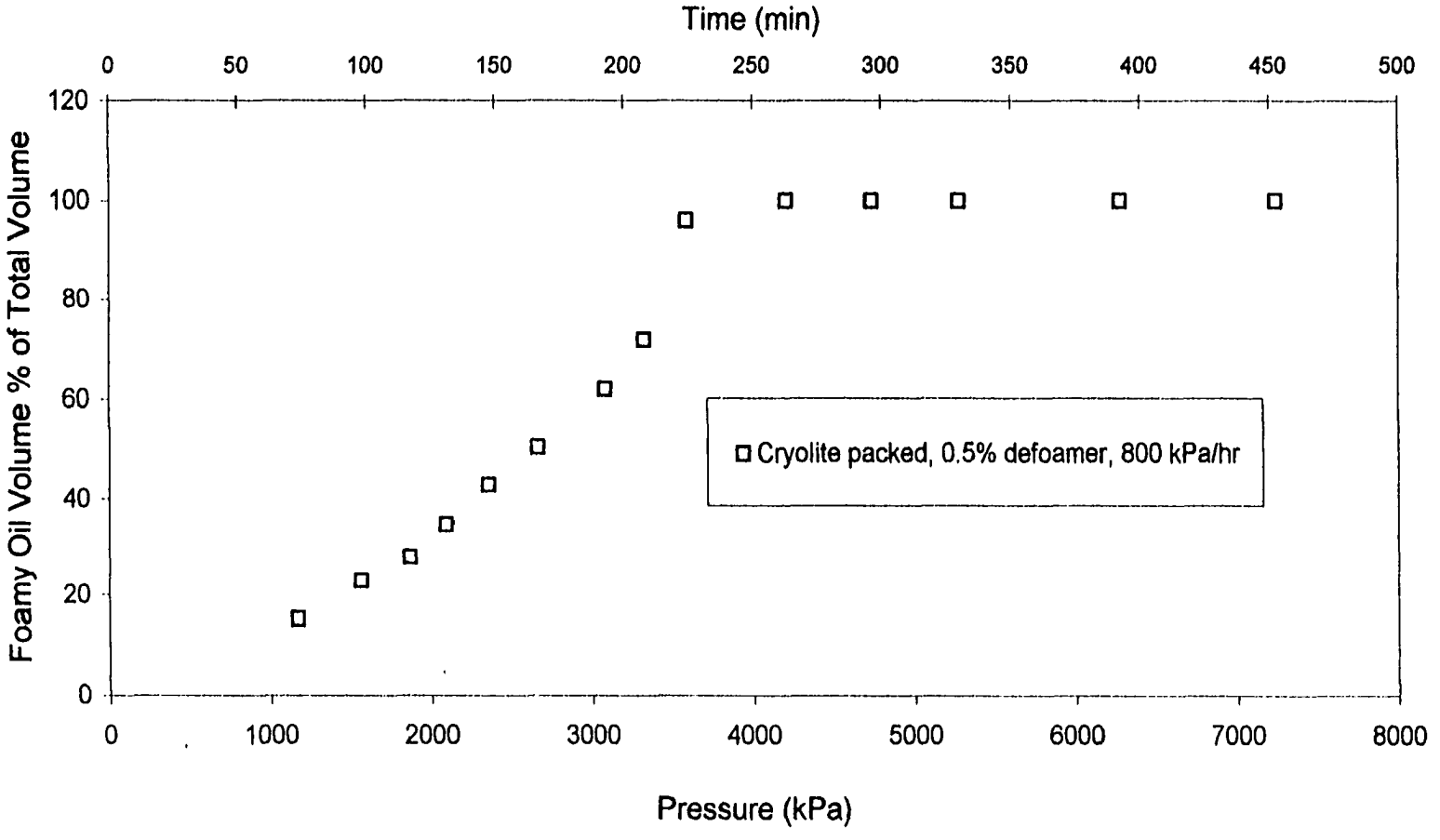

Figure 5.30 - Micromodel Run 7 depletion data.

Reproduced with permission of the copyright owner. Further reproduction prohibited without permission.

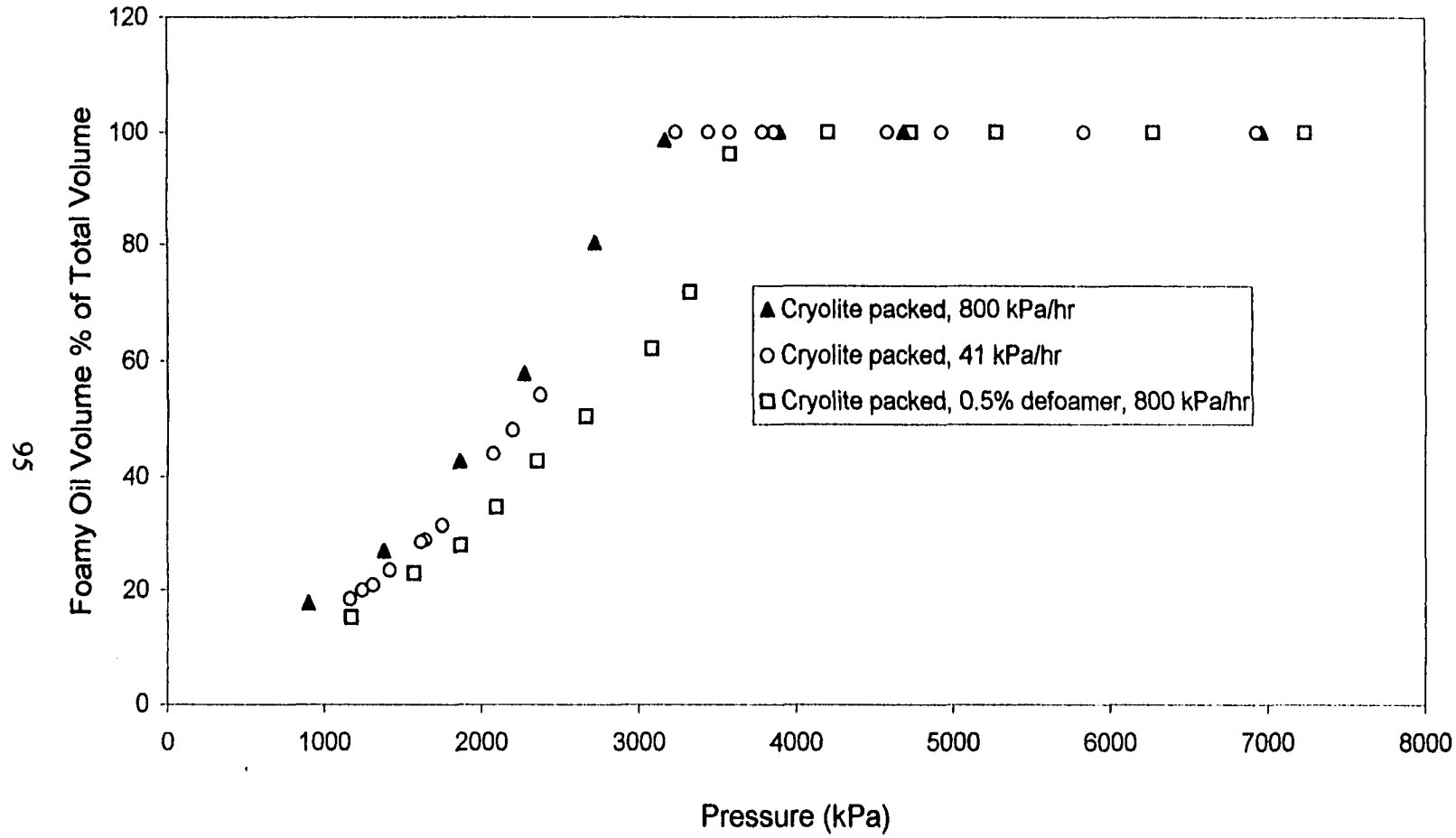

Figure 5.31 - Cryolite-packed micromodel Runs 4, 6 and 7 performed with and without the addition of defoamer and at slow and fast pressure depletion rates.

Reproduced with permission of the copyright owner. Further reproduction prohibited without permission.

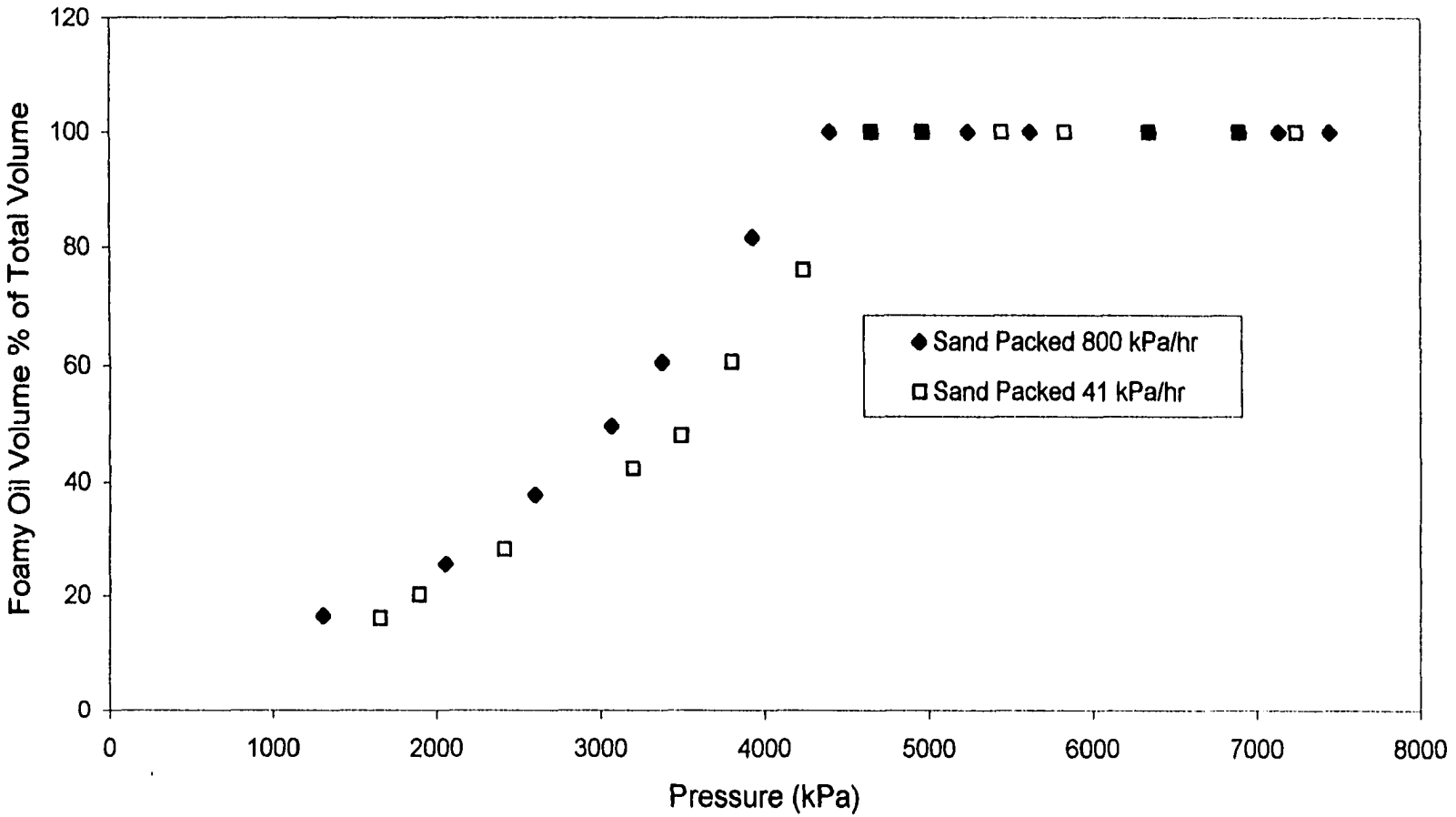

Figure 5.32 - Sand-packed micromodel Runs 8, and 9 performed at slow and fast pressure depletion rates.

mesh size, the shape of the grains were most likely different for the reason that the Cryolite was crushed in the laboratory using simple crushing techniques whereas the sand was is naturally rounded grains. Because of having different grain shape (sharper and irregular), Cryolite packed micromodel would have narrower pore throats than the sand-packed micromodel that has regular grain shapes. Therefore, in Cryolite packed micromodel, bubble/s formed within pore body walls would have to overcome a larger resistance to flow through a pore throat than in the sand case. Hence, a larger foamy oil volume would result in the Cryolite case. Figure 5.33 presents the Cryolite and sand packed micromodel depletion runs at different pressure depletion rate. Calculation of the bubble point pressure (3600 kPa, 520 psi) from the experimental data for Cryolite runs showed almost the same degree of supersaturation, 2068 kPa, 300 psi. Because of this, supersaturation would contribute to the higher foamy oil volume in the Cryolite case.

The higher foamy oil volume seen in the Cryolite case could be due to wettability problem. Figure 5.33 suggests that sand has higher wettability to oil resulting in high residual oil saturation. Hence, the foamy oil production would be lower. Cryolite, on the other hand, is not highly oil wet. This would manifests in lower residual oil saturation and higher produced foamy oil. For the Cryolite, the higher produced foamy oil volume was caused by the combination of the capillary force and by the wettability.

5.3.3 Visualization of the Foamy Oil Phenomena

Visualization of foamy oil solution gas mechanism was achieved by a specially designed micromodel that could be run with and without being packed with porous media. As was discussed in the Experimental Set-up and Procedure, Section 4.5 Micromodel Design and Set-up, two cameras and associated videotape recorder were used to record the experiments. One camera had a modified lens assembly to give a high magnification of the process while the other was used to capture an overall view of the micromodel. With the high magnification camera, the smallest bubble visible was of the order of four μm. As the depletion process started and the pressure dropped

Reproduced with permission of the copyright owner. Further reproduction prohibited without permission.

Reproduced with permission of the copyright owner. Further reproduction prohibited without permission.

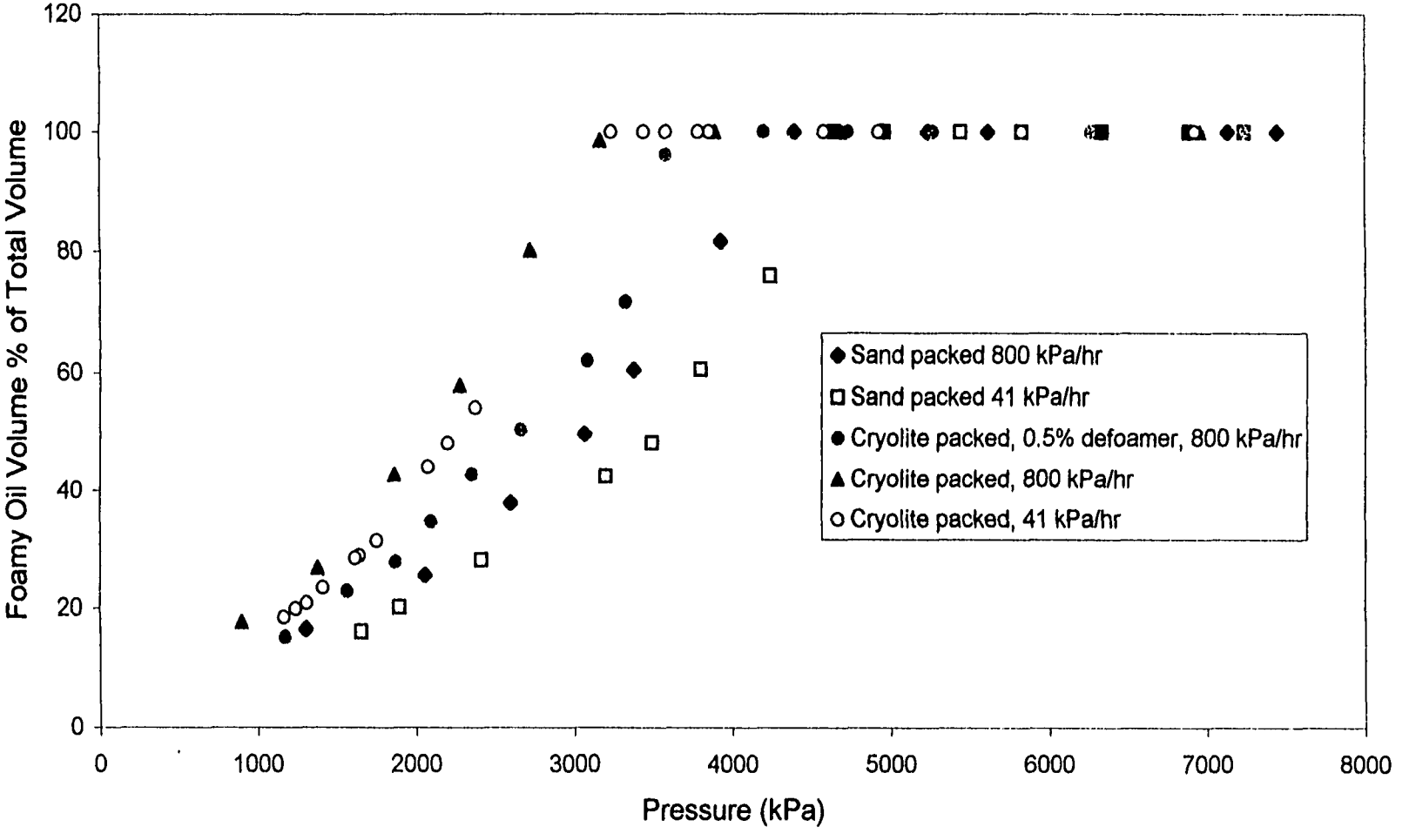

Figure 5.33 - Comparison of Cryolite and sand packed micromodel runs at slow and fast pressure depletion rates.

below the bubble point pressure, gas was clearly seen coming out of solution and forming gas bubbles at the furthest point from production outlet. This was repeated in all the experiments with and without porous media. In addition, this nucleation site was continuously active almost two-thirds of the time of experiments. While the above-mentioned nucleation site was active at the bottom of the micromodel, other parts of the micromodel showed no bubble nucleation, and that the micromodel was full of dark oil. This nucleation site was observed to be active on all micromodel runs for the fast and slow (41 and 800 kPa/hr) pressure depletion rates. As pressure dropped further to around 400 psi, other nucleation sites became active in random locations and time. This is in contrast to the prevailing and the expected notion that gas bubbles would form closest to the production outlet. One possibility of this is that there is a strong nucleation site on the micromodel. Another possibility is that the local supersaturation is higher furthest away from the production end than that close to the production outlet. It is worth noting that the micromodel was taken apart and cleaned at the end of each run. Also the polycarbonate windows were replaced at end of each run.

It was thought that a videotape would serve better to explain and show the process as it was happening in real time. Therefore, a one-hour videotape is included with this thesis. The videotape summarizes all the experiments performed in the micromodel. Due to the length of the experiments, only what was thought to be important is included in the videotape. Some still images are presented below to show the visualized foamy oil solution gas process. The videotape and its descriptions is included in Appendix B.

As the pressure dropped to a certain level below the bubble point pressure, bubbles started to nucleate. The nature of nucleation in both the fast and slow depletion process was observed to be the same in the location of the nucleation, growth and flow towards the production outlet. At the start of nucleation, bubbles were observed to nucleate at the bottom of the micromodel. This nucleation site clearly shows that

Reproduced with permission of the copyright owner. Further reproduction prohibited without permission.

nucleation is heterogeneous. Multiple bubbles were observed to nucleate from this site. Figure 5.34 shows a bubble being nucleated at the bottom of the micromodel.

(a) (b) (c)

Figure 5.34 – Bubble nucleation at the beginning the depletion process. a) bubble being nucleated, b) Bubble detachment and growth, c) Repeat of the nucleation of bubbles.

This nucleation site produced series of bubbles and remained active for a considerable length of time. This means that the nucleation is not instantaneous, but rather progressive where new bubbles continued to nucleate later in the depletion process. Following this, a transition period when nucleation at this site slowed down and eventually became inactive. After that, other random nucleation sites become active. In this stage of nucleation, multi-bubbles were seen to spring-out throughout the micromodel. This was repeated randomly throughout the micromodel. In this stage, the nucleated-bubbles initially had spherical shape, and stayed still until they reached a certain size. They grow through coalescence and diffusion. The moment they start to move, their shapes changed from spherical to elongated ones. They move to the closest pressure sink. In most cases, they would flow perpendicular to the production outlet direction and towards a lager moving bubble or train of bubbles. Also, during this nucleation stage, it was observed that in the vicinity of a larger moving bubble nucleation did occur. Moreover, nucleation was observed to occur behind a larger moving bubble, where supposedly the supersaturation was the lowest as the

Reproduced with permission of the copyright owner. Further reproduction prohibited without permission.

supersaturation was decreased due to the diffusion of gas into the larger bubble. In some of these nucleation events, bubbles seemed to come out from the bulk liquid oil. If one considers each nucleation site separately, this stage resembles an instantaneous nucleation, where bubbles would nucleate, and then grow. However, the overall depletion is certainly not. Figures 5.35, 5.36 and 5.37 show spherical multi-bubbles nucleated during this stage.

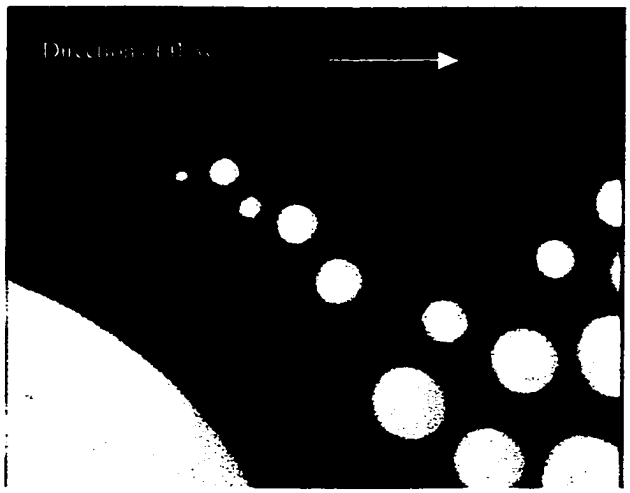

Figure 5.35 – Spherical bubbles being nucleated

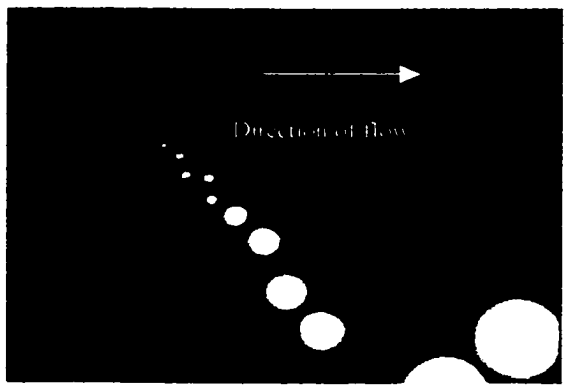

Figure 5.36 – Spherical bubbles being nucleated near a larger moving bubble.

Reproduced with permission of the copyright owner. Further reproduction prohibited without permission.

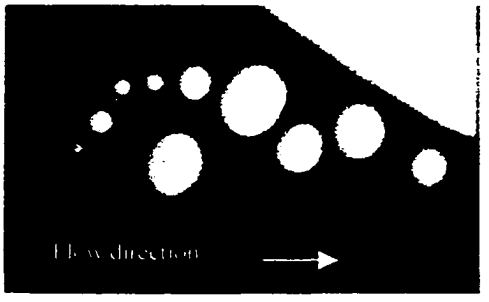

Figure 5.37 – Spherical bubbles being nucleated behind a larger moving bubble

Next, a ramified pattern occurred throughout the micromodel in random locations. This stage was the last stage of depletion process. The captured continuous images of this stage are shown in the videotape at videotape counter number of 477 to 525.

In micromodel runs performed in the presence of porous media, nucleation also started at the bottom of the micromodel, furthest point away from the production end. Few images at the pore level were taken with the high magnification camera, it was decided that an overall picture showing the flow of gas towards the production end would be more useful. So, in runs involving porous media, most of the process was recorded using the video camera showing the entire micromodel visual area. The images of the runs carried out in the presence of porous media are included in the videotape and a few are reproduced here to show the solution gas process. The images are for the 800 kPa/hr depletion rate performed in the presence of Ottawa sand. Figures 5.38, 5.39, 5.40, and 5.41 below show the growth of gas phase during the pressure depletion run in the micromodel. The micromodel was positioned vertically and the production end was at top of the micromodel.

Reproduced with permission of the copyright owner. Further reproduction prohibited without permission.

Figure 5.38 – Initial condition of the sand-packed micromodel at a pressure of 6895 kPa (1000 psi), flow was from left to right, top to bottom.

Figure 5.39 – Growth of gas phase at a pressure of about 4137 kPa (600 psi), flow was from left to right, top to bottom.

Figure 5.40 – Growth of gas phase at a pressure of 3450 kPa (500 psi) , flow was from left to right, top to bottom.

Figure 5.41 – Growth of gas phase at a pressure of 2415 kPa (350 psi).

Reproduced with permission of the copyright owner. Further reproduction prohibited without permission.

Observations from the visual micromodel experiments show that at the beginning of the depletion process (below the bubble point pressure), bubbles nucleated on the wall at one nucleation site. In micromodel experiments where no porous medium was present, these different stages were more apparent than with porous media. The nucleated bubbles were initially spherical and later elongated and formed very long oval shaped bubbles. The elongation could be caused by the geometry of the micromodel. This very long bubble had variable width, as narrow as one to two grains and as wide as 10 grains. The long bubbles followed the same path to the production outlet. Moreover, towards the end of the depletion process, the nucleation and growth patterns change to random and throughout the whole micromodel. At this stage, growth became ramified "tongues" of gas patterns and not spherical or individual bubbles. The experiment was continued until the micromodel was filled with gas.

In the absence of foamy oil phenomena, one would expect that there would not be any difference in the production response when a defoamer is added. Also, it was observed that the pressure response when a defoamer was added was different than when no defoamer was involved. In the defoamer case, pressure at the outlet end fluctuated wildely due to the production of gas slugs. This pressure response was not seen in any of the other runs which did not involve the addition of defoamer.

Reproduced with permission of the copyright owner. Further reproduction prohibited without permission.

5.4 Discussion of Sand Pack Experimental Results

The last part of this study was the sand pack experiments. Two sand pack coreholders were used. The first was a 125 cm long and 4.75 cm in diameter and the second was 60 cm long and 7.6 cm in diameter. The same recombined oil was used in all of the sand pack depletion experiments. The absolute permeability of the sand packs was around 12 darcies. After the absolute permeability was determined, water was displaced using dead oil to establish the irreducible water saturation. Then the dead oil was displaced by the recombined Lloydminster oil (live oil). During the recombined oil injection, a back pressure regulator was used for controlling the pressure at the outlet end of the sand pack. The injection of the dead and live oil was done at a very slow injection rates due to the high injection pressure caused by the high viscosity of the dead oil and by the back pressure which was above the initial pressure of the depletion experiment, 6895 kPa (1000 psi). The backpressure was set above the initial pressure of the experiment to insure that there was no gas flashed out during the saturation process.

It was already established in the PVT and micromodel runs that addition of defoamer to the recombined oil altered the process of foamy oil by lowering the dispersed gas phase. The result of this was a lower foamy oil production. The purpose of these sand pack depletion experiments was to investigate the effect of the defoamer on the foamy oil process, and to investigate production of foamy oil at very slow depletion rate, 103 kPa/day (15 psi/day).

The first depletion run was performed in the long sand pack at a slow pressure depletion rate of 103 kPa/day (15 psi/day). Figure 5.42 shows the production history of this run. The cumulative oil production was 175 cc, giving a recovery factor of 22% pore volume, PV. This run showed that at a low-pressure depletion rate, production of reasonably high foamy oil recovery was possible.

Reproduced with permission of the copyright owner. Further reproduction prohibited without permission.

Reproduced with permission of the copyright owner. Further reproduction prohibited without permission.

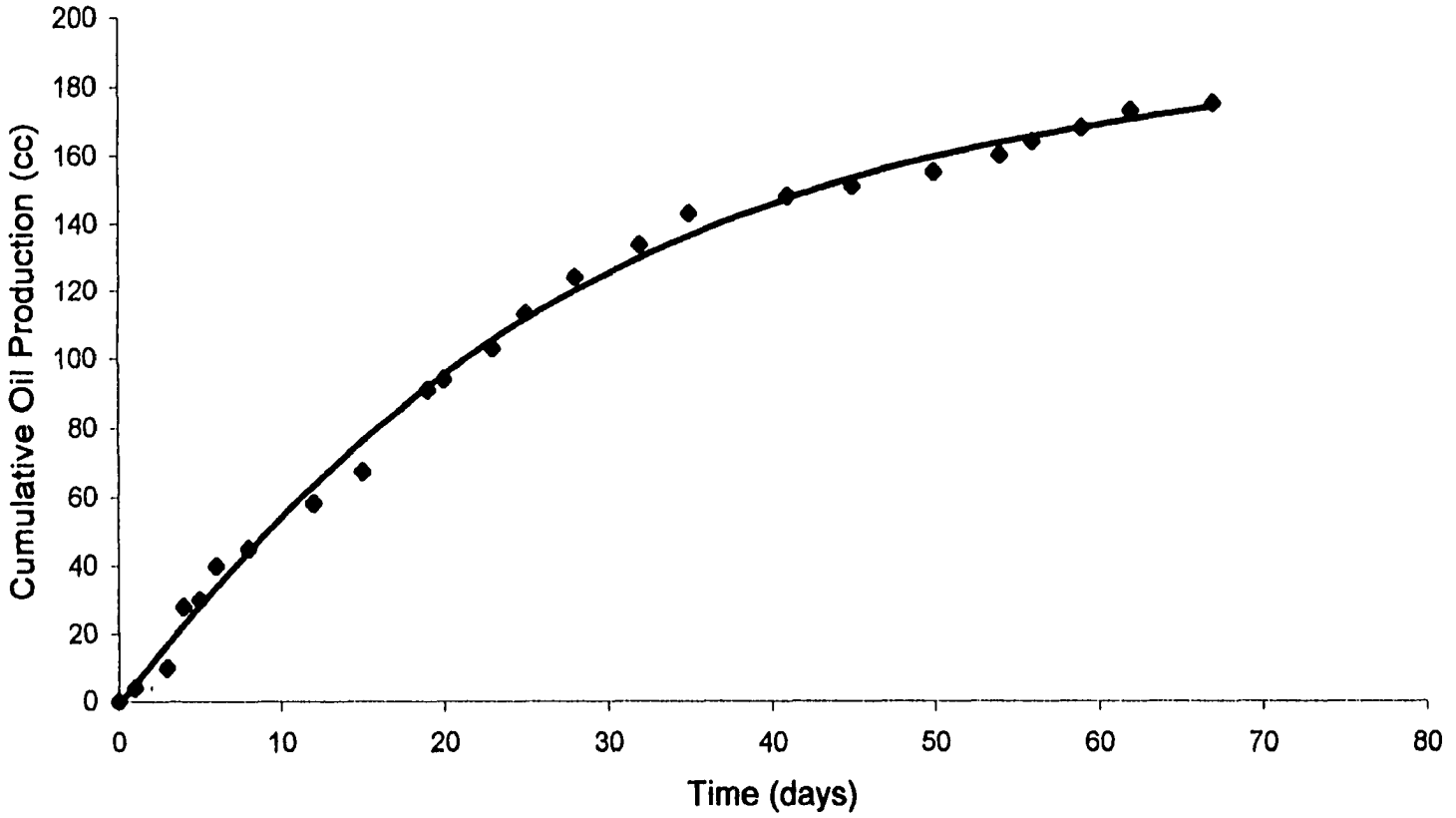

Figure 5.42 Cumulative oil production of Run 2 performed in the long sand pack.

The next runs, a 0.5% (by volume) defoamer was added to two depletion experiments, which were carried out using the short and long coreholders. The two runs were performed at a pressure depletion rate of 414 kPa/day (60 psi/day). Figures 4.43 and 4.44 show the cumulative production as a function of time for short and long sand pack when 0.5% defoamer was added . The cumulative oil recovery for the short and the long coreholders were 6 and 8% PV, respectively. Another depletion run was performed with the same pressure depletion rate of 414 kPa/day (60 psi/day), but with out the addition of the defoamer. The cumulative foamy oil production was 200 cc, corresponding to 25% PV. Figure 5.45 shows the cumulative production with respect to time for the run with no defoamer added. Comparing the runs done at the same depletion rates, the addition of defoamer decreased the foamy oil production by a considerable amount. The addition of the defoamer helped gas bubbles to disengage from the dispersed gas phase into free gas. In runs where defoamer was added, intermittent slugs of gas where produced. Comparing the production of the runs with and without the addition of defoamer, one would come to the conclusion that not only the pressure depletion rate is responsible for the high recovery of foamy oil but also the dispersed gas phase volume.

Laboratory experimental work on foamy oil has usually been performed at depletion rates higher than rates attainable in the field. Hence, the extrapolation of these results is not directly applicable to reservoirs. In this study, slow depletion rates comparable to foamy oil reservoirs pressure depletion rates were used. The recovery was in the order of 20% (PV). This oil production was obtained without the sand production. It is believed that with sand production recovery will be higher. Furthermore, when defoamer was added to some runs, pressure fluctuated wildly at the outlet end. This fluctuation was not seen in any other run that did not involve the addition of defoamer. Pressure fluctuation, other parameters same, at the outlet end is an indication of gas slug production; and as a result, higher GOR. Comparing runs with and without the addition of defoamer, one concludes that in the latter case foamy

Reproduced with permission of the copyright owner. Further reproduction prohibited without permission.

Reproduced with permission of the copyright owner. Further reproduction prohibited without permission.

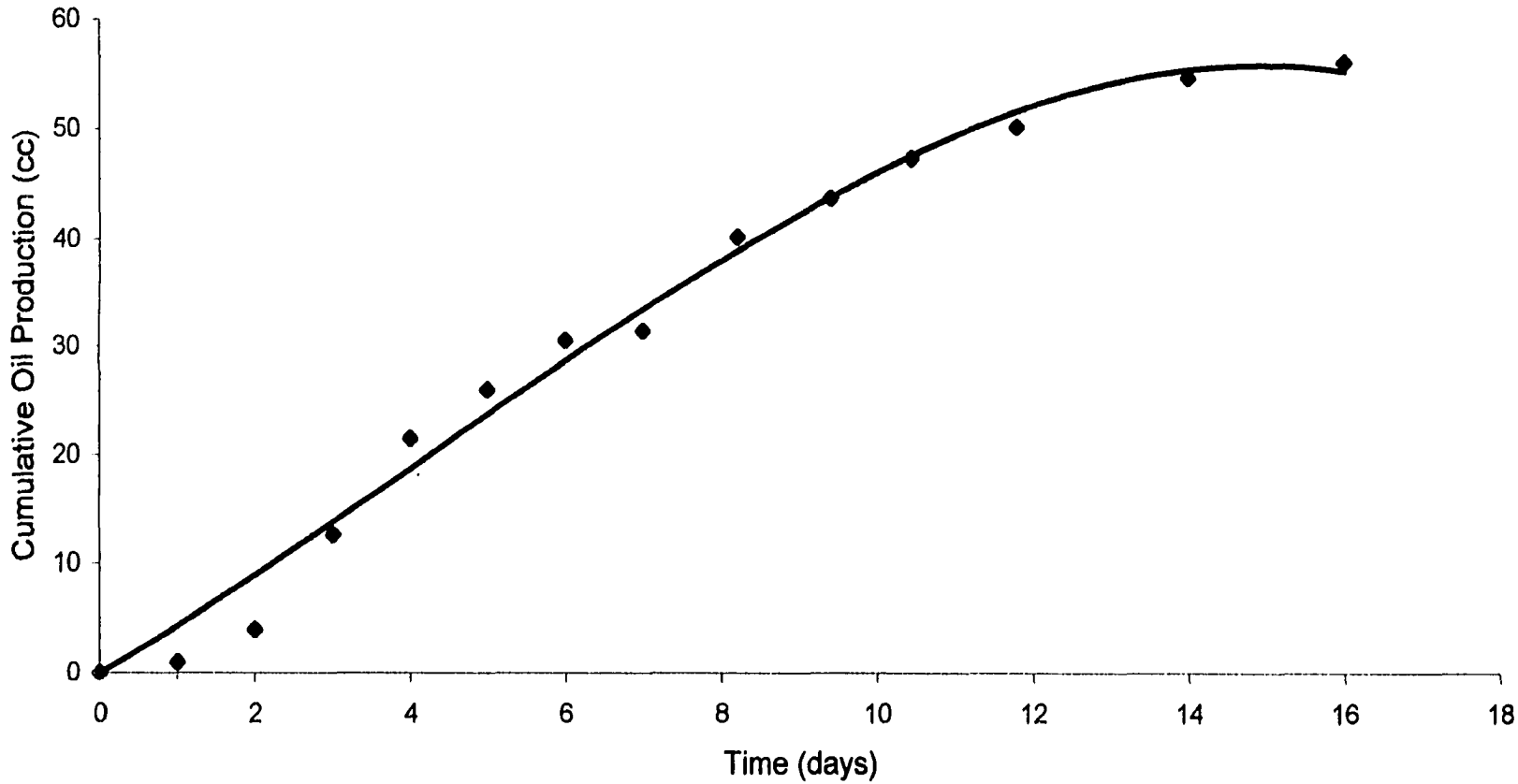

Figure 5.43 Cumulative oil production of Run 6 performed in the short sand pack.

Reproduced with permission of the copyright owner. Further reproduction prohibited without permission.

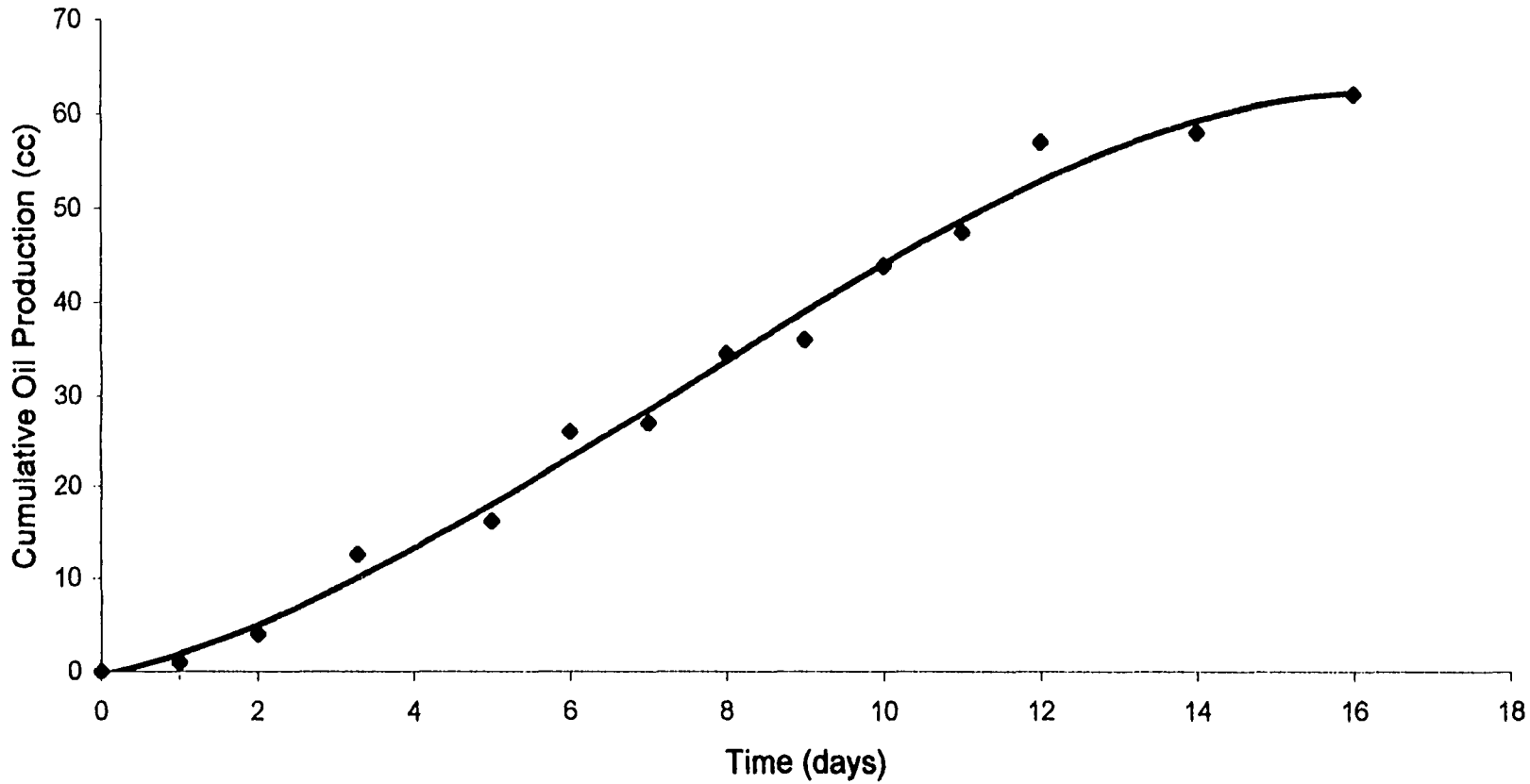

Figure 5.44 Cumulative oil production of Run 5 performed in the long sand pack.

Reproduced with permission of the copyright owner. Further reproduction prohibited without permission.

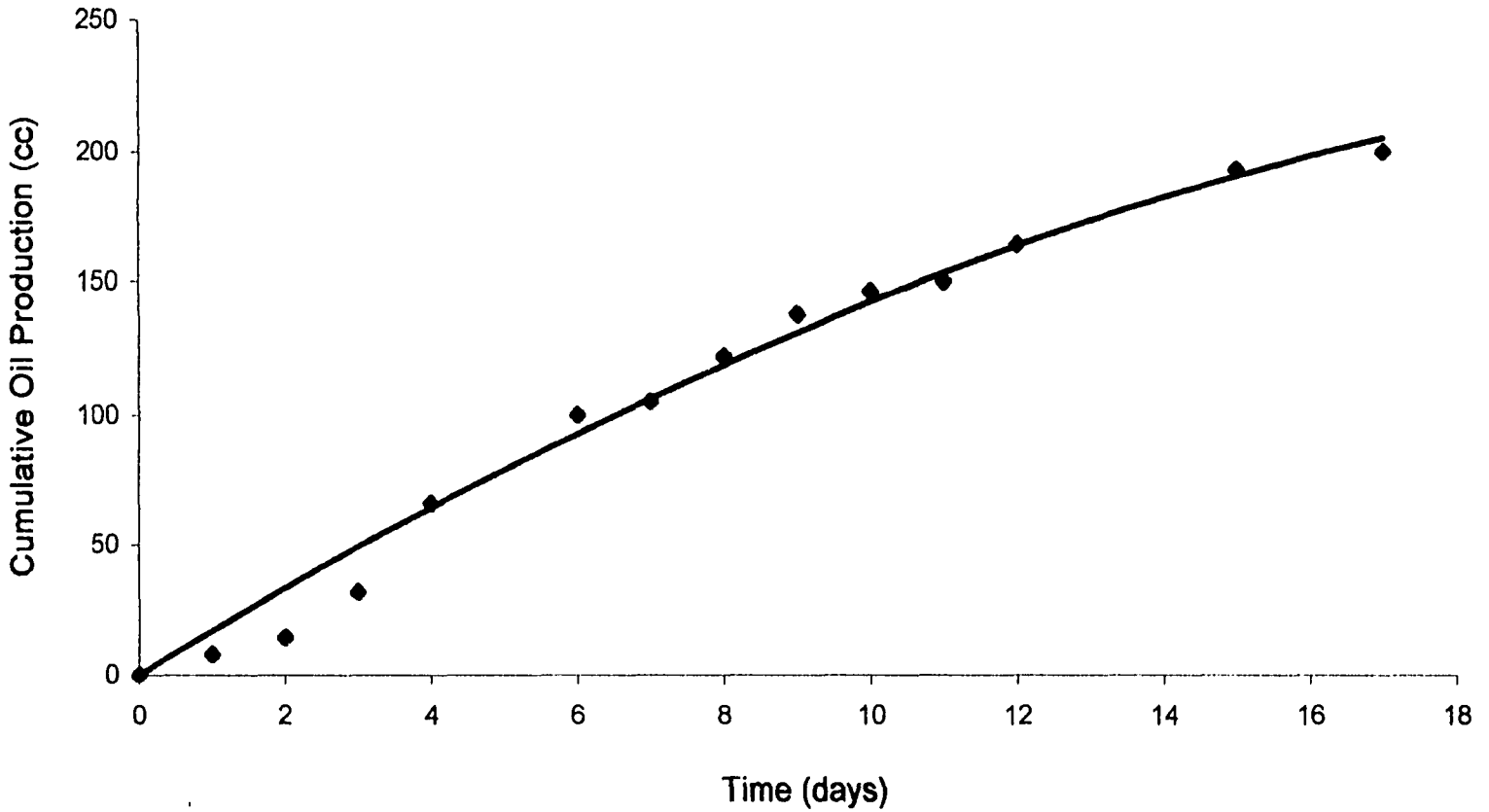

Figure 5.45 Cumulative oil production of Run 2 performed in the long sand pack.

oil flow occurred. In other words, gas bubbles did not coalesce to form gas slugs and flowed as a dispersed gas phase with the oil phase.

Reproduced with permission of the copyright owner. Further reproduction prohibited without permission.

Chapter VI

6. Conclusions

A comprehensive and complex high-pressure foamy oil study was carried out in a PVT cell, micromodel, and sand packs. The research comprised of constant composition expansion (CCE) experiments designed to investigate the "foamy oil solution gas process" under different conditions of mixing/ no mixing and addition of a defoamer. The second part of the study was measurement of foamy oil viscosity. Three different viscometers (Cambridge, capillary, and Haake RV-2) were used for the measurements of foamy oil rheology. A unique feature of this work was visualization of the foamy oil rheology and flow in a high-pressure micromodel. The micromodel was capable of being packed with porous media. The last part of the study involved slow sand pack experiments in two different sand packs with and without the addition of the defoamer.

The experimental techniques employed in this study to investigate the PVT and rheology of foamy oil showed that the dispersed gas phase volume was a time-dependent property of foamy oil and it influenced its viscosity.

The following summarizes the results obtained from the PVT and the foamy oil rheology experiments.

1. CCE runs showed that the faster the pressure depletion rate the higher is the dispersed gas phase volume.
2. For the same pressure depletion rate, the mixing case gave lower foamy oil volume as a percentage of total volume than the quiescent run, indicating less dispersed gas phase.
3. The addition of 0.5% (by vol.) of a defoamer helped to liberate gas bubbles that would otherwise be entrained in the liquid phase, and as a result, decreased the dispersed gas phase. Comparing runs done at the same pressure depletion rate, the addition of the defoamer resulted in a lower foamy oil volume. Hence, the

Reproduced with permission of the copyright owner. Further reproduction prohibited without permission.

time-dependent properties of foamy oil were controlled by the dispersed gas phase.

4. Packing of glass beads into the PVT cell changed the trend of the foamy oil volume (as percentage of total volume) curve. The packing provided nucleation sites and aided in coalescence and gas separation to free gas phase.
5. The apparent viscosity of foamy oil as measured by Cambridge viscometer was lower for the faster depletion rate; and the longer the sample left to stabilize the higher the apparent viscosity of foamy oil. The capillary viscometer results showed less variation, within 5% from each other.
6. The Cambridge viscometer results appear to correlate better with the observed behaviour in the PVT cell than the capillary viscometer results.
7. The Haake viscometer measurements were very low and were deemed unreliable due to gas phase development inside the viscometer chamber where the depletion took place.
8. Based on the knowledge gained during course of the study, it is concluded that the Cambridge viscometer gives numbers that are consistent with the PVT data; however, these numbers are not correlated with simulator.

For the micromodel experiments and the visualization of the foamy oil depletion process, the following summarizes the experimental results obtained:

1. Several PVT cell CCE runs were repeated in the micromodel with no porous media present. The results showed good repeatability and were in very good agreement with the same PVT cell runs indicating that the micromodel was representative of the depletion process.
2. In all micromodel experiments, nucleation was observed to start at the bottom of the micromodel, furthest away from the production outlet.
3. Several nucleation regimes were observed to occur during the depletion process.

Reproduced with permission of the copyright owner. Further reproduction prohibited without permission.

a. At the beginning of the nucleation process, one nucleation site was observed to be active for considerable length of time. This stage could be characterized as a heterogeneous progressive nucleation.
b. The second stage of nucleation is distinguished by random multiple nucleation sites occurring throughout the entire micromodel and producing spherical bubbles. The individual site could be categorized as an instantaneous nucleation.
c. The Last stage of nucleation observed is also random and occurred throughout the micromodel, but the bubbles were not spherical, instead ramified patterns "tongues" of gas. The nucleation could be categorized as heterogeneous progressive nucleation.

4. When the micromodel was packed with a porous medium, nucleation was seen to start at the bottom of the micromodel too. The gas builds up at the bottom of the micromodel, and then it flows upwards to the production outlet in a displacement pattern where gas displaces oil.
5. For the same pressure depletion rate, the micromodel packed with Cryolite gave higher foamy oil production as compared to sand-packed-micromodel run.

The sand pack experiments were carried out using two different core holders at slow depletion rates and with/without the addition of defoamer. The following summarizes the conclusions derived from slow depletion in sand packs:

1. For the same pressure depletion rate, the run with the defoamer gave lower cumulative oil production than the run without the defoamer. The dispersed gas phase seems responsible for the higher foamy oil production and the low producing gas oil ratio.
2. At very slow pressure depletion rate of 103.4 kPa/day (15 psi/day), lower than actual reservoir depletion rate, the oil recovery was 22% PV, which proves that foamy oil production is possible at lower depletion rates.

The concluding remarks of the overall study are that the measurement of the foamy oil parameters, CCE, apparent viscosity, apparent solution GOR, and production

Reproduced with permission of the copyright owner. Further reproduction prohibited without permission.

is technique dependent and it is time dependent. In other words, the way a run is conducted and the geometry of the instrument influence the measurement. As a general conclusion of this study, the longer the bubbles remain dispersed in liquid oil, there is an ample time for the foamy oil to flow towards the production end. As a result, higher recovery factors will be attained.

The process of cold production has been in operation for 10 years or so, and it is gaining popularity among heavy oil producers. It is believed that foamy oil solution gas drive occurs in heavy oil reservoirs exhibiting foamy oil characteristics. The work performed in this study confirmed that dispersed flow does occur. In addition, the production of foamy oil in sandpacks was high at depletion rates comparable to field rates. The high oil viscosity acts as a stabilizing factor for the dispersed gas bubbles. Therefore, the gas bubbles take longer to separate from the liquid oil giving the foamy oil longer time to flow towards the production end. In addition, critical gas saturation will be higher as the dispersed gas fraction remains in the liquid oil. This will improve the recovery of oil. The dispersed gas bubbles provide a driving energy to the oil. Sand production, will improve the efficiency of the foamy oil displacement by providing "highways" for the foamy oil flow. The no communication condition observed in the field (a producing well stop flowing) can be explained through the deterioration of the foamy oil properties. That is if the foamy oil has to flow long distance (time longer than the time it takes the dispersed bubbles to coalesce and form continuous gas phase), then foamy oil "looses" its properties and oil flow slows down to a trickle or stop. Stimulation, which is a common practice in the field, will initiate foamy oil flow. So, the conducive conditions for the foamy oil flow to occur in heavy oil solution gas drive reservoirs are: high permeability, high dispersed gas fraction, high critical gas saturation, high pressure gradient, and short drainage area.

Reproduced with permission of the copyright owner. Further reproduction prohibited without permission.

Chapter VII

7. Recommendations

Based on the experience gained from this research, the following recommendations are offered to extend the scope of this research:

1. Critical gas saturation is an important parameter that affects the recovery of oil in solution gas drive reservoirs. Further research of this parameter is needed to clarify its role on foamy oil solution gas drive mechanism.
2. In the this study, micromodel runs were performed in vertical position, a challenge for future work is to modify the micromodel set-up to allow runs to be performed in other positions; i.e., horizontal position, producing from bottom, etc. This would help in understanding gravity effects and on the dispersed gas bubbles. In addition, this will clarify the observation of the occurrence of nucleation at the upstream section of the micromodel.
3. Improvement and modification of the visual set-up to allow observation of sub-micron bubbles would verify and ascertain the existence of microbubbles.
4. It is known that most foamy oil production is associated with sand production; an attempt to study the sand production effects (in combination with foamy oil) on dispersed gas bubbles would improve the understanding of foamy oil process.

Reproduced with permission of the copyright owner. Further reproduction prohibited without permission.

References

Andres, R. P.: Homogeneous Nucleation in a Vapor, in Nucleation, Zettlemoyer, A. C., Ed., Marcel Dekker, New York, 1969.

Angus, S., Armstrong, B., and de Reuck, K.: International thermodynamic Tables of the Fluid State Carbon Dioxide, Pergramon Press, Toronto, 1973.

Aubert, J.H., and Kraynik, A.M.: "Aqueous Foams," Scientific American, Vol. 254, p. 74-82, May 1986.

Berger, P.D., and Gast, J.A.: "J. Coat. Tech., Vol. 48, No. 55, 1976.

Bernath, L.: "Theory of Bubble Formation in Liquids," Industrial and Eng. Chem., vol. 44, 1952.

Blander, M. and Katz, J. L.: "Bubble Nucleation in Liquids," AIChE. J., Vol. 21, No. 5, Sep. 1975.

Bora, R.: An Experimental Investigation of Foamy Oil in Porous Media, Ph.D. dissertation, U. of Calgary, 1998.

Claridge, E. L., Prats, M.: "A Proposed Model and Mechanism for Anomalous Foamy Heavy Oil Behaviour," SPE 29243, presented at the International Heavy Oil Symposium, Calgary, AB, Canada, June 19-21, 1995.

Clift, R. et al.: Bubbles, Drops, and Particles, Academic Press, New York, 1978.

Craft, B.C. and Hawkins, M., revised by Terry, R.E.: Applied Petroleum Reservoir Engineering, 2nd ed., Prentice Hall, Englewood Cliffs, NJ, 1991.

Dunning, W. J.: General and Theoretical Introduction, in Nucleation, Zettlemoyer, A. C., Ed., Marcel Dekker, New York, 1969.

Elkins, L. F., Morton, D. and Blackwell, W. A.: "Experimental Fireflood in a Very Viscous Oil-Unconsolidated Sand Reservoir," S. E. Pauls Valley Field, Oklahoma, SPE 4086, 1972.

Reproduced with permission of the copyright owner. Further reproduction prohibited without permission.

Firoozabadi, A. et al.: "Measurements of Supersaturation and Critical Gas Saturation," SPE 28669, SPE Formation Evaluation, December 1992.

Firoozabadi, A. et al.: "Reply to Discussion of Measurements of Supersaturation and Critical Gas Saturation," SPE 28669, SPE Formation Evaluation, June 1994.

Fogg, P.G.T. and Gerrard, W.: Solubility of Gases in Liquids: A Critical Evaluation of Gas/Liquid Systems in Theory and Practice, John Wiley & sons, New York, NY, 1991.

Hammami, et al.: "Asphaltene Precipitation From Live Oils: An Experimental Investigation of the Onset/Endpoint Conditions and Reversibility," a presentation given at the National Petroleum Show; Leading Technologies Forum, Calgary, June 9-11, 1998.

Hatschek, E., The Viscosity of Liquids, London, 1928.

Heilen, W., Klocker, O., and Adams, J.: "Influence of Defoamers on the Efficiency of Waterborne Coating Systems," J. Coat. Tech. Vol. 66, No. 47, p 47-53, Feb. 1994.

Islam, M. R. and Chakma, A.: "Mechanics Of Bubble Flow In Heavy Oil Reservoirs," SPE 20070, 1990.

Kamath, J. and Boyer, R. E.: "Critical Gas Saturation and Supersaturation in Low-Permeability Rocks," SPE 26663, presented at the 1995 SPE Annual Technical Conference and Exhibition, Houston, Oct. 3- 6, 1993.

Kashchiev, D., and Firoozabadi, A.: "Kinetics of the Initial Stage of Isothermal Gas Phase Formation," J. Chem. Phys., Vol. 98, No. 6, March 1993.

Kennedy, H. T. and Olson, C. R.: "Bubble Formation in Supersaturated Hydrocarbon Mixtures," SPE 232-G, presented at the Petroleum Meeting of AIME, Houston, TX, Oct. 1-3, 1952.

Kortekaas, T. F. M. and Van Poelgeest, F.: "Liberation of Solution Gas During Pressure Depletion of Virgin and Watered-Out Oil Reservoirs," SPE 19693, presented at the 64th Annual Technical Conference and Exhibition of the Society of Petroleum Engineers, San Antonio, TX, October 8-11, 1989.

Reproduced with permission of the copyright owner. Further reproduction prohibited without permission.

Kraus, W. P. et al.: "Pseudo-bubble Point Model for Foamy Oil," paper CIM 93-45, presented at the Annual Technical Conference of the Petroleum Soc. of CIM, Calgary, May 9-12, 1993.

La Mer, V. K.: "Nucleation in Phase Transitions," Industrial and Engineering Chemistry, Vol. 44, No. 6., 1952.

Lebel, J. P.: "Performance Implications of Various Reservoir Access Geometries (for Cold Heavy Oil/Bitumen Production)," presented at the 11th Annual Heavy Oil and Oil Sands Technical Symposium, March 1994.

Lepski, B., Bassiouni, Z., and Wolcott, J.: "Second-Contact Water Displacement Oil Recovery Process," SPE 35360, presented at the SPE/DOE Tenth Improved Oil Recovery, Tulsa, OK, April 21-24, 1996.

Li, X. and Yortsos, Y. C.: "Critical Gas Saturation: Modeling and Sensitivity Studies," SPE 26662, presented at the Annual Technical Conference and Exhibition of the Society of Petroleum Engineers, Houston, TX, October 3-6, 1993.

Li, X. and Yortsos, Y. C.: "Visualization and Numerical Studies of Bubble Growth During Pressure Depletion," SPE 22589, presented at the 56th Annual Technical Conference and Exhibition of the Society of Petroleum Engineers, Dallas, TX, Oct. 1991.

Loughead, D. J.: "Lloydminster Heavy Oil Production-Why So Unusual?," 9th Annual Heavy Oil and Oil Sands Technology Symposium, Calgary, AB, March 11, 1992.

Maini, B. B., Sarma, H. K. and George, A. E.: "Significance of Foamy-Oil Behaviour in Primary Production of Heavy Oils," JCPT, Vol. 32, No. 9, Nov. 1993.

Maini, B. B.: "Foamy-Oil Flow in Primary Production of Heavy Oil under Solution Gas Drive," SPE 56541, presented at Annual Technical Conference and Exhibition of the Society of Petroleum Engineers, Dallas, TX, Oct.3-6, 1999.

McCain, W.D.: The Properties of Petroleum Fluids, PennWell Books, Tulsa, OK, 1973.

Reproduced with permission of the copyright owner. Further reproduction prohibited without permission.

McGee, J.: "Selecting Chemical Defoamers and Antifoams," Chemical Engineering, Vol. 96, p. 131-6, April 1989.

Mitchell, B. J.: "Gap Fluid," Oil and Gas J., Sep. 1971.

Moulu, J. C.: "Solution-Gas Drive: Experiments and Simulation," J. Petroleum Science and Engineering, 2, p. 379-386, 1989.

Odeh, A. S.: "Effect of Viscosity Ration on Relative Permeability," Petroleum Transactions of AIME, Vol. 216, 1959.

Pal et al.: Rheology of Emulsions, in Emulsions: Fundamentals and Applications in the Petroleum Industry, Schramm, L. L., Ed. Advances in Chemistry Series 231, American Chemical Society, Washington, DC, 1992.

Poon, D. and Kisman, K.: "Non Newtonian Effects on the Primary Production of Heavy Oil Reservoirs," paper CIM/AOSTRA 91-33, presented at the CIM/AOSTRA Technical Conference, Banff, AB, April 21-24, 1991.

Ross, S.: " Profoams and Antifoams," Colloids and Surfaces A: Physicochemical and Engineering Aspects, Vol. 118, No. 3, p. 187- 192, Nov. 18, 1996.

Shen, C. and Batycky J.: "Some Observations of Mobility Enhancement of Heavy Oils Flowing Through Sand Pack Under Solution Gas Drive," paper CIM 96-27, 47th Annual Technical Meeting of the Petroleum Society of CIM, Calgary, AB, Canada, June 10-12, 1996.

Sheng, J. J. et al: "A Dynamic Model to Simulate Foamy Oil Flow in Porous Media," SPE 36750, 1996.

Sheng, J. J.: Foamy Oil Flow in Porous Media, a Ph.D. thesis, U. of Alberta, 1997.

Smith, G. E.: "Fluid Flow and Sand Production in Heavy-Oil Reservoirs Under Solution-Gas Drive," SPE 15094, SPE Production Eng., May 1988.

Stewart, C. R. et al.: "The Role of Bubble Formation in Oil Recovery by Solution Gas Drives in Limestones," paper No. 410-G, presented at the Fall Meeting of the

Reproduced with permission of the copyright owner. Further reproduction prohibited without permission.

Petroleum Branch, American Institute of Mining and Metallurgical Engineers, San Antonio, TX, October 17-20, 1954.

Tremblay, B. et al.: "CT Imaging of Wormhole Growth During Solution-Gas Drive," SPE 39638, JPT Canada, a Supplement to JPT, June 1998.

Tremblay, B. et al.: "Simulation of Cold Production in Heavy Oil Reservoirs: Wormhole Dynamics," SPE/DOE 35387, 1996.

Wallhorn, E.; Heilen, W.; Silber, S.: "Defoamers - Nothing but Empirical Results?," European-Coatings-Journal. No. 10, p 911-918, 1997.

Wankat, P. C., Rate Controlled Separations, Elsevier Scientific Publishing Co., London, 1990.

Wilkinson, P. M., van Schayk, A., Spronken, J. P. M. and van Dierendonck, L. L.: "The Influence of Gas Density and Liquid Properties on Bubble Breakup," Chemical Engineering Science, Vol. 48, No. 7, 1993.

Walton, A. G.: Nucleation in Liquids and Solutions, in Nucleation, Zettlemoyer, A. C., Ed., Marcel Dekker, New York, 1969.

Yeung, K. C., and Adamson, M. F.: "Burnt Lake Project- Bitumen Production from Cold Lake Oil Sands Deposit Without Steam," AOSTRA/ Canadian Heavy Oil Association Conference, Calgary, AB, June 10-12, 1992.

Yeung, K. C.: "Cold Flow Production of Crude Bitumen at the Burnt Lake Project," Northeastern Alberta, AOSTRA/ Canadian Heavy Oil Association Conference, Calgary, AB, 1996.

Yortsos, Y. C. and Parlar, M.: "Phase Change in Binary Systems in Porous Media: Application to Solution-Gas Drive," SPE 19697, 1989.

Yuster, S. T.: "Theoretical Consideration of Multiphase Flow in Idealized Capillary Systems," Proceeding of the Third World Petroleum Congress- Section II, 1951.

Reproduced with permission of the copyright owner. Further reproduction prohibited without permission.

Appendix A

CCE and Viscosity Data for Different Runs

Reproduced with permission of the copyright owner. Further reproduction prohibited without permission.

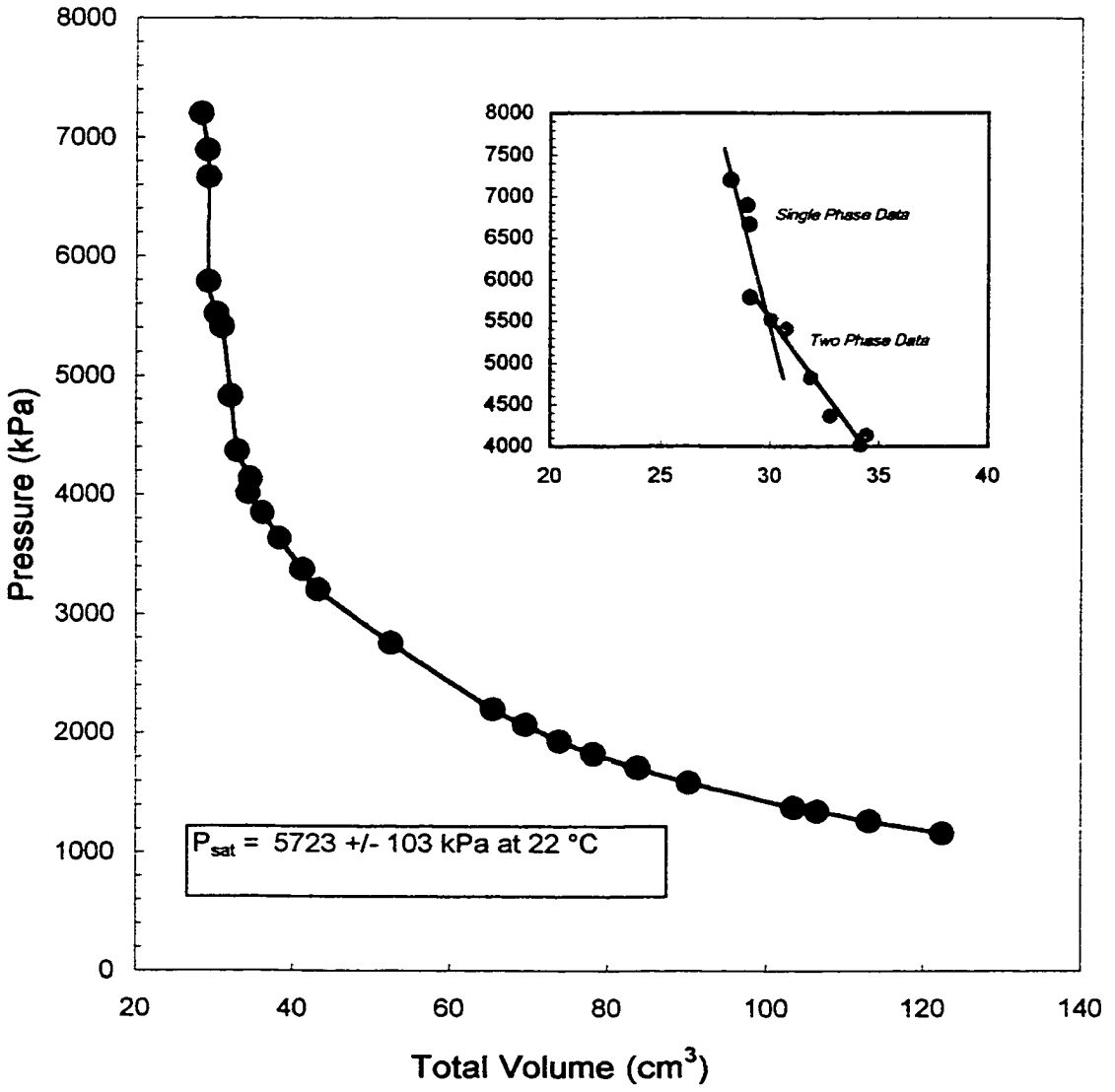

Figure 5.9A - CCE data and Bubble point determination for the case of no mixing and pressure depletion rate of 41 kPa/hr and room temperature.

Reproduced with permission of the copyright owner. Further reproduction prohibited without permission.

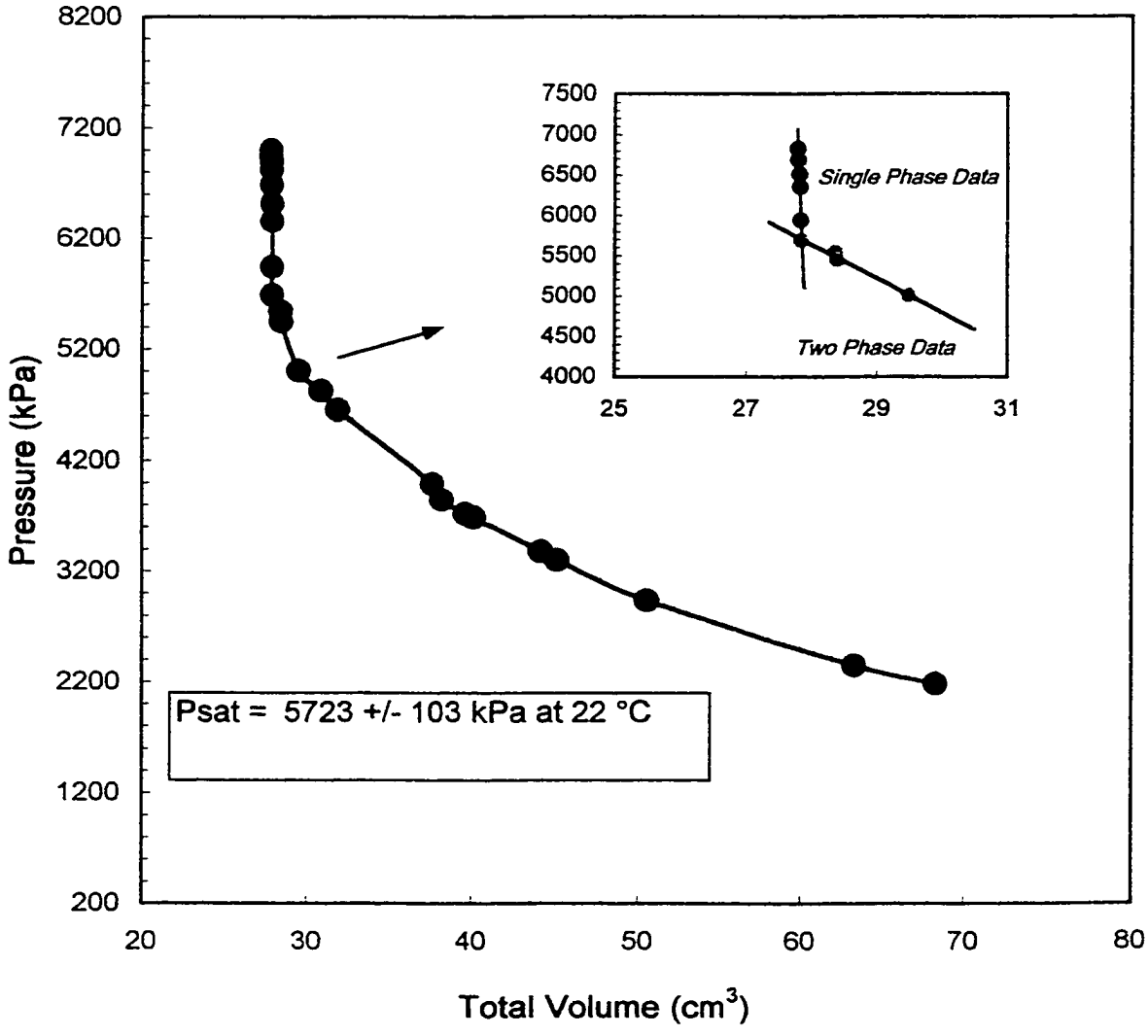

Figure 5.10A - CCE data and Bubble point determination for the mixing case and pressure depletion rate of 41 kPa/hr and room temperature.

Reproduced with permission of the copyright owner. Further reproduction prohibited without permission.

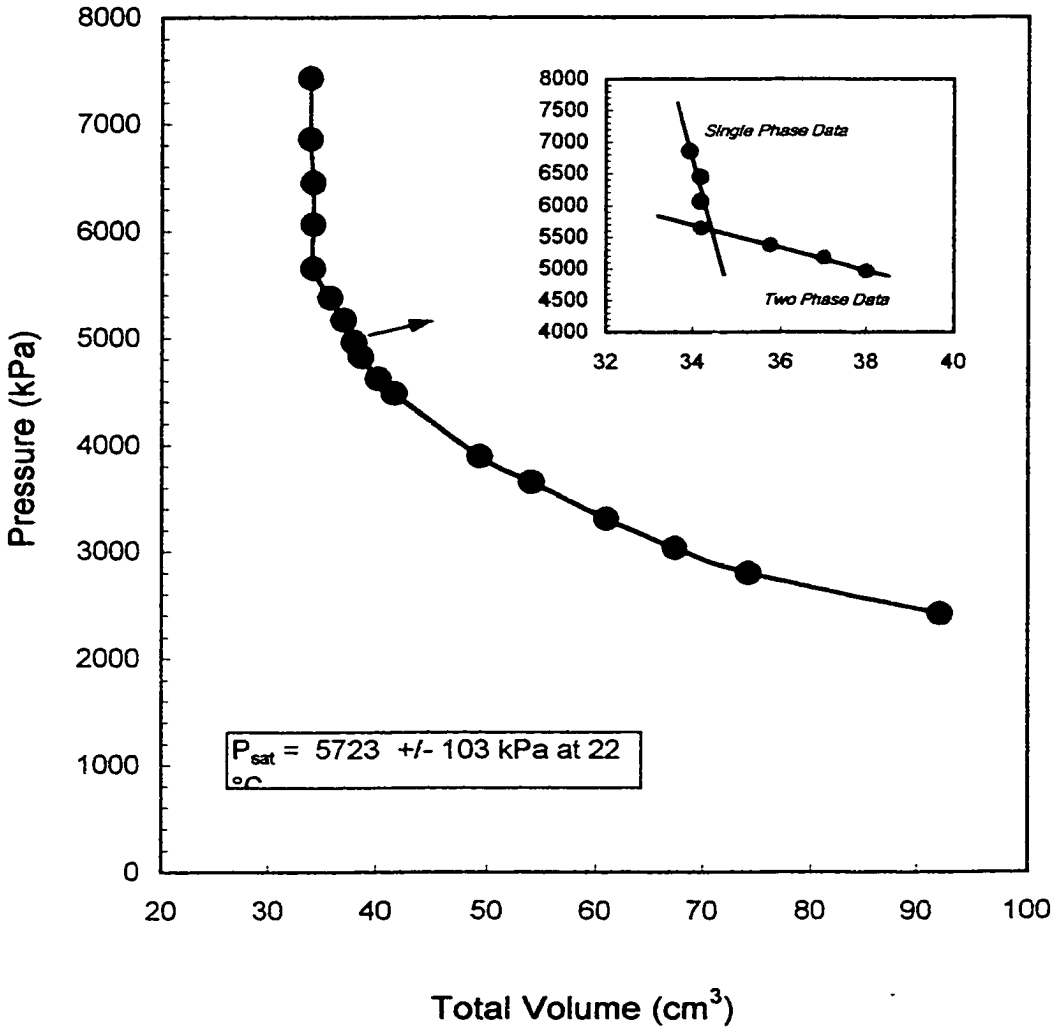

Figure 5. 11A - CCE of foamy oil at the depletion of 800 kPa/hr and room Temperature with glass beads filled PVT cell.

Reproduced with permission of the copyright owner. Further reproduction prohibited without permission.

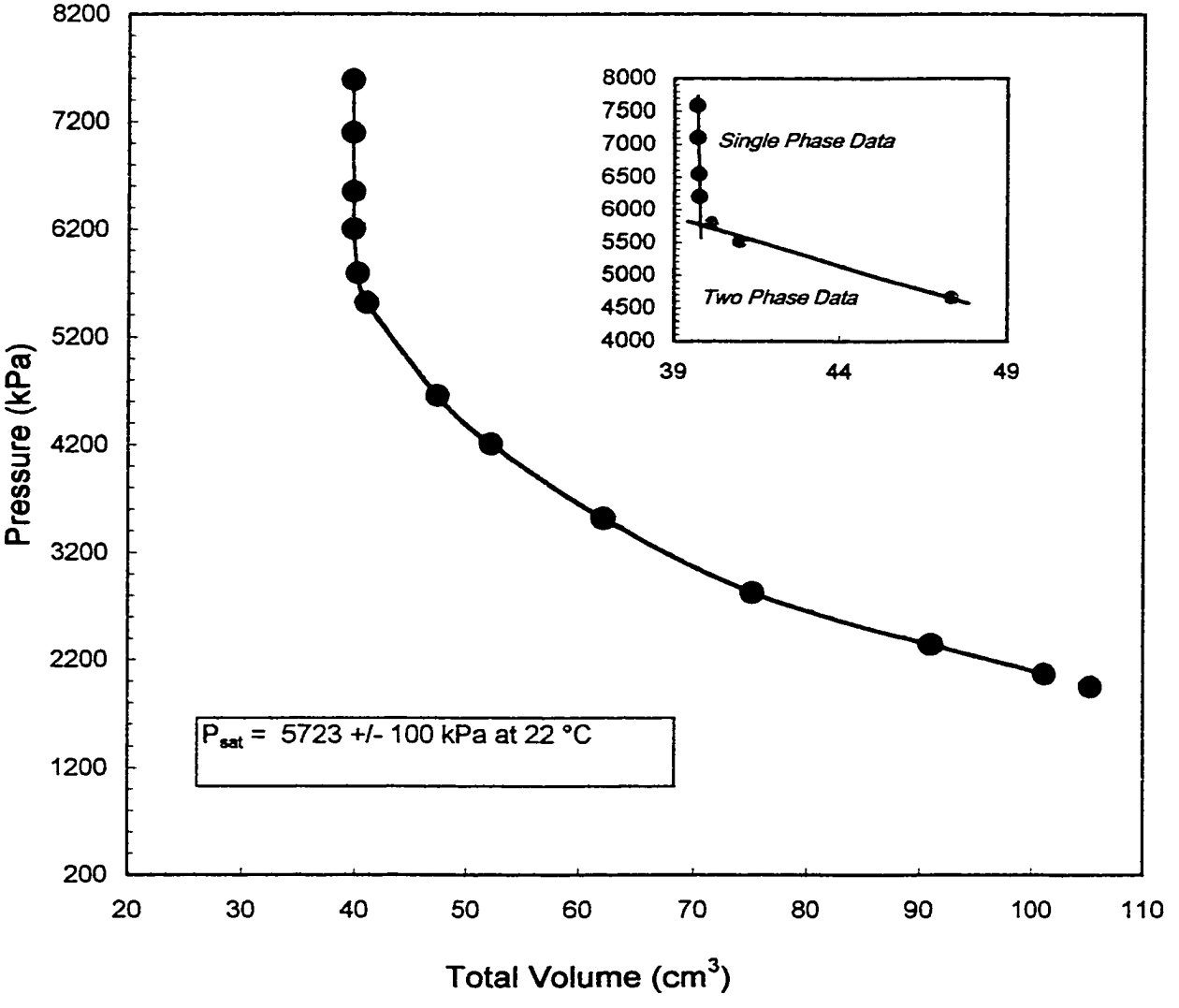

Figure 5.12A - CCE of foamy oil at pressure depeletion rate of 800 kPa/hr and room temperature, for the case of mixing (repeat) insert showing bubble point pressure

Reproduced with permission of the copyright owner. Further reproduction prohibited without permission.

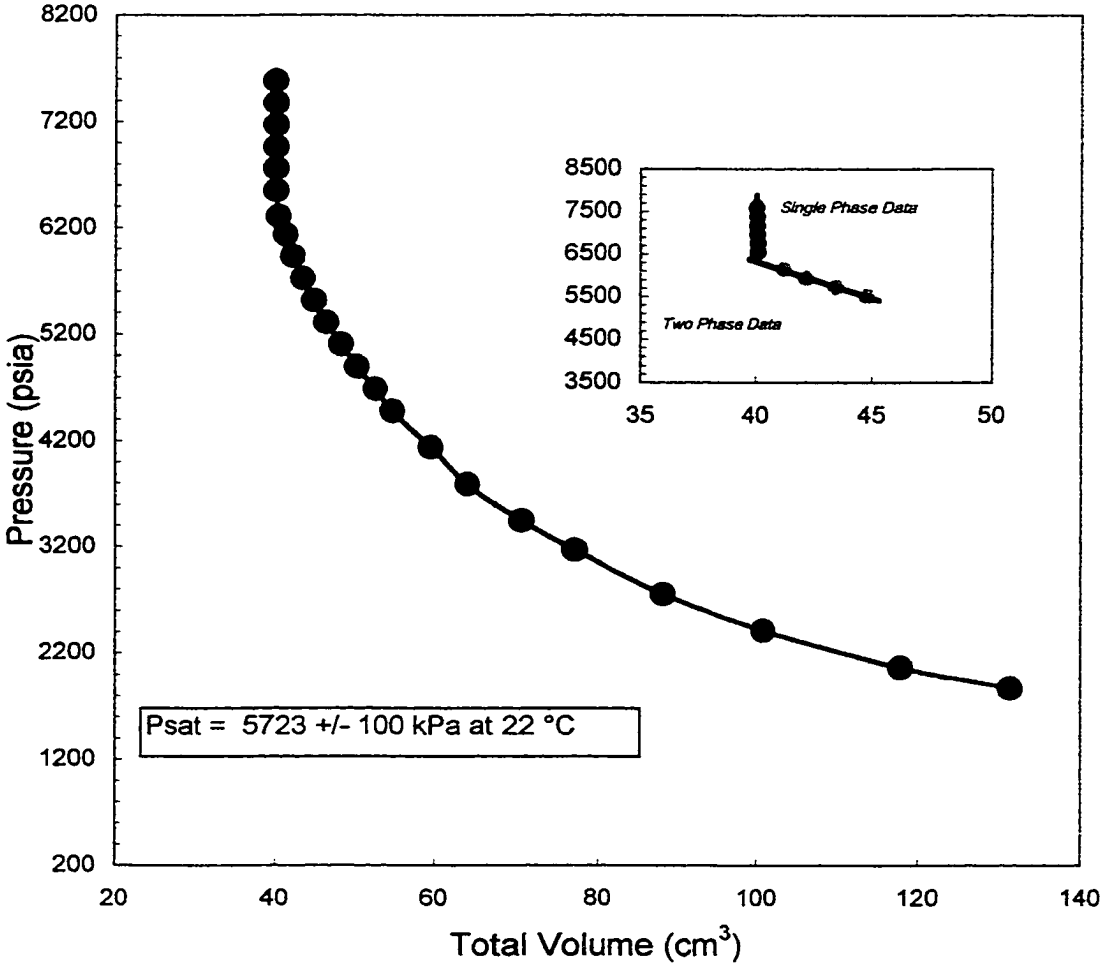

Figure 5.13A - CCE of foamy oil at pressure depeletion rate of 800 kPa/hr and room temperature, for the case of mixing, insert showing bubble point pressure.

Reproduced with permission of the copyright owner. Further reproduction prohibited without permission.

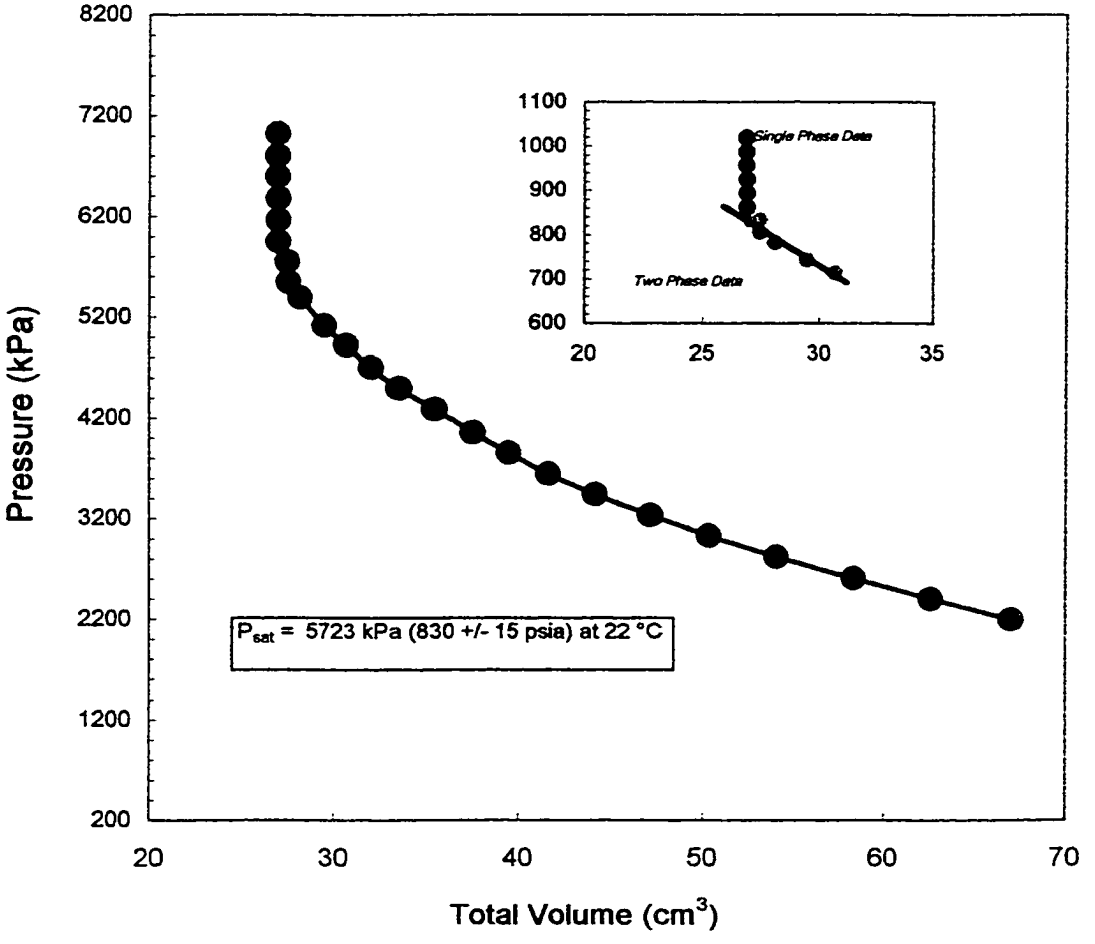

Figure 5.14A - CCE of foamy oil at the depletion of 800 kPa/hr and room Temperature with 0.5% defoamer added for mixing case.

Reproduced with permission of the copyright owner. Further reproduction prohibited without permission.

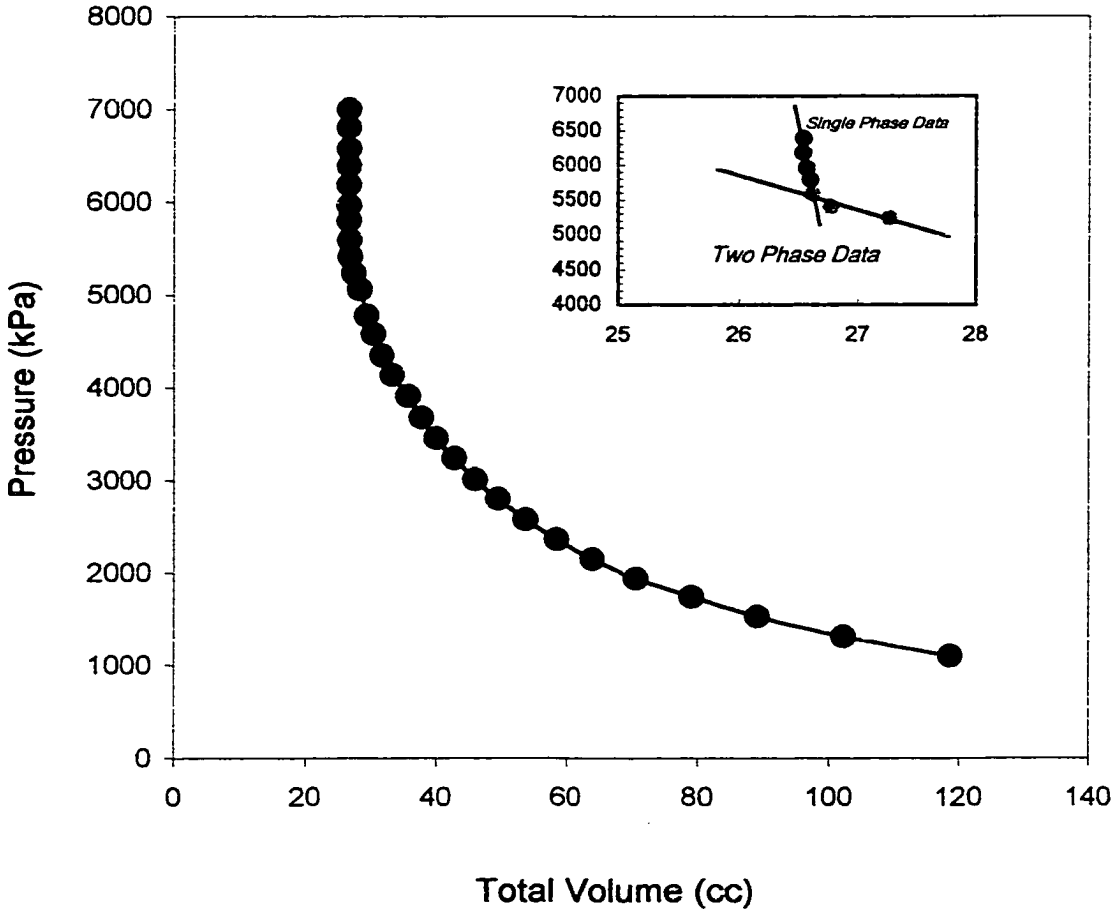

Figure 5.15A1 - CCE of foamy oil at the depletion of 800 kPa/hr and room Temperature with 0.5% defoamer added for no mixing case.

Reproduced with permission of the copyright owner. Further reproduction prohibited without permission.

Reproduced with permission of the copyright owner. Further reproduction prohibited without permission.

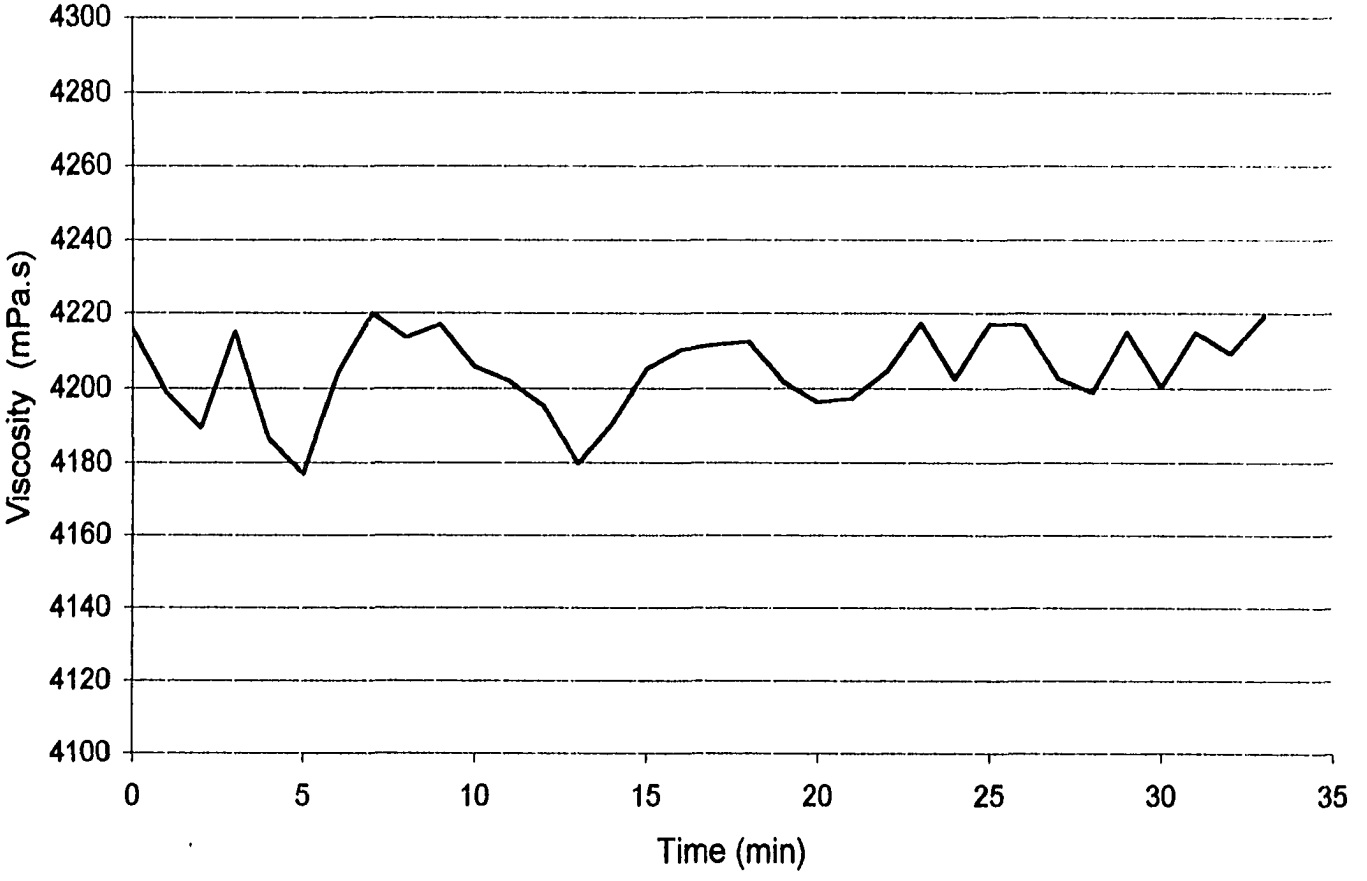

Figure 5.15A - Viscosity of foamy oil at 2068 kPa (300 psi) for 800 kPa/hr pressure depletion rate and room temperature.

Reproduced with permission of the copyright owner. Further reproduction prohibited without permission.

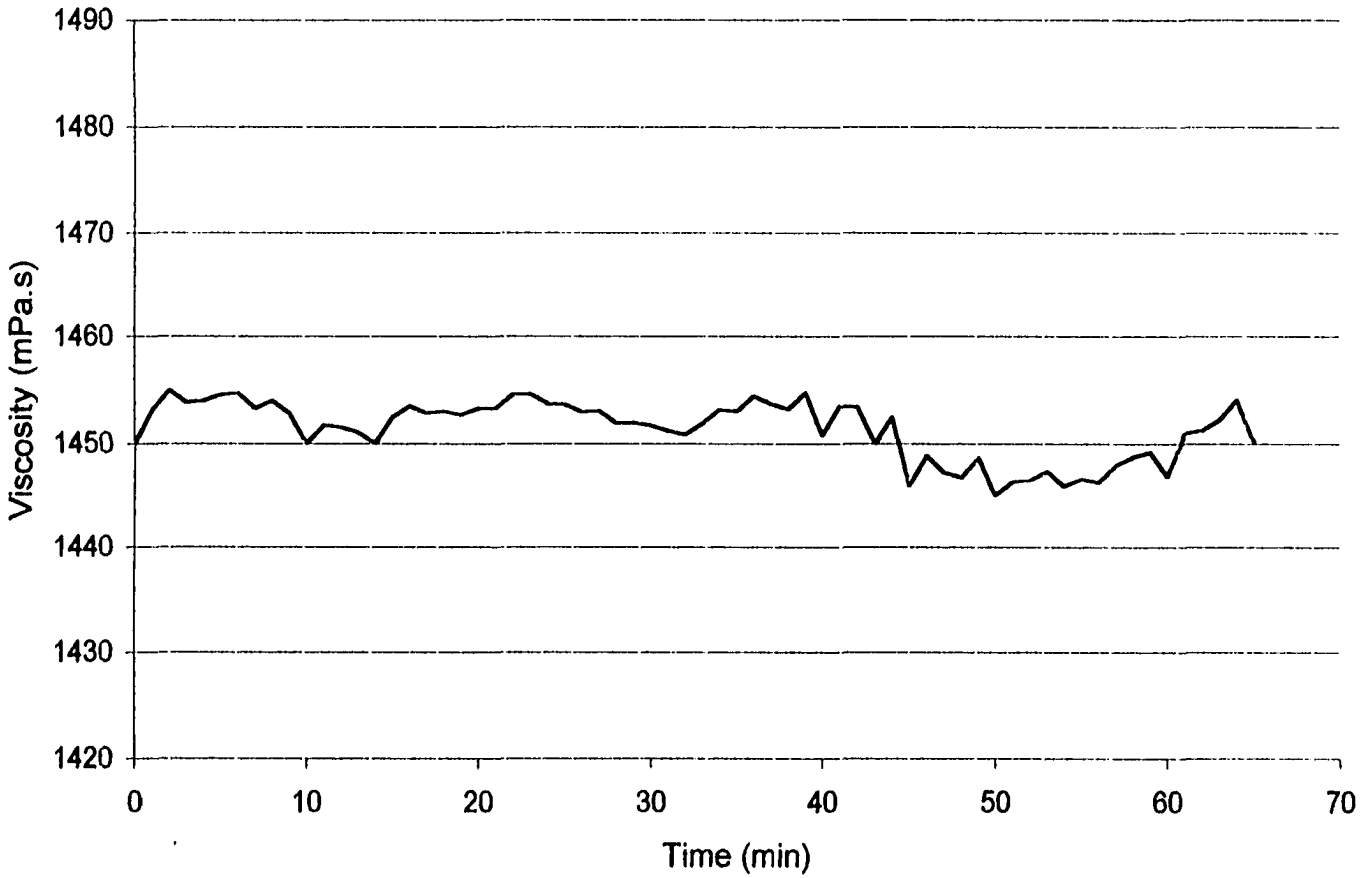

Figure 5.16A - Viscosity of foamy oil at 4689 kPa (680 psi) for 800 kPa/hr pressure depletion rate and room temperature.

Reproduced with permission of the copyright owner. Further reproduction prohibited without permission.

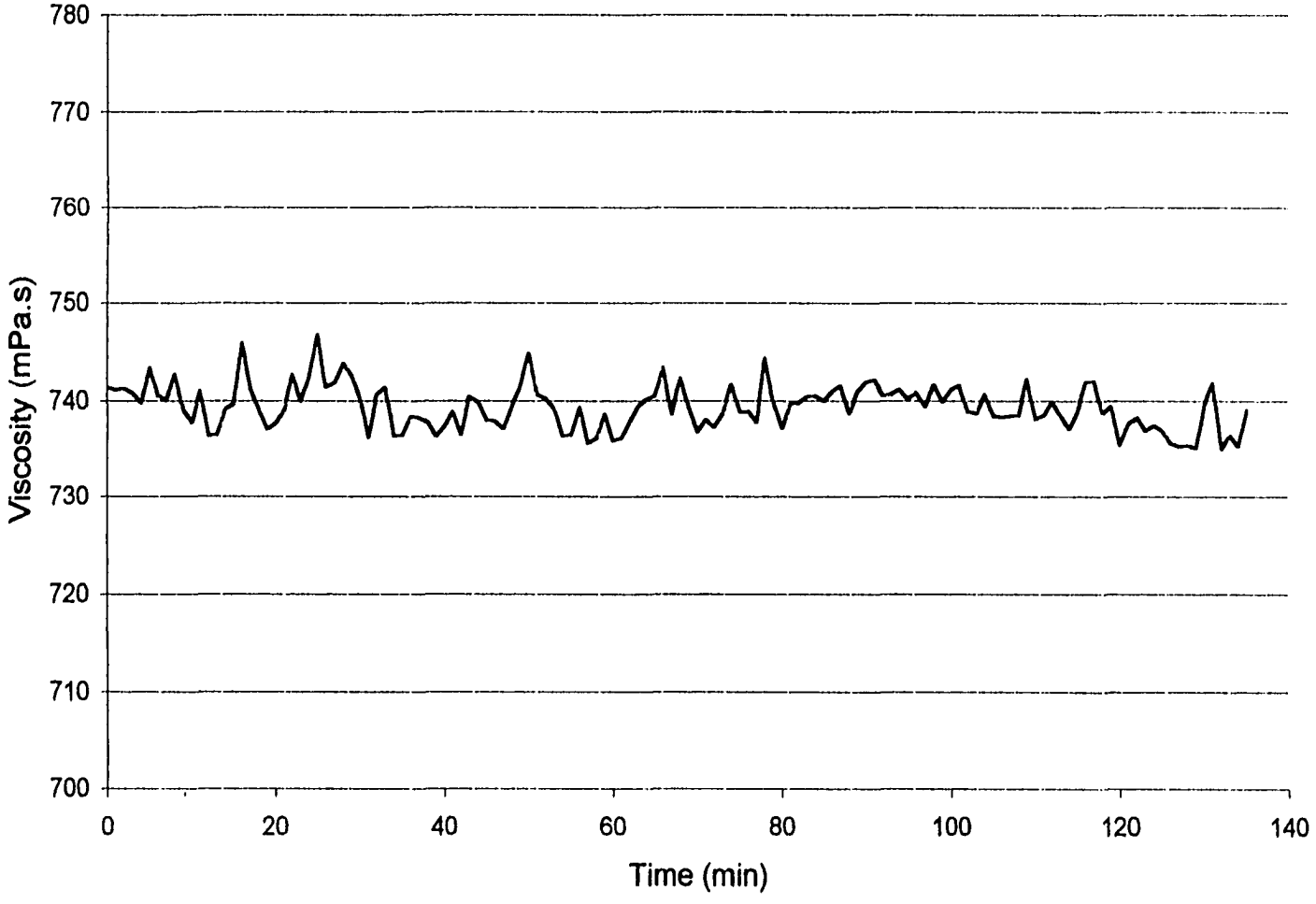

Figure 5.17A - Viscosity of foamy oil at 5516 kPa (800 psi) for 800 kPa/hr pressure depletion rate and room temperature.

Reproduced with permission of the copyright owner. Further reproduction prohibited without permission.

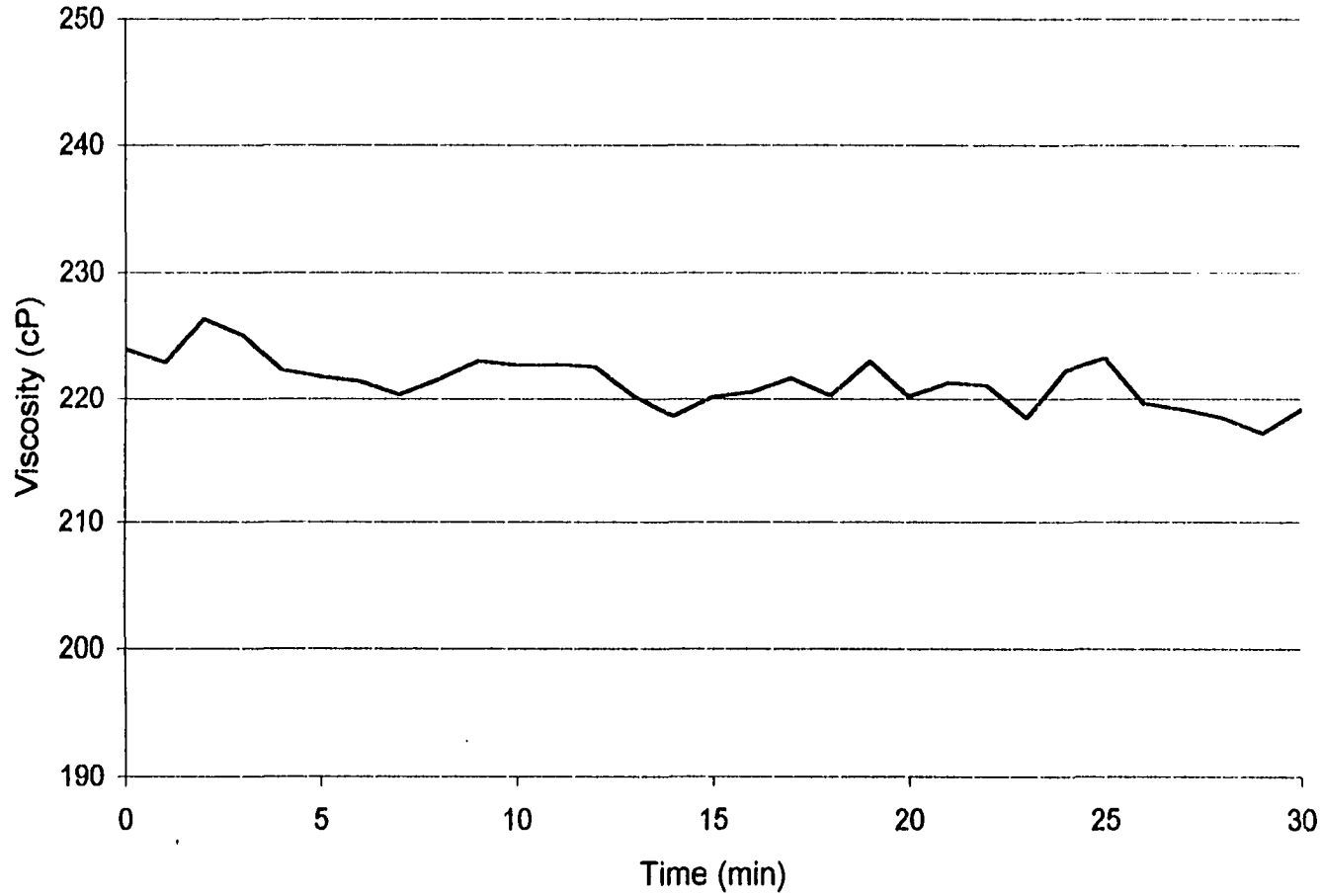

Figure 5.18A - Viscosity of foamy oil at 6343 kPa (920 psi) for 800 kPa/hr pressure depletion rate and room temperature.

Reproduced with permission of the copyright owner. Further reproduction prohibited without permission.

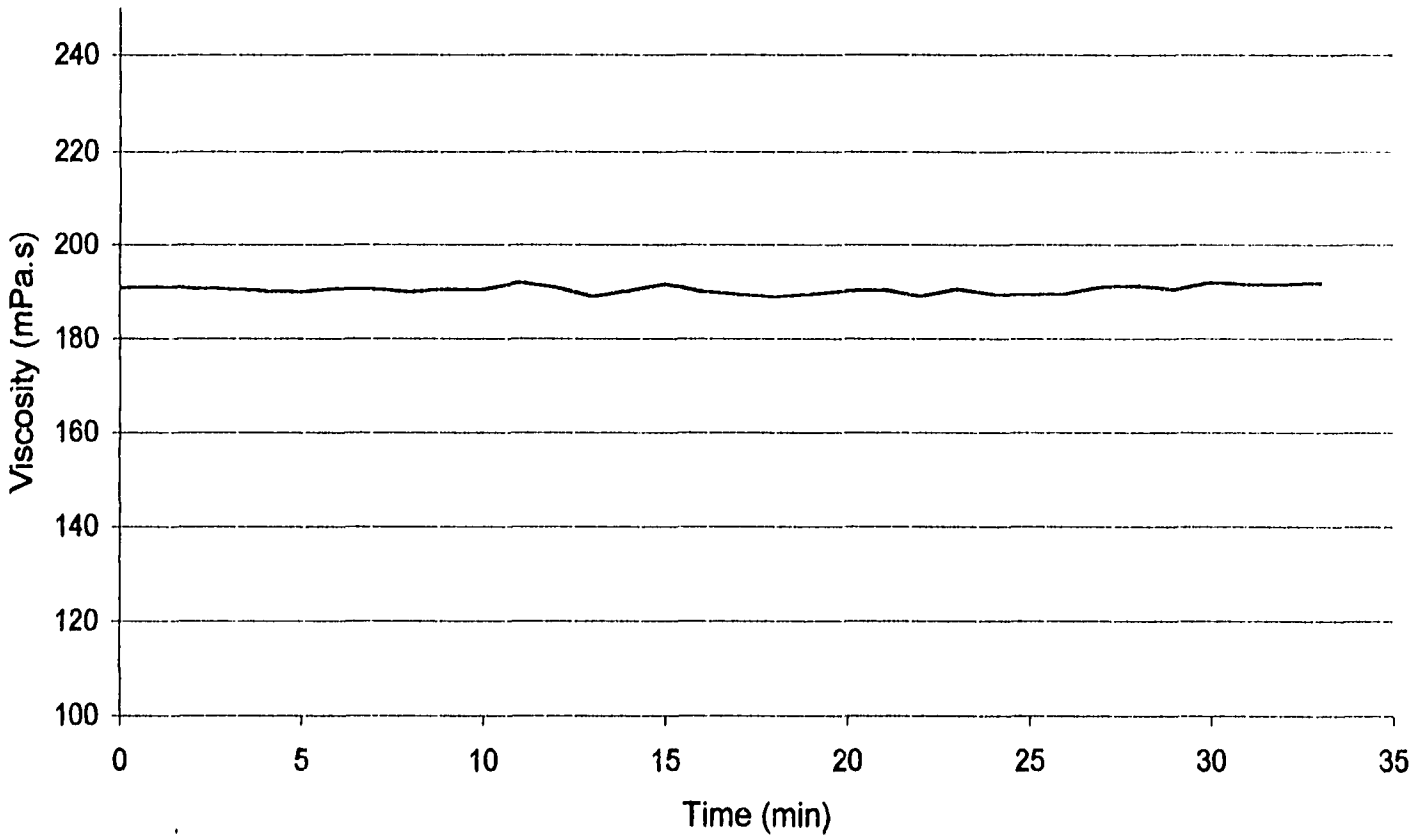

Figure 5.19A - Viscosity of foamy oil at 6895 kPa (1000 psi) for 800 kPa/hr pressure depletion rate and room temperature.

Reproduced with permission of the copyright owner. Further reproduction prohibited without permission.

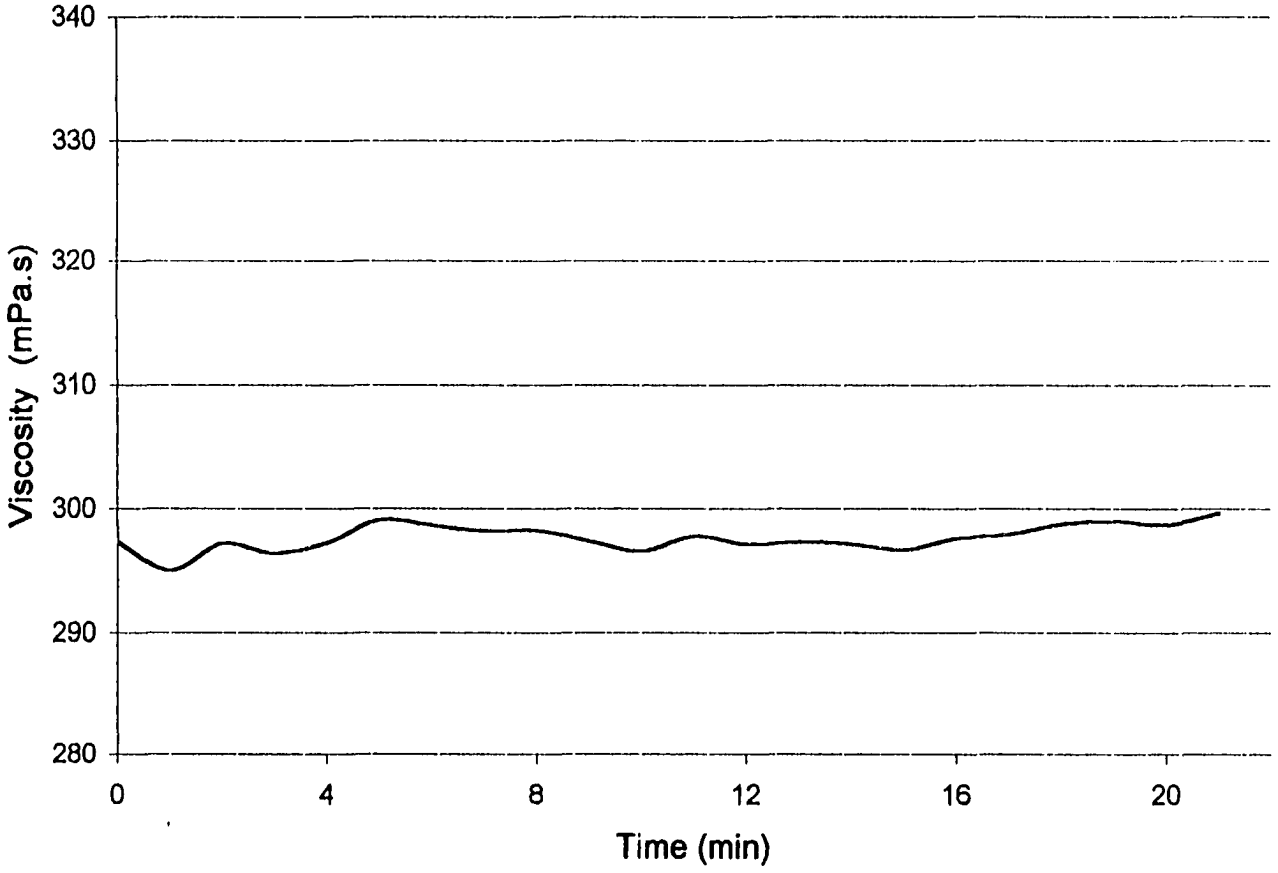

Figure 5.20A - Viscosity of foamy oil at 7584 kPa (1100 psi) performed at a pressure depletion rate of 800 kPa/hr and room temperature.

Reproduced with permission of the copyright owner. Further reproduction prohibited without permission.

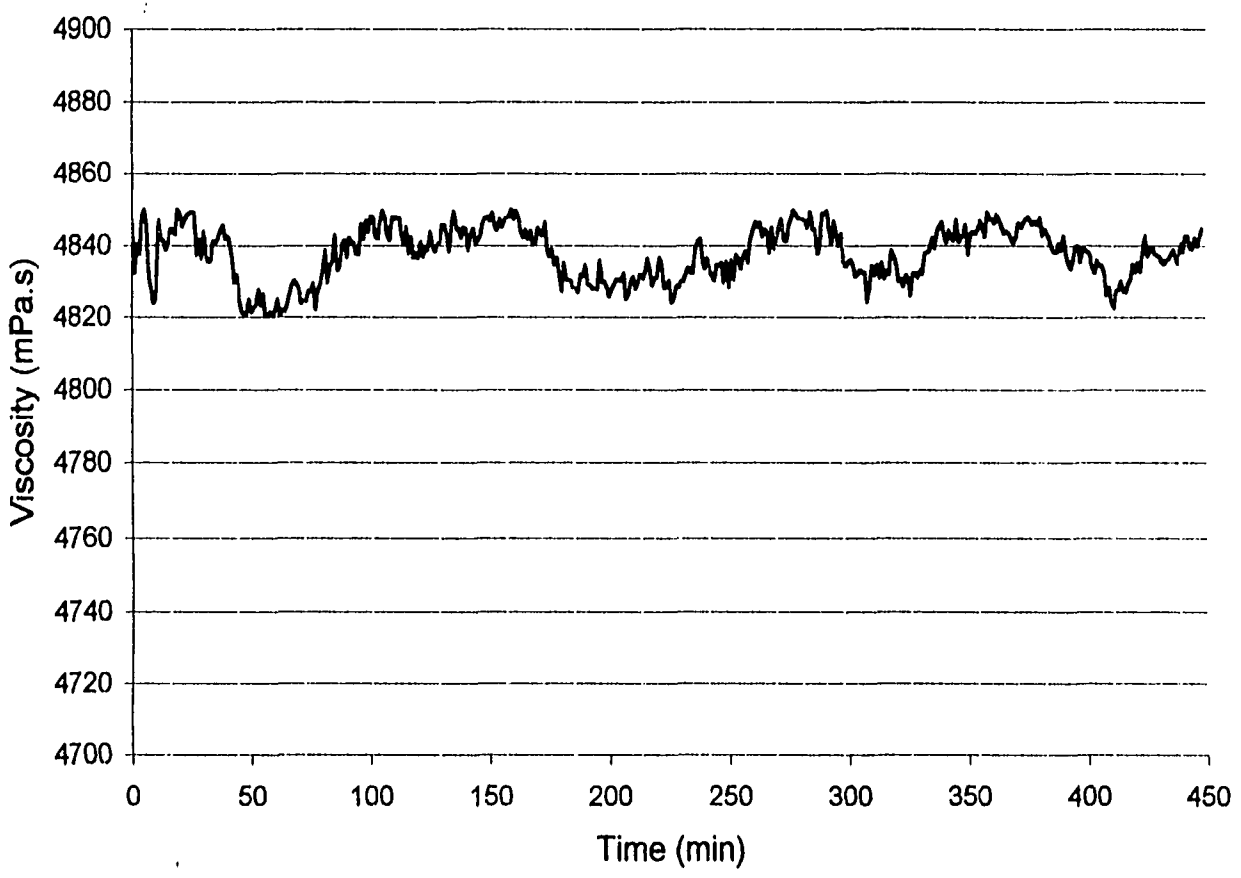

Figure 5.21A- Viscosity of foamy oil with o.5% (by vol.) defoamer at 2068 kPa (300 psi) for pressure depletion rate of 800 kPa/hr and room temperature.

Reproduced with permission of the copyright owner. Further reproduction prohibited without permission.

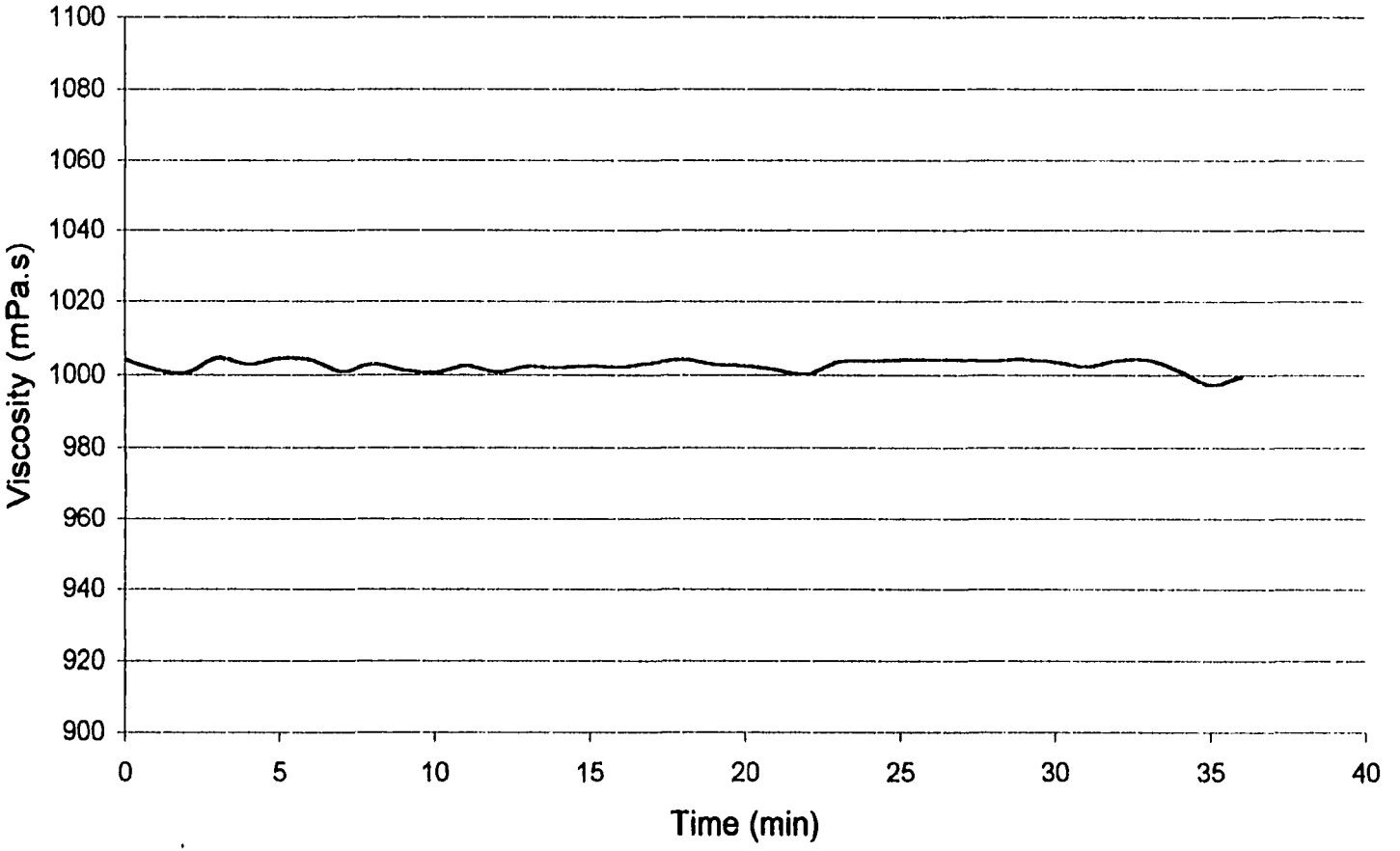

Figure 5.22A - Viscosity of foamy oil with o.5% (by vol.) defoamer at 5516 kPa (800 psi) for pressure depletion rate of 800 kPa/hr and room temperature.

Reproduced with permission of the copyright owner. Further reproduction prohibited without permission.

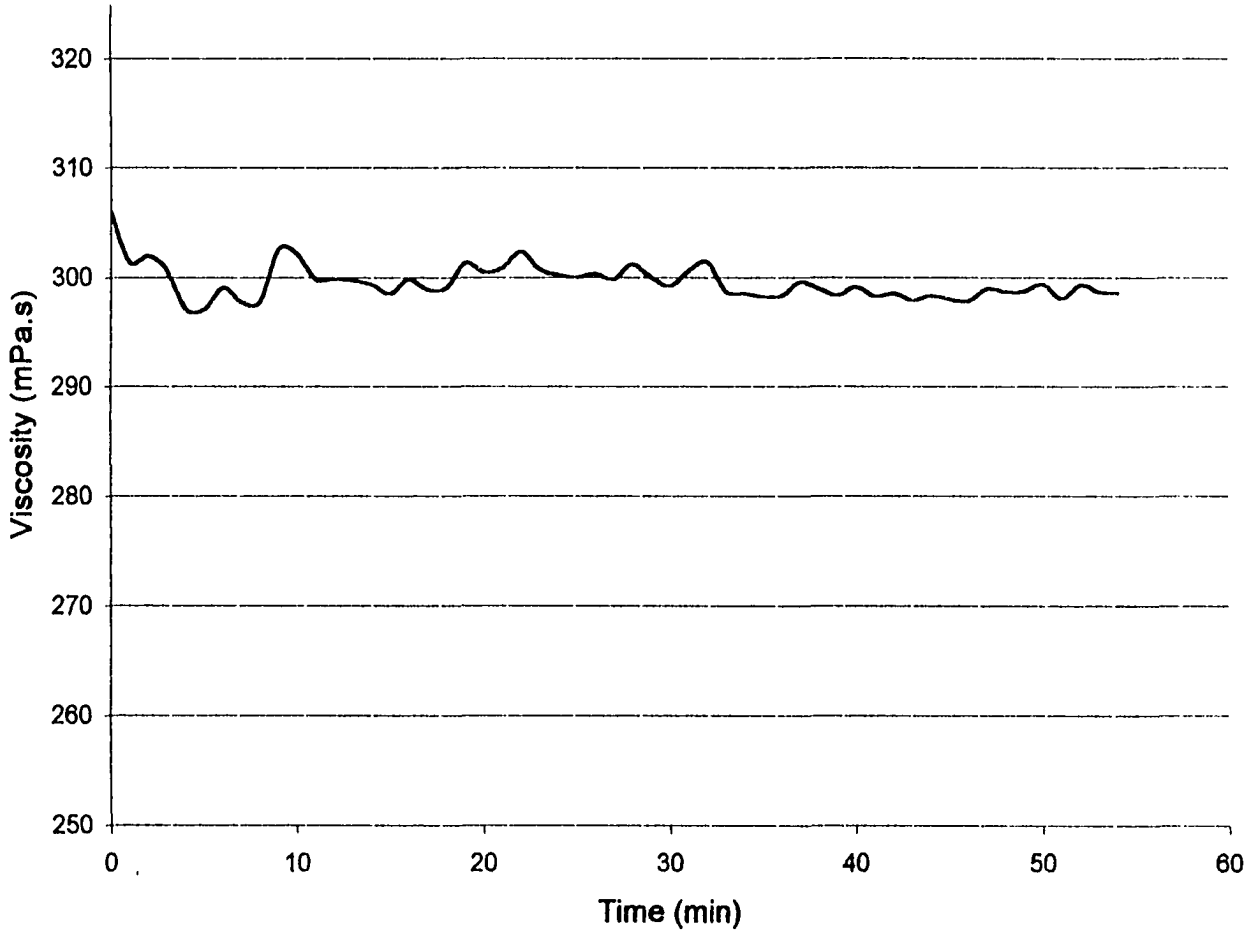

Figure 5.23A - Viscosity of foamy oil with o.5% (by vol.) defoamer at 6343 kPa (920 psi) for pressure depletion rate of 800 kPa/hr and room temperature.

Reproduced with permission of the copyright owner. Further reproduction prohibited without permission.

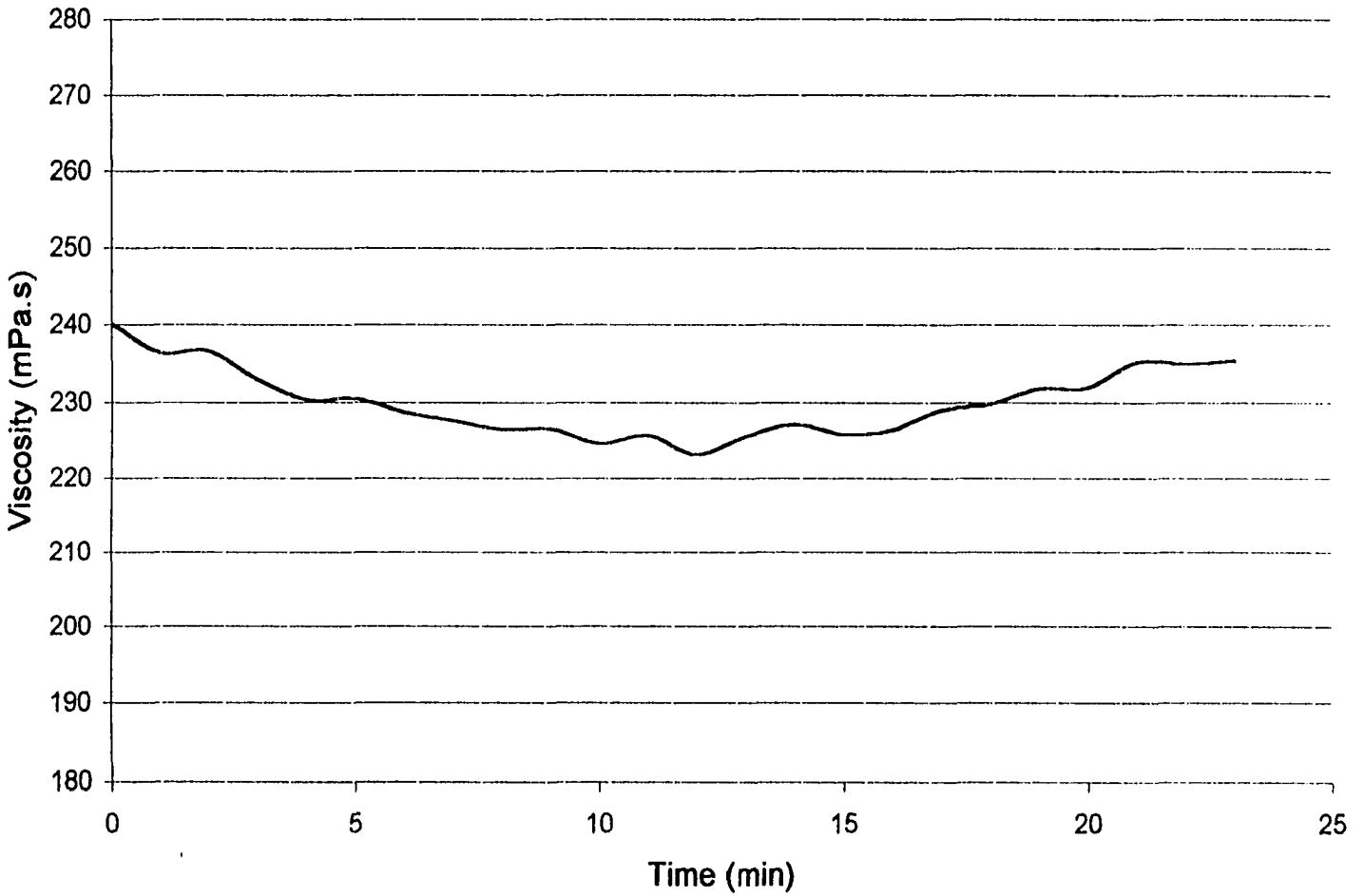

Figure 5.24A - Viscosity of foamy oil with o.5% (by vol.) defoamer at 6895 kPa (1000 psi) for pressure depletion rate of 800 kPa/hr and room temperature.

Reproduced with permission of the copyright owner. Further reproduction prohibited without permission.

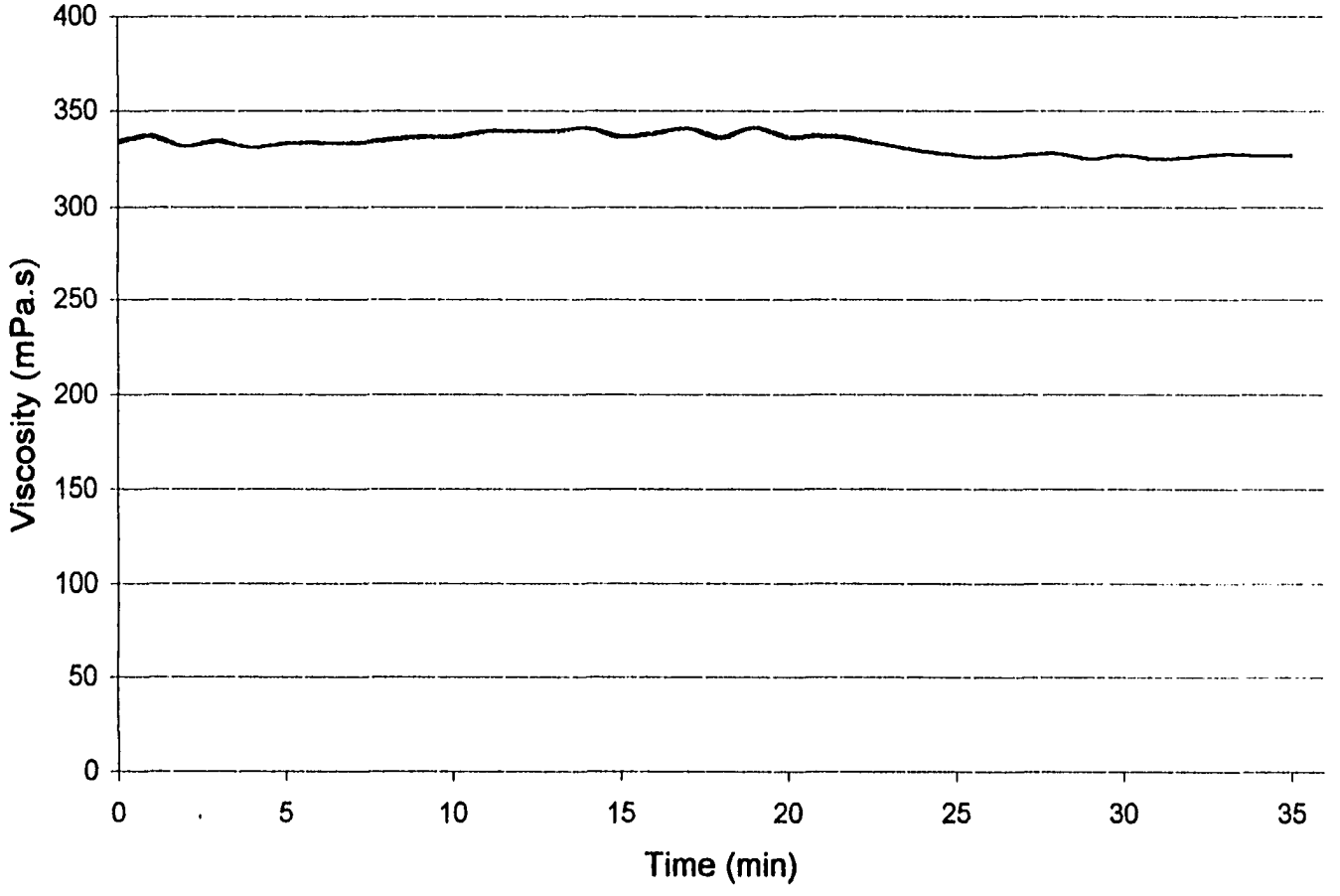

Figure 5.25A - Viscosity of foamy oil with 0.5% (by Vol.) defoamer at 7584 kPa (1100 psi) for pressure depletion rate of 800 kPa/hr and room temperature.

Reproduced with permission of the copyright owner. Further reproduction prohibited without permission.

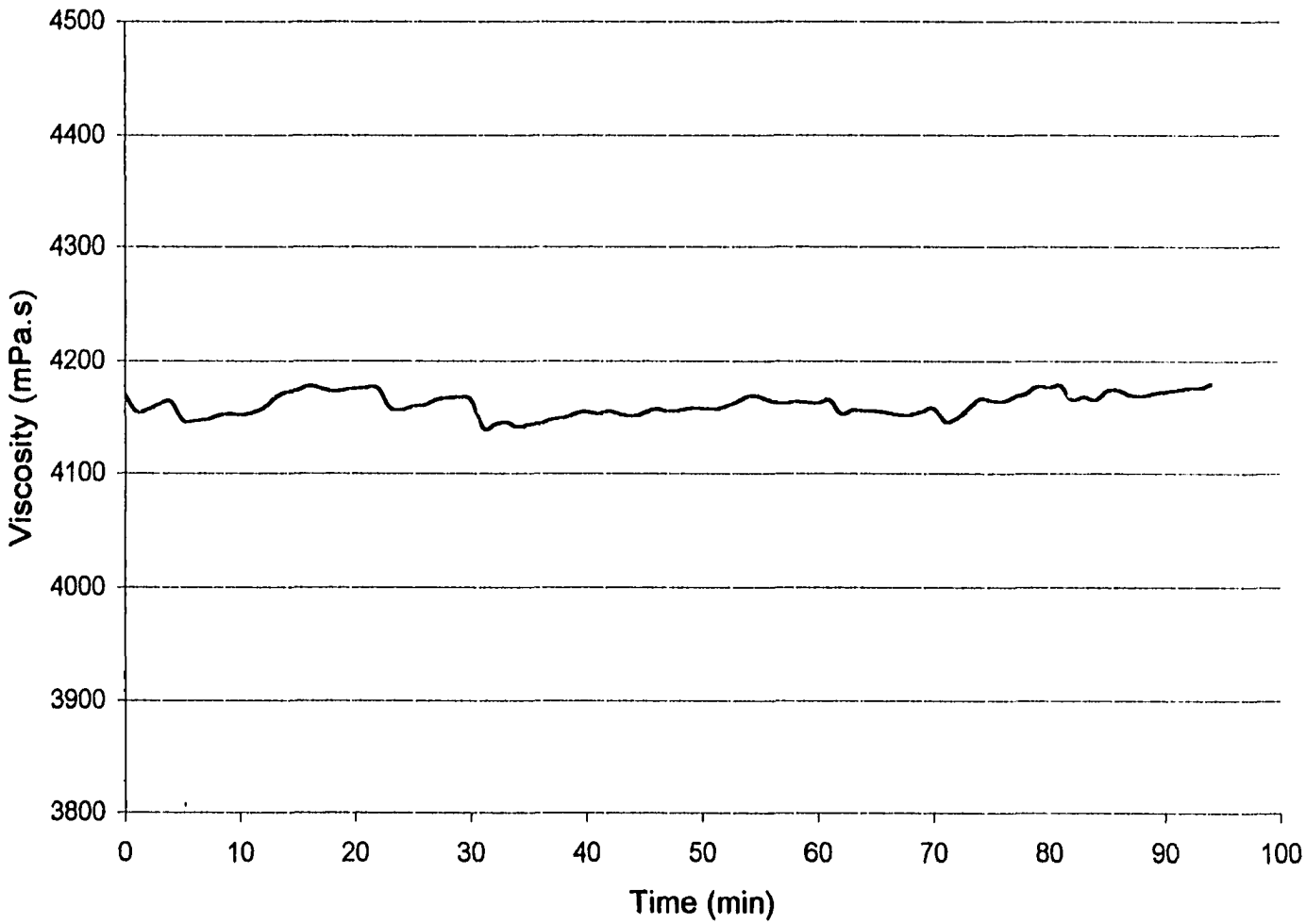

Figure 5.26A - Viscosity of foamy oil at 2068 kPa (300 psi) for 800 kPa/hr pressure depletion rate and room temperature.

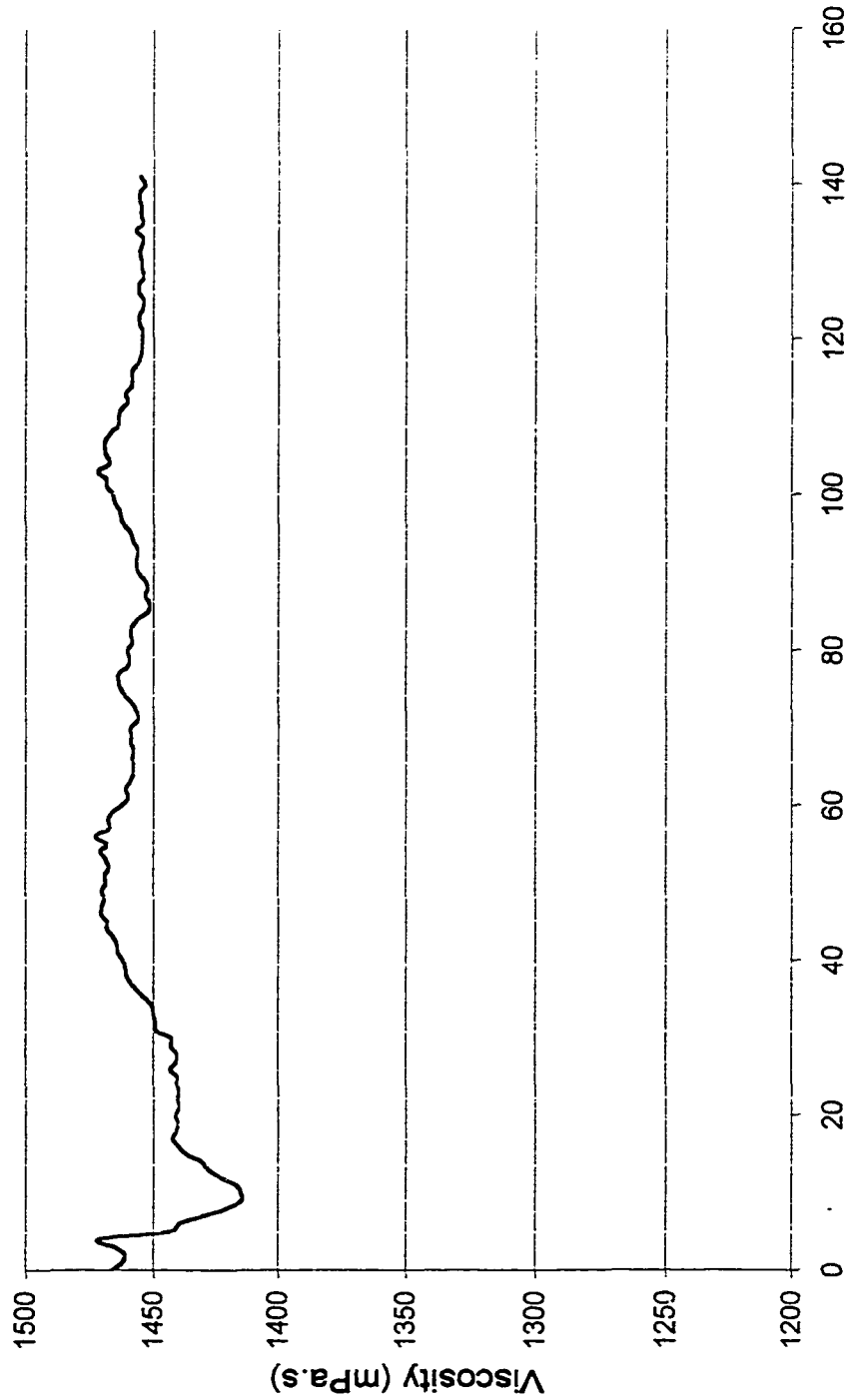

Figure 5.27A- Viscosity of foamy oil at 4689 kPa (680 psi) for 800 kPa/hr pressure depletion rate and room temperature.

Reproduced with permission of the copyright owner. Further reproduction prohibited without permission.

Reproduced with permission of the copyright owner. Further reproduction prohibited without permission.

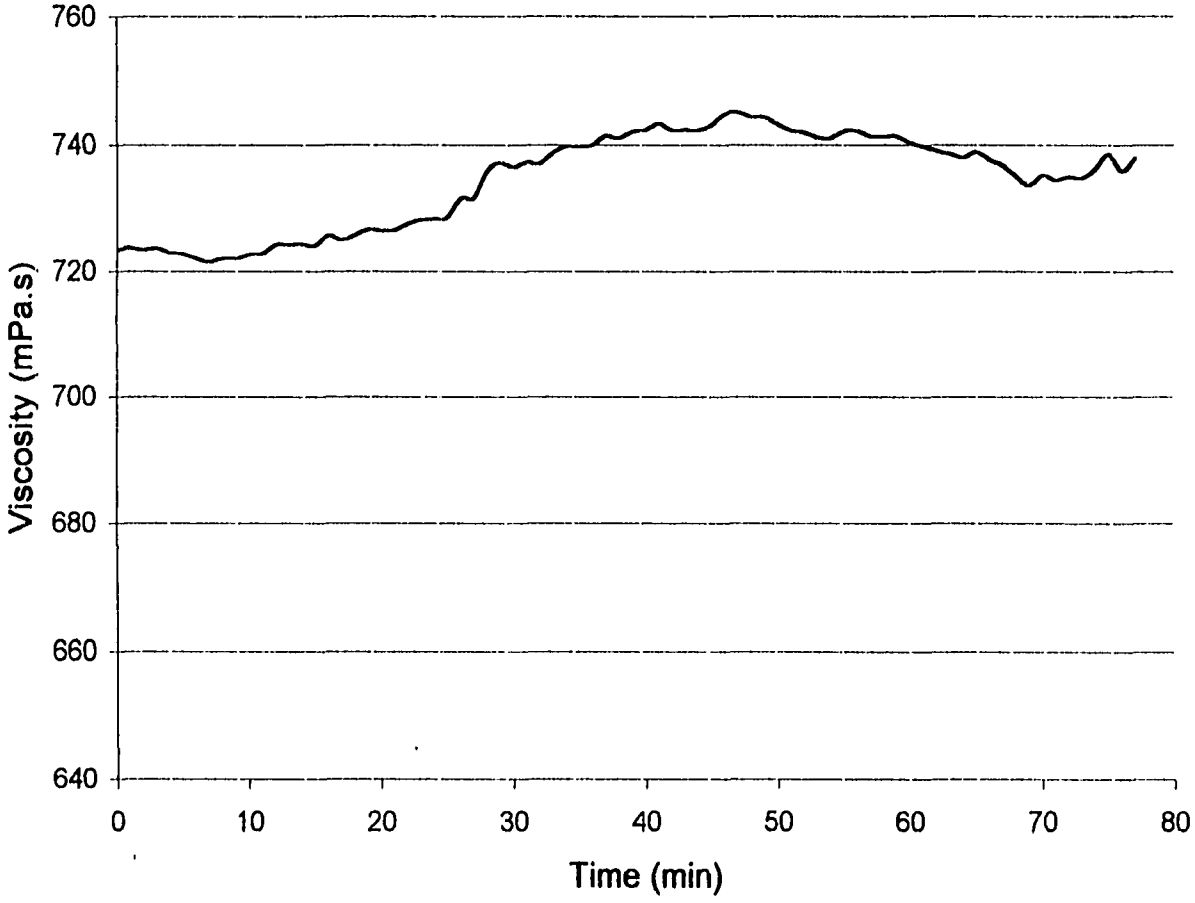

Figure 5.28A - Viscosity of foamy oil at 5516 kPa (800 psi) for 800 kPa/hr pressure depletion rate and room temperature.

Reproduced with permission of the copyright owner. Further reproduction prohibited without permission.

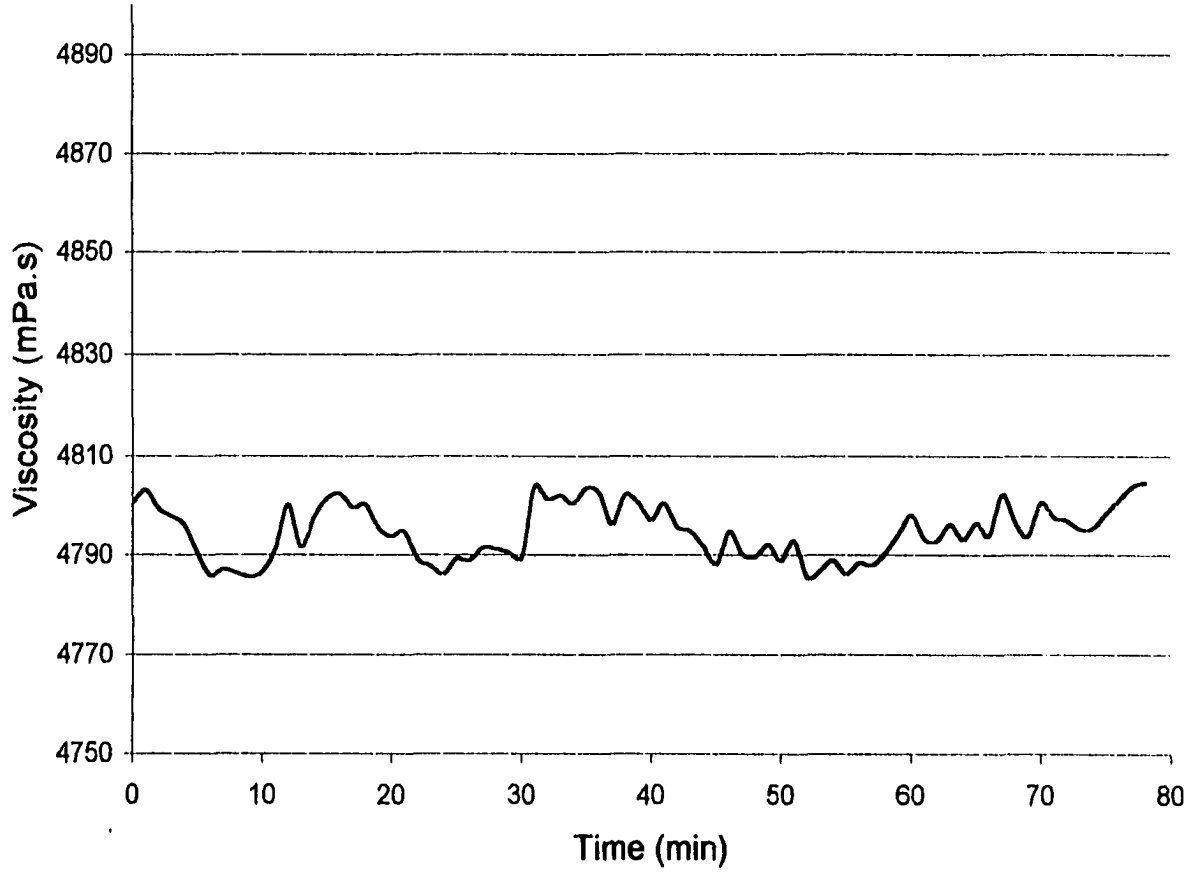

Figure 5.29A - Viscosity of foamy oil with o.5% (by vol.) defoamer at 2068 kPa (300 psi) for pressure depletion rate of 800 kPa/hr and room temperature using 10000-piston.

Reproduced with permission of the copyright owner. Further reproduction prohibited without permission.

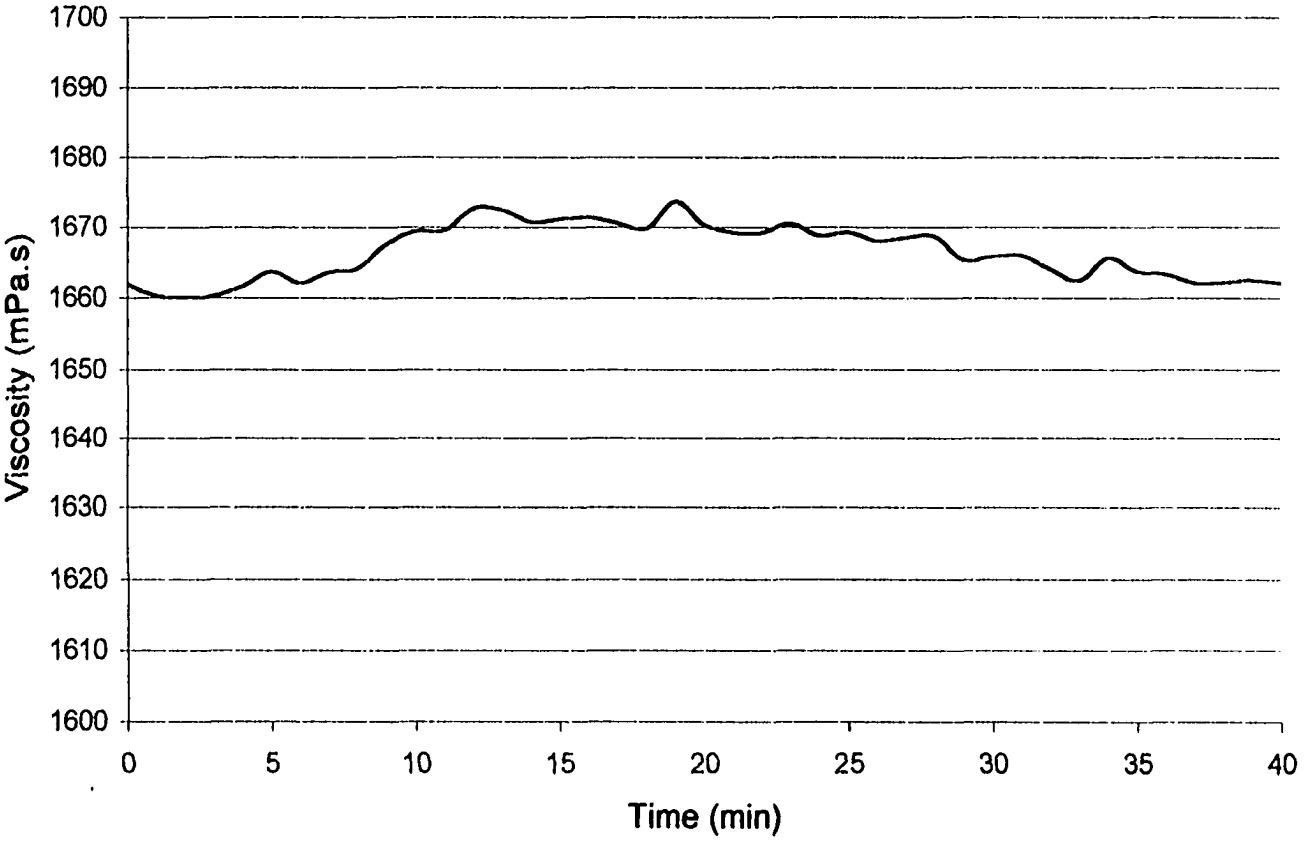

Figure 5.31A - Viscosity of foamy oil with o.5% (by vol.) defoamer at 4689 kPa (680 psi) for prssure depletion rate of 800 kPa/hr and room temperature using 10000-piston (overlap run with 2000piston).

Reproduced with permission of the copyright owner. Further reproduction prohibited without permission.

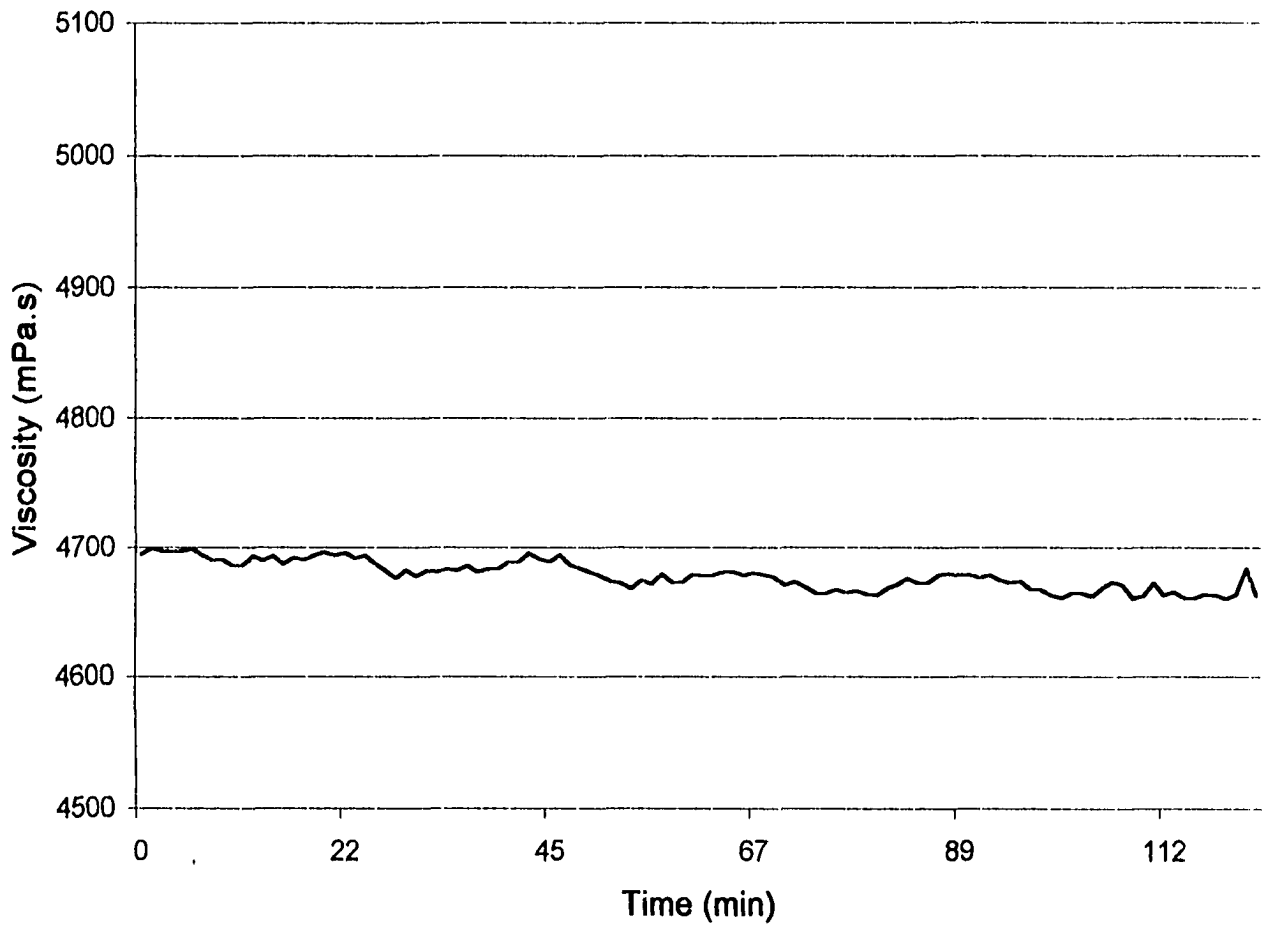

Figure 32A - Viscosity of foamy oil at 2068 kPa (300psi) for pressure depletion rate of 41 kPa/hr and room temperature.

Reproduced with permission of the copyright owner. Further reproduction prohibited without permission.

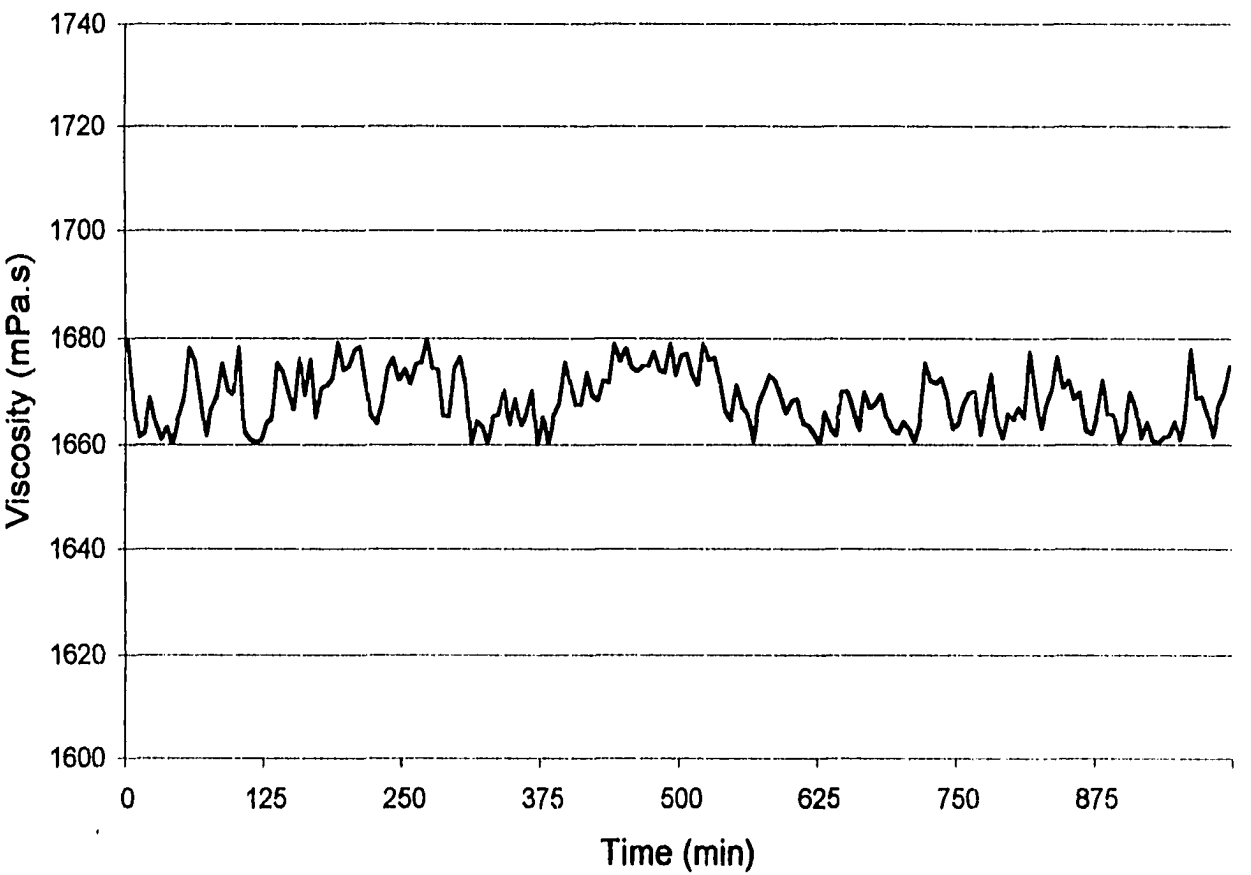

Figure 5.33A - Viscosity of foamy oil at 4689 kPa (680 psi) for pressure depletion rate 41 kPa/hr and room temperature.

Reproduced with permission of the copyright owner. Further reproduction prohibited without permission.

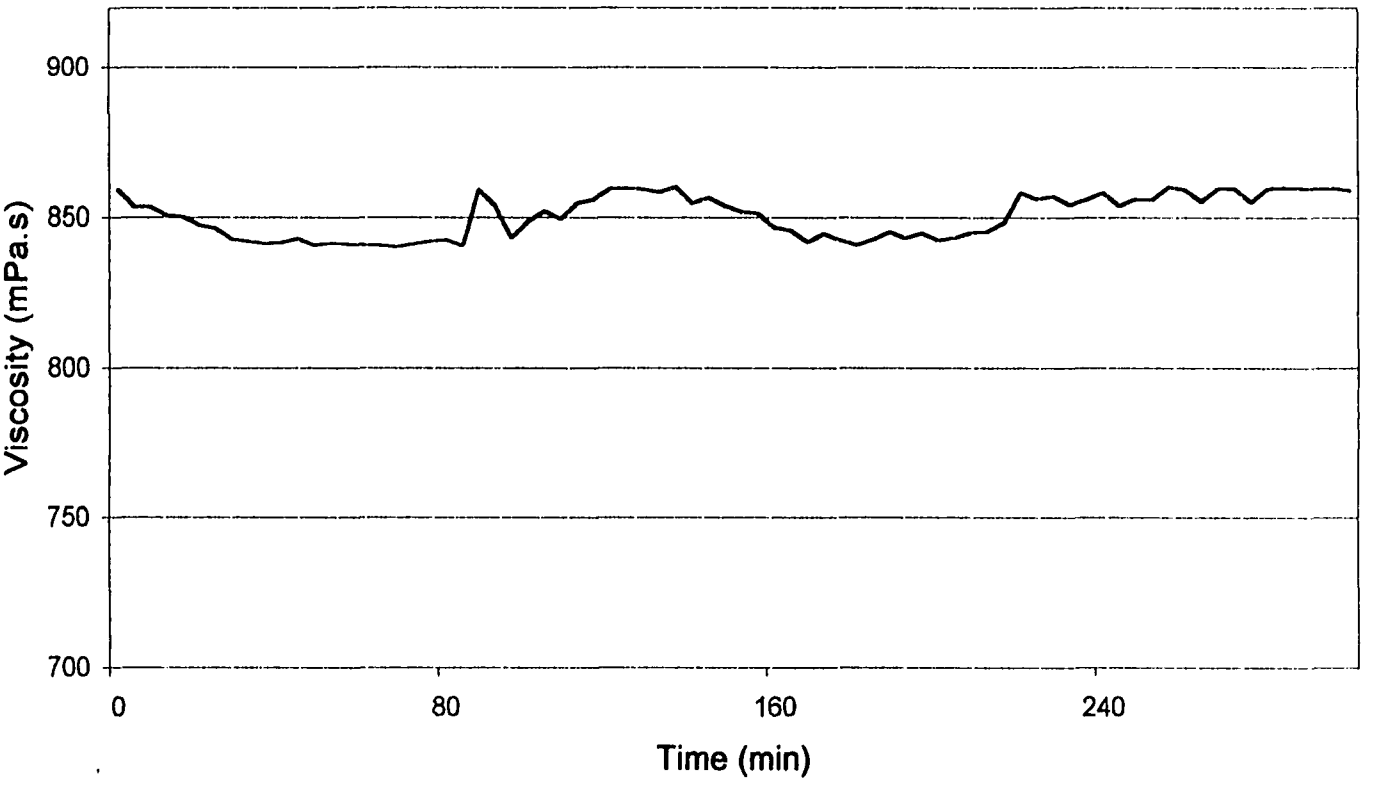

Figure 5.34A - Viscosity of foamy oil at 5516 (800 psi) for pressure depletion rate of 41 kPa/hr and room temperature.

Reproduced with permission of the copyright owner. Further reproduction prohibited without permission.

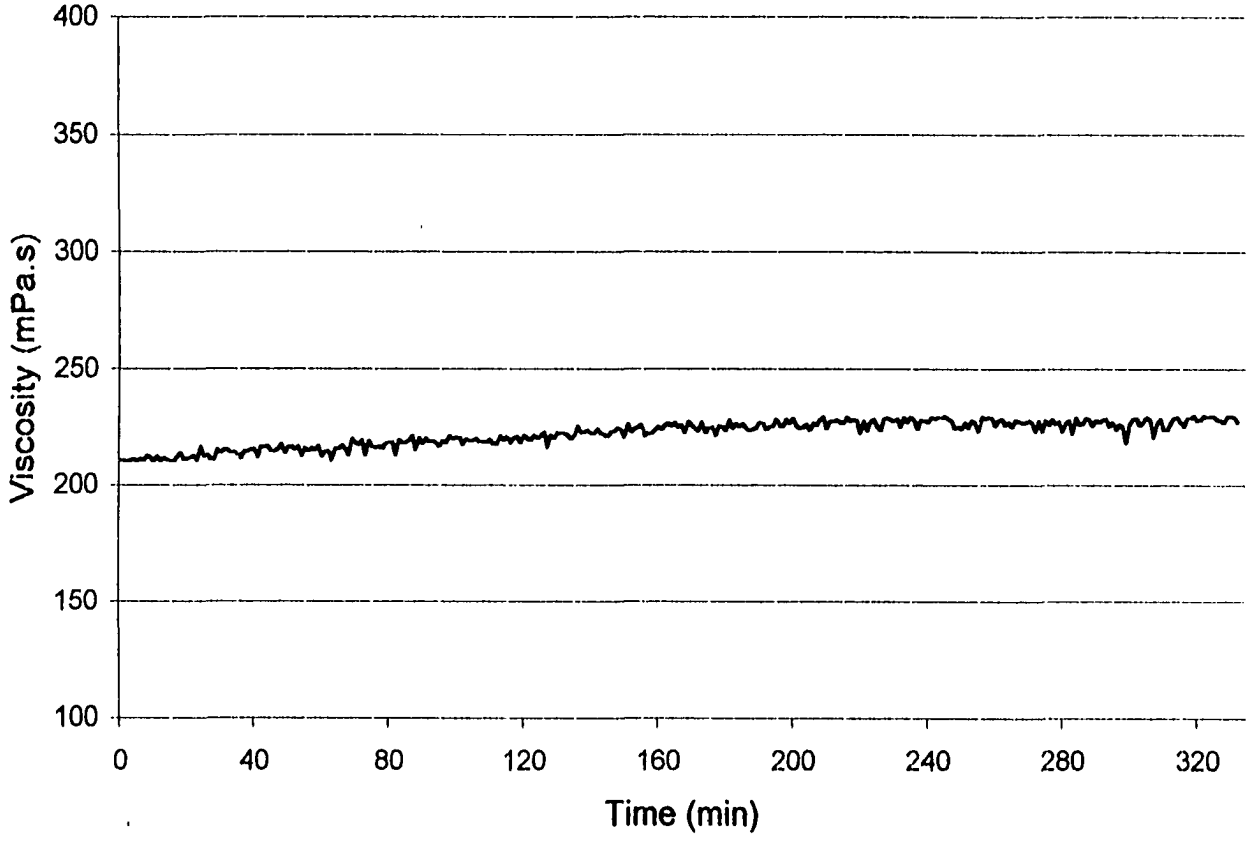

Figure 5.35A- Viscosity of foamy oil at 6343 kPa (920 psi) for pressure depletion rate of 41 kPa/hr and room temperature.

Reproduced with permission of the copyright owner. Further reproduction prohibited without permission.

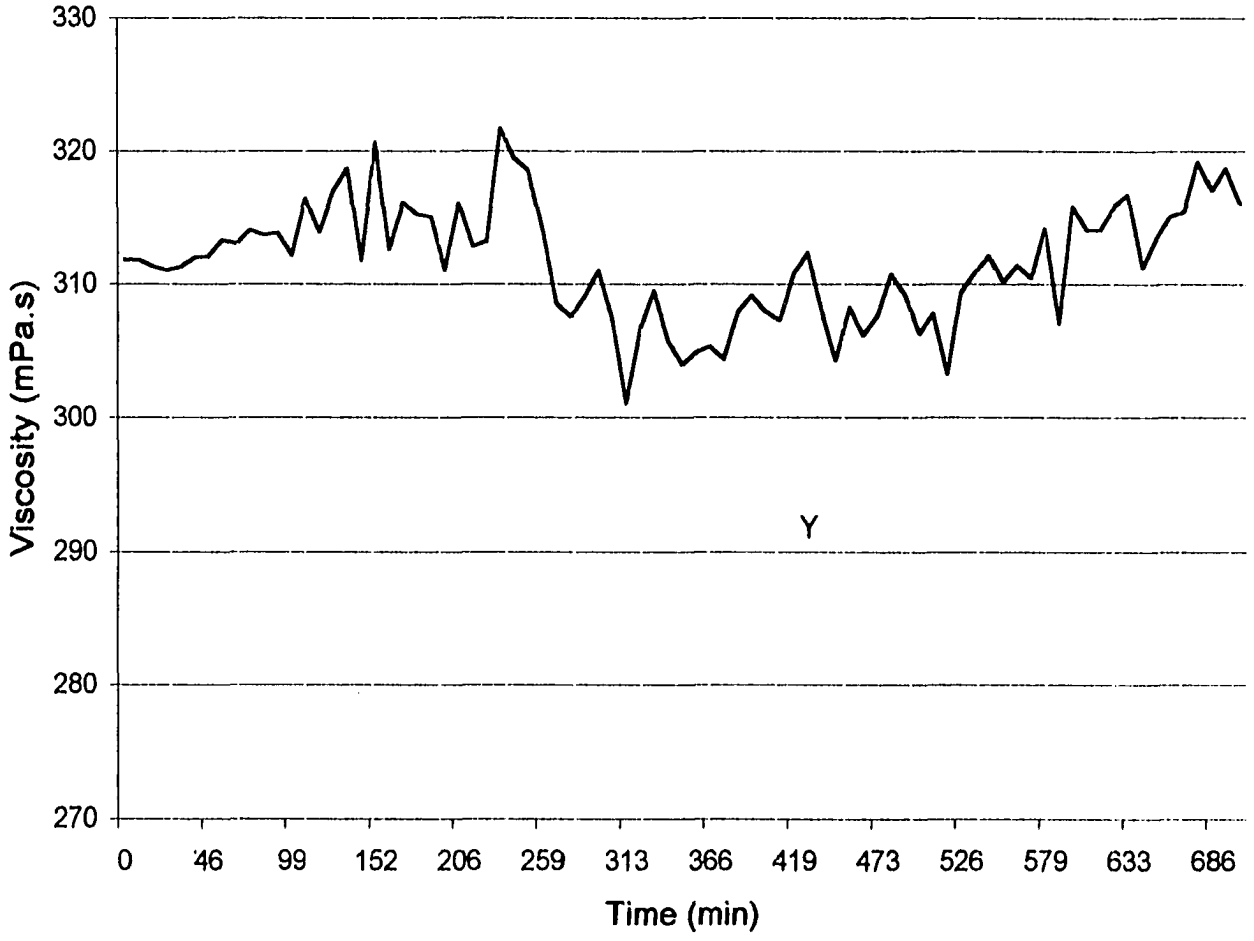

Figure 5.36A - Viscosity of foamy oil at 7584 kPa (1100 psi) for pressure depletion rate of 41 kPa/hr and room temperature.

Reproduced with permission of the copyright owner. Further reproduction prohibited without permission.

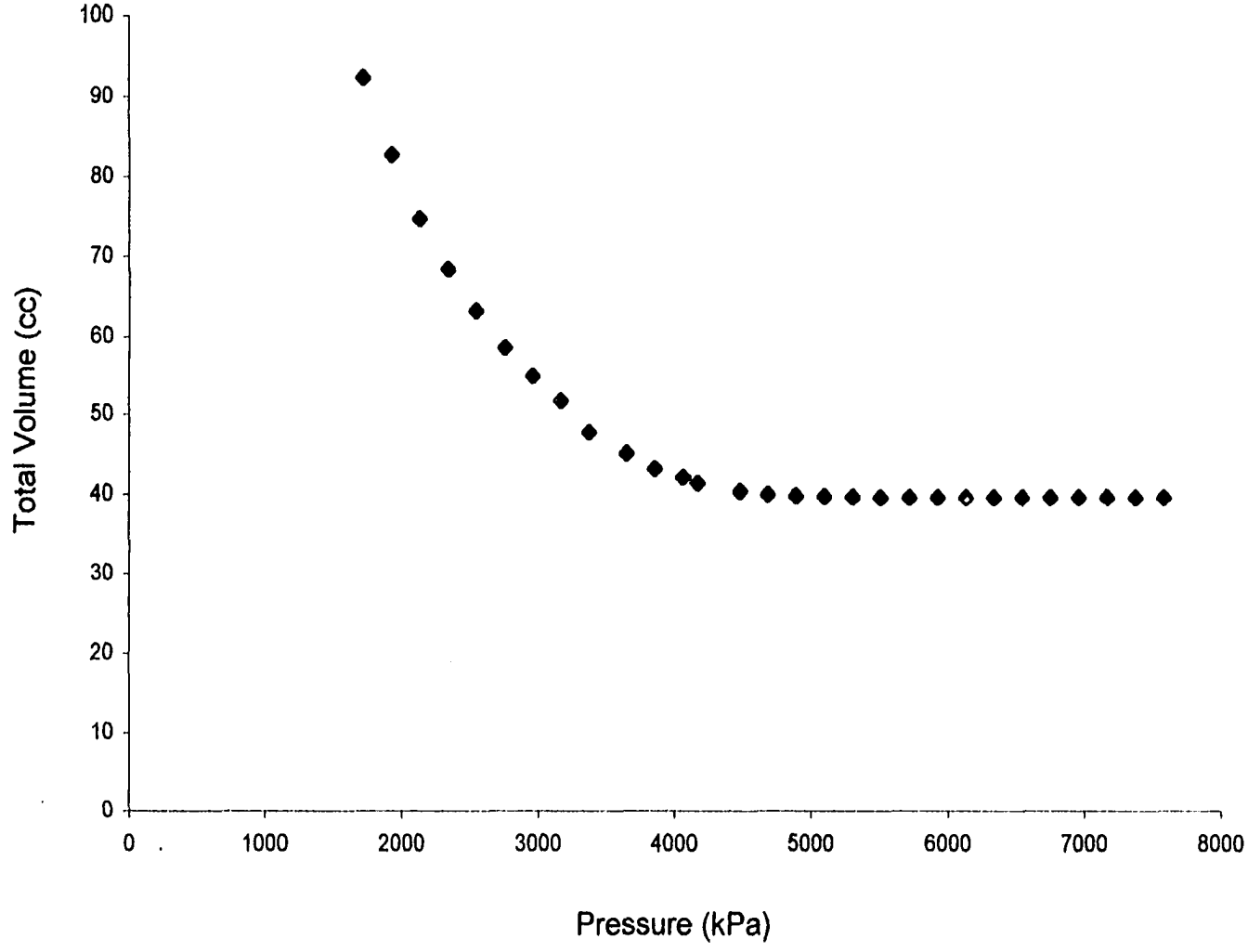

Figure 5.2T - Total volume of foamy oil for no mixing case at a depletion rate of 800 kPa/hr and room temperature.

Reproduced with permission of the copyright owner. Further reproduction prohibited without permission.

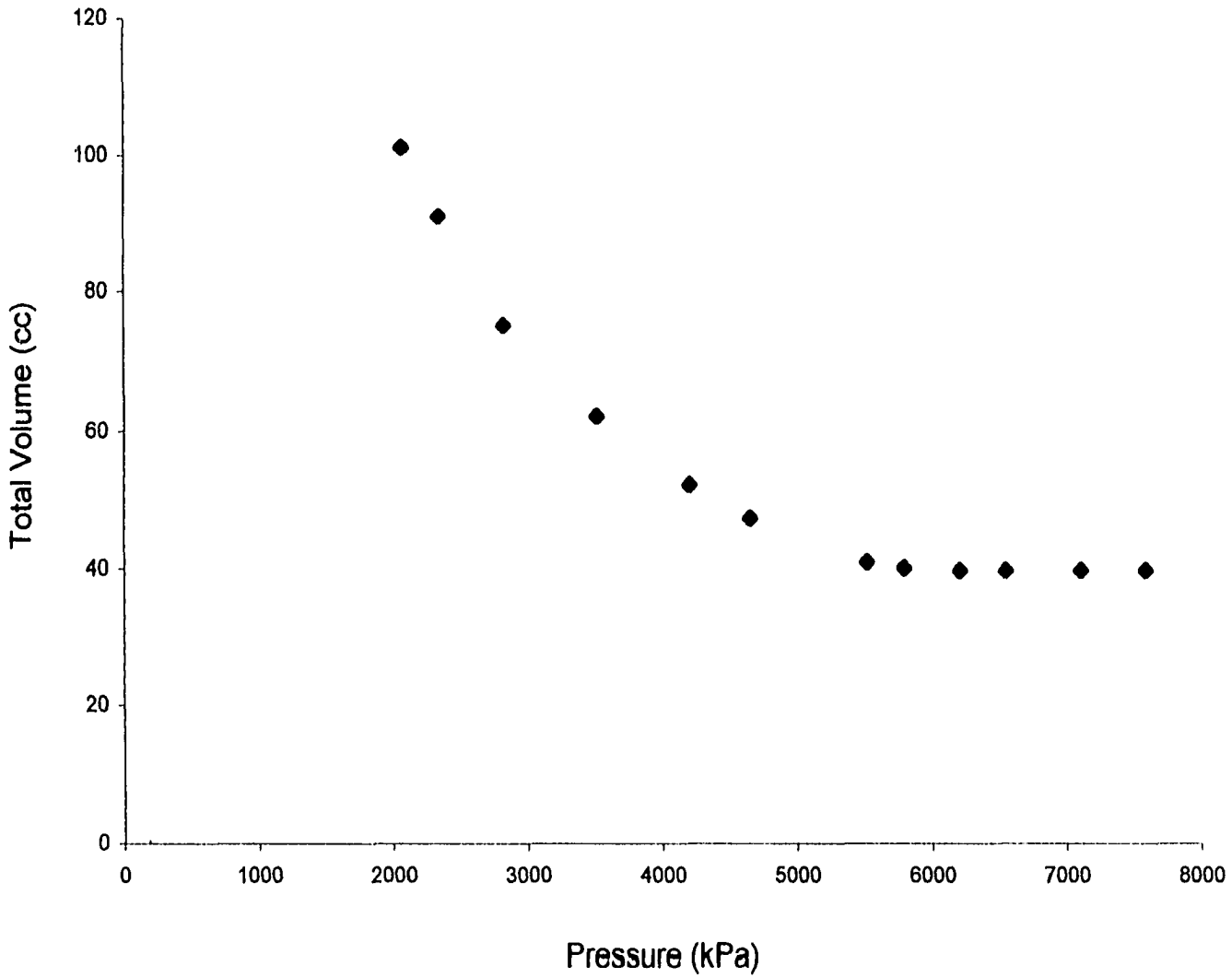

Figure 5.3T - Total volume of foamy oil for mixing case at a depletion rate of 800 kPa/hr and room temperature.

Reproduced with permission of the copyright owner. Further reproduction prohibited without permission.

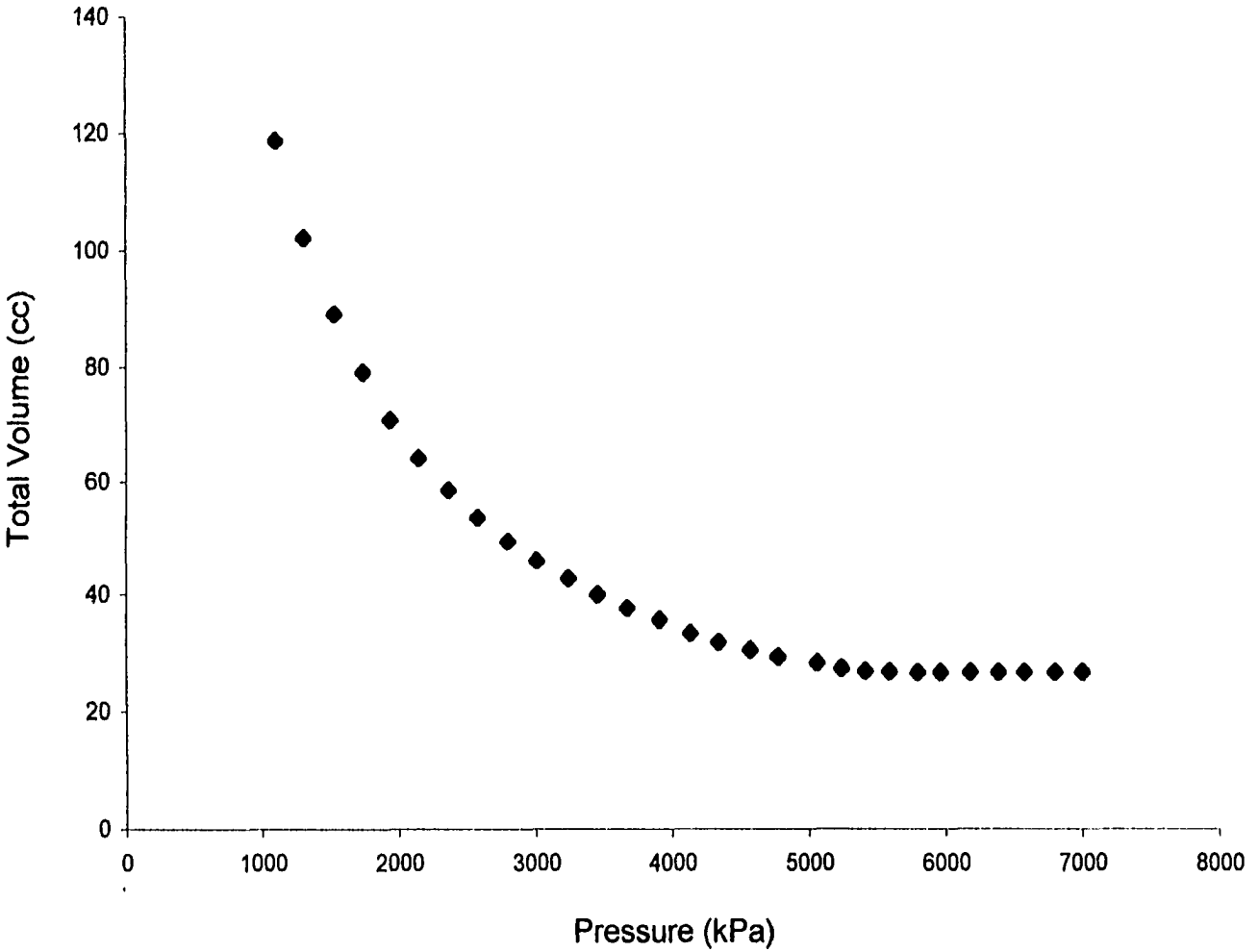

Figure 5.4T - Total volume of foamy oil for 0.5% (by vol.) defomer and no mixing case at a depletion rate of 800 kPa/hr and room temperature.

Reproduced with permission of the copyright owner. Further reproduction prohibited without permission.

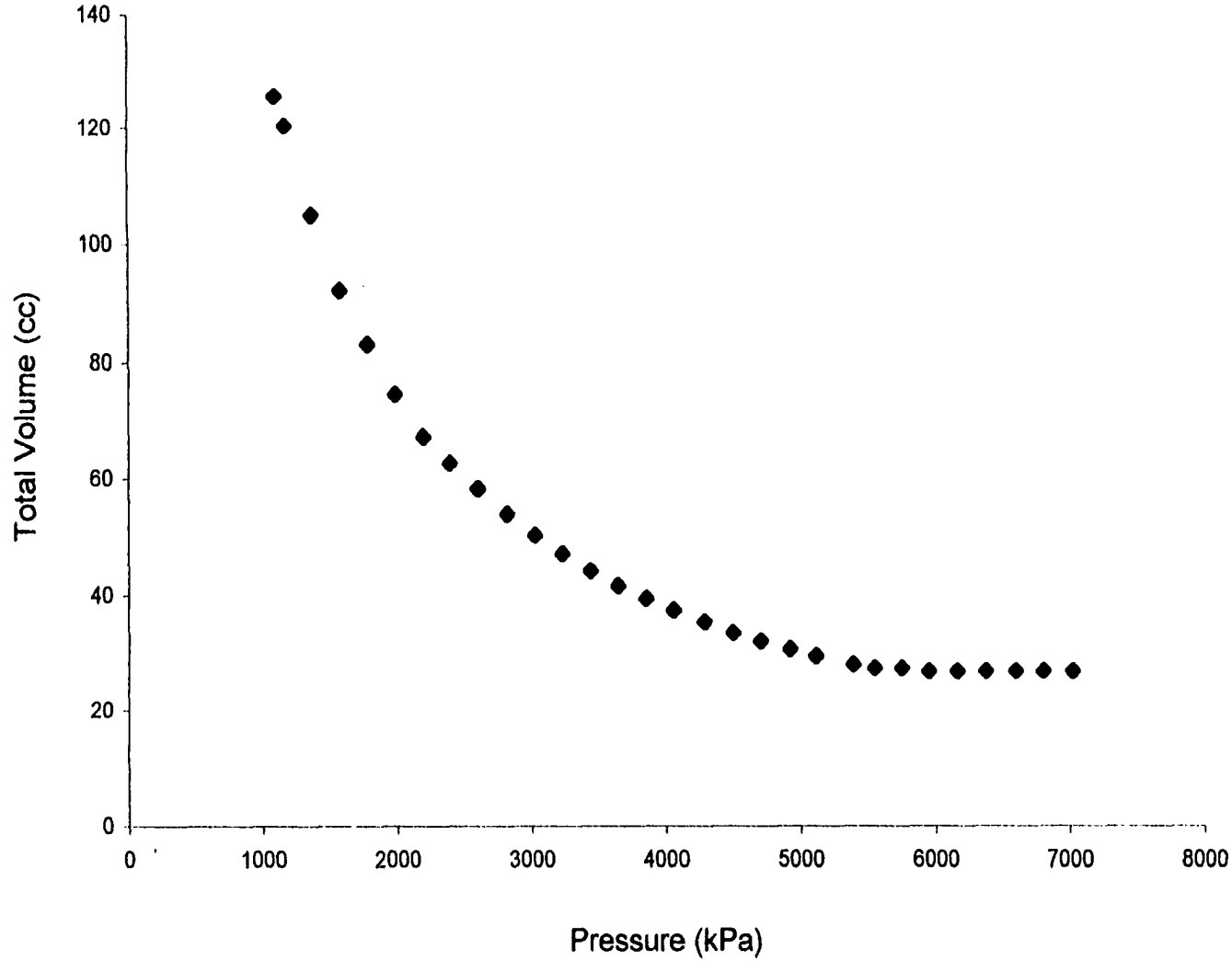

Figure 5.5T - Total volume of foamy oil for 0.5% (by vol.) defomer and mixing case at a depletion rate of 800 kPa/hr and room temperature.

Reproduced with permission of the copyright owner. Further reproduction prohibited without permission.

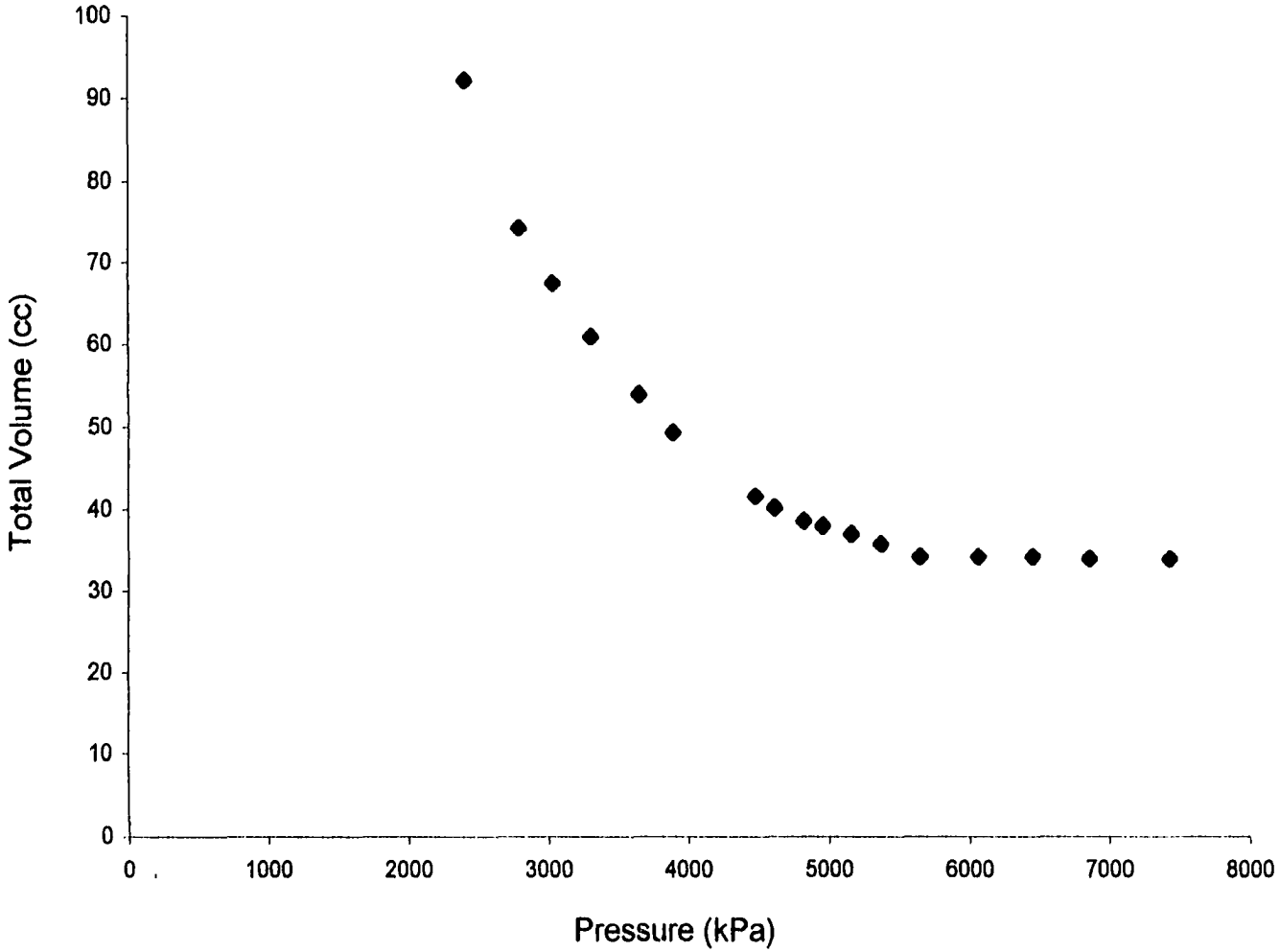

Figure 5.7T - Total volume of foamy oil for glass beads bed case at a depletion rate of 800 kPa/hr and room temperature.

Reproduced with permission of the copyright owner. Further reproduction prohibited without permission.

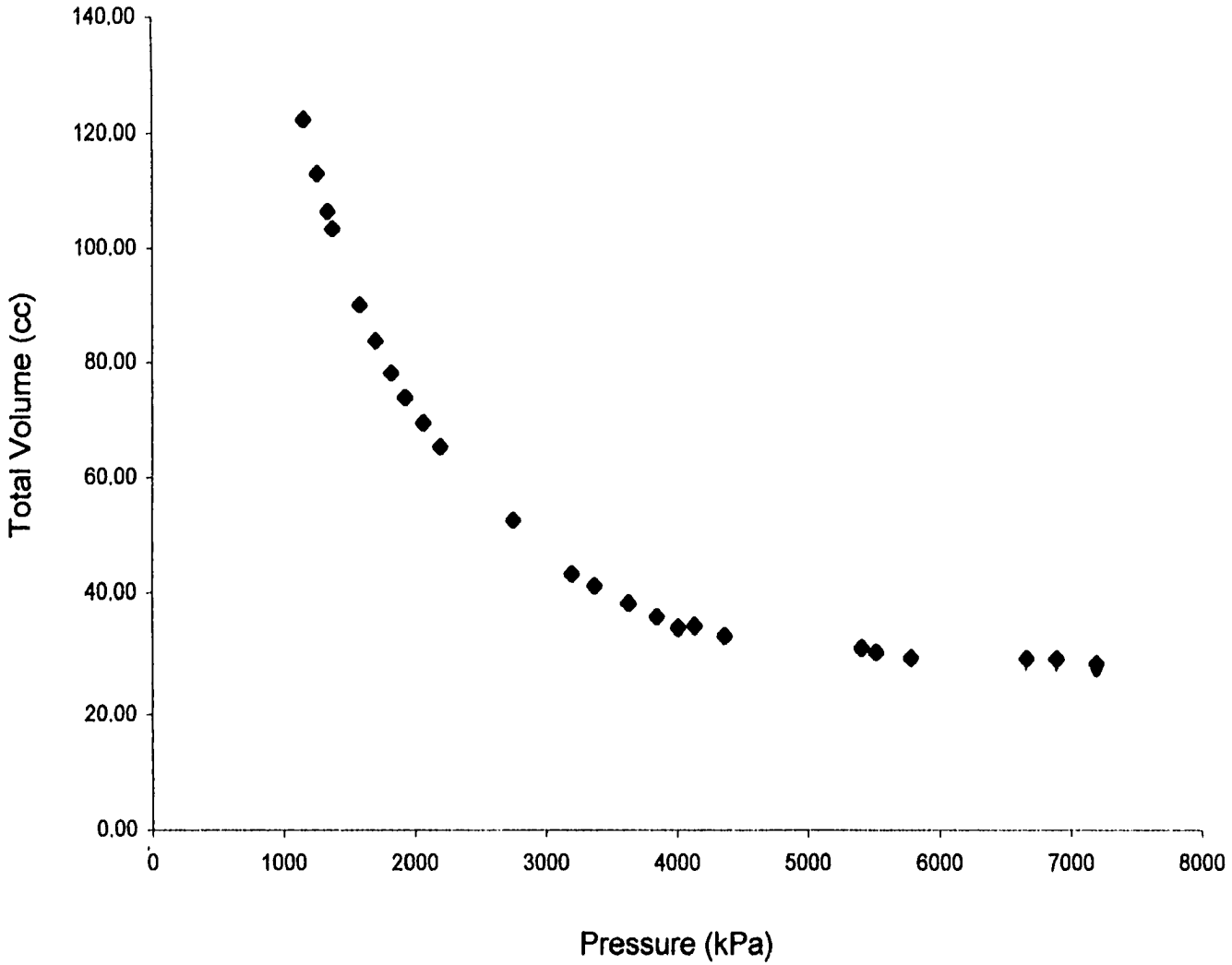

Figure 5.9T - Total volume of foamy oil for no mixing case at depletion rate of 41 kPa/hr and room temperature.

Reproduced with permission of the copyright owner. Further reproduction prohibited without permission.

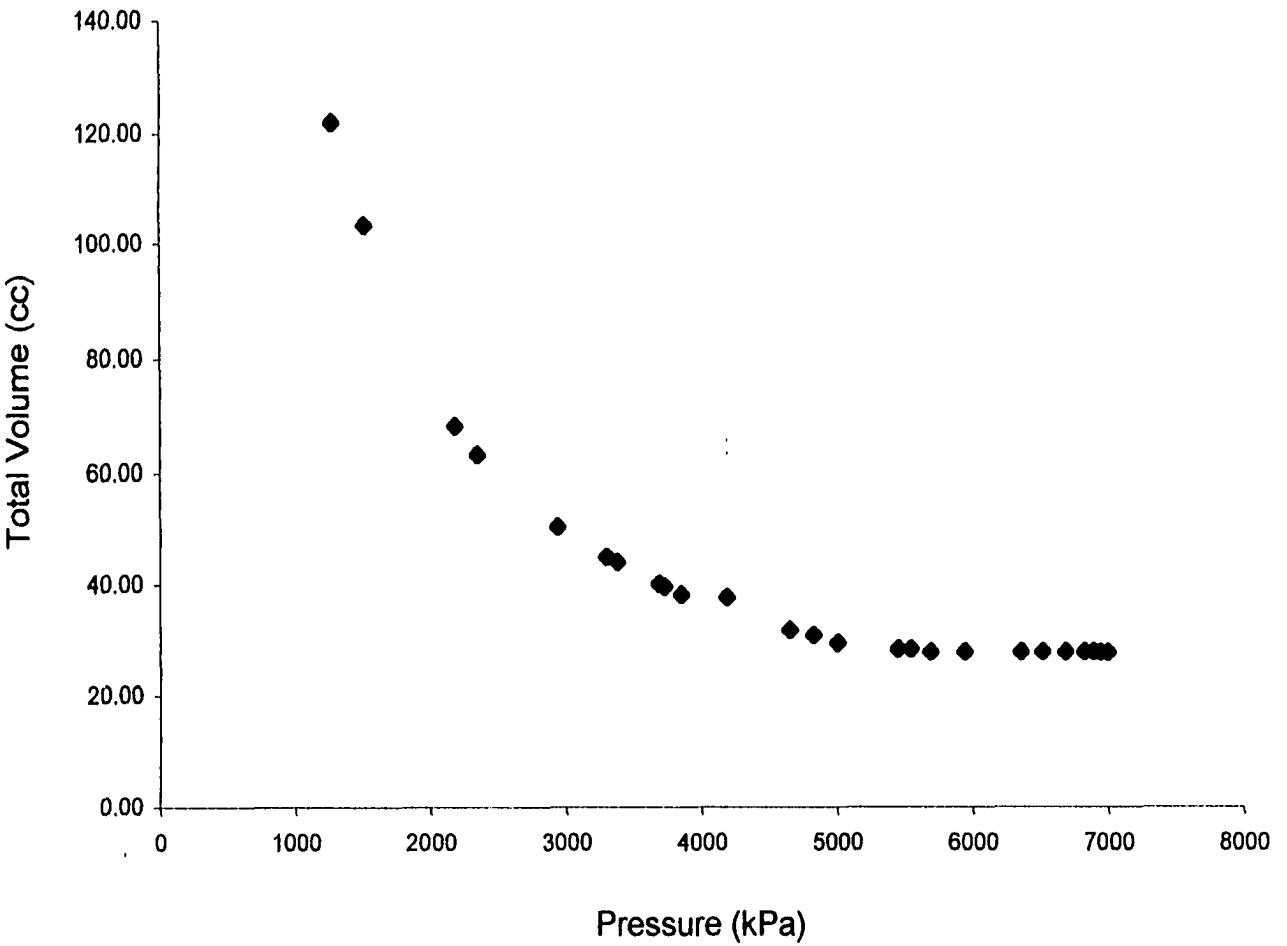

Figure 5.10T - Total volume of foamy oil for mixing case at depletion rate of 41 kPa/hr and room temperature.

Reproduced with permission of the copyright owner. Further reproduction prohibited without permission.

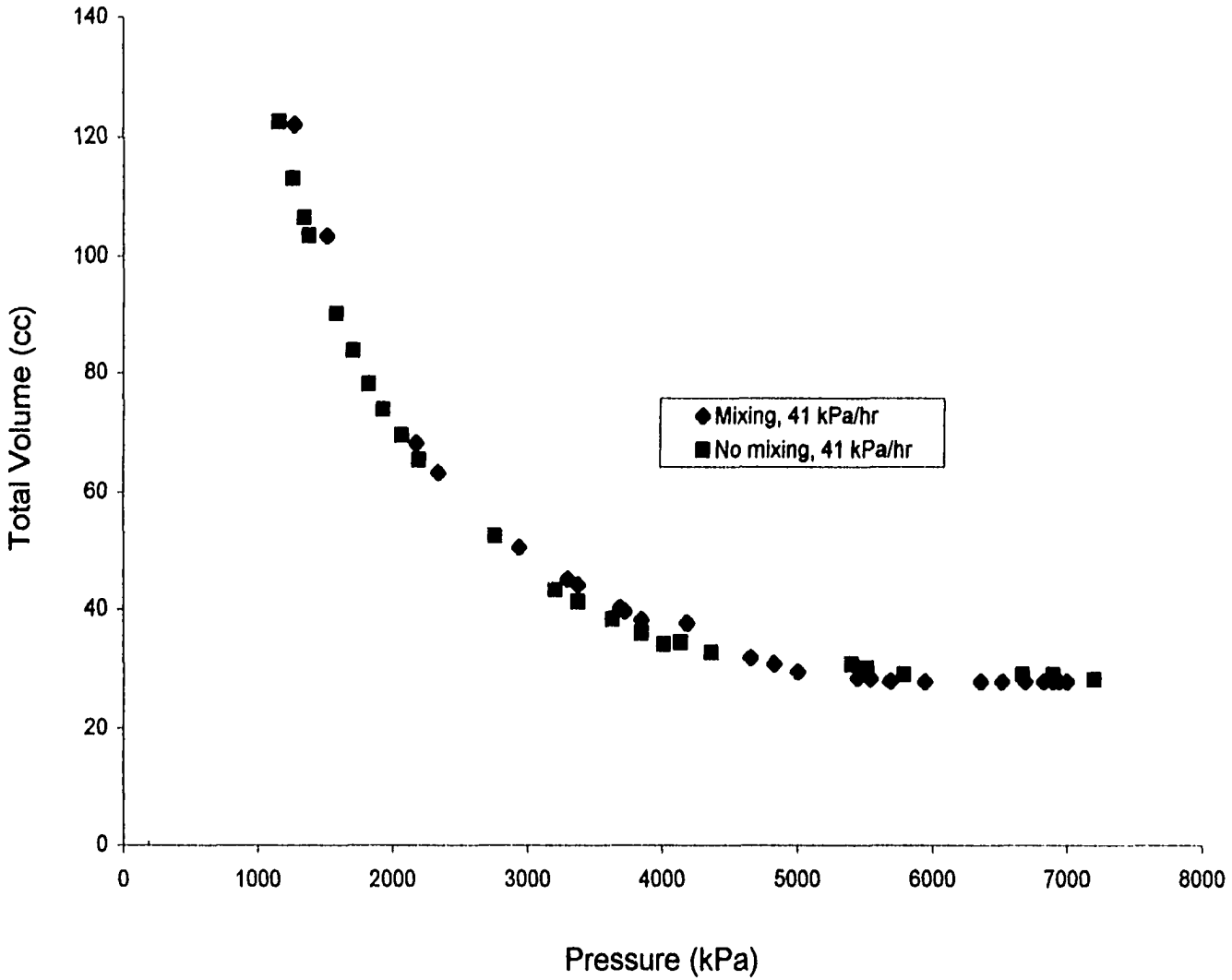

Figure 5.11T - Comparison of total volume at depletion rate of 41 kPa/hr and room temperature for mixing and no mixing cases.

Reproduced with permission of the copyright owner. Further reproduction prohibited without permission.

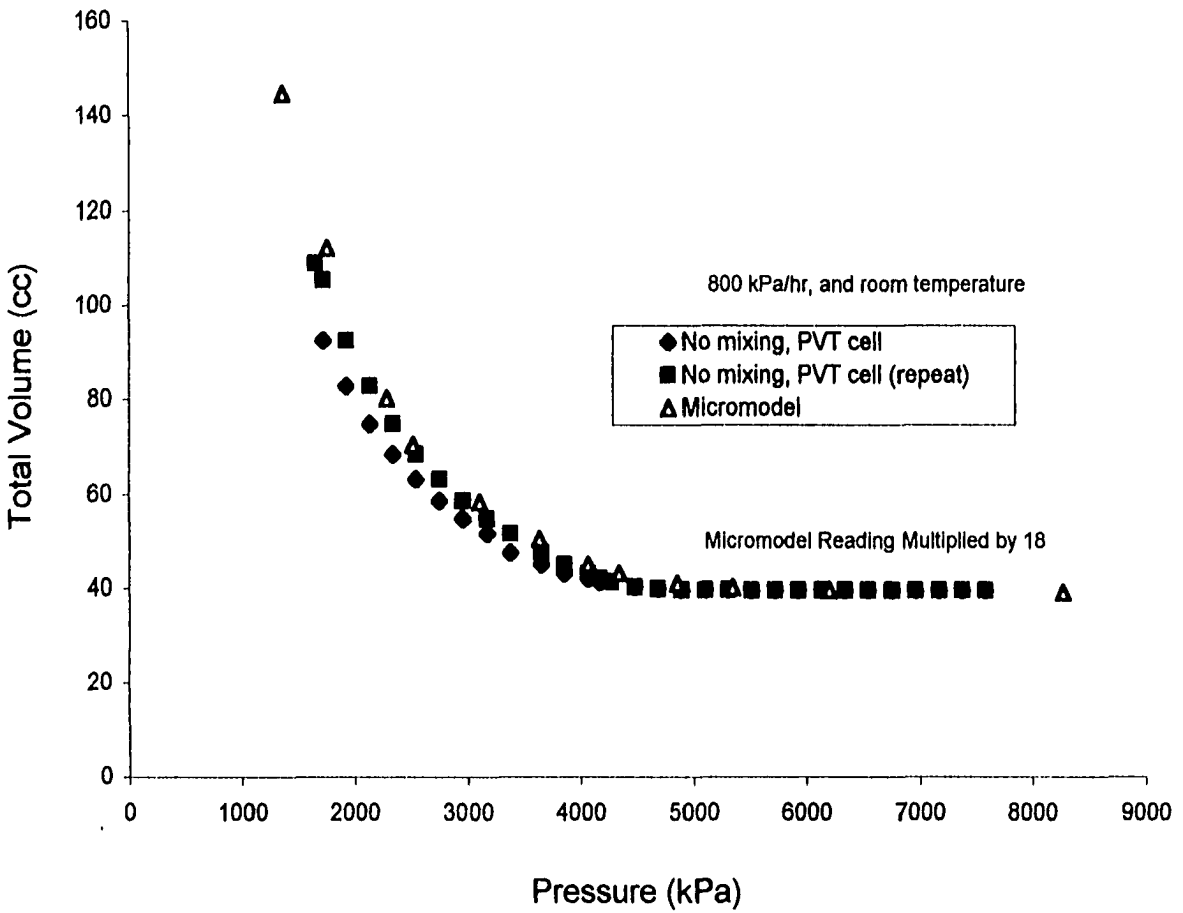

Figure 5.26T - Comparison of PVT cell CCE (total volume) and micromodel pressure depletion at a pressure depletion rate of 800 kPa/hr.

Reproduced with permission of the copyright owner. Further reproduction prohibited without permission.

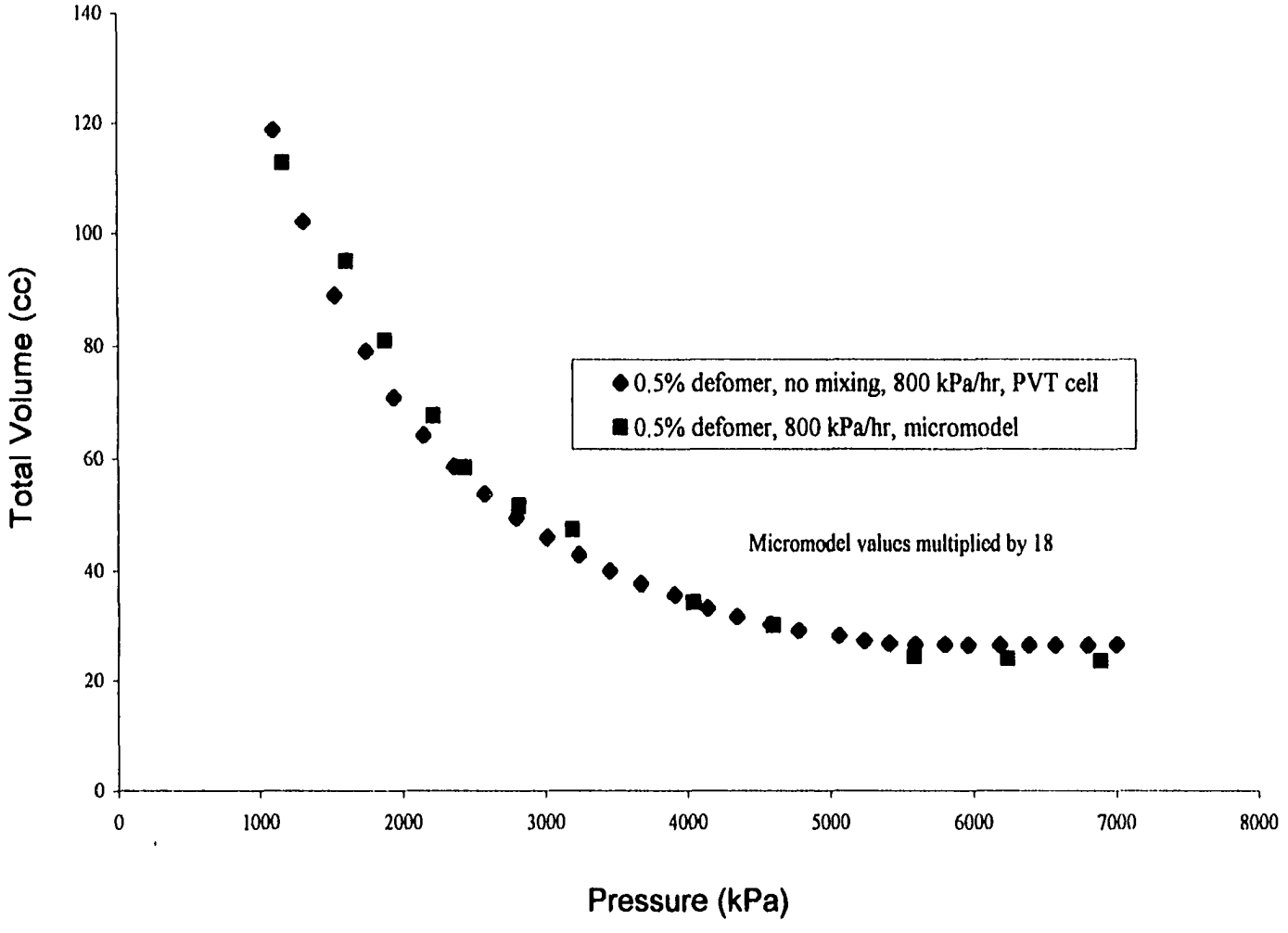

Figure 5.27T - Comparison of PVT cell CCE (total volume) and micromodel runs of 0.5% defoamer at a pressure depletion rate of 800 kPa/hr.

Reproduced with permission of the copyright owner. Further reproduction prohibited without permission.

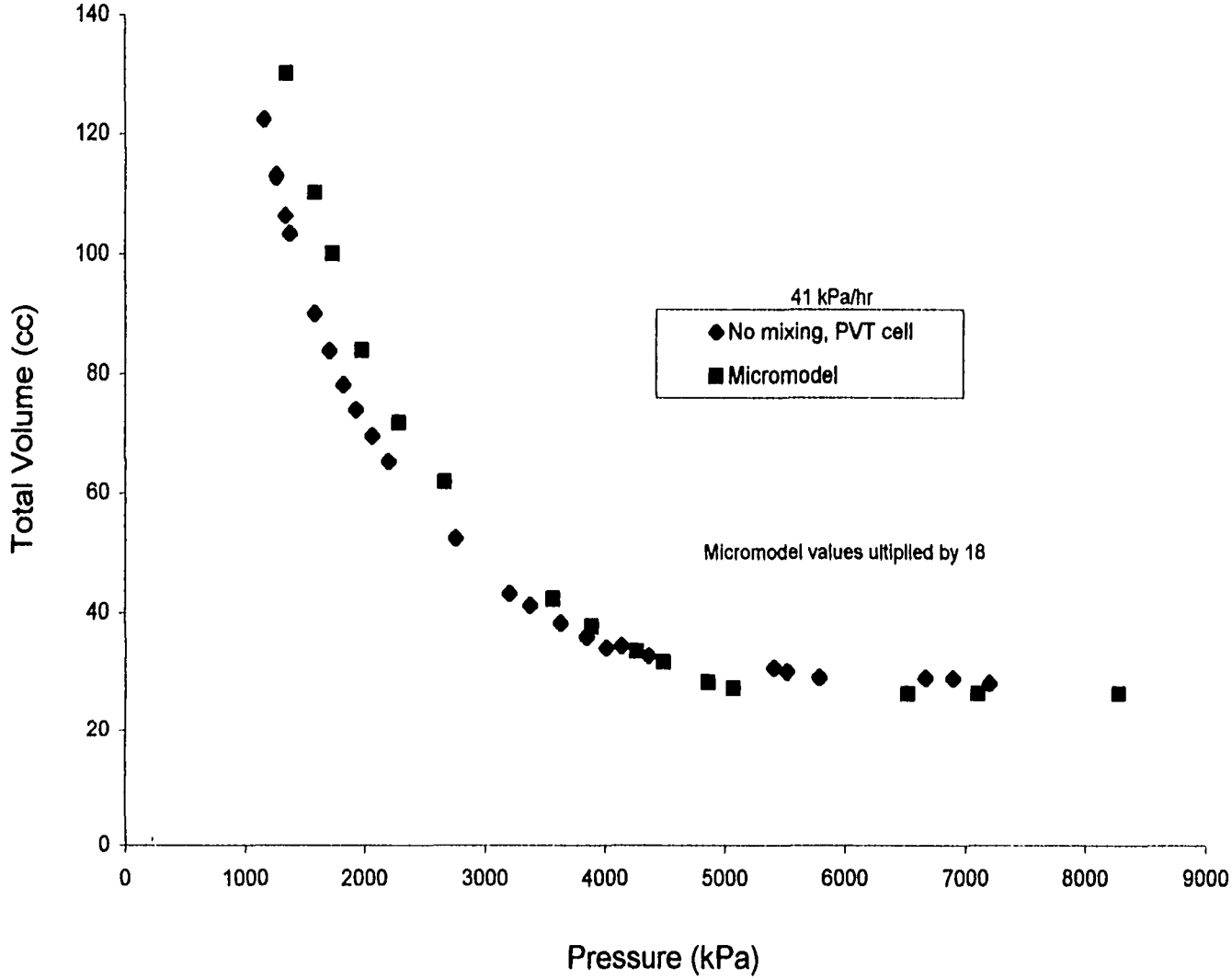

Figure 5.28T - Comparison of PVT cell (total volume) CCE and micromodel run at pressure depletion rate of 41 kPa/hr.

Reproduced with permission of the copyright owner. Further reproduction prohibited without permission.

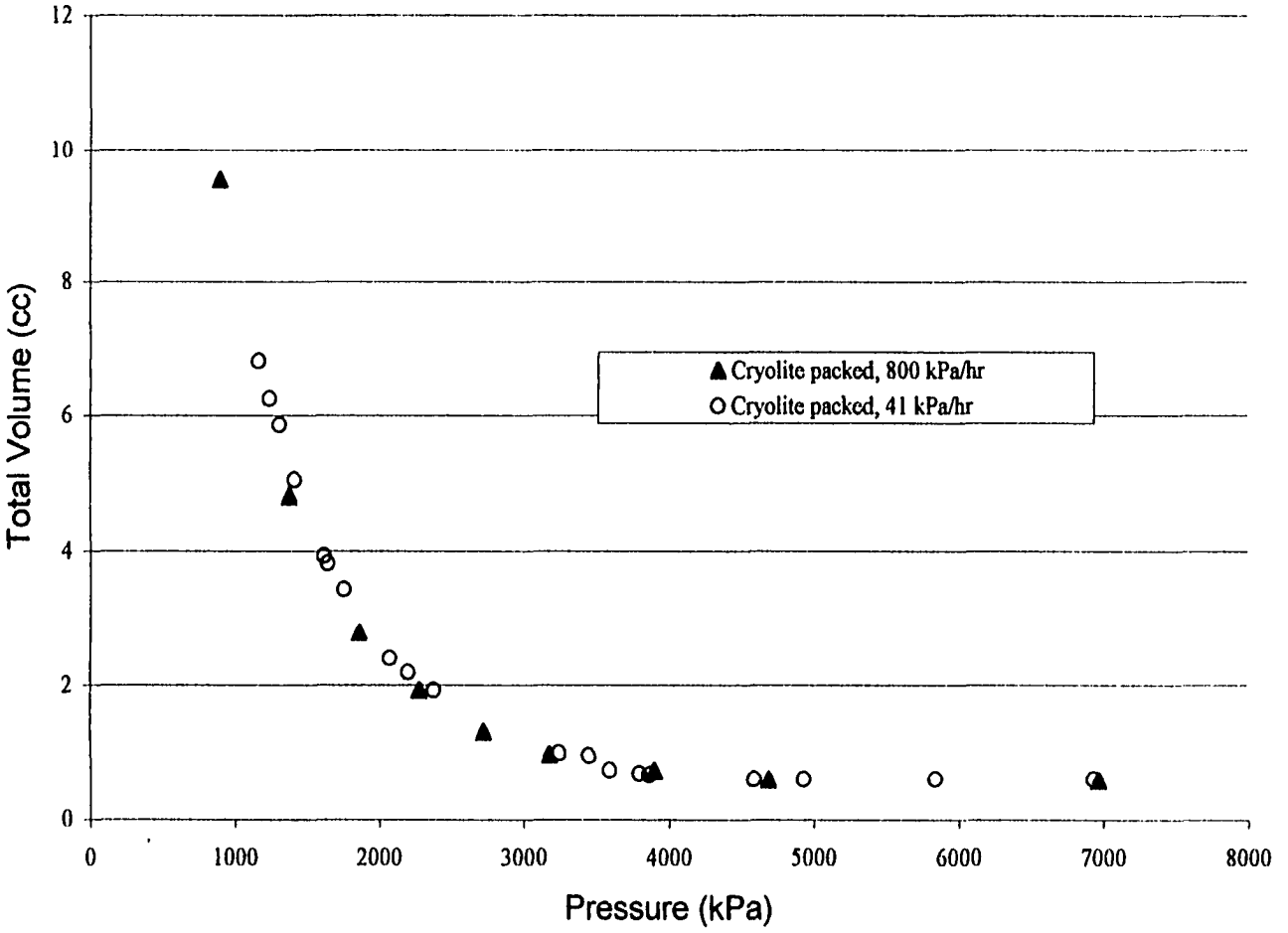

Figure 5.29T - Total volume for Cryolite-packed micromodel runs for 41 and 800 kPa/hr pressure depletion rates

Reproduced with permission of the copyright owner. Further reproduction prohibited without permission.

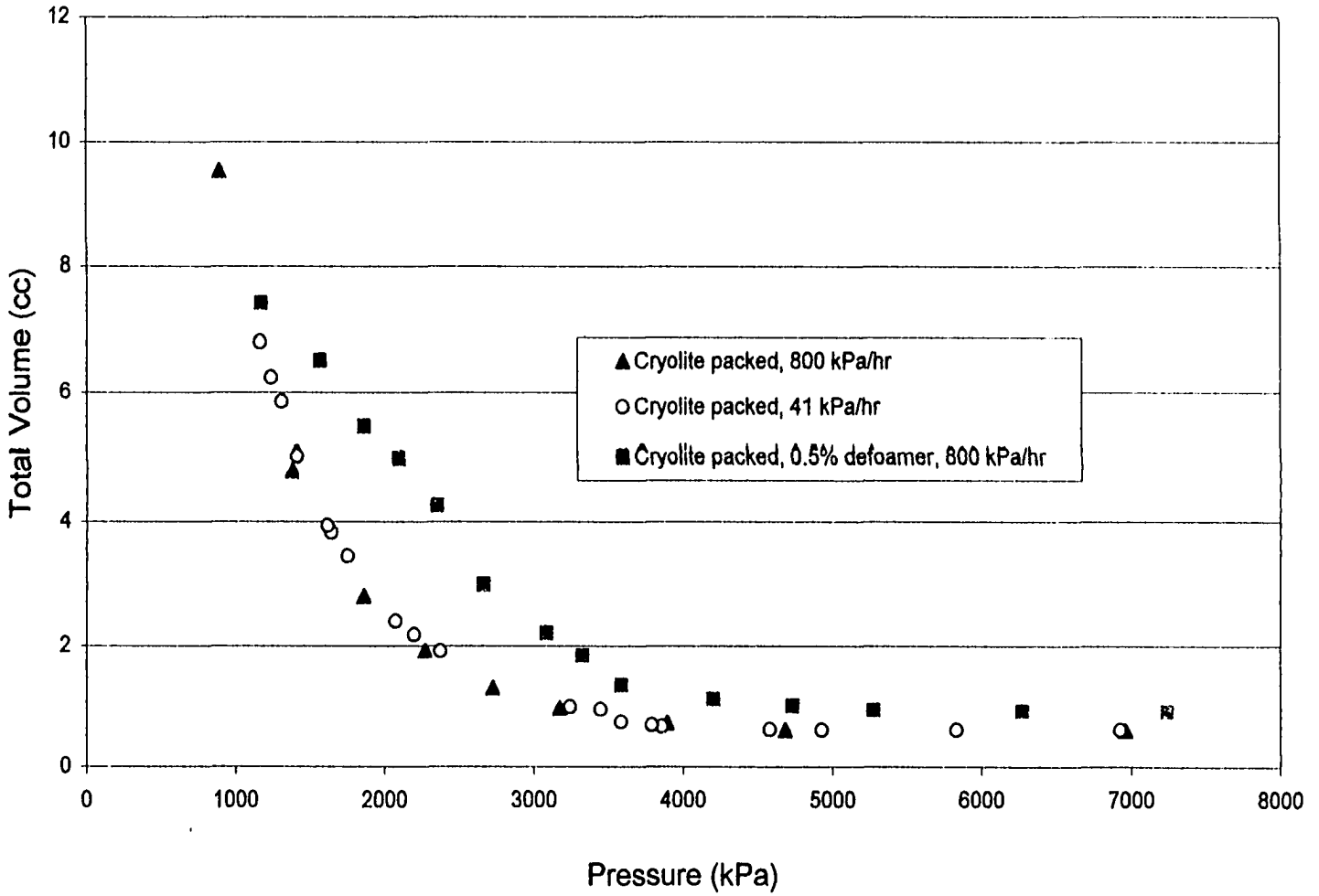

Figure 5.31T - Total volume of Cryolite-packed micromodel runs at different conditions and pressure depletion rates.

Reproduced with permission of the copyright owner. Further reproduction prohibited without permission.

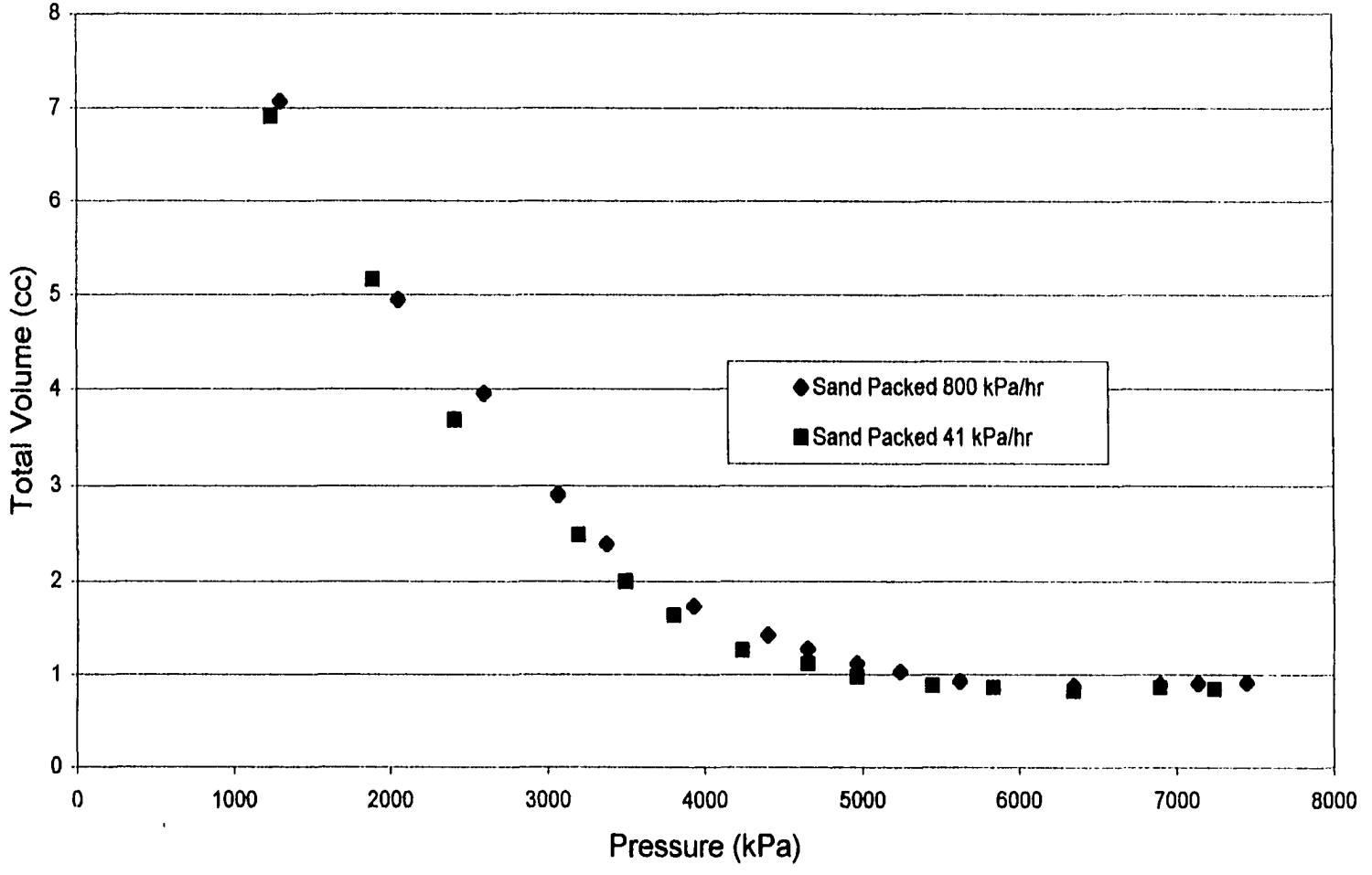

Figure 5.32T - Total volume for sand-packed micromodel runs at 41 and 800 kPa/hr pressure depletion depletion rates.

Reproduced with permission of the copyright owner. Further reproduction prohibited without permission.

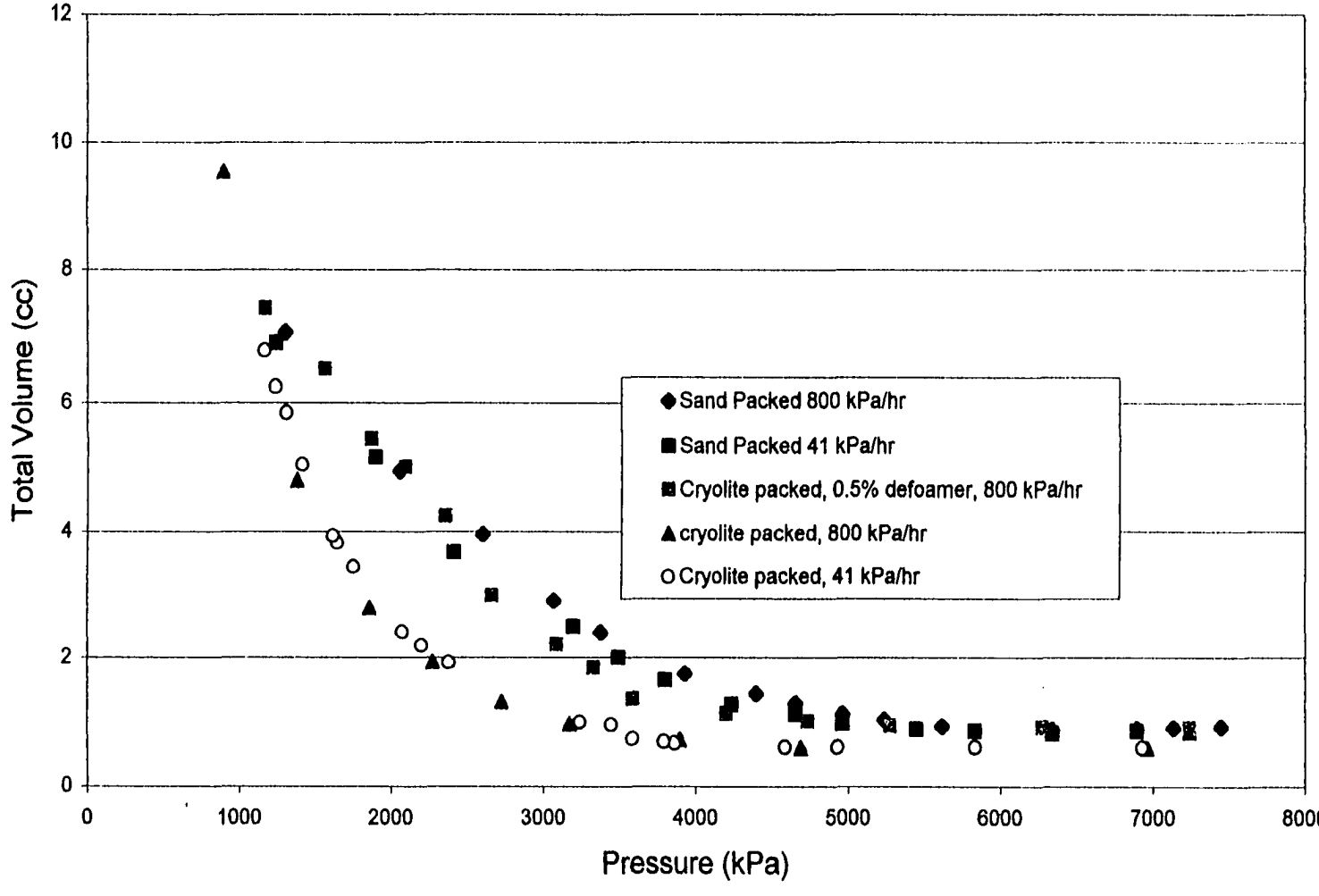

Figure 5.33T - Comparison of total volume for Cryolite and sand packed micromodel runs.

Appendix B

Videotape of the Micromodel Depletion process

Reproduced with permission of the copyright owner. Further reproduction prohibited without permission.

The videotape is described below using the counter of the videotape recorder as a guide whose zero corresponds to the beginning of the tape. The micromodel was positioned vertically. The sapphire cell the production end was connected at the top of the micromodel. The top of the micromodel is on the right of the screen and that the direction of flow is from the left to right.

(Tape Counter) Rec. Time	Event
(0-64) 0:02.35	Bubble nucleation at bottom of the micromodel, followed by bubble growth as elongated bubbles.
(64) 0:02.35	Narrow gas bubble moving towards the outlet.
(66-140) 0:2.41-0:6.05	More nucleation at bottom of the micromodel from different runs, followed by growth and flow of bubbles towards the outlet end.
(142-185) 0:6.10-0:8.18	Spherical bubbles at about the midpoint of the micromodel growing locally, then they move towards the production outlet, they change shape during their flow towards the outlet.
(186-232) 0:8.21-0:10.45	Nucleation of multi-bubbles. They start as spherical in shape and stand still, after they grow to a certain size; they start to move towards the closest moving bubble/train of bubbles.
(233-297) 0:10.49-0:14.2	Other spherical bubble nucleation, followed by a period of growth with virtually no movement until they attain a certain size then they start to move.
(300-475) 0:14.3-0:25.18	Bubbles moving while others being nucleated within the vicinity of the larger bubbles, then they move perpendicular to the production outlet direction.
(477-525) 0:25.26-0:28.4	Heterogeneous nucleation sites of multi-bubbles.

Reproduced with permission of the copyright owner. Further reproduction prohibited without permission.

(Tape Counter) Rec. Time	Event
(526-535) 0:28.47-0:29.2	Bubble movement towards the production end.
(536-552) 0:29.3-0:30.35	More bubble nucleation at bottom of the micromodel of different run followed by bubble movement.
(557-574) 0:30.56-0:32.1	More bubble nucleation at bottom of micromodel for a different run of slow depletion.
(575-600) 0:32.14-0:34.0	Nucleation of bubble at same site but more rapid nucleation rate.
(600-625) 0:32.14-0:35.53	Slow down of the nucleation from the one site eventually stopped nucleating, signaling a change in the nucleation stage.
(626-705) 0:35.53-0:42.1	Spherical bubbles start to appear on other parts of micromodel which they would not move until they attain a certain size after which they start moving to the closet pressure sink. Their shapes change to an elongated ones.
(706) 0:42.12	Coalescence of the bubble with a lager one.
(711-735) 0:42.3-0:44.25	Movement of bubbles at later stage of the depletion where bubble flow in perpendicular to the production end direction in order to flow to the closest longer moving bubble.
(736-760) 0:44.3-0:46.27	Nucleation changes to ramified and throughout the entire micromodel.
(774-786) 0:47.36-0:48.36	Porous media flow of high magnification where some bubbles are seen to flow with the liquid oil.
(787-795) 0:48.41-0:49.21	Porous media run showing the gas growth where it starts at a point away from the outlet.

Reproduced with permission of the copyright owner. Further reproduction prohibited without permission.

(Tape Counter) Rec. Time	Event
(797-811) 0:49.31-0:50.41	Another porous media run which shows the same process of gas buildup flow towards the production end, and at the end of the run the micromodel is full oil gas.
(812-845) 0:50.48-0:53.37	Gas movement at high magnification during the depletion process, it shows that gas does move through the pore throats, unfortunately the picture is not clear due to the dark color of oil.
(846-870) 0:53.41-0:55.47	Sand run showing the same gas buildup and flow towards the production end. The gas buildup starts at the bottom of the micromodel.
(871-885) 0:55.52-0:57.0	The gas migrates towards the production end.
(886-930) 0:57.06-0:57.12	Gas building up starts again at the bottom of the model and repeats the same thing observed with previous runs.
(931-965) 1:01.1-1:04.2	Another sand run showing the same process of gas build up that starts at the bottom of the model and flow towards the production end.

Table 5.4 – Descriptions of the foamy oil depletion process captured in videotape.

Reproduced with permission of the copyright owner. Further reproduction prohibited without permission.